LINKING THE BACTERIAL CYTOSKELETON
TO CELL WALL SYNTHESIS ACTIVATION:
DISCOVERY OF THE [FTSZ-FZLA]-FTSWI SIGNALING PATHWAY

by

Patrick J. Lariviere

A dissertation submitted to Johns Hopkins University in conformity with the
requirements for the degree of Doctor of Philosophy.

Baltimore, Maryland
May, 2019

© Patrick J. Lariviere 2019
All rights reserved

Abstract

Bacterial division requires the coordination of cytoskeleton constriction and insertion of new peptidoglycan (PG) into the existing cell wall by PG synthase enzymes. At the launch of this work, we hypothesized that FtsZ filament curvature promotes cell constriction. We therefore chose to study FzlA, a division protein that stabilizes highly curved FtsZ filaments, as a tool for assessing the contribution of FtsZ filament curvature to constriction. We show that in *Caulobacter crescentus*, FzlA must bind to FtsZ for division to occur and that FzlA-mediated FtsZ curvature is correlated with efficient division. We observed that FzlA influences constriction rate, and that this activity is mildly correlated with its ability to bind and curve FtsZ polymers. Further, we found that a slowly constricting fzlA mutant strain develops "pointy" poles, suggesting that FzlA influences the relative contributions of radial versus longitudinal PG insertion at the septum. These findings implicate FzlA as a critical coordinator of envelope constriction rate through its interaction with FtsZ, though they did not strongly show that FtsZ curvature is a major driver efficient constriction in *C. crescentus*.

We then asked if FzlA is able to regulate constriction because it signals through the division-specific PG synthesis pathway and discovered a promising genetic link. We found that hyperactive mutants of the PG synthases FtsW and FtsI specifically render *fzlA*, but not other division genes, non-essential. However, FzlA is still required to maintain proper constriction rate and efficiency in a hyperactive PG synthase background. Intriguingly, loss of *fzlA* in the presence of hyperactivated FtsWI causes cells to rotate about the division plane during constriction and sensitizes cells to cell-wall-specific antibiotics. We demonstrate that FzlA-dependent signaling to division-specific PG synthesis is conserved in another α-proteobacterium, *Agrobacterium tumefaciens*. These data establish that FzlA helps link FtsZ to cell wall remodeling and is required for signaling to both activate and spatially orient PG synthesis during division. Overall, our findings support the paradigm that activation of SEDS-PBP PG synthases is a broadly conserved requirement for bacterial morphogenesis.

Primary Reader: Erin D. Goley, Ph.D.

Secondary Reader: Jie Xiao, Ph.D.

Acknowledgements

I would first like to acknowledge everyone who contributed scientifically to this body of work. I thank my advisor, Dr. Erin Goley, for providing invaluable training, guidance, and input throughout all stages of the research and writing processes. I thank Dr. Piotr Szwedziak and Dr. Jan Löwe for solving the structure of FzlA and being great collaborators. I thank Chris Mahone for selflessly contributing protein interaction data for my first paper. I again thank Chris Mahone, as well Allison Daitch, for making major contributions to my second paper and for being very easy to work with. I also thank Gustavo Santiago-Collazo, Matthew Howell, Rilee Zeinert, Dr. Pam Brown, and Dr. Peter Chien for their valuable contributions to my second paper. I would also like to acknowledge Dr. Phil Cox and James Valderrama for their contributions to the early stages of my thesis work, and Anant Bhargava for helping to streamline the process of single cell image analysis. I also thank Dr. Zachary Pincus and Dr. Adrien Ducret (from the Brun lab) for assistance with Celltool and MicrobeJ respectively. We thank Dr. Josh Modell and Dr. Michael Laub for providing strains, as well as the Manley lab and Aurelia Battesti for providing us with plasmids. I also thank Mike Delannoy, Barbara Smith, and Selam Woldemeskel for developing the SEM protocol; Mike and Barbara for training on SEM equipment; Caren Freel Meyers and Amer Al-khouja for HADA synthesis; Brandon King for providing support with experiments; and William Mills for help during his rotation. I would of course like to thank members of both the Goley and the Xiao labs for insightful discussions during all stages of my research. And finally, I would like to thank Dr. Jie Xiao, Dr. James Berger, Dr. Geraldine Seydoux, and Dr. Trina Schroer for their guidance and advise as my thesis committee.

Having hopefully acknowledged all of the intellectual contributions to this work, I would now like to acknowledge everyone who made getting through grad school possible. I would first

like to again thank Erin for her steady mentorship throughout my graduate career. Erin taught me how to do rigorous and honest science without cutting corners. Of the many pieces of wisdom that Erin imparted on me, among the most important is that we perform science to uncover the truth, not just to fit the data into a particular model. I can remember a particular instance when I had hit a wall scientifically and could not resolve conflicting pieces of data with our current model at the time. Distraught, I asked Erin if there was any way to massage the data to make it work. But Erin calmly explained that if we needed to throw out our current model, then so be it, we would come up with a completely new one, because we were trying to seek the truth. My graduate career was filled will small, but impactful teaching moments like this, and I will always be grateful for Erin's patience and sage advice.

Erin also did a great job at fostering a safe, supportive, and fun environment to work in – I feel lucky to have made truly lifelong friends in her lab. Thanks to Liz and Kousik for first mentoring me, then quickly befriending me, and for making the lab a great place to be early on. Thanks to Selam for making the lab a great place to be and for stoking some healthy, light-hearted competition. Thanks to Chris, Allison, and Jordan for similarly being great labmates and for bringing some energy into lab in my later stages of grad school. I would also like to acknowledge members of the Margolis lab for helping me to blow off some steam. I will truly miss the MarGoley lab dynamic and hanging out on in the hallways (where science really gets done) of the 5th floor of WBSB.

Finally, I would also like to thank members of the BC department and the BCMB program administration for all of their help, in particular Carolyn Machamer and Arhonda Gogos – I greatly appreciate all of your support.

Table of Contents

Abstract .... **ii**

Acknowledgements .... **iv**

List of Tables .... **ix**

List of Figures .... **x**

Chapter 1: Cell division in *Caulobacter crescentus*: A molecular-scale model **1**

1.1 Introduction 1

1.2 Z-ring composition, structure, and dynamics 3
  1.2.1 FtsZ: The building block of the Z-ring 4
  1.2.2 Z-ring structure and dynamics 6

1.3 Building the Z-ring: Spatiotemporal regulation of Z-ring formation 8
  1.3.1 Cell cycle control of FtsZ protein levels 9
  1.3.2 Z-ring site selection 10
  1.3.3 Cell cycle control of FtsZ self-interaction: A putative model 14
  1.3.4 Focusing the Z-ring 15
  1.3.5 Attachment of the Z-ring to the membrane 16

1.4 The Z-ring: A scaffold for the rest of the divisome 19

1.5 Divisome-associated elongation 20

1.6 Constriction: A PG synthesis-driven process 22
  1.6.1 Force generation through PG synthesis 23
  1.6.2 Constriction-specific PG synthesis machinery 24
  1.6.3 FtsZ-mediated PG synthase localization and activation 27
  1.6.4 Stress response-mediated constriction regulation 30
  1.6.5 Downstream PG synthase activation pathways 31

1.7 Envelope maintenance 33

1.8 Cell separation, polar organization, and the final events of division 36
  1.8.1 Cell separation 36
  1.8.2 Recruitment of polarity determining factors 39
  1.8.3 Z-ring disassembly and MreB dispersal 39
  1.8.4 Cell pole shape determination 41

1.9 Conclusions and Outlook 42

1.10 Figures and Legends 44

Chapter 2. FzlA, an essential regulator of FtsZ filament curvature, controls constriction rate during *Caulobacter* division **52**

2.1 Introduction 52

2.2 FzlA forms a GST-like homodimer 54

2.3 Attempts to co-crystallize FtsZ and FzlA were unsuccessful 56

2.4 FzlA interacts with the GTPase domain of FtsZ 56
2.5 Creation of FzlA mutant library..... 57
2.6 *fzlA* mutants display a range of localization and division defects 58
2.7 FzlA mutant proteins display distinct defects in activities towards FtsZ *in vitro* 60
2.8 FzlA-FtsZ binding is necessary for allelic complementation..... 64
2.9 Mutant *fzlA* strains display growth and shape defects 65
2.10 *fzlA* mutant strains display reduced constriction rates 67
2.11 Discussion..... 69
2.12 Tables 75
2.13 Figures and Legends..... 79

Chapter 3. An essential regulator of bacterial division links FtsZ to cell wall synthase activation..... 115

3.1 Introduction 115
3.2 *fzlA* lies upstream of *ftsWI* in a PG synthesis pathway 117
3.3 ftsW**I* specifically permits loss of *fzlA* 119
3.4 FzlA contributes to efficient division in a hyperactive PG synthase background..... 119
3.5 *fzlA* is required for maintenance of proper cell shape 121
3.6 The [FtsZ-FzlA]-FtsWI pathway contributes to resistance to PBP-targeting antibiotics 122
3.7 The *fzlA-ftsW* genetic interaction is conserved in diverse α-proteobacteria..... 124
3.8 Discussion..... 125
3.9 Figures and Legends 130

Materials and Methods..... 153

4.1 Plasmid construction 153
4.2 Strains..... 154
4.3 Spot dilutions, growth analysis, and synchrony 154
4.4 Protein Purification 155
4.5 Crystallization and structure determination..... 156
4.6 Bacterial Two-Hybrid (BTH) Analysis..... 157
4.7 Co-immunoprecipitation 157
4.8 FtsZ activity assays 158
4.9 Antibodies and Immunoblot analysis..... 159
4.10 Light microscopy imaging and analysis..... 159
4.11 Cell shape analysis 161

4.12 Scanning electron microscopy sample preparation and imaging................................ 162
4.13 Transposon library preparation, sequencing, and analysis.. 162
4.14 Quantification and Statistical Analysis 164
4.15 Data Availability.. 164
References 165
Curriculum Vitae.. 181

List of Tables

Table 1. Crystallographic data. 75
Table 2. FzlA mutant phenotypes and activity.. 76
Table 3. Additional FzlA mutant phenotype and activity.. 77

List of Figures

Figure 1. Overview of division in _Caulobacter_. 44

Figure 2. Architecture of the Caulobacter divisome.......... 46

Figure 3. Timing of divisome localization. 47

Figure 4. A dynamic activator model for FtsZ-mediated constriction initiation. 49

Figure 5. Cell separation pathways.......... 50

Figure 6. FzlA forms a homodimer in the GST structural family. 79

Figure 7. Close-up of a stereo image of the electron density map of FzlA. 80

Figure 8. FzlA self-interacts _in vivo_. 81

Figure 9. FzlA Interacts with the GTPase domain of FtsZ. 83

Figure 10. Structure-function analysis workflow. 84

Figure 11. _fzlA_ mutant strains display a range of division and localization deficiencies. 86

Figure 12. Many _fzlA_ mutant strains displayed wild-type phenotypes or were unstable or insoluble. 88

Figure 13. Protein levels of mCherry-FzlA under induction conditions. 90

Figure 14. _fzlA_ mutant strains grown with xylose to induce WT FzlA grow normally.......... 91

Figure 15. _fzlA_ mutant strains grown without inducers display a range of growth phenotypes that correlate with their activities in the presence of vanillate.......... 93

Figure 16. Protein levels of mCherry-FzlA under depletion conditions.......... 95

Figure 17. FtsZ forms rings in cells expressing _fzlA_ mutant alleles. 96

Figure 18. FtsZ binding and/or helix formation is perturbed for a number of FzlA mutant proteins.......... 98

Figure 19. High speed co-pelleting of FzlA mutant proteins and FtsZ. 100

Figure 20. Low speed co-pelleting of FzlA mutant proteins and FtsZ. 102

Figure 21. Some FzlA mutant proteins are able to form higher order structures in the presence of FtsZ. 104

Figure 22. High speed co-pelleting of FzlA$^{\mathrm{WB1}}$ or FzlA$^{\mathrm{NB1}}$ and FtsZ. 106

Figure 23. Three _fzlA_ mutant genes are capable of allelic replacement, causing a range of division and morphological defects. 107

Figure 24. Protein levels of FzlA in _fzlA_ allelic exchange strains. 109

Figure 25. _fzlA_ mutant strains show protracted constriction. 110

Figure 26. Pre-constriction time and change in cell length for _fzlA_ allelic exchange strains. 112

Figure 27. Model of FzlA function in regulating constriction 114

Figure 28. Hyperactive _ftsWI_ mutants suppress loss of _fzlA_. 130

Figure 29. _ftsW**I*_ rescue the fitness/morphological defects of two _fzlA_ mutants.......... 132

Figure 30. In the presence of hyperactive PG synthases, the interaction between FtsZ and FzlA determines division efficiency, but not growth rate or viability. 133

Figure 31. Mutation of FzlA's essential C-terminus phenocopies loss of _fzlA_ in an _ftsW**I*_ background. 135

Figure 32. FzlA contributes to efficient division in a hyperactive PG synthase background.......... 137

Figure 33. _fzlA_ is required for global shape maintenance. 139

Figure 34. FtsZ, MreB, and PG synthesis localization is unaffected in _ftsW**I*_ Δ_fzlA_ cells. 141

Figure 35. Interaction of FtsZ with FzlA is necessary for proper division site shape maintenance. 143

Figure 36. Loss of *fzlA* leads to increased cell wall antibiotic sensitivity. 145
Figure 37. Effect of loss of FzlA and FzlA-FtsZ interaction on resistance to cell wall antibiotics. 146
Figure 38. Multiple non-essential division genes become essential in a hyperactive PG synthase background. 148
Figure 39. The ability of hyperactive *ftsW* to suppress loss of *fzlA* is conserved. 150
Figure 40. FzlA is required for activation of FtsWI and regulates the geometry of PG insertion. 152

Chapter 1: Cell division in *Caulobacter crescentus*: A molecular-scale model

1.1 Introduction

For a replicating bacterium, the objective of cell division is relatively simple: split into two viable cells that are themselves capable of growing and dividing. Despite the simplicity of this goal, the mechanism for achieving successful division in *Caulobacter crescentus* (hereafter, *Caulobacter*) is in fact exceedingly sophisticated. The first layer of complexity involves proper timing of division initiation, such that the start of division is coordinated with the other events of the cell cycle. *Caulobacter* cells begin their life cycle as motile, flagellated swarmer cells, which grow, but do not themselves divide (Terrana and Newton, 1975; Aaron *et al.*, 2007). In their natural habitat, swarmer cells are believed to swim around in search of a nutrient-rich zone. Upon finding such an environment, swarmer cells undergo a cell-type transition in which they lose their flagella and grow a long, thin extension of the cell body called the stalk. At this time, stalked cells begin to replicate their DNA, grow, and initiate the pre-constriction phase of the cell division program. At some point after DNA replication has begun, cells begin to constrict, eventually dividing into two daughter cells.

Division in *Caulobacter* requires that cells undergo a complex series of synchronized shape changes in the cell envelope. In Gram-negative cells including *Caulobacter*, the envelope is the multi-layered casing around the cell made up of an inner membrane (IM), an outer membrane (OM), and a cell wall in between the two, occupying the space known as the periplasm. The cell wall in *Caulobacter* is a semi-rigid structure made of the macromolecule peptidoglycan (PG), which helps resist turgor pressure and maintain cell shape (Cabeen and Jacobs-Wagner, 2005; Woldemeskel and Goley, 2017). PG itself is made of glycan strands of repeating disaccharides that run along the circumference of the cell and are attached to each other by pentapeptide crosslinks (Hayhurst *et al.*, 2008; Gan *et al.*, 2008; Huang *et al.*, 2008). Incorporation of new PG material into the cell wall (also referred to as PG or cell wall remodeling) drives both constriction, the inward invagination of the envelope, and elongation, the longitudinal extension of the envelope that occurs before and during constriction in *Caulobacter*.

The next layer of the complexity of division lies within the sheer number of factors involved in facilitating cell wall remodeling and other events during the division process. The components of the cell division machinery are collectively known as the divisome, with each protein playing one or more specialized role(s) in division. The structural core of the divisome, FtsZ, forms a cytokinetic ring referred to as the Z-ring. In *Caulobacter*, the Z-ring marks the site of division, which is located approximately at midcell. There, the Z-ring acts as a scaffold for the rest of the division machinery, including the enzymes that insert new PG into the cell wall. Such a scaffold nucleates an intricate network of interactions among the various divisome proteins that is crucial for allowing division to occur.

The last level of complexity in *Caulobacter* division lies in the requirement for tight coordination of the activities of the numerous members of the divisome in time and space, such that the envelope can undergo the correct shape changes at the right time. Here we present a description of division in *Caulobacter.* We have divided division into five concrete steps, which we will explain in brief here and in greater detail in the following sections. Note that we introduce these events each in turn for simplicity, but they are not strictly separate. Instead, they are tightly coordinated and overlapping in time and space. These steps are as follows: 1. Formation of the Z-ring 2. Cell elongation at midcell 3. Envelope maintenance 4. Activation of the constriction machinery and constriction 5. Cell separation and polar organization (**Fig. 1**). Z-ring formation marks the beginning of the cell division program in *Caulobacter* and consists of localizing the Z-ring to midcell at the correct point in time in the cell cycle with the help of other divisome proteins and additional factors. Following assembly of the Z-ring, proteins involved in cell elongation and envelope maintenance localize to the ring to initiate growth at midcell, and preserve integrity of the cell wall. While cells elongate, additional division proteins gradually localize to midcell in a stepwise fashion. We will refer to these later arriving division proteins as the constriction machinery, as they are more directly responsible for either activating or effecting constriction. Once all of the constriction machinery has assembled, constriction initiates, whereby the entire envelope starts to invaginate. When cells are close to finishing division, that is they are characterized by deep constrictions, polarity determining factors arrive at midcell and factors responsible for separating the two future daughter cells help execute the last stages of the division process. Finally, the cell splits into two, thus completing division. Having introduced the major steps of division, we will go into each in more detail in the rest of this chapter. First, however, we will introduce the Z-ring and describe what is known about its structure and dynamics.

1.2 Z-ring composition, structure, and dynamics

The Z-ring is an essential apparatus required for division in most bacteria, including *Caulobacter*, though the full range of its activities are still being investigated. A guiding principle in this endeavor has been that the structure of the Z-ring dictates its functions within the cell, and so a detailed understanding of its architecture has been a longstanding goal. The fundamental building block of the Z-ring is the GTPase FtsZ, a tubulin-like protein that polymerizes into head-to-tail assemblies of monomers to form protofilaments. *In vivo*, these FtsZ protofilaments assemble into a dynamic, annular superstructure - the Z-ring - along the circumference of the cell's short axis at midcell. Formation of this structure is crucial for FtsZ to serve as a scaffold for the rest of the divisome, a concept that we will explore in a later section. In order to lay the groundwork for understanding the functions of the Z-ring during division, this section will focus first on the composition of the Z-ring, then on its structure and dynamics.

1.2.1 FtsZ: The building block of the Z-ring

FtsZ is a widely conserved protein (Vaughan *et al.*, 2004) that is essential for division in *Caulobacter* and most other bacterial species. First characterized in *E. coli*, *ftsZ* was identified by complementation of a mutation that conferred cell filamentation at restrictive temperature, indicating that it is required for division. Subsequent studies established FtsZ as a crucial positive regulator of division by demonstrating its overexpression rescued various division mutant phenotypes (Lutkenhaus *et al.*, 1986; Bi and Lutkenhaus, 1990). FtsZ was then found to localize to midcell at the site of division, first in *E. coli*, then in *Bacillus subtilis*, forming a ring-like structure now known as the Z-ring (Bi and Lutkenhaus, 1991; Wang and Lutkenhaus, 1993; Ma *et al.*, 1996).

FtsZ is considered to be a tubulin homolog through amino acid sequence and structural comparison (Mukherjee *et al.*, 1993; Löwe and Amos, 1998; Löwe, 1998; Vaughan *et al.*, 2004). Like tubulin, FtsZ is a GTPase, capable of binding and hydrolyzing GTP in its GTPase domain (de Boer *et al.*, 1992; RayChaudhuri and Park, 1992; Mukherjee *et al.*, 1993). However, unlike tubulin, *Caulobacter* FtsZ contains two additional motifs: a C-terminal conserved (CTC) peptide and a disordered C-terminal linker (CTL), which connects the GTPase domain to the CTC (Sundararajan *et al.*, 2015).

Like tubulin, FtsZ monomers form protofilaments in a nucleotide-dependent manner *in vitro* (Mukherjee and Lutkenhaus, 1994), with GTP binding and hydrolysis influencing polymer assembly and disassembly dynamics (Mukherjee and Lutkenhaus, 1998; Mukherjee and Lutkenhaus, 1999). FtsZ binds GTP to initiate polymerization, with FtsZ-GTP subunits assembling in an end-to-end fashion (Mukherjee and Lutkenhaus, 1994; Löwe and Amos, 1999) . GTP is quickly hydrolyzed into GDP, which subsequently destabilizes the filaments (Scheffers and Driessen, 2002; Chen and Erickson, 2005). Finally, subunits fall off the protofilament and exchange GDP for GTP to begin the cycle anew (Scheffers and Driessen, 2002; Chen and Erickson, 2005). By electron microscopy (EM), FtsZ protofilaments form straight or gently curved polymers in the presence of GTP, but they can also form highly curved mini-ring-shaped assemblies under strongly stabilizing conditions (i.e., on DEAE-dextran) with GDP present (Mukherjee and Lutkenhaus, 1994; Erickson *et al.*, 1996; Mukherjee and Lutkenhaus, 1998; Mukherjee and Lutkenhaus, 1999; Goley *et al.*, 2010b). Additional structural and *in vitro* data indicate that individual FtsZ protofilaments can associate with one another further to form higher order structures, depending on *in vitro* conditions. Specifically, FtsZ protofilaments can interact laterally to form small filament bundles (made up of as few as two filaments), larger multi-filament bundles, or structured sheets, with such lateral interactions appearing to be required for division in *E. coli* (Erickson *et al.*, 1996; Yu and Margolin, 1997; Mukherjee and Lutkenhaus, 1999; Löwe and Amos, 1999; Oliva *et al.*, 2004; Milam and Erickson, 2013; Guan *et al.*, 2018).

1.2.2 Z-ring structure and dynamics

In vivo, by conventional fluorescence microscopy (FM), FtsZ localizes to midcell to form the band-like Z-ring (Ma *et al.*, 1996). Super-resolution microscopy has provided additional insight into the architecture of the Z-ring. Viewing cells from a top-down perspective, photoactivated localization microscopy (PALM) shows that FtsZ is tightly focused at midcell, with a mean longitudinal width of 71-108 nm in *Caulobacter* (Biteen *et al.*, 2012; Holden *et al.*, 2014; Woldemeskel *et al.*, 2017). Imaging *Caulobacter* cells in cross-section by PALM confirms the suspected ring-like structure, with FtsZ most concentrated near the membrane (Holden *et al.*, 2014), similar to the ring-like organization observed in other organisms (Fu *et al.*, 2010; Strauss *et al.*, 2012). *Caulobacter* Z-rings were found to have a diameter roughly corresponding with cell diameter [150 nm (near the z resolution limit) to 650 nm, depending on what stage of division the cell is in] and a mean radial thickness of around 65 nm (Biteen *et al.*, 2012; Holden *et al.*, 2014). *Caulobacter* Z-rings, similar to other organisms, have a clustered distribution of FtsZ suggesting the *Caulobacter* Z-ring is patchy and discontinuous (Strauss *et al.*, 2012; Holden *et al.*, 2014; Coltharp *et al.*, 2016; Lyu *et al.*, 2016).

Whole cell cryo-electron tomography (cryo-ET) has provided a higher resolution view of the *Caulobacter* Z-ring. In one study, curved filamentous FtsZ structures have been observed at midcell roughly 16 nm from the membrane (Li *et al.*, 2007). Over-expression of FtsZ or expression of a less dynamic form of FtsZ increased the number these structures, suggesting they are in fact made of FtsZ (Li *et al.*, 2007). These structures are similar in width to single FtsZ protofilaments (5 nm wide by cryo-ET vs. 4 nm wide FtsZ structure by crystallography), with neighboring structures being either approximately parallel or slightly overlapping (Li *et al.*, 2007). Moreover, these structures are relatively short at 80-160 nm in length and are heterogeneously distributed at midcell, providing additional evidence for a discontinuous Z-ring (Li *et al.*, 2007). A follow-up study showed that in the initial stages of constriction, FtsZ filaments were often found localized to one side of the cell at a site of invagination, suggesting the heterogeneous distribution of the Z-ring begins early in the division process (Yao *et al.*, 2017). However, in similar experiments from another group, the Z-ring instead appears as a single connected, continuous filament (Szwedziak *et al.*, 2014). Since cryo-ET does not use labeling, not all of the FtsZ in a cell may be visualized, which may account for discrepancies between the two sets of experiments. Questions therefore still remain about the continuous nature of the *Caulobacter* Z-ring, though evidence presented in subsequent sections, as well as the super-resolution light microscopy data discussed above, support the discontinuous ring model.

Although the Z-ring displays a relatively ordered architecture, it is highly dynamic at multiple timescales. On a longer timescale, the structure of the Z-ring is dynamic through the cell cycle: FtsZ moves from the pole to midcell during the swarmer to stalked cell transition, assembles into a focused ring, then decreases in diameter throughout the constriction process (Goley *et al.*, 2011; Holden *et al.*, 2014). On a much shorter timescale, fluorescence recovery after photobleaching (FRAP) experiments from *E. coli* suggest that the Z-ring exchanges with cytoplasmic FtsZ on the order of seconds, with the speed of this process dependent on FtsZ's GTPase rate (Stricker *et al.*, 2002; Anderson *et al.*, 2004). In addition to subunit exchange, recent work in other species suggests the Z-ring exhibits another form of dynamics: treadmilling. In both *E. coli* and *B. subtilis*, by three dimensional structured-illumination microscopy (3D-SIM) or total internal reflection fluorescence microscopy (TIRFM), FtsZ polymers/clusters appear to move around the circumference of the cell (Bisson-Filho *et al.*, 2017; Yang *et al.*, 2017).

However, FtsZ molecules are actually motionless, and the polymers themselves likely do not "move" either (Bisson-Filho *et al.*, 2017; Yang *et al.*, 2017). Yang et al and Bisson-Filo et al instead propose that FtsZ clusters treadmill, potentially achieving dynamics through addition of FtsZ subunits (or oligomers or polymers) at the leading edge of the cluster and loss of FtsZ from the lagging edge (Bisson-Filho *et al.*, 2017; Yang *et al.*, 2017), allowing FtsZ clusters to have the appearance of movement. The speed of this movement is dependent on the GTPase rate of FtsZ, indicating that polymerization and depolymerization dictate FtsZ dynamics within the cell (Bisson-Filho *et al.*, 2017; Yang *et al.*, 2017). Experiments to assess FtsZ treadmilling in *Caulobacter* have not yet been reported, likely because its smaller diameter complicates resolution of the Z-ring. However, since FtsZ treadmilling is conserved in both Gram-positive and Gram-negative bacteria, we can infer that it occurs in *Caulobacter* as well.

1.3 Building the Z-ring: Spatiotemporal regulation of Z-ring formation

Having detailed the architecture of the Z-ring, we will now consider *how* the Z-ring forms. The timing of Z-ring formation must be tightly controlled since precise timing of the *Caulobacter* cell cycle is necessary to ensure that cells balance replication speed with fitness of both mother and daughter cells. Z-ring formation is prevented in swarmer cells both by transcriptional and post-translational limitation of FtsZ levels, and by inhibition of FtsZ polymerization. Removal of these blocks occurs only when swarmer cells are ready to transition into the division-competent stalked cells, thus allowing the Z-ring to assemble. Spatial regulation of Z-ring formation is also crucial for the division process, ensuring that division yields two properly sized daughters. As cells enter the stalked phase, the site of Z-ring formation is set at approximately midcell in a process that is tightly coupled to the cell cycle. Shortly after the midcell division plane is established, FtsZ rapidly assembles into a ring-like structure. Additional factors are required to “focus” the ring to a defined width. Concurrently, at least one other factor is thought to attach FtsZ polymers to the membrane in order to bring the Z-ring proximal to its site of action. The result is a highly ordered super-structure that is now ready to serve as the backbone for the rest of the divisome for the remainder of the division process.

1.3.1 Cell cycle control of FtsZ protein levels

The initiation of division is regulated, at least in part, through temporal control of division protein concentrations. As such, FtsZ protein levels in *Caulobacter* fluctuate over the course of the cell cycle (Quardokus and Brun, 2002); FtsZ is absent or in low abundance in swarmer cells, with its expression increasing around the time of the swarmer to stalked cell transition (Quardokus and Brun, 2002). FtsZ levels peak in pre-divisional cells, before finally dropping significantly after division is complete (Quardokus and Brun, 2002). At least two mechanisms are responsible for the control of FtsZ protein levels: transcriptional regulation and proteolysis. *ftsZ* mRNA levels were found to fluctuate over the course of the cell cycle in a manner dependent on the cell cycle regulator CtrA(Kelly *et al.*, 1998; Laub *et al.*, 2000). Depletion of CtrA leads to a corresponding increase in *ftsZ* expression, whereas overexpression of CtrA reduces *ftsZ* expression (Kelly *et al.*, 1998). CtrA therefore represses *ftsZ* expression during the swarmer phase by directly binding to its promoter (Laub *et al.*, 2002), and as its own levels decrease upon transition to the stalked cell phase, *ftsZ* levels go up. Other cell-cycle associated transcriptional regulators – DnaA, GcrA, and CcrM – have been implicated in directly activating *ftsZ* expression, allowing for its transcription throughout the majority of the division process (Hottes *et al.*, 2005; McAdams and Shapiro, 2009; Gonzalez and Collier, 2013;

Haakonsen *et al.*, 2015). Additionally, transcripts of other division genes (*ftsA*, *ftsQ*, *ftsW*, *ftsI*, *ftsK*, *fzlA*, *ftsB, kidO, murG*) have also been found to fluctuate over the course of the cell cycle (Laub *et al.*, 2000; Goley *et al.*, 2011). Multiple transcriptional regulators probably control these transcript levels, as *kidO*, *fzlA*, and *ftsK* have CtrA binding motifs and *ftsA*, *ftsQ*, and *ftsB* have both CtrA and CcrM motifs.

The levels of FtsZ and at least a few other divisome proteins are also regulated post-translationally. When either *ftsZ*, *ftsQ*, or *ftsA* are constitutively transcribed, levels of the corresponding protein still change over the cell cycle similar to WT cells (Kelly *et al.*, 1998; Martin *et al.*, 2004), suggesting cell cycle-linked protein degradation by proteolysis. The AAA+ protease ClpXP, which was first found to degrade FtsZ in *E. coli* (Camberg *et al.*, 2009), was determined to be partially responsible for the cell cycle-dependent proteolysis of FtsZ in *Caulobacter* (Bhat *et al.*, 2013; Williams *et al.*, 2014). Another protease, ClpAP, also degrades both *Caulobacter* FtsZ and FtsA in a cell cycle-dependent manner (Williams *et al.*, 2014). Deletion of ClpA or inactivation of ClpX leads to accumulation of FtsZ in swarmer cells (Williams *et al.*, 2014), indicating that these proteases are critical for preventing premature FtsZ accumulation and Z-ring formation. Initiation of the cell division program is therefore inhibited during G1 phase and only begins once FtsZ (and FtsA) transcript and protein levels increase sufficiently to support Z-ring formation upon transition to S phase.

1.3.2 Z-ring site selection

As cells enter S phase, and FtsZ levels increase, the Z-ring is now ready to assemble. Formation of the Z-ring is not, however, merely dependent on the presence of FtsZ. In fact, despite multiple forms of negative regulation of FtsZ accumulation during G1 phase, a small amount of FtsZ is actually present in cells localized to the pole opposite the flagellum, indicating a mechanism is in place to regulate FtsZ localization. It is only upon transition to S phase, concurrent with the increase in FtsZ protein levels, that FtsZ relocates from the pole to midcell (**Fig. 1** and **Fig. 3**). How, then, does FtsZ exhibit dynamic localization and how is localization eventually limited to midcell? Additionally, how is FtsZ localization regulated temporally? A negative regulator of FtsZ polymerization, the dimeric ATPase MipZ, is primarily responsible for regulating localization of the Z-ring in time and space (Thanbichler and Shapiro, 2006). MipZ is technically non-essential, though its deletion (or depletion) causes severe perturbations in division including cell filamentation and loss of nearly all constriction sites (Thanbichler and Shapiro, 2006; Radhakrishnan *et al.*, 2010). In swarmer cells, MipZ localizes to the flagellated pole (opposite from the FtsZ-localized pole). Coincident with FtsZ's relocation to midcell, MipZ becomes bipolar in cells that have recently undergone the swarmer to stalked cell transition (**Fig. 1** and **Fig. 3**), forming a gradient with maxima at the poles and a minimum at midcell (Thanbichler and Shapiro, 2006; Goley *et al.*, 2011). Overexpessing *mipZ*, which causes it to become diffuse throughout the cytoplasm, makes FtsZ localize to the poles instead of midcell. MipZ therefore dictates FtsZ localization, with FtsZ present at the minimum of the MipZ gradient. What is the mechanism of this regulation? *In vitro*, MipZ has been shown to destabilize FtsZ filaments and promote polymer turnover. MipZ is thus proposed to negatively regulate FtsZ polymerization *in vivo* through its formation of a gradient, spatially limiting where FtsZ can localize and polymerize. This regulation is necessary for allowing FtsZ polymers to condense into a focused Z-ring, since depletion of MipZ leads to the formation of FtsZ puncta instead of rings (Thanbichler and Shapiro, 2006).

If MipZ is able to dictate FtsZ's localization, how then is its own localization determined? The DNA partitioning protein ParB, which binds to the centromeric DNA locus *parS* to help segregate the chromosome in a ParA-dependent manner, also directly interacts with and colocalizes with MipZ (Thanbichler and Shapiro, 2006). MipZ localization is dependent on ParB, becoming diffuse upon ParB depletion. MipZ's localization is therefore determined by the localization of the ParB-*parS* complex. During G1 phase, ParB-*parS* localizes to the flagellated pole; upon DNA replication in S phase, one copy of ParB-*parS* is segregated to the opposite cell pole. Localization of ParB-*parS* to the poles therefore underlies MipZ gradient formation (Thanbichler and Shapiro, 2006). In light of these localization dependencies, it is therefore unsurprising that proper FtsZ localization to midcell requires initiation of DNA replication (Quardokus and Brun, 2002). When the DNA replication initiator DnaA is depleted, FtsZ forms constrictions at subpolar regions of the cell (Quardokus and Brun, 2002). Interestingly, FtsZ also appears to become punctate in some cells blocked for DNA replication (Quardokus and Brun, 2002), reminiscent of MipZ depletion. Further study is required to flesh out the links between DNA replication and the localization patterns of MipZ and FtsZ.

MipZ's dimerization state also influences both its own and FtsZ's localization within the cell, as indicated by a study involving MipZ mutants with aberrant ATP binding, hydrolysis, and/or dimerization (Kiekebusch *et al.*, 2012). Polar ParB recruits ADP-bound MipZ monomers to the poles. MipZ then exchanges ADP for ATP, causing MipZ to dimerize and release ParB. Dimeric MipZ begins to diffuse from the pole, but its diffusion is limited by sequence non-specific interactions with the chromosome. This dimeric form of MipZ is also able to inhibit FtsZ polymerization. MipZ eventually hydrolyzes ATP and becomes monomeric again, releasing from the chromosome and going back to the poles due to its high affinity for ParB. These dynamics allow for formation of a MipZ gradient in the cell with the poles serving as the points of highest concentration. Since a large concentration of dimeric MipZ is still close to the poles, FtsZ is forced to polymerize near midcell where the concentration of MipZ is the lowest (Kiekebusch *et al.*, 2012). More accurately, however, the Z-ring does not actually localize to the exact midpoint between the poles – rather, it tends to assemble slightly closer to the non-stalked pole. Shtylla proposes that this is due to the presence of more free ParB at the stalked pole, allowing slightly more MipZ to localize to this pole, pushing the MipZ minimum closer to the other pole (Shtylla, 2017).

In addition to chromosome segregation, cell polarity also helps MipZ regulate Z-ring placement spatially and temporally. Disrupting proper cell polarity through deletion of *tipN*, a polarity determinant, has multiple effects on MipZ activity, which in turn adversely affects Z-ring localization (Schofield *et al.*, 2010). TipN directly influences ParA localization, both spatially and temporally, impacting the timing and location of ParB, and finally MipZ localization (Schofield *et al.*, 2010). Accordingly, in *tipN* deleted cells, MipZ establishes its bipolar gradient both less robustly, with weaker MipZ maxima at each pole, and also later in the cell cycle, which causes the Z-ring to form later (Schofield *et al.*, 2010). Additionally, the MipZ gradient was flipped in TipN deleted cells, with a higher concentration of MipZ found at the non-stalked pole instead of the stalked pole, causing reversed Z-ring asymmetry (Schofield *et al.*, 2010). Since proper MipZ localization depends on the timing of ParAB-mediated DNA segregation, itself a tightly timed process, MipZ-mediated Z-ring formation is intimately linked to the cell cycle both temporally and spatially.

1.3.3 Cell cycle control of FtsZ self-interaction: A putative model

Another mode of Z-ring assembly inhibition, which is still poorly understood, entails temporal regulation of FtsZ self-interaction. Two non-essential FtsZ-binding proteins, GdhZ, an NAD+-dependent glutamate hydrolase, and KidO, an NADH binding protein, are proposed to negatively regulate FtsZ self-association in a cell cycle-dependent manner (Radhakrishnan *et al.*, 2010; Beaufay *et al.*, 2015). *In vivo*, KidO and GdhZ are present in high concentrations during G1 phase and are diffusely localized, but their protein levels decrease during S phase in a CtrA-dependent manner. Intriguingly, qualitative observations suggest that deletion of either protein may cause the Z-ring to assemble earlier than normal (Radhakrishnan *et al.*, 2010; Beaufay *et al.*, 2015). However, a more quantitative analysis would be useful in confirming this hypothesis. *In vitro*, GdhZ (which can also convert NAD+ into NADH) inhibits FtsZ polymerization in an NAD+- or a glutamate- dependent manner, while KidO inhibits FtsZ polymer bundling in an NADH-dependent manner (Radhakrishnan *et al.*, 2010; Beaufay *et al.*, 2015). Beaufay et al have proposed a model by which GdhZ and KidO regulate Z-ring formation (Beaufay *et al.*, 2015): GdhZ and KidO inhibit self-interaction of what little FtsZ is present in G1 phase, preventing Z-ring formation (Beaufay *et al.*, 2015). Upon a downshift in *gdhZ* and *kidO* transcript levels during S phase, FtsZ self-interaction is no longer inhibited, and it is now able to form the Z-ring (Beaufay *et al.*, 2015). These negative regulators are proposed to act in synergy, with GdhZ supplying the NADH required for KidO's activity (Beaufay *et al.*, 2015). Finally, GdhZ's glutamate hydrolysis activity may link FtsZ polymerization state to metabolism (Beaufay *et al.*, 2015), though the implications of this are still unclear. Though Beaufay et al present a tantalizing model to explain Z-ring assembly regulation, more data are required to fully validate it.

1.3.4 Focusing the Z-ring

Although MipZ is necessary for localizing FtsZ to the future division site, it is not sufficient for forming a coherent Z-ring. Additional factors are indeed required to help focus the Z-ring into a narrow band that can efficiently promote constriction. Key players in this process in *Caulobacter* are the non-essential, cytoplasmic, coiled-coil proteins ZapA and ZauP (**Fig. 2**), which are recruited to midcell by FtsZ shortly after FtsZ itself arrives (**Fig. 3**) (Goley *et al.*, 2011; Woldemeskel *et al.*, 2017). ZapA directly interacts with both ZauP and FtsZ, and mediates recruitment of ZauP to midcell. Similar to deletion of *zapA* in *E. coli*, deletion of *Caulobacter zapA, zauP,* or both causes the Z-ring to become more dispersed and less tightly focused along the longitudinal axis. The mechanism through which this occurs may be distinct from *E. coli*, however, based on a few divergent observations. The most recent cellular scale model in *E. coli* suggests that ZapA's ability to focus the Z-ring depends on connections to the chromosome mediated by two proteins, MatP and ZapB, which forms a ring concentric to ZapA (Buss *et al.*, 2015; Buss *et al.*, 2017). However, *Caulobacter* lacks homologs to these factors, and ZauP, which forms a ring with the same diameter of ZapA, does not bind DNA. Like ZapB in *E. coli*, ZauP midcell foci persist upon FtsZ depletion, suggesting that ZauP may form a stable scaffold, albeit independent of the chromosome. The observation that *zapB* and *zauP* homologs are mutually exclusive further indicates that there is a separate mode of Z-ring focusing. The details of this proposed ZauP-dependent process are still unknown, however. On the molecular scale, *E. coli* ZapA's ability to bundle FtsZ was initially thought to be important for its activity *in vivo*, though this has been called into question (Buss *et al.*, 2013). Therefore, the finding that *Caulobacter* ZapA does not affect FtsZ polymerization or bundling suggests an alternate mechanism may indeed be more plausible. *E. coli* ZapA has also been shown to crosslink FtsZ, which may instead contribute to its activity *in vivo* (Dajkovic *et al.*, 2010). Further testing will be required to determine if *Caulobacter* ZapA also crosslinks FtsZ.

Additional divisome proteins also help to focus the Z-ring. Genetic perturbation of the membrane anchor FzlC or the putative membrane anchor FtsEX, a complex of the proteins FtsE (a cytoplasmic ATPase) and FtsX (a transmembrane protein), has effects on Z-ring focusing (Meier *et al.*, 2016; Meier *et al.*, 2017). FzlC and FtsE each interact directly with FtsZ, as demonstrated in *Caulobacter* and *E. coli* respectively (Corbin *et al.*, 2007; Meier *et al.*, 2016). Overexpression of either *ftsEX* or *fzlC* causes Z-rings to become broader, and overexpression of *ftsE* alone results in punctate FtsZ. Deletion of *fzlC* alone does not impact FtsZ width, but deletion of *ftsE* alone or *fzlC* and *ftsE* together yields dispersed Z-rings. Interestingly, overexpression of *fzlC* in a background lacking *ftsE* largely rescues its phenotype, making Z-rings become more focused again. Finally, *ftsE*, but not *fzlC*, displays synthetic interactions with *zapA*. Proper stoichiometry between FtsZ and the assembly factors FtsE, FzlC, and potentially ZapA, therefore appear to be required for properly focused Z-rings. As will be discussed below, FzlC (and possibly FtsEX) is a membrane anchor for FtsZ, so varying the number of FtsZ polymers attached to the membrane likely has an impact on how focused the Z-ring appears to be.

1.3.5 Attachment of the Z-ring to the membrane

By PALM and cryo-ET, the *Caulobacter* Z-ring forms proximal to the membrane in stalked cells, and because FtsZ on its own does not interact strongly with the membrane, a separate protein (or proteins) is required to anchor FtsZ to the membrane. FtsA is thought to be the primary FtsZ membrane anchor in many species, but it arrives at the site of division in

Caulobacter well after initial Z-ring assembly (Goley *et al.*, 2011). *Caulobacter* therefore likely has at least one additional FtsZ membrane anchor that functions early in the cell cycle, with one candidate being FzlC. FzlC, an FtsZ binding protein that arrives early at the Z-ring (**Fig. 2** and **Fig. 3**) (Meier *et al.*, 2016), has been shown by fluorescence microscopy to localize to membranes both in *Caulobacter* when FtsZ is depleted, and when heterologously expressed in *E. coli*. Additionally, FzlC is found in the membrane fraction of whole cell lysate of *Caulobacter* cells and it directly interacts with phospholipid vesicles *in vitro*. Compellingly, FzlC was found to drive localization of FtsZ to vesicle membranes *in vitro*, specifically interacting with the C-terminus of FtsZ, a known binding site for other membrane anchors. In aggregate, these data implicate FzlC as a membrane anchor for FtsZ, likely acting before FtsA arrives (Meier *et al.*, 2016). However, while overexpression of FzlC causes division defects, it is not essential and can be deleted without causing deleterious effects on Z-ring assembly (Meier *et al.*, 2016). It is therefore possible that another early divisome protein is able to anchor the Z-ring in a redundant way.

FtsEX has been proposed to be another membrane anchor for FtsZ. FtsEX belongs to the ABC transporter protein family, with FtsE predicted to be a cytoplasmic ATPase, and FtsX thought to be a transmembrane protein (**Fig. 2**) (Arends *et al.*, 2009; Meier *et al.*, 2016). FtsE has been shown to interact with FtsZ in *E. coli* by co-immunoprecipitation, suggesting FtsEX could link FtsZ to the membrane (Corbin *et al.*, 2007). In *Caulobacter*, FtsE arrives at the division plane early (**Fig. 3**), around the same time as FzlC (Goley *et al.*, 2011). Overexpression or deletion of FtsE causes the Z-ring to become punctate, consistent with a direct interaction between FtsE and FtsZ (Meier *et al.*, 2017). In addition, FtsE genetically interacts with FzlC. Deletion of both gives a synthetic sick phenotype, whereas overexpression of *fzlC* reduces the severity of an *ftsE* deletion phenotype (Meier *et al.*, 2016). Taken together, these data present a case that FtsEX may serve as a membrane anchor, though biochemical evidence of this activity will be required to advance this hypothesis.

The last known FtsZ membrane anchor to arrive to the divisome is FtsA (**Fig. 2** and **Fig. 3**), an essential division protein in *Caulobacter* that is widely conserved across bacteria (Sackett *et al.*, 1998; Rothfield *et al.*, 1999; Pichoff and Lutkenhaus, 2005; Goley *et al.*, 2011). FtsA has been shown to anchor FtsZ to the membrane in a number of *in vitro* and *in vivo* systems (Pichoff and Lutkenhaus, 2005; Szwedziak *et al.*, 2012; Szwedziak *et al.*, 2014), an activity facilitated by its FtsZ-interacting domain (Pichoff and Lutkenhaus, 2007) and a C-terminal amphipathic helix capable of binding to the membrane (Pichoff and Lutkenhaus, 2005; Szwedziak *et al.*, 2012). An actin homolog, FtsA is an ATPase capable of both forming protofilaments and binding to membranes *in vitro*, with polymerization being required for membrane attachment (Szwedziak *et al.*, 2012; Krupka *et al.*, 2014). Cryo-ET of liposomes containing *Thermotoga maritima* FtsZ and FtsA demonstrate that, at least *in vitro*, FtsA protofilaments can form a ring-like structure sandwiched between the membrane and FtsZ protofilaments (Szwedziak *et al.*, 2014). *E. coli* FtsA has been shown to stimulate FtsZ dynamics at the membrane *in vitro* (Loose and Mitchison, 2014), indicating FtsA is not simply a passive membrane anchor. Interestingly, genetic data suggests that FtsA functions in a distinct manner compared to one of the other *Caulobacter* FtsZ membrane anchors, FzlC (Meier *et al.*, 2016). Overexpression of *fzlC* in *Caulobacter* cells causes Z-rings to become wider and cells to become slightly longer, whereas overexpression of *ftsA* induces broad Z-rings and patchy FtsZ localization, as well as severe cell filamentation (Meier *et al.*, 2016). The ability of FtsA to regulate FtsZ dynamics could account for these phenotypic differences, although it is has not been tested if FzlC also possesses this activity.

Alternatively, or in addition, FtsA is believed to be involved in signaling to the PG synthetic machinery in the divisome, whereas FzlC has genetic interactions with factors involved in PG hydrolysis, further highlighting functional differences between the two.

1.4 The Z-ring: A scaffold for the rest of the divisome

Having explored how the Z-ring is assembled, we are now ready to consider the function of the Z-ring in the context of division. Itself a well-defined and tightly focused structure, the Z-ring helps to ensure that the division site is also well-defined by spatially constraining the site of envelope remodeling. The Z-ring achieves this feat by acting as a scaffold for the divisome, precisely positioning the division machinery near midcell in the longitudinal axis.

What comprises the division machinery? The divisome is made up of over thirty proteins that are involved in remodeling the envelope during division, which we have categorized into functional groups: Z-ring formation factors (ZapA, ZauP, FzlC, FtsA), discussed in the previous section; elongation machinery (MreB, MurG, RodZ); constriction machinery (FzlA, FtsN, FtsQ, FtsI, FtsK, FtsL, FtsW, FtsB, PbpX, PbpY, DipI); envelope maintenance machinery (the Tol-Pal complex); cell separation factors (AmiC, LdpF, CtpA); Z-ring disassembly factors (KidO, GdhZ, ClpXP); polarity determining factors (TipN, TipF); and multifunctional factors (FtsEX, DipM, SdpA, SdpB) (**Fig. 2**). Note that we have categorized a handful of factors as multifunctional since they contribute to multiple processes, which will be discussed throughout the chapter.

The order and timing of midcell localization for most of these proteins has been determined, with timing of functional group localization corresponding well to the activity associated with that group (Goley *et al.*, 2011). In general, proteins within each functional group localize to the Z-ring in close temporal proximity to one another (**Fig. 3**). The Z-ring formation factors are the first to arrive to midcell, which ensure proper focusing and membrane attachment. Shortly after this, the elongation and envelope maintenance machineries both begin to localize to the future site of division. The constriction machinery assembles to the Z-ring in a more drawn out fashion, with the first factor appearing early, and the subsequent proteins arriving up until constriction starts. The factors involved in cell separation, Z-ring disassembly, and polarity determination localize to midcell last, only after constriction has initiated. All members of the divisome require FtsZ for localization and there is a non-linear hierarchy of assembly (Goley *et al.*, 2011), with numerous protein-protein and protein-envelope interactions likely important for divisome assembly.

Having introduced the concept that the Z-ring serves as a scaffold for the divisome, we are now ready to describe the next steps in division and the role that each divisome protein plays in more detail. First we will discuss divisome-associated elongation, followed by constriction. We will then examine the importance envelope maintenance in the division process. Finally, we will consider cell separation and the completion of division.

1.5 Divisome-associated elongation

Caulobacter cells begin to elongate shortly after assembling the Z-ring, and both before and during constriction, suggesting a potential link between the division machinery and elongation. In a landmark study, Aaron et al showed that *Caulobacter* elongation occurs primarily via insertion of PG at the midcell, colocalized with the Z-ring (Aaron *et al.*, 2007). Insertion of PG was found to start in relatively young stalked cells, before the initiation of constriction. Additionally, this process was found to be FtsZ-dependent since loss of FtsZ leads to PG incorporation throughout the entire length of the cell (Aaron *et al.*, 2007). Intriguingly, links have been found between FtsZ and the elongation machinery, also known as the elongasome. Soon after Z-ring assembly, at least two members of the elongasome arrive at midcell (Goley *et al.*, 2011). MreB, an actin homolog located in the cytoplasm that scaffolds the elongasome and MurG, a PG precursor synthesizing enzyme also found in the cytoplasm, localize to the future site of division in an FtsZ-dependent manner (**Fig. 3**) (Aaron *et al.*, 2007; Goley *et al.*, 2011). FtsZ is therefore thought to at least passively regulate elongation (Aaron *et al.*, 2007), though the details of this mechanism are still hazy.

Two additional elongasome proteins, MraY (a PG precursor synthesis enzyme) and RodZ (a transmembrane MreB binding protein, required for its circumferential motion in *E. coli*), have also been shown to localize to midcell either concurrent with constriction in *E. coli* (MraY) or prior to constriction in *Cauobacter* (RodZ) (**Fig. 2** and **Fig. 3**) (Alyahya *et al.*, 2009; Morgenstein *et al.*, 2015; Liu *et al.*, 2018). However, it is unclear if the rest of the elongasome localizes to midcell. On the one hand, patchy localization has been reported for numerous other elongasome proteins, including PG modifying enzymes, with localization to midcell only occurring after exposure to cell shape stressors such as osmolarity upshift or MreB inhibition (Divakaruni *et al.*, 2007; White *et al.*, 2010; Hocking *et al.*, 2012). On the other hand, MreB localization itself is either patchy or primarily midcell localized, depending on the stage of the cell cycle (Figge *et al.*, 2004; Gitai *et al.*, 2004; Aaron *et al.*, 2007; Goley *et al.*, 2011). A comprehensive study assessing elongasome localization throughout the cell cycle will be required to address these concerns.

Inversely, some proteins associated with the elongasome also play a role in division. MurG and, probably MraY, contribute to cell wall remodeling during constriction, since division also requires the synthesis of PG precursors. It has also been proposed in *E. coli* that MreB somehow “transfers” PG synthesis enzymes to FtsZ prior to constriction (Fenton and Gerdes, 2013), though this hypothesis relies heavily on two-hybrid data and has not been validated in *Caulobacter*. Additional work will be required to clarify the relationship between the *Caulobacter* elongasome and divisome.

1.6 Constriction: A PG synthesis-driven process

Constriction in *Caulobacter* is marked by the simultaneous increase in length and decrease in width at a particular spot. Like elongation, constriction is thought to be facilitated by the insertion of new PG into the cell wall at midcell. Vital to this process is the constriction machinery, made up of the constriction-specific PG synthesis enzymes and their regulators, and of course the Z-ring, which plays a crucial role in recruiting, scaffolding, and potentially activating the constriction machinery at midcell. The members of the constriction machinery localize to the Z-ring in an ordered fashion, with the first protein, FzlA, arriving around the same time that elongation starts (Goley *et al.*, 2011). Subsequently, the rest of the constriction machinery factors (FtsA, FtsN, FtsQ, FtsI, FtsK, FtsL, FtsW, FtsB) gradually assemble at the Z-ring, with the arrival of FtsB coinciding with the initiation of constriction (Goley *et al.*, 2011). In our model for constriction initiation, we propose that FtsZ activates the constriction-specific PG synthases through its dynamics, physical signals, and/or interaction partners (**Fig. 4**). A number of downstream constriction activators likely help transduce the activation signal from FtsZ to the PG synthases, potentially occupying multiple pathways.

1.6.1 Force generation through PG synthesis

One of the major questions concerning not only *Caulobacter* division, but bacterial division in general, is what *drives* constriction? That is, what generates the force needed to push or pull the cell envelope inward at the site of division? Early models implicated FtsZ as the primary driver of constriction, since FtsZ alone was able to facilitate liposome constriction *in vitro* (Osawa *et al.*, 2008; Osawa and Erickson, 2013). FtsZ-mediated constriction was proposed to work either through maximization of lateral bonds through Z-ring condensation or through FtsZ curvature-mediated bending of the IM (Lan *et al.*, 2009; Erickson *et al.*, 2010; Xiao and Goley, 2016; Erickson and Osawa, 2017; Coltharp and Xiao, 2017). The second model is supported by evidence that FtsZ protofilaments can deform membranes with directional specificity (Osawa *et al.*, 2009), with FtsZ filament curvature likely driving membrane bending in a GTP-hydrolysis independent manner (Erickson and Osawa, 2017; Osawa and Erickson, 2018). However, these FtsZ-centric models have been disfavored recently for a few major reasons. The force required to counter turgor pressure and constrict the IM at the division site is predicted to be 400 pN, whereas the Z-ring is calculated to only produce between 8-100 pN of force (Lan *et al.*, 2007; Allard and Cytrynbaum, 2009; Lan *et al.*, 2009; Paez *et al.*, 2009; Xiao and Goley, 2016; Coltharp and Xiao, 2017) . Additionally, FtsZ leaves the divisome in *E. coli* before completion of constriction and before the PG synthases leave, indicating FtsZ is not required for this later step (Söderström *et al.*, 2014; Söderström *et al.*, 2016; Xiao and Goley, 2016). Finally, alteration of FtsZ GTPase rate does not affect the constriction rate in *E. coli*, indicating that any mechanism of FtsZ-mediated force that requires GTP hydrolysis cannot be rate-limiting for constriction (Coltharp *et al.*, 2016; Xiao and Goley, 2016; Yang *et al.*, 2017). Instead, mutation of FtsI, a PG synthase highlighted below, was found to slow the constriction rate in *E. coli*, suggesting that midcell PG synthesis is the primary driver of constriction in that organism (Coltharp *et al.*, 2016). This hypothesis is supported by computational work suggesting that the chemical energy released upon PG bond formation generates sufficient force for constriction (Lan *et al.*, 2007; Banerjee *et al.*, 2016; Xiao and Goley, 2016; Coltharp and Xiao, 2017). A PG-centric force generation model may hold not across all species, however. Alteration of FtsZ GTPase rate in *B. subtilis does* influence the constriction rate and inhibition of FtsZ in *S. aureus* blocks constriction initiation (but not its completion), indicating that GTP hydrolysis can be rate-limiting during constriction in other organisms (Bisson-Filho *et al.*, 2017; Monteiro *et al.*, 2018). Regardless of these differences, it is clear that both the PG synthesis machinery and the Z-ring play central roles in constriction in *Caulobacter*. The following sections will therefore explore the contributions of *Caulobacter*'s PG synthases and their regulators, including FtsZ, to constriction.

1.6.2 Constriction-specific PG synthesis machinery

During constriction, the cell wall is remodeled at the division plane through the addition of new PG (Aaron *et al.*, 2007; Divakaruni *et al.*, 2007). As described above, PG consists of glycan strands attached to each other by peptide crosslinks. Addition to this network requires that these glycan strands are extended or polymerized *de novo* through glycosyltransferase (GTase) enzymatic activity and that new peptide crosslinks are made via transpeptidase (TPase) activity. The enzymes responsible for this activity, the constriction specific GTases and TPases, together will be referred to as the PG synthetic machinery in this text from this point on. This machinery is thought to be crucial for facilitating efficient constriction, though the activities of its individual components and their collective mechanism of action is still poorly defined in *Caulobacter* and other organisms.

Perhaps the best understood constriction-specific PG synthetic enzyme in *Caulobacter* is the TPase FtsI, also known as PBP3. FtsI plays an essential role in constriction, with loss of functional FtsI in *Caulobacter* causing cell filamentation (Costa *et al.*, 2008). FtsI is similarly essential for constriction in *E. coli* (Goehring and Beckwith, 2005; Typas *et al.*, 2012), with partial inhibition of function slowing the rate of constriction (Coltharp *et al.*, 2016) and full knockdown completely blocking division (Spratt, 1977b; Pogliano *et al.*, 1997). A single pass transmembrane protein, FtsI contains a small cytoplasmic motif and periplasmic transpeptidase domain capable of catalyzing the PG transpeptidation reaction (Wissel and Weiss, 2004; Sauvage *et al.*, 2014:3). FtsI localizes to the IM and, along with the rest of the constriction machinery, is recruited to midcell in an FtsZ-dependent manner before the initiation of constriction (**Fig. 2** and **Fig. 3**) (Costa *et al.*, 2008; Goley *et al.*, 2011). FtsI localization at the *Caulobacter* midcell was found to be highly dynamic by FRAP (Costa *et al.*, 2008). Higher resolution imaging in *E. coli* and *B. subtilis* showed that their division-specific TPases (FtsI in *E. coli*; Pbp2B in *B. subtilis*) move around the circumference of the division site in a manner dependent on FtsZ treadmilling speed (Bisson-Filho *et al.*, 2017; Yang *et al.*, 2017), insinuating that *Caulobacter* FtsI may demonstrate similar dynamics. Conversely, in *Streptoccocus pneumoniae*, FtsZ treadmilling does not influence the rate of directional movement of the FtsI homolog PBP2X (Perez *et al.*, 2019). Further work on *Caulobacter* FtsI will be required to determine whether or not its dynamics depend on FtsZ treadmilling.

Another essential member of the constriction machinery in *Caulobacter* is FtsW, which has been shown to bind to FtsI in *E. coli* (Karimova *et al.*, 2005; Fraipont *et al.*, 2011). FtsW, whose depletion leads to filamentation and loss of constriction initiation (Goley *et al.*, 2011), is a multipass transmembrane protein that is part of the SEDS (shape, elongation, division, and sportulation) family (Meeske *et al.*, 2016). Located at the IM (**Fig. 2**) (Fraipont *et al.*, 2011), FtsW arrives at midcell just before the start of constriction (**Fig. 3**) (Goley *et al.*, 2011). FtsW was recently shown to be a GTase in a number of species (*Caulobacter* was not tested, however), whose enzymatic activity is regulated by its cognate PBP, FtsI (Taguchi *et al.*, 2019). It is worth mentioning that, based on *in vitro* work, *E. coli* FtsW was previously hypothesized to act as a flippase for the PG precursor lipid II, transferring lipid II from the cytoplasmic face of the inner membrane to the periplasmic side (Mohammadi *et al.*, 2011; Mohammadi *et al.*, 2014). However, *in vivo* data has failed to demonstrate FtsW's flippase activity in *E. coli* (Sham *et al.*, 2014). As an aside, it will also be important to identify the lipid II flippase in *Caulobacter*, as this is likely a key player in all processes requiring PG synthesis, including division. The leading candidate is MurJ, which was shown to be required for flipping lipid II in *E. coli* (Sham *et al.*, 2014) and has a homolog in *Caulobacter*.

Caulobacter has additional putative PG synthases that may contribute to constriction. Pbp1A, PbpC, PbpX, PbpY, and PbpZ are bifunctional penicillin binding proteins (PBPs) located at the IM, each containing a transmembrane domain, a TPase domain, and a GTase domain (Yakhnina and Gitai, 2013; Strobel *et al.*, 2014). Each of these PBPs is nonessential and, with the exception of PbpZ, each individually is sufficient for supporting growth and/or division (Yakhnina and Gitai, 2013; Strobel *et al.*, 2014). However, deletion of *pbpX* leads to a mild elongation phenotype and deletion of all five together is lethal (Yakhnina and Gitai, 2013; Strobel *et al.*, 2014). PbpX and PbpY localize along the length of the cell at the IM prior to constriction, with PbpX relocating to midcell at or just prior to constriction initiation and PbpY arriving shortly after (**Fig. 2** and **Fig. 3**) (Yakhnina and Gitai, 2013; Strobel *et al.*, 2014). Additionally, both PbpX and PbpY have been found to interact with the divisome proteins FtsN, FtsL, and DipM by bacterial two-hybrid analysis, strengthening the claim that these PBPs are involved in division (Strobel *et al.*, 2014). Intriguingly, PbpC and Pbp1A do not localize to midcell (PbpZ localization could not be determined) (Yakhnina and Gitai, 2013), so enrichment of a bifunctional PBP at midcell is not absolutely required for division. Altogether, the sequence homology, localization, and interaction data strongly suggest that PbpX and PbpY play an auxiliary role in division, possibly as a secondary function to general PG maintenance. The nature of the roles that PbpZ, PbpC, and Pbp1A play in division is still unknown.

1.6.3 FtsZ-mediated PG synthase localization and activation

So what role does FtsZ play in constriction, then? FtsZ of course is necessary for localizing the constriction machinery to the site of division, and it now seems that treadmilling is important for directing movement of PG synthases at the division site. As described in previous sections, FtsZ in *E. coli* and *B. subtilis* has been shown to treadmill around the circumference of the cell, with its GTPase rate dictating treadmilling speed (Bisson-Filho *et al.*, 2017; Yang *et al.*, 2017). FtsI in *E. coli* (or Pbp2B in *B. subtilis*), but not *S. pneumoniae* (PBP2X), moves around the cell at a speed that is dependent on FtsZ treadmilling (Bisson-Filho *et al.*, 2017; Yang *et al.*, 2017; Perez *et al.*, 2019). In *B. subtilis*, but not *E. coli*, treadmilling speed also correlates with the rate of PG synthesis (Bisson-Filho *et al.*, 2017; Yang *et al.*, 2017). Interestingly, in *S. aureus*, it was recently shown that FtsZ treadmilling is required for an early phase of constriction, but is dispensable later on (Monteiro *et al.*, 2018). *S. aureus* FtsZ may therefore activate PG synthases early in division, but is not required for their continued regulation, highlighting mechanistic similarities to both *E. coli* and *B. subtilis* FtsZ (Monteiro *et al.*, 2018). Altogether, these data suggest *Caulobacter* FtsZ probably treadmills too and is therefore important for spatial regulation of PG insertion. However, they do not provide any coherent insight as to whether FtsZ regulates the rate of PG synthesis, which may well vary from species to species.

Based on the FtsZ treadmilling studies, to what extent FtsZ regulates PG remodeling is still in question, with evidence from *E. coli* pointing toward a passive role for FtsZ and evidence from *B. subtilis* indicating a more active role for FtsZ. Studies from our lab have helped to shed light on this point, suggesting that FtsZ may more actively regulate PG synthase activity in *Caulobacter*. FtsZ's CTL, the flexible linker between the GTPase domain and C-terminal peptide, has been shown to be essential for proper PG synthesis in *Caulobacter*, a function that is conserved across α-proteobacteria (Sundararajan *et al.*, 2015; Howell *et al.*, 2019). Cells producing an FtsZ variant lacking its CTL (FtsZ-ΔCTL) form bulges instead of constrictions at midcell, similar to the cell shape changes induced by β-lactam treatment (Sundararajan *et al.*, 2015). Muropeptide analysis revealed that PG composition in these cells is altered, indicating a defect in the activity of cell wall remodeling enzyme(s) downstream of FtsZ (Sundararajan *et al.*, 2015). Because the rest of the divisome appears to still form properly in the presence of FtsZ-ΔCTL, it was proposed that FtsZ regulates PG synthesis in a CTL-dependent manner, possibly by facilitating mechanical signaling to the PG synthesis machinery (Sundararajan *et al.*, 2015).

Another pathway by which *Caulobacter* FtsZ regulates activation of PG synthase is through the FtsZ-bending protein, FzlA. An early localizing FtsZ binding protein (**Fig. 3**), FzlA is cytoplasmic (**Fig. 2**) and has been shown to curve FtsZ protofilaments *in vitro* (Goley *et al.*, 2010b). Mutations in FzlA that resulted in weakened interaction with FtsZ also caused a decrease in constriction rate relative to elongation rate, indicating that FzlA, through its interaction with FtsZ, regulates the rate of constriction (Lariviere *et al.*, 2018).

More recently, we demonstrated that FzlA is specifically required for regulating the activation of FtsWI in both *Caulobacter* and *A. tumefaciens* (Lariviere *et al.*, 2019). Loss of FzlA can be suppressed by hyperactive forms of FtsWI, suggesting it lies upstream of these enzymes in a PG synthesis activation pathway. Even in the presence of hyperactive PG synthases, FzlA is still required for efficient constriction. Interestingly, in the presence of hyperactive PG synthases, FzlA appears to be required for proper morphogenesis and resistance to cell wall metabolic stress: cells lacking *fzlA* but possessing hyperactive PG synthases are S-shaped and are more sensitive to β-lactam antibiotics. Overall, these findings suggest FzlA is required for regulating the geometry and rate of PG insertion through its interaction with FtsZ (Lariviere *et al.*, 2019). Further, these results both confirm the paradigm hypothesized for elongation-specific PG synthases by Rohs et al (Rohs *et al.*, 2018) that SEDS-PBP enzymes require activation and, further, expand it to a division context (Lariviere *et al.*, 2019).

Based on the above data, we propose two models by which FtsZ could regulate PG remodeling during division, whereby the Z-ring acts as either a “dynamic scaffold” or a “dynamic activator”. In the dynamic scaffold model, which is in line with FtsZ function in *E. coli*, FtsZ treadmilling is required only for distributing the PG synthases at the site of division, not for affecting their activity. According to the dynamic activator model, which more accurately describes FtsZ function in *B. subtilis*, FtsZ treadmilling is needed to both distribute and activate the PG synthases at midcell. We therefore propose that *Caulobacter* FtsZ is also a dynamic activator (**Fig. 4**). We can envision several possible mechanisms through which *Caulobacter* FtsZ might activate PG synthesis according to a dynamic activator model, which need not be mutually exclusive: mechanical signaling to PG synthases requiring force transduction through the CTL; FzlA-dependent signaling to PG synthases; and treadmilling-dependent distribution and/or activation of PG synthases (**Fig. 4**). FtsZ does not directly bind to FtsW or FtsI, therefore each of these proposed mechanisms likely requires that signal transduction from FtsZ to the PG synthases goes through one or more intermediary factors (**Fig. 4**). Substantial future work will be required to determine the precise mechanisms and proteins through which FtsZ activates PG synthesis in *Caulobacter*.

1.6.4 Stress response-mediated constriction regulation

Downstream of FtsZ, additional factors are likely required to regulate the PG synthetic machinery activity, ensuring that constriction occurs at the correct time. However, before discussing this regulation under normal conditions, we will consider how the PG synthases can be deactivated (leading to a constriction block) under stress, as this will provide us with valuable insight into the activation process. The best studied stress that leads to a late stage constriction block in *Caulobacter* is DNA damage. Induction of DNA damage results in the upregulation of numerous genes involved in DNA repair, as well as two genes responsible for inhibiting division in *Caulobacter, sidA* and *didA*. *sidA* is a member of the canonical DNA damage response SOS regulon, with its expression driven by cleavage of the SOS repressor LexA (Modell *et al.*, 2011). *didA*, on the other hand, is not part of the SOS regulon, with its expression driven instead by a poorly understood transcriptional activator, DriD (Modell *et al.*, 2014). Normally, when cells sense DNA damage, they halt division to allow time for DNA repair. However, when *sidA* or *didA* are deleted, division occurs more quickly and leads to more growth defects in the presence of DNA damage (Modell *et al.*, 2011; Modell *et al.*, 2014). Deletion of both genes together greatly enhances this effect, indicating SidA and DidA are both needed for proper division inhibition in response to DNA damage (Modell *et al.*, 2011; Modell *et al.*, 2014). Overproduction of either protein alone in the absence of DNA damage results in division inhibition, indicating each protein is sufficient to block division (Modell *et al.*, 2011; Modell *et al.*, 2014). SidA and DidA each localize to midcell, with SidA binding FtsW and both binding FtsN (Modell *et al.*, 2011; Modell *et al.*, 2014). FtsN is an essential transmembrane divisome protein (**Fig. 2** and **Fig. 3**), which binds to PG via a periplasmic SPOR domain (Möll and Thanbichler, 2009). FtsN likely binds to FtsW and FtsI, putatively forming an FtsWIN complex (Karimova *et al.*, 2005; Alexeeva *et al.*, 2010; Fraipont *et al.*, 2011; Modell *et al.*, 2011; Modell *et al.*, 2014). Because neither SidA nor DidA recruitment to midcell results in delocalization of any of the divisome proteins tested, including FtsW, FtsI, or FtsN, Modell et al proposed that they inactivate the FtsWIN complex (Modell *et al.*, 2014). In support of this hypothesis, mutations in FtsW and FtsI which have been shown to increase constriction rate under WT conditions (Lambert *et al.*, 2018), as well as a mutation in FtsN proposed to hyperactivate constriction under WT conditions, suppress the ability of SidA or DidA to block division (Modell *et al.*, 2014). These data suggest FtsWIN may occupy either an inactive state or an active state (Modell *et al.*, 2014), though it is still unclear precisely how SidA and DidA alter the transition from one to the other.

1.6.5 Downstream PG synthase activation pathways

Having discussed regulation of the PG synthesis machinery in response to stress, we now have a better understanding of how PG synthase regulation downstream to FtsZ may occur under normal conditions. FtsN is thought to activate the PG synthases FtsW and FtsI, since mutation of

FtsN can suppress a constriction block caused by SidA and DidA overproduction, thus allowing FtsW and FtsI to function (Modell *et al.*, 2014). Because FtsN forms a complex with FtsW and FtsI, this activation is likely direct (Modell *et al.*, 2014). However, data from *E. coli* suggests FtsN may also activate FtsW and FtsI via an indirect route as well. FtsN is proposed signal to the PG synthases through the FtsQLB complex, comprising the IM transmembrane proteins FtsQ, FtsL, and FtsB (**Fig. 2** and **Fig. 3**) (Goley *et al.*, 2011; Liu *et al.*, 2015; Tsang and Bernhardt, 2015; Glas *et al.*, 2015). This may occur through direct interactions with FtsQLB in the periplasm and/or through FtsA in the cytoplasm. This latter assertion not only suggests that FtsA is more than a passive membrane anchor for FtsZ, but also implicates a parallel, overlapping pathway in constriction initiation (Liu *et al.*, 2015; Tsang and Bernhardt, 2015). Thus, by analogy to *E. coli*, there are potentially a number of ways in which FtsN activates FtsWI in *Caulobacter*, all of which require validation before we can propose a fully fleshed out model. Further, the interaction between FtsQ and FtsB appears to be essential in *E. coli* (Kureisaite-Ciziene *et al.*, 2018), though it is unclear whether this interaction contributes to activation by FtsN, FtsA, or both.

In addition to the above factors, several other proteins have been implicated in constriction activation in *Caulobacter.* FtsK is a DNA translocase, with transmembrane and cytoplasmic portions (**Fig. 2**), that localizes to midcell just prior to constriction (**Fig. 3**) and is essential for proper chromosome segregation (Wang *et al.*, 2006; Grainge, 2010; Goley *et al.*, 2011; Wolfe *et al.*, 2014). In *E. coli*, FtsK binds members of the FtsWI and FtsQLB complexes, and a temperature sensitive mutant allows for partial suppression of deletion of FtsQ, FtsB, FtsN, and FtsA (Geissler and Margolin, 2005; Grainge, 2010). FtsK has therefore been proposed to play a regulatory function in the divisome, possibly licensing constriction initiation after DNA segregation has occurred, though no mechanism has been described (Grainge, 2010). FzlA is another essential activator of constriction in *Caulobacter* as described earlier. Yet another essential protein required for division in *Caulobacter*, DipI, was recently discovered. Believed to reside in the periplasm (**Fig. 2**), DipI localizes to midcell just prior to constriction initiation (**Fig. 3**), and is thought to bind FtsQLB (Osorio *et al.*, 2017). Osorio et al therefore propose that DipI helps FtsQLB to activate the PG synthesis machinery, though the details of this mechanism are unresolved (Osorio *et al.*, 2017).

As a note, we have characterized the above pathways as downstream of FtsZ in our dynamic activator model, in which they relay activating signals from FtsZ to PG synthases (**Fig. 4**). However, at this time it is unclear how biophysical signals from FtsZ are relayed to FtsQLB, FtsN, FtsK, and/or DipI, or if any of these pathways are parallel to FtsZ activation signals instead of downstream. Future work will focus on characterizing how these constriction activators interact genetically with one another and how they transduce an activation signal from FtsZ to PG synthases.

1.7 Envelope maintenance

Addition of new PG to the cell wall is not sufficient for efficient division to occur in *Caulobacter*. The integrity of the envelope needs to be maintained during division in order to ensure that the entire *Caulobacter* envelope invaginates in a concerted manner and that cells do not lyse in the process of division. The IM and OM, separated by a distance of 31.5 nm in *Caulobacter* (Goley *et al.*, 2010a), must be physically linked in order to maintain envelop integrity and to ensure equal rates of constriction of both membranes. The Tol-Pal complex is a multi-protein system that spans the entire length of the envelope and serves precisely such a function, with TolA, TolQ, and TolR located at the inner membrane, TolB at the periplasm, and Pal at the outer membrane (**Fig. 2**) (Gerding *et al.*, 2007; Yeh *et al.*, 2010). Given the location of each protein within the envelope, TolA is thought to bind Pal in the periplasm, physically tethering the IM to the OM. Accordingly, by cryo-EM, the OM to PG distance increases in cells depleted of Pal and the PG to IM distance increases in cells depleted of TolA (Yeh *et al.*, 2010), indicating loss of a functional Tol-Pal system weakens the IM to OM connection. Depletion of TolA or Pal leads to membrane blebbing throughout the cell, including at the division plane, with loss of TolB causing blebbing at the division plane as well (Yeh *et al.*, 2010). Because blebbing results from loss of envelope integrity and impaired IM-PG-OM attachment, its occurrence at the site of division prevents efficient and concerted constriction of the envelope. However, while this envelope maintenance function is important for constriction, it is unlikely to be specific to it. TolQ, followed by TolA, localizes to midcell well before constriction is initiated, around the time that the elongation machinery assembles (**Fig. 3**) (Yeh *et al.*, 2010; Goley *et al.*, 2011); the rest of the Tol-Pal machinery is presumed to follow suit. This early assembly, in conjunction with the presence of cell-wide shape defects in Tol-Pal depletion strains, suggests that the Tol-Pal system is likely active during elongation as well.

Another envelope maintenance protein well characterized in *Caulobacter* is the LytM and LysM domain-containing protein, DipM. Located in the periplasm (**Fig. 2**), DipM is proposed to be involved in PG hydrolysis, causing cell lysis when it is overexpressed (Goley *et al.*, 2010a; Möll *et al.*, 2010; Poggio *et al.*, 2010). Like the Tol-Pal proteins, deletion of *dipM* causes membrane blebbing at the site of division and throughout the rest of the cell (Goley *et al.*, 2010a; Möll *et al.*, 2010). And similar to TolQ, DipM localizes to midcell early, around the time that the elongation machinery arrives (**Fig. 3**) (Goley *et al.*, 2010a; Möll *et al.*, 2010; Poggio *et al.*, 2010;

Goley *et al.*, 2011). Intriguingly, cells depleted of DipM were found to have thicker PG throughout the entire length of the cell, indicating that DipM is important for regulating PG width (Goley *et al.*, 2010a). Further, it has been hypothesized that proper PG width is required to maintain contact between TolA and Pal in the periplasm, with thicker PG pushing TolA and Pal out of reach of each other (Goley *et al.*, 2010a). This results in loss of IM-OM contact and would explain the OM blebbing present in Δ*dipM* cells.

DipM is likely not a PG hydrolase itself, however. While zymogram analysis shows that DipM can bind PG, this assay cannot differentiate PG binding from hydrolysis (Uehara *et al.*, 2010; Möll *et al.*, 2010). By RBB-labeled sacculus dye release assay, a more reliable method for measuring PG hydrolysis, DipM does not show hydrolytic activity on its own (Meier *et al.*, 2017). Instead, DipM's crucial function is likely to recruit and/or activate other PG hydrolases in order to drive PG breakdown (Meier *et al.*, 2017; Zielińska *et al.*, 2017). SdpA and SdpB are two such putative lytic transglycoslyases, which reside in the periplasm and localize to midcell early in the division process in a FtsN- and DipM-dependent manner (**Fig. 2** and **Fig. 3**) (Zielińska *et al.*, 2017). Deletion of *sdpA* and *sdpB* causes membrane blebbing, highlighting their importance in envelope maintenance (Zielińska *et al.*, 2017). Further deletion of *dipM* in a background lacking *sdpA* and *sdpB* results in a synthetic sick/lethal phenotype, indicating DipM may have other downstream targets (Zielińska *et al.*, 2017). What lies upstream of DipM? Interestingly, FtsN has been shown to interact with DipM by bacterial two hybrid analysis, and is also required for recruitment of DipM, SpdA, and SdpB to midcell (Möll *et al.*, 2010; Zielińska *et al.*, 2017). Although it is unclear precisely how the late arriving FtsN recruits the early arriving DipM, the localization dependencies and interaction data indicate a potential link between the constriction and envelope maintenance machineries, suggesting that FtsN may help coordinate their activities

(Möll *et al.*, 2010). Finally, while DipM, SdpA, and SdpB are all involved in envelope maintenance during constriction, like Tol-Pal, they are likely also important during elongation due to their early midcell localization and cell-wide envelope defects.

1.8 Cell separation, polar organization, and the final events of division

Following the initiation and continuation of constriction, the final stage of division is marked by a few major events. During cell separation, the IMs fuse, compartmentalizing the cytoplasm into two separate daughters; PG hydrolases cleave PG connecting the daughter cells in a process we will refer to as terminal PG hydrolysis; and finally, the OMs fuse. Prior to or concurrent with these events, polarity factors are recruited to the constriction site to mark the creation of a new pole. Towards the end of division, MreB disperses and the Z-ring begins to be dismantled. Finally, the completion of division results in two new daughter cells, with two new poles, shaped by the constriction process, in place of the division plane.

1.8.1 Cell separation

A number of factors have been implicated in cell separation that function in at least three pathways: 1. The FtsEX-LdpF pathway; 2. The AmiC pathway; 3. The DipM-SdpAB pathway (Meier *et al.*, 2017) (**Fig. 5A**). FtsEX, which we introduced as a putative FtsZ membrane anchor, has also been implicated in terminal PG hydrolysis (Meier *et al.*, 2017). LdpF is a LytM-domain containing protein that is predicted to be periplasmic, and like DipM, LdpF is thought to lack the endopeptidase activity typically associated with LytM proteins due to the absence of key active site residues (Meier *et al.*, 2017; Zielińska *et al.*, 2017). [Note that while LdpF is thought to be active at midcell, it localizes diffusely throughout the cell, so it is not included in **Fig. 2** (Meier *et* *al.*, 2017).] AmiC is an N-acetylmuramoyl-L-alanine amidase, responsible for cleaving the bond between MurNac and the pentapetide stem in PG (Meier *et al.*, 2017; Zielińska *et al.*, 2017; Dubey and Priyadarshini, 2017). AmiC is predicted to reside in the periplasm and localizes to midcell shortly after constriction starts (**Fig. 2** and **Fig. 3**) (Meier *et al.*, 2017; Zielińska *et al.*, 2017). Finally, DipM, as previously mentioned, is another early recruit involved in envelope maintenance, that is a periplasmic PG binding protein (Goley *et al.*, 2010a; Möll *et al.*, 2010; Poggio *et al.*, 2010). The soluble lytic transglycosylases (SLTs) SdpA and SdpB, which have putative lytic transglycosylase activity, are dependent on DipM for localization for midcell (Zielińska *et al.*, 2017).

Genetic perturbation of the cell separation factors has informed functional grouping according to phenotype (**Fig. 5B**). Loss of *ftsE*, *amiC*, or *ldpF* alone or together results in a similar chaining phenotype with varying severity (Meier *et al.*, 2017; Zielińska *et al.*, 2017). Specifically, cells lacking one or more of these factors constrict to a very late point, then extend thin connections between daughter cells that remain unresolved. In an *ftsE amiC* double mutant, unfused inner membrane connections were observed in these thin cell-cell connections, implicating these genes in inner membrane fusion (**Fig. 5B**). Deletion of *dipM*, *sdpA*, or *sdpB*, on the other hand, yields short, blunt, septum-like connections, in which the OM has not constricted fully, but the IMs have fused (Goley *et al.*, 2010a; Möll *et al.*, 2010; Meier *et al.*, 2017; Zielińska *et al.*, 2017). Deletions of *ftsE* or *ldpF* are each synthetic sick or synthetic lethal with loss of *amiC* or *dipM*; depletion of AmiC is additionally synthetic lethal with Δ*dipM* (Meier *et al.*, 2017; Zielińska *et al.*, 2017). Loss of both *ftsE* and *ldpF* results in a mild synthetic sick phenotype (Meier *et al.*, 2017). In light of these phenotypic and genetic interaction data, we can describe a preliminary model of the three cell separation pathways (**Fig. 5A**). In the FtsEX-LdpF pathway, FtsEX may transduce a signal from FtsZ to LdpF, which then activates an unknown PG hydrolase (Meier *et al.*, 2017). FtsX and LdpF interact by bacterial two-hybrid analysis, indicating a series of direct protein-protein interactions from FtsZ to LdpF (Meier *et al.*, 2017). In the AmiC pathway, DipM weakly activates the PG hydrolase AmiC, supported by *in vitro* evidence that AmiC cleaves PG in the presence of DipM (but not LdpF) (Meier *et al.*, 2017). Interestingly, LdpF is required for AmiC localization to midcell (Zielińska *et al.*, 2017), suggesting the activity of the AmiC pathway may be partially dependent on the FtsEX-LdpF pathway. As for the DipM-SdpAB pathway, DipM likely activates the putative hydrolases SdpA and SdpB (Zielińska *et al.*, 2017). We would like to note here that the membrane anchor FzlC also interacts genetically with a number of cell separation factors (Meier *et al.*, 2016). Loss of *dipM*, *ftsE*, or *amiC* in a *fzlC* deletion background yields synthetic sick phenotypes (Meier *et al.*, 2016), indicating that FzlC may be involved in cell separation, possibly helping to integrate the three pathways described above.

In addition to the above factors, an additional protein, CtpA, is implicated in cell separation in *Caulobacter*. Essential in *Caulobacter*, CtpA is a putative tyrosine phosphatase that resides on or near the IM (**Fig. 2**) and localizes to midcell before constriction starts (**Fig. 3**) (Shapland *et al.*, 2011). Although CtpA does not have detectable activity *in vitro*, it has homology to other tyrosine phosphatases, and mutation of its predicted catalytic site leads to growth inhibition (Shapland *et al.*, 2011). Depletion of CtpA not only causes cell chaining and inefficient cell separation, but also results in OM blebbing throughout the cell body (Shapland *et al.*, 2011). CtpA is therefore proposed to regulate a factor/factors involved in OM maintenance, cell separation, or both (Shapland *et al.*, 2011). Further work is required to identify CtpA's specific targets.

1.8.2 Recruitment of polarity determining factors

The last proteins recruited to the divisome are the polarity determining factors, TipN and TipF (Huitema *et al.*, 2006; Lam *et al.*, 2006; Goley *et al.*, 2011). Predicted to be transmembrane proteins at the IM (**Fig. 2**), TipN and TipF are responsible for marking the new cell pole that will be formed after division, a function necessary for properly localized flagellar development, chromosome segregation, and daughter cell length determination (Huitema *et al.*, 2006; Lam *et al.*, 2006; Ptacin *et al.*, 2010). TipN arrives at midcell in an FtsZ-dependent fashion after constriction is well underway, and is itself necessary for recruitment of TipF to midcell (**Fig. 3**) (Huitema *et al.*, 2006; Goley *et al.*, 2011). TipN recruitment to midcell also depends on the Tol-Pal system, with which it was shown to interact by co-immunoprecipitation (Yeh *et al.*, 2010).

1.8.3 Z-ring disassembly and MreB dispersal

Upon completion of division, the former constriction site becomes the new poles, FtsZ levels decrease in both daughter cells (Williams *et al.*, 2014), and the Z-ring is disassembled. In the new swarmer cell, a small amount of FtsZ remains at the new pole, whereas in the new stalked cell, FtsZ immediately leaves the new pole for the new midcell (Goley *et al.*, 2011; Williams *et al.*, 2014). Several mechanisms are proposed to facilitate these changes. The cytoplasmic proteases ClpXP and ClpAP, which were previously shown to limit FtsZ levels in G1 phase through degradation, are hypothesized to also be involved in Z-ring disassembly. Although ClpA remains diffuse throughout the entire *Caulobacter* cell cycle, ClpX localizes to midcell just before completion of division (**Fig. 2** and **Fig. 3**) (Williams *et al.*, 2014). ClpXP may therefore assist in Z-ring disassembly by reducing FtsZ concentration at the old constriction site/new poles to a point below its critical concentration and thereby favoring depolymerization. GdhZ and KidO, cytoplasmic inhibitors of FtsZ self-interaction in G1 phase, may also contribute to Z-ring disassembly. Expression of GdhZ and KidO is downregulated during S phase, but increases again starting in pre-divisional cells (Radhakrishnan *et al.*, 2010; Beaufay *et al.*, 2015). KidO subsequently localizes to midcell shortly after the initiation of constriction, whereas GdhZ appears to arrive some time before constriction starts (**Fig. 2** and **Fig. 3**) (Radhakrishnan *et al.*, 2010; Goley *et al.*, 2011; Beaufay *et al.*, 2015). Around the time that constriction finishes, KidO and GdhZ are thought to help disassemble the Z-ring by blocking FtsZ self-interaction (Radhakrishnan *et al.*, 2010), though it is unclear how they delay their activity until completion of division. Finally, the other negative regulator of Z-ring assembly, MipZ, likely plays a role in disassembly of FtsZ foci at newborn cell poles. MipZ localizes to the new pole in stalked cells as soon as chromosome segregation has occurred (Thanbichler and Shapiro, 2006; Goley *et al.*, 2011), suggesting it helps to quickly displace FtsZ from the last division site. Altogether, Z-ring disassembly from the old division site appears to be due to a combination of decreased FtsZ levels and localized inhibition of self-interaction.

It is also worth mentioning that MreB disperses from the division plane toward the end of division, after constriction has initiated and before the cell has completed separation (**Fig. 3**) (Goley *et al.*, 2011). Precisely why or how MreB leaves midcell at this time is not currently known, though we can speculate that if MreB contributes to elongation earlier during division, its departure may allow for an increased focus of PG synthesis on constriction.

1.8.4 Cell pole shape determination

Following cell separation, a single *Caulobacter* cell splits into two, and the constriction site becomes two new poles. Because the shape of the poles can be influenced by numerous factors during constriction, analysis of its shape is sometimes useful for assessing the efficiency of different processes during division. Cell pole shape can be characterized according to two metrics: “pointiness”, a measure of how tapered or blunt the pole looks, and envelope topology, which indicates if the OM, PG, and IM are still properly attached. As pole pointiness is dictated by the events of division, it is logically determined by the ratio of the elongation rate to the constriction rate, such that cells elongating faster relative to constriction will have pointier poles. This has been shown to be the case in *E. coli*, where a mutation in FtsI causes cells to start to develop pointy poles during division (Taschner *et al.*, 1988; Costa *et al.*, 2008). In *Caulobacter*, however, it has previously been shown that poles become pointier well after division has finished (Aaron *et al.*, 2007), so it is less clear to what extent division also plays a role in pole shape determination in this species. Consideration of division protein mutants that alter cell pole pointiness has helped to shed some light on this matter. Mutation of FzlA has been shown to yield pointy poles, likely because it slows the rate of constriction relative to elongation (Lariviere *et al.*, 2018). Overexpression of FzlC also leads to pointy poles, though the reason for this is still unclear (Meier *et al.*, 2016). Finally, deletion of DipM leads to blunter poles, though again it is not clear if DipM deletion impacts constriction and/or elongation rate (Möll *et al.*, 2010). A properly functioning divisome is therefore required for WT pole pointiness, though studies with finer temporal resolution will be required to determine if DipM and FzlC influence pole pointiness during or following division.

The other metric for pole shape, envelope topology, is determined by members of the envelope maintenance machinery described in previous sections, including DipM and the Tol-Pal system. Loss of envelope integrity due to DipM or Tol-Pal deletion/depletion leads to OM blebbing during constriction, which is often still present at the new poles following division, either in the form of a small bulge or a larger bleb (Goley *et al.*, 2010a; Möll *et al.*, 2010; Yeh *et al.*, 2010). All in all, the determination of cell pole shape is highly sensitive to the interplay amongst multiple division processes.

1.9 Conclusions and Outlook

In this chapter we have outlined what is currently known about division in *Caulobacter*. The Z-ring is a central player in division, helping to coordinate temporally overlapping processes. Multiple assembly factors regulate Z-ring formation in both time and space, defining the division plane at midcell after chromosome replication has begun. The Z-ring subsequently recruits a host of divisome proteins, the first of which contribute to cellular elongation from the midcell. Upon arrival of the constriction machinery, FtsZ is hypothesized to activate PG synthesis through one or multiple putative mechanisms, including dynamics-, mechanical-, or protein interaction-based signal transduction, involving up to a dozen potential additional regulators. Since both elongation and constriction involve cell wall remodeling, maintenance of envelope integrity is crucial for effective division. As a cell nears the end of division, PG hydrolysis drives cell separation, the Z-ring begins to disassemble, and the cell finally splits into two daughter cells.

Though numerous studies in recent years have greatly informed our understanding of division in *Caulobacter*, we would like to highlight some of the remaining fundamental unanswered questions. To what extent do FtsZ and PG remodeling contribute to the forces required for constriction to occur? Direct evidence that PG remodeling generates a constrictive force is still lacking. What is the nature of FtsZ's role in activating PG synthesis in *Caulobacter*? How is this activation mechanistically facilitated and to what degree, if at all, do dynamics, force transduction, and downstream protein signaling each play a role in PG synthase regulation? How do the constriction machinery activators (FtsN, FtsQ, FtsL, etc…) interact with one another and effect constriction? Is the PG remodeling that facilitates elongation during division distinct from or related to the PG remodeling that drives constriction? How are the activities of constriction-specific PG synthases and PG hydrolases regulated with respect to one another? How are the activities of the factors involved in cell separation coordinated to drive OM fusion, terminal PG hydrolysis, and IM fusion? Finally, how is division influenced by metabolic processes?

In order to address these questions and gain a better understanding of division in *Caulobacter*, the use of emerging tools will be invaluable. Advanced imaging techniques such as PALM and cryo-ET have proved useful for gaining a higher resolution view of microscopic processes. Computational analyses of single-cell experiments have allowed for the rapid and easy generation of high quality datasets. Additionally, the declining cost of whole genome sequencing and the proliferation of other genomics techniques, such as transposon-sequencing and CRISPR-based editing, should make genetic analysis faster and more accessible. The use of cutting edge technologies to complement tried-and-true approaches like genetics and *in vitro* biochemistry will drive future discoveries in the field. Our hope is that their implementation in the study of *Caulobacter* will provide insight into the fundamental nature of division.

1.10 Figures and Legends

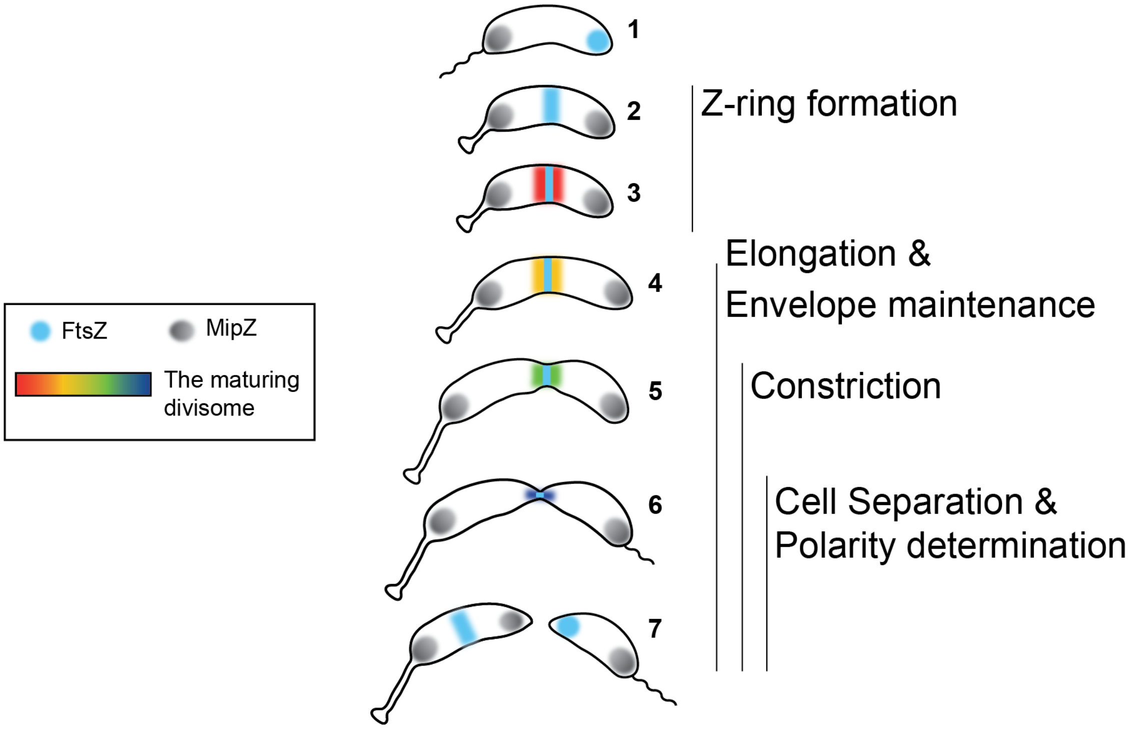
FtsZ
MipZ
The maturing divisome
1
2
3
4
5
6
7
Z-ring formation
Elongation & Envelope maintenance
Constriction
Cell Separation & Polarity determination

Figure 1. Overview of division in *Caulobacter*.

Caulobacter cells undergo a series of events during division, facilitated by maturation of the divisome. (1) Cells begin in the swarmer phase, with unipolar MipZ and FtsZ at opposite poles. (2) During the swarmer to stalked cell transition, MipZ localizes to both poles to initiate Z-ring formation, forcing FtsZ to localize in an unfocused band at midcell. (3) Z-ring formation factors arrive (red) to help focus the Z-ring and tether FtsZ to the membrane. (4) The elongation machinery (yellow) arrives and cells begin to elongate by PG insertion at midcell; at the same time, the envelope maintenance machinery (also yellow) arrives to ensure envelope integrity is preserved throughout the division process. (5) The constriction machinery (green) arrives and constriction begins. (6) As constriction progresses, factors involved in cell separation and polarity determination (dark blue) arrive at midcell to help terminate division and mark the future site of the new pole. (7) Division terminates when the cell finally splits apart, forming two new daughter cells.

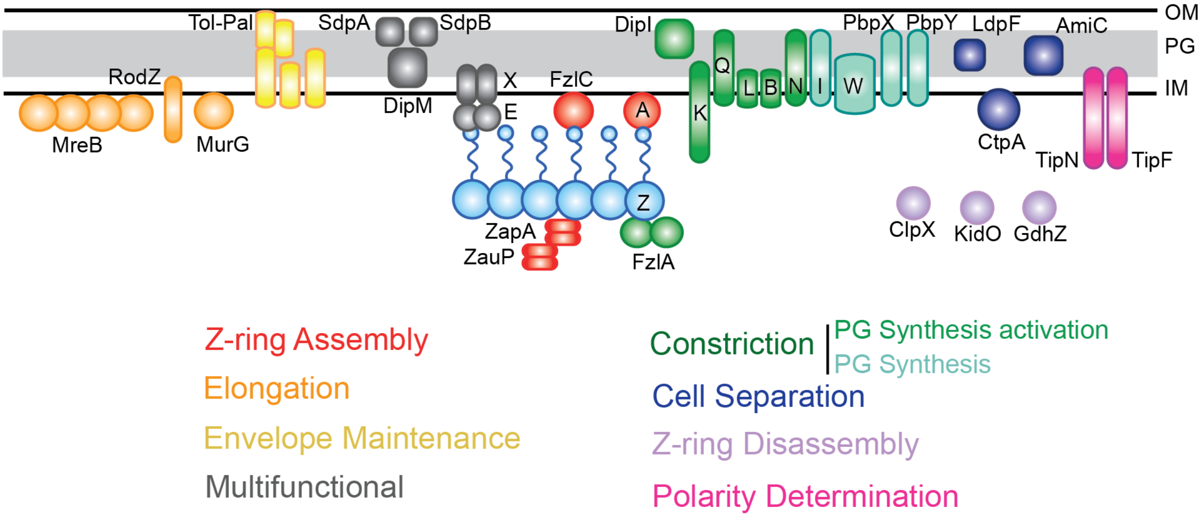
OM
PG
IM
Tol-Pal
SdpA
SdpB
DipI
PbpX
PbpY
LdpF
AmiC
RodZ
X
FzlC
Q
L
B
N
I
W
DipM
E
A
K
MreB
MurG
CtpA
TipN
TipF
Z
ZapA
ZauP
FzlA
ClpX
KidO
GdhZ
Z-ring Assembly
Elongation
Envelope Maintenance
Multifunctional
Constriction
PG Synthesis activation
PG Synthesis
Cell Separation
Z-ring Disassembly
Polarity Determination

Figure 2. Architecture of the Caulobacter divisome.

Depiction of all of the known members of the *Caulobacter* divisome at the envelope at midcell (IM = inner membrane; PG = peptidoglycan; OM = outer membrane). Members of the divisome have been placed into functional groups: Z-ring assembly factors (red); elongation machinery (orange); envelope maintenance machinery (yellow); multifunctional factors (gray); constriction machinery, subdivided into PG synthesis activation factors (green) and PG synthesis enzymes (turquoise); cell separation factors (dark purple); Z-ring disassembly factors (lavender); polarity determination factors (magenta). Note that the divisome is a dynamic structure and not all of its components are necessarily localized to midcell at the same time, as shown here. See figure 3 for divisome localization timing. Adapted from Goley *et al.*, 2011.

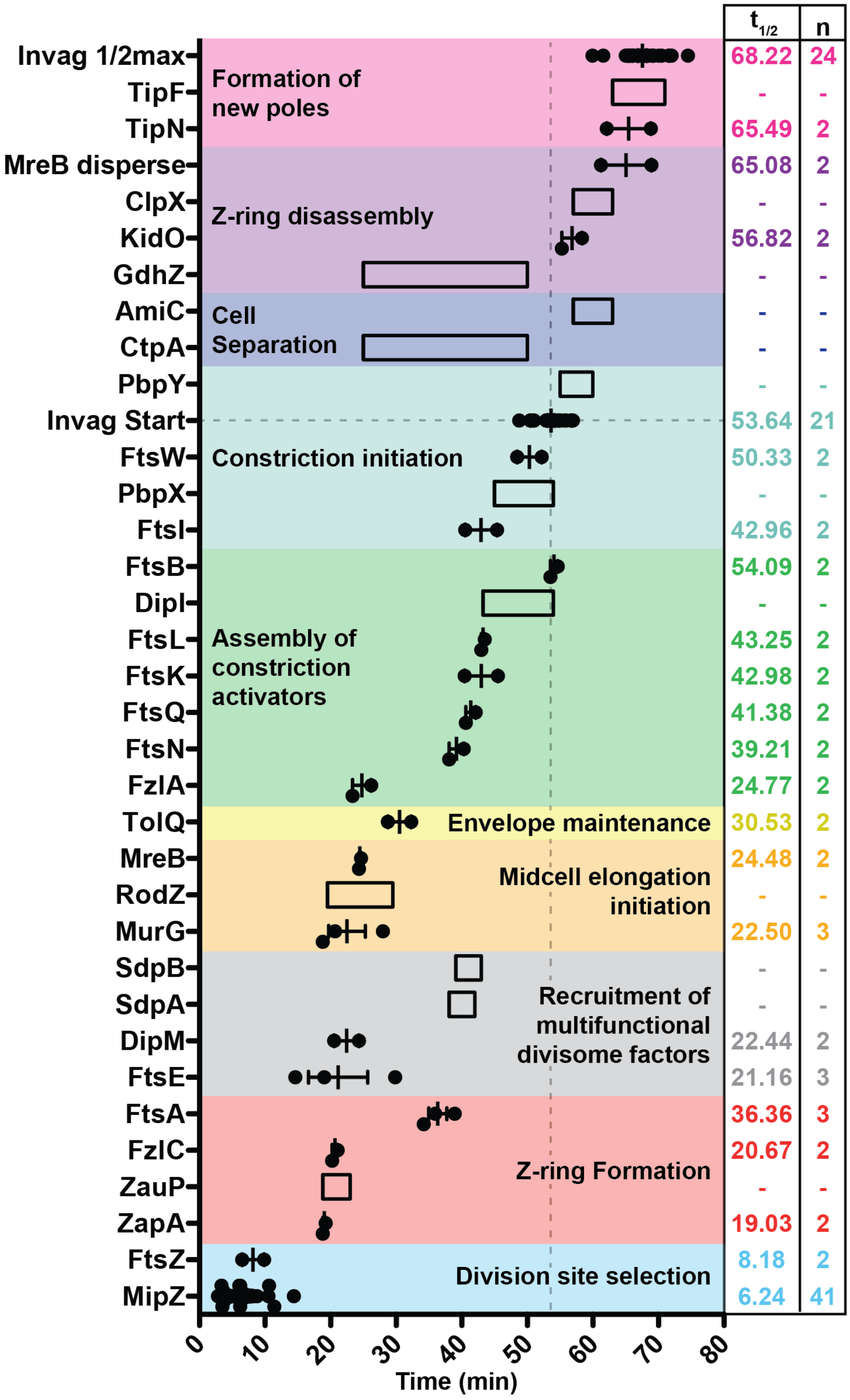

Figure 3. Timing of divisome localization.

Midcell localization timing and order of the members of the divisome. The half-maximal midcell localization time of each protein (the time at which half of all of a protein has localized to midcell; $t_{1/2}$) was either calculated from measured data (black circles, reported in Goley *et al.*, 2011) or predicted (empty boxes). Measured data were taken from Goley *et al.* 2011 in which timing of localization of 19 different divisome proteins were assessed in parallel. For proteins where $t_{1/2}$ was predicted, localization timing was extracted from the literature. When possible, the timing of protein localization was compared to the timing of localization of another, already characterized protein. Absent such information, a best guess was made (ie, a protein was predicted to arrive around the same time as interaction partners or before/after a major event, such as constriction initiation). Adapted from Goley *et al.*, 2011.

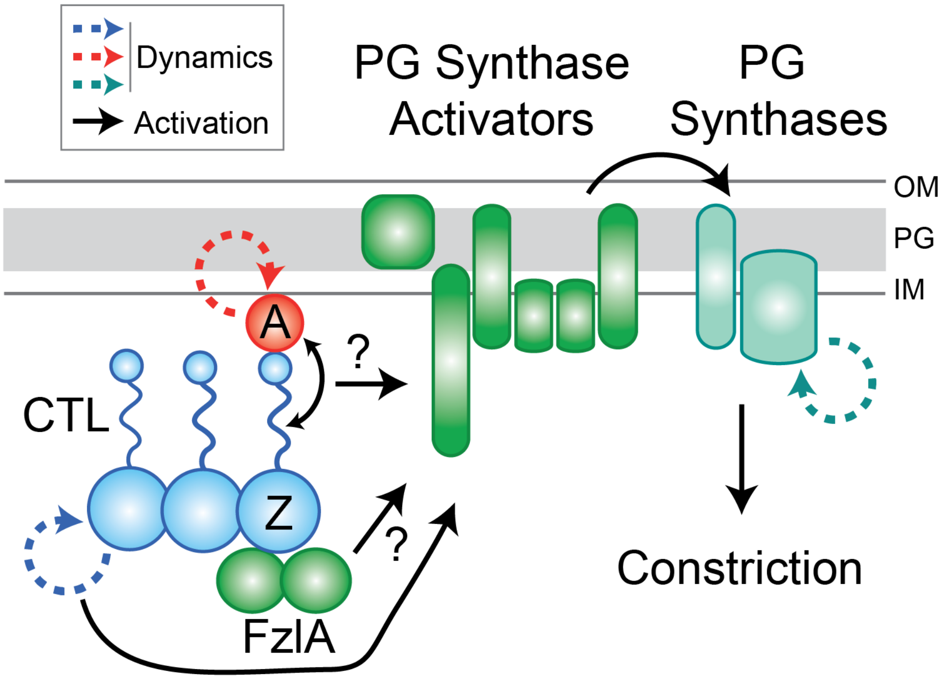

Figure 4. A dynamic activator model for FtsZ-mediated constriction initiation.

Model for FtsZ-directed activation of constriction in *Caulobacter*. FtsZ is proposed to signal through the PG synthase activators (e.g. FtsQLB, FtsN, FtsK) to PG synthases (e.g. FtsWI), initiating PG remodeling and potentially impacting PG synthase dynamics (turquoise dashed line), to start constriction. There are a number of putative mechanisms by which FtsZ may signal to the PG synthase activators (black arrows, as shown) or potentially directly to the PG synthases (not shown): Through FtsZ's CTL, which may influence protein-protein interactions directly or indirectly, possibly through mechanical signaling and/or through an interaction with FtsA (double-headed black arrow); through a FzlA-mediated protein-protein interaction; and/or through FtsZ dynamics (blue dashed line), which may influence protein-protein interactions indirectly. FtsA dynamics (red dashed line) may also play a role in constriction activation, though precisely how is still unclear.

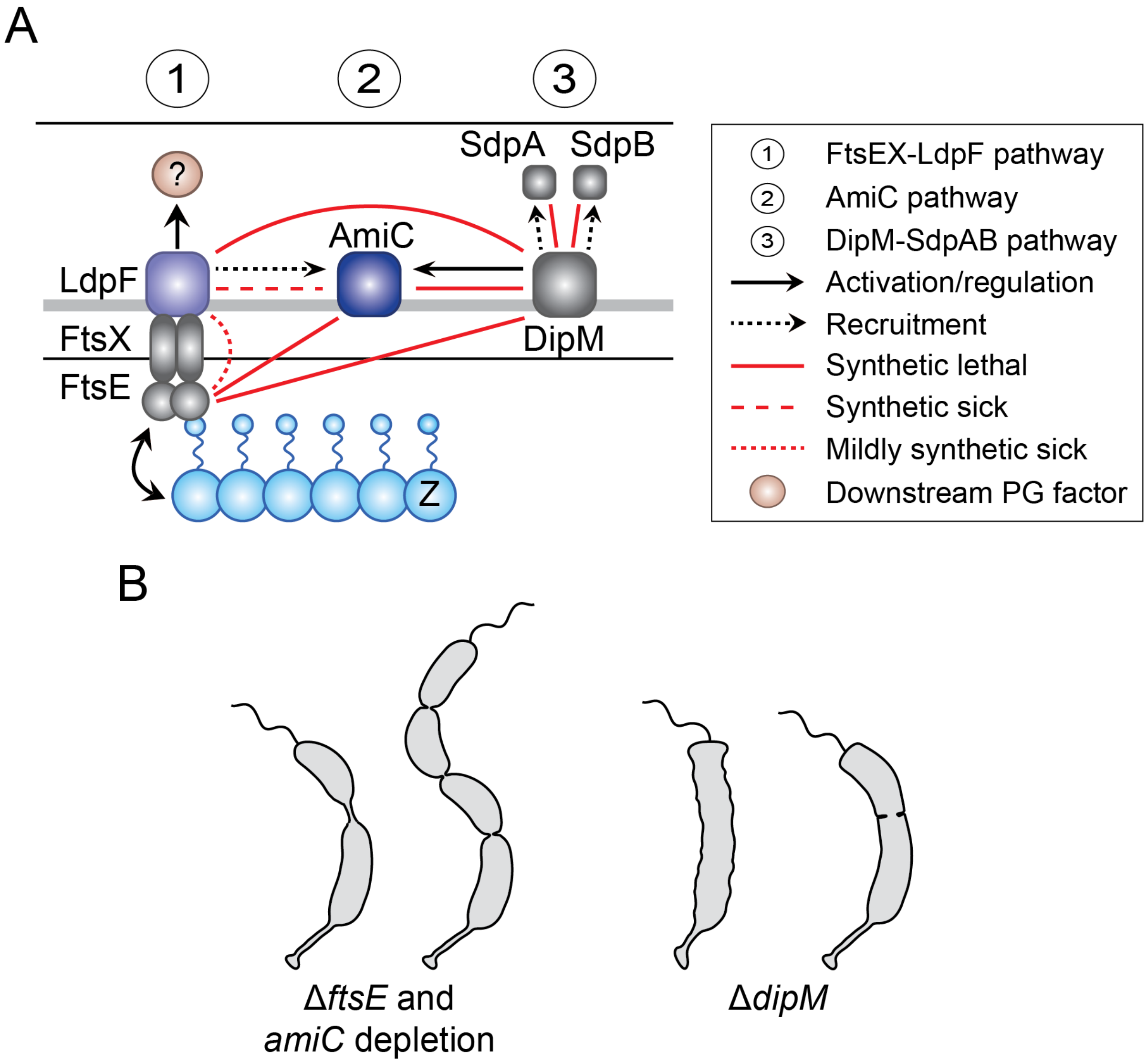
A
①
②
③
SdpA
SdpB
?
AmiC
LdpF
FtsX
FtsE
DipM
Z
① FtsEX-LdpF pathway
② AmiC pathway
③ DipM-SdpAB pathway
Activation/regulation
Recruitment
Synthetic lethal
Synthetic sick
Mildly synthetic sick
Downstream PG factor
B
Δ*ftsE* and
amiC depletion
Δ*dipM*

Figure 5. Cell separation pathways.

(A) Model for cell separation pathways in *Caulobacter*. (1) In the FtsEX-LdpF pathway, FtsEX and LdpF are proposed to signal to an unidentified PG hydrolase to initiate cell separation. FtsZ, which interacts with FtsEX, may serve as an upstream activator for this pathway. (2) In the AmiC pathway, LdpF recruits AmiC to midcell, and DipM subsequently activates AmiC's PG hydrolase activity. (3) In the DipM-SdpAB pathway, DipM recruits the putative PG hydrolases SdpA and SdpB to midcell, which then begin PG hydrolysis. Synthetic interactions between genes (red solid, dashed, and dotted lines) indicate varying degrees of highlight the complexity of the interactions among and between pathways. Adapted from Meier *et al.*, 2017.

(B) Deletion or depletion phenotypes of *ftsE*, *amiC*, and *dipM* in *Caulobacter*. Deletion of *ftsE* and depletion of AmiC yields a heterogeneous population of chained cells, with some connected by a long, skinny connection and others connected by a much shorter connection. Deletion of *dipM* leads to filamentation, envelope defects, blunter poles, and septum-like constriction sites. The gene deletions correspond with the cell separation pathways depicted in panel A and highlight the heterogeneity of roles that each protein/pathway plays in cell separation.

Chapter 2. FzlA, an essential regulator of FtsZ filament curvature, controls constriction rate during *Caulobacter* division

2.1 Introduction

Cell division in bacteria is a highly complex process that requires coordination of numerous distinct events in time and space. The cell must invaginate and remodel the inner membrane, cell wall, and outer membrane, all while maintaining envelope integrity. FtsZ, an essential and widely conserved tubulin-like GTPase (de Boer *et al.*, 1992), acts as a central hub for the assembly and action of dozens of proteins (the divisome) that collectively remodel the cell envelope (Goley *et al.*, 2011; Sundararajan and Goley, 2017). Prior to division, FtsZ protofilaments coalesce at midcell and with the help of accessory proteins, form a focused superstructure called the Z-ring (Wang and Lutkenhaus, 1996; Woldemeskel *et al.*, 2017; Meier *et al.*, 2017). The Z-ring is in turn anchored to the inner membrane by adapter proteins (Ma *et al.*, 1996; Pichoff and Lutkenhaus, 2005; Szwedziak *et al.*, 2014; Meier *et al.*, 2016). The Z-ring successively recruits components of the divisome (Rueda *et al.*, 2003; Aarsman *et al.*, 2005; Goehring *et al.*, 2006; Goley *et al.*, 2011; Du and Lutkenhaus, 2017), which include factors involved in peptidoglycan (PG) synthesis and hydrolysis (Boyle *et al.*, 1997; Weiss *et al.*, 1999; Daniel *et al.*, 2000; Bernhardt and De Boer, 2003; Goley *et al.*, 2010a). However, the mechanisms by which the Z-ring facilitates or organizes envelope constriction have not yet been fully elucidated.

The biochemical and biophysical properties of FtsZ are proposed to be central to its role in division (Erickson *et al.*, 2010). FtsZ assembles into polymers in a guanosine nucleotide-dependent manner, with both straight and curved filament conformations observed *in vitro* and *in vivo* (Lu *et al.*, 2000; Mingorance *et al.*, 2005; Li *et al.*, 2007). Membrane-targeted FtsZ is able to deform membranes in the same direction as FtsZ filament curvature (Osawa *et al.*, 2009), suggesting a force generation mechanism that could be used to drive constriction (Erickson *et al.*, 2010). However, it is unknown if FtsZ filament curvature contributes to division in cells or how this activity might be regulated during the tightly timed constriction process. A critical downstream outcome of Z-ring function is synthesis and remodeling of PG at the division site, and mounting evidence suggests that this requires active direction of PG metabolism by FtsZ (Xiao and Goley, 2016; Coltharp and Xiao, 2017). In *Caulobacter crescentus*, FtsZ influences the chemical composition of the PG in a manner requiring its C-terminal linker (Sundararajan *et al.*, 2015). Moreover, recent studies in both *Escherichia coli* and *Bacillus subtilis* demonstrated that FtsZ dynamics *in vivo* drive the dynamics of PG synthetic enzymes during division (Bisson-Filho *et al.*, 2017; Yang *et al.*, 2017). In *B. subtilis*, but not *E. coli*, FtsZ dynamics dictate the rate of constriction during division (Coltharp *et al.*, 2016; Bisson-Filho *et al.*, 2017; Yang *et al.*, 2017). It is still unknown how FtsZ and PG metabolism are mechanistically coupled or if FtsZ filament curvature plays a role in regulating PG synthesis or constriction dynamics.

Here, we have studied FzlA, a *C. crescentus* division protein that promotes formation of stable, highly curved FtsZ filaments *in vitro* (Goley *et al.*, 2010b), both as a handle for probing the effect of FtsZ curvature on division, and with the aim of scrutinizing the ability of FtsZ to influence constriction rate. FzlA is an essential FtsZ-binding protein conserved across α-proteobacteria (Goley *et al.*, 2010b). Depletion of FzlA leads to cell filamentation, but leaves Z-ring and divisome assembly unperturbed, suggesting that FzlA is required for active constriction (Goley *et al.*, 2010b; Goley *et al.*, 2011). *In vitro*, FzlA not only binds to FtsZ, but promotes formation of stable, double-stranded helices containing two highly curved FtsZ protofilaments (Goley *et al.*, 2010b). We previously hypothesized that FzlA promotes constriction through its ability to regulate FtsZ filament curvature and, perhaps, the generation of FtsZ-mediated force (Goley *et al.*, 2010b).

We now present the crystal structure of FzlA and use it to inform a structure-function analysis of FzlA with respect to its interaction with FtsZ. We demonstrate that the FtsZ-FzlA interaction is essential for division, and that FzlA-mediated FtsZ curvature is correlated with division efficiency. Specifically, we demonstrate that FzlA modulates the rate of constriction during division through its interaction with and curving of FtsZ filaments. We find that slowly constricting *fzlA* mutant strains form tapered, "pointy" poles, consistent with our observations that mutation of *fzlA* decreases the rate of constriction relative to the rate of elongation during division. These results implicate FzlA as a key regulator of envelope constriction through its interaction with FtsZ, and are consistent with a role for FtsZ curvature in efficient cell envelope constriction in *C. crescentus*.

2.2 FzlA forms a GST-like homodimer

To guide our investigation into the interaction of FzlA with FtsZ and its role in cytokinesis, we sought to solve its structure using X-ray crystallography. To this end, we expressed an N-terminal hexahistidine-tagged version of *C. crescentus fzlA* in *E. coli*. FzlA could be purified in large quantities and crystallized readily. The cubic crystals, both native and heavy metal derivatives, diffracted well, so that it was possible to collect all the data in house (**Table 1**).

Subsequent data processing, phasing, model building, and refinement produced an electron density map at 2 Å and the corresponding model was of very good quality. It was possible to resolve residues 3-228 of FzlA and the asymmetric unit contained one molecule (**Fig. 6A** and **Fig. 7** for stereo view of a portion of the structure). Based on sequence homology, FzlA was classified as a member of the GST protein family in *C. crescentus* (Goley *et al.*, 2010b). Indeed, the structure of FzlA can be superimposed on that of GST from *Proteus mirabilis* (PDB 1PMT) (Rossjohn *et al.*, 1998) with an RMSD of 2.09 Å over 179 Cα atoms (**Fig. 6B**). FzlA does not bind glutathione (Goley *et al.*, 2010b), however, and lacks the catalytic histidine and serine/cysteine residues found in other GST proteins (Ma *et al.*, 2009; Federici *et al.*, 2010), suggesting that it no longer retains glutathione transferase activity. Applying crystal symmetry revealed that FzlA is most likely a homodimer (interface area 1263 Å^2 as determined by PISA) (**Fig. 6C**). In contrast to the rest of the structure, residues 212-228 at the C-terminus do not show any secondary structure, but are still ordered (**Fig. 6C**). In the course of our work, the structure of a FzlA homolog from *Sinorhizobium meliloti* (SmFzlA) was deposited in the PDB (PDB 4MDC). The two structures can be superimposed with an RMSD of 1.03 Å over 176 Cα atoms.

Though FzlA runs as an apparent monomer by calibrated size exclusion chromatography (Goley *et al.*, 2010b), both CcFzlA and SmFzlA crystallized as dimers, and we found that FzlA self-interacts by bacterial two-hybrid (BTH) analysis (**Fig. 8A**). As a further test for dimerization in *C. crescentus* cells, we performed co-immunoprecipitation with differentially tagged variants of FzlA. We created a *C. crescentus* strain (EG2452) with *3xflag-fzlA* replacing *fzlA* at its native locus and *mCherry-fzlA* integrated at the *vanA* chromosomal locus, with expression driven by the inducible P_{van} promoter. Cells expressing both tagged variants of *fzlA* were lysed and anti-FLAG conjugated agarose beads were used to immunoprecipitate 3xFLAG-FzlA and its binding partners (**Fig. 8B**). Immunoblot analysis demonstrated that mCherry-FzlA robustly and specifically co-immunoprecipitates with 3xFLAG-FzlA. Though FtsZ co-immunoprecipitates with 3xFLAG-FzlA in the presence of a chemical crosslinker (data not shown), it does not precipitate in the absence of crosslinker (**Fig. 8B**). These data indicate that the interaction between 3xFLAG-FzlA and mCherry-FzlA is direct and not mediated by FtsZ. In conjunction with the structural and BTH analysis data, these results suggest that FzlA forms a dimer *in vivo*.

2.3 Attempts to co-crystallize FtsZ and FzlA were unsuccessful

Since FzlA was previously shown to bind FtsZ (Goley *et al.*, 2010b), we attempted to co-crystallize FtsZ and FzlA at the MRC-LMB crystallization facility to gain deeper insight into the nature of this interaction. His_6-FzlA was mixed with either full length FtsZ or FtsZΔCTL. We expected that full length FtsZ might not crystallize readily due to flexibility of the linker domain and we had found that FzlA interacts with FtsZΔCTL. Protein mixtures were made containing either a 1:1 ratio of FtsZ:FzlA or an excess of either FtsZ or FzlA, then incubated at room temperature or 4°C to allow for crystal growth. Co-crystallization proved to be unsuccessful and the only crystals that could be found were FzlA alone. For these experiments, His_6-FzlA and FtsZ/FtsZΔCTL were purified individually, as described in the methods section.

2.4 FzlA interacts with the GTPase domain of FtsZ

Since co-crystallization proved to be unsuccessful, we instead performed co-sedimentation assays with His_6-FzlA and either FtsZ, FtsZΔCTL (FtsZ lacking the C-terminal linker), or FtsZΔCTLC (FtsZ lacking the C-terminal linker and conserved C-terminal peptide) to determine what domain of FtsZ mediates interaction with FzlA. FzlA co-sedimented with each FtsZ variant, suggesting that the GTPase domain of FtsZ is the site of interaction with FzlA (**Fig. 9**).

2.5 Creation of FzlA mutant library

With the structure of FzlA in hand, we undertook a directed mutagenesis approach to probe the role of the FzlA-FtsZ interaction in division (**Fig. 10A**). We identified surface residues that were charged and/or conserved across α-proteobacteria and used site-directed mutagenesis to create a library of 34 *fzlA* mutant variants, each encoding a protein containing one to four non-conservative point mutations (**Fig. 10B**, **Table 2,** and **Table 3)**. We anticipated that these mutations might disrupt FtsZ binding, helix formation, or other unknown functions of FzlA. We were particularly interested in identifying mutations that were proficient in FtsZ binding, but deficient in curving FtsZ filaments, so that we could probe the link between FtsZ curvature and cell division.

As discussed below, we screened each mutant strain for FzlA localization, cell morphology and growth, and steady state FzlA protein levels *in vivo*, then selected a subset for biochemical characterization and further follow-up (**Fig. 10A**). Based on our results, we created a strategy for naming the mutants for ease of reference. Eleven mutants displayed **W**T (W) characteristics *in vivo*, so we named these *fzlA*^{W1}- *fzlA*^{W11} and did not characterize these further (**Table 3**). Seven mutants had poor protein **st**ability (ST) by immunoblotting, named *fzlA*^{ST1}-*fzlA*^{ST7}, and were also not pursued further. Six mutants displayed poor **sol**ubility (SOL) *in vitro*, named *fzlA*^{SOL1}-*fzlA*^{SOL6}, which could not be purified for biochemical assays. The remaining mutants were functionally grouped and named primarily according to their biochemical activity towards FtsZ, as described below: **w**eakened **b**inding (WB) to FtsZ, *fzlA*^{WB1}; **u**nknown **n**on-essential activity (UN), *fzlA*^{UN1}-*fzlA*^{UN2}; **u**nknown **e**ssential activity (UE), *fzlA*^{UE1} & *fzlA*^{UE2}; **n**o **b**inding to FtsZ (NB), *fzlA*^{NB1}& *fzlA*^{NB2}; and **n**o **h**elices (NH), *fzlA*^{NH1}- *fzlA*^{NH3} (**Table 2**).

2.6 *fzlA* mutants display a range of localization and division defects

To functionally characterize our panel of FzlA mutant strains, we devised an *in vivo* microscopy-based assay to identify strains deficient in division and/or FzlA localization. *mCherry* was fused to the 5' end of each mutant *fzlA* allele and placed under the control of a vanillate-inducible promoter. These fusions were integrated at the *vanA* locus in a strain background containing xylose-inducible *fzlA* at the *xylX* locus and a *fzlA* deletion at its native locus (**Fig. 11A**). Cells were grown to log phase with xylose to induce WT *fzlA*, then washed and grown with vanillate to induce mutant *fzlA* and deplete WT FzlA for 24 hours. Each strain was subsequently imaged by phase contrast and fluorescence microscopy and FzlA levels were probed by immunoblotting [**Fig. 11B** (includes mutants discussed at length) and **Fig. 12A** (includes mutants that were not further characterized) and **Fig. 13**]. Strains were also imaged with xylose alone to only produce WT FzlA (**Fig. 14A**) or with neither inducer (**Fig. 15A**). We additionally determined growth rate and cell viability using spot dilutions to assess the fitness of each strain (**Fig. 11C-D**, **Fig. 12B**, **Fig. 14B**, and **Fig. 15B**).

As previously shown, mCherry-FzlA localizes to midcell and complements the loss of FzlA, yielding cells of WT length and growth rate (Goley *et al.*, 2010b). Screening the library of mutant strains yielded a wide range of FzlA localization and length phenotypes in the presence of vanillate (**Table 2** and **Table 3**). Many of these mutants were indistinguishable from WT in viability, length, and FzlA localization (*fzlA*^{W1}- *fzlA*^{W10}) (**Fig. 12**). Numerous mutants had diffuse FzlA localization, increased cell length, and reduced growth rate and viability (*fzlA*^{NB1} - *fzlA*^{NB2}, *fzlA*^{ST1}- *fzlA*^{ST7}, *fzlA*^{SOL1}- *fzlA*^{SOL5}) (**Fig. 11** and **Fig. 12**). Three mutants (*fzlA*^{NH1}, *fzlA*^{UE1}, *fzlA*^{UE2}) had localized FzlA, yet displayed elongated cell morphologies, reductions in growth rate, and had lower colony forming units (CFUs). Five mutants (*fzlA*^{UN1}, *fzlA*^{UN2}, *fzlA*^{NH1}, *fzlA*^{NH2}, and *fzlA*^{SOL6}) similarly had FzlA localization and a mixed population of elongated and short cells, but were less impaired in growth rate and/or viability. Interestingly, one mutant (*fzlA*^{WB1}) had diffuse FzlA, but was otherwise comparable to WT cells in terms of cell length, growth, and viability.

It should be noted that in nearly all mutant strains (except for the poor stability mutants), vanillate induction resulted in varying degrees of mutant FzlA overexpression **(Fig. 13)**. Although some of these mutant proteins appeared to be more highly expressed than others, all except the poor stability mutant proteins were expressed at levels greater than native WT FzlA. Therefore, any division defects in these mutants are unlikely to be due to insufficient protein levels. Further, the previous observation that FzlA overexpression does not result in increased cell length (Goley *et al.*, 2010b), suggests mutant protein levels do not likely underlie the division defects observed *in vivo*.

Expression of WT FzlA alone in cells without induction of mCherry-mutant FzlA supported normal growth of each strain, as expected (**Fig. 14**). However, we were curious if any mutant FzlA screening strains could grow in the absence of either inducer. We found when we grew cells in the absence of xylose or vanillate that numerous mutant strains had cells that became elongated and had reduced viability (*fzlA*^{WB1}, *fzlA*^{UE1}-*fzlA*^{UE2}, *fzlA*^{NB1}-*fzlA*^{NB2}, *fzlA*^{NH1}, *fzlA*^{W9}, *fzlA*^{ST1}-*fzlA*^{ST7}, *fzlA*^{SOL1}-*fzlA*^{SOL6}), as expected (**Fig. 15**). Surprisingly, however, WT cells and many of the mutant strain cells exhibited WT cell length and were viable (*fzlA*^{UN1}, *fzlA*^{NH2}-*fzlA*^{NH3}, *fzlA*^{W1}-*fzlA*^{W8}, and *fzlA*^{W10}) (**Fig. 15**). α-FzlA immunoblotting of the mutants that were subsequently characterized biochemically revealed that in the absence of inducers, low levels of the mCherry-FzlA variants and WT FzlA were present (**Fig. 16**). This suggests that the P_{van}, and to a lesser extent P_{xyl}, promoters were leaky. The low expression levels of the functional or partially functional mutant FzlA variants were apparently sufficient to enable growth.

After the initial screening, we sought to visualize the Z-ring in a subset of mutant strains deficient in division. Since depletion of FzlA does not obviously affect Z-ring organization by conventional microscopy (Goley *et al.*, 2010b), we hypothesized that mutation of FzlA would not affect it either. To test this, we imaged cells depleted of WT FzlA, producing both mCherry-mutant FzlA and Venus-FtsZ (**Fig. 17**). For each strain tested, we observed that Z-ring structure was similar to WT, and that filamentous cells typically contained one or two focused Z-rings per cell. This is similar to what has been previously reported in *C. crescentus* cells blocked for division at stages downstream of Z-ring assembly, where relatively few Z-rings are observed even in filamentous cells (Costa *et al.*, 2008; Modell *et al.*, 2014; Osorio *et al.*, 2017). We also found that in strains where FzlA mutant proteins formed rings or foci, FtsZ co-localized with FzlA. In mutant strains where FzlA was diffuse, such as $fzlA^{NB1}$ and $fzlA^{NB2}$, FtsZ still formed rings. We therefore conclude that the division and/or localization defects that we observed are not due to global defects in Z-ring assembly.

2.7 FzlA mutant proteins display distinct defects in activities towards FtsZ *in vitro*

Having screened the *fzlA* mutant strains for localization and division phenotypes *in vivo*, we compiled a list of mutant proteins for characterization of activity towards FtsZ *in vitro*. We did not pursue the $fzlA^{W}$ or $fzlA^{ST}$ mutants, since they were fully functional or displayed poor protein stability *in vivo* by immunoblot analysis, respectively (**Fig. 13**). We additionally did not follow up on FzlA^{UN2}, since its mutated residue (Y223A) was included in another mutant, FzlA^{UE1} (Y223A, D227K, F228A) and the phenotype of the triple mutant was identical to that of FzlA^{UE2} bearing the single D227K mutation. We attempted to purify the remaining 15 mutant proteins by expressing them as His$_6$-SUMO fusions, followed by affinity purification and cleavage of the His$_6$-SUMO tag. Six of these mutant proteins (FzlA^{SOL1}-FzlA^{SOL6}, **Table 3**) were insoluble when expressed in *E. coli*, so we focused our efforts on the nine biochemically tractable mutant proteins that corresponded with non-WT phenotypes *in vivo* (**Table 2**). Following purification, we subjected these nine mutant proteins to a series of biochemical assays, testing for FtsZ binding, higher order structure formation, and helix formation (**Fig. 18**).

We first optimized these assays using untagged WT FzlA, since the conditions previously reported used His$_6$-FzlA (Goley *et al.*, 2010b). His$_6$-FzlA was previously shown to bind, form helices with, and lower the GTPase rate of FtsZ using HEK polymerization buffer (50 mM HEPES-KOH [pH7.2], 50 mM KCl, 0.1 mM EDTA) with 2.5 mM $MgCl_2$ and 2 mM GTP. For our study, we sought to characterize the activity of untagged FzlA mutant proteins, in order to control against any potential His$_6$ artifacts. We purified His$_6$-SUMO-WT FzlA, then cleaved the affinity tag. Interestingly, when we conducted the FtsZ interaction assays with untagged FzlA using HEK polymerization buffer and the same conditions as before, although FzlA still bound FtsZ efficiently, we rarely observed FtsZ helix formation or an effect on GTPase rate. After optimizing numerous variables, we found that untagged FzlA promotes formation of FtsZ helices efficiently at pH 6.5, but not pH 7.2 (data not shown). This may reflect the difference in the predicted pI of the two forms of FzlA: His$_6$-FzlA is predicted to have a pI of 7.4 and untagged FzlA is predicted to have a pI of 6.8. Untagged FzlA would therefore be above its pI at pH 7.2 whereas the His$_6$-tagged version would be below its pI. Lowering the pH to 6.5 would be predicted to place both proteins below their pI and render each a net positive charge. Since FtsZ still efficiently polymerizes and hydrolyzes GTP at this lower pH, we carried out all FzlA-FtsZ interaction assays using these conditions.

Although the pH and salt concentration of the *E. coli* cytoplasm has been reported to be close to neutral and 250 mM potassium, respectively, there is no information on the conditions of the *C. crescentus* cytoplasm. Given the distinct environmental niches occupied by *E. coli* and *C. crescentus* it may not be fair to assume equivalent pH and salt concentrations in *C. crescentus*. Therefore, it is difficult to know what the appropriate "physiological" conditions might be to inform conditions for our *in vitro* assays. In order to maximize our ability to distinguish possible differences between our mutant FzlA proteins and WT, we used pH 6.5, 50 mM KCl buffer for all of our *in vitro* assays. We acknowledge that it is impossible to fully recapitulate the chemical and physical conditions of the cell – even when these are known - in a test tube, so all activities observed *in vitro* must be viewed with the caveat that they may not occur in the context of the cell.

Having identified *in vitro* conditions that maximized WT FzlA activity (pH 6.5, 50 mM KCl), which were in line with commonly used conditions for FtsZ activity assays (Chen *et al.*, 2007; Pacheco-Gómez *et al.*, 2011; Milam and Erickson, 2013), we were now ready to probe the activities of different mutant proteins and attempt to identify potentially subtle defects in activity. To test for binding to FtsZ, we performed a high speed co-pelleting assay in which FtsZ polymers pellet on their own and can bring bound FzlA to the pellet (**Fig. 18A** and **Fig. 19**). In the absence of FtsZ polymers, FzlA remains in the supernatant (Goley *et al.*, 2010b) (**Fig. 18Ai**). To quantify formation of higher order structures, we used a low speed co-pelleting assay where neither FzlA nor FtsZ polymers pellet in isolation, but both co-sediment when combined under polymerizing conditions due to formation of large helical structures (Goley *et al.*, 2010b) (**Fig. 18B** and **Fig. 20)**. To confirm the formation of higher order structures, we used right-angle light scattering (RALS) (**Fig. 21**). Lastly, we used negative stain transmission electron microscopy (TEM) to directly observe helix formation.

It has been previously shown that WT FzlA co-pellets with FtsZ at both high and low speeds, forms large structures by RALS, and makes helices by TEM (Goley *et al.*, 2010b). Subjecting the nine biochemically tractable mutant proteins to these assays gave a range of activities compared to WT. FzlA^{UN1} (UN=unknown non-essential) behaved similarly to WT FzlA in all assays (**Fig. 18**). Two additional mutant proteins (FzlA^{UE1} & FzlA^{UE2}; UE=unknown essential activity) also bound to FtsZ and formed helices, but were binned into a separate group based on their phenotypes *in vivo* (discussed below). FzlA^{NB2} (NB=no binding to FtsZ) was found to neither bind nor form helices or other higher order structures with FtsZ. Additionally, three mutant proteins (FzlA^{NH1}, FzlA^{NH2}, FzlA^{NH3}; NH=no helices) appeared to uncouple FtsZ binding from helix formation: they bound to FtsZ, albeit to a lesser extent than WT FzlA, but did not form helices.

Two mutant proteins, FzlA^{WB1} (WB=weak binding to FtsZ) and FzlA^{NB1}(NB=no binding to FtsZ), appeared to self-aggregate (**Fig. 18Ai**), making it difficult to assess binding to FtsZ by high speed co-pelleting under the standard conditions used in this study (pH 6.5, 2:1 FzlA:FtsZ). Increasing pH to 7.2 and using a 1:1 FzlA:FtsZ ratio significantly reduced aggregation and allowed us more confidently assess binding by high speed pelleting. Under these conditions, neither mutant co-sedimented with FtsZ significantly better than when alone (**Fig. 22**). Interestingly, under our standard conditions, FzlA^{WB1} still formed structures by low speed pelleting and helices by TEM, whereas FzlA^{NB1} did not (**Fig. 18B-C**). FzlA^{WB1} therefore appears to weakly bind FtsZ since it is able to form helices, while FzlA^{NB1} does not bind at all.

FzlA was previously shown to reduce FtsZ's GTPase activity (Goley *et al.*, 2010b), similar to other FtsZ polymer stabilizing proteins (Gueiros-Filho and Losick, 2002; Hale *et al.*, 2011; Durand-Heredia *et al.*, 2012). We measured GTPase rate of FtsZ in the presence of FzlA mutant proteins to determine if variants retained the ability to lower activity (**Table 2**). The mutant proteins that interacted more strongly with FzlA and formed helices lowered the GTPase rate more than the weak interactors, though FzlA^{WB1} (which forms helices, but weakly binds FtsZ) did not significantly lower FtsZ's GTPase rate. From these data we conclude that reduction in GTPase rate generally correlates with helical FzlA-FtsZ bundle formation.

2.8 FzlA-FtsZ binding is necessary for allelic complementation

To clarify the contributions of FzlA's biochemical activities to cell division, we next asked if any of the nine *fzlA* mutant alleles corresponding with the mutant proteins we characterized biochemically, were able to replace WT *fzlA* as the only copy of the gene in the cell. To this end, we attempted allelic exchange at the *fzlA* locus using each of the above nine mutant genes. However, we were only able to successfully replace WT *fzlA* with three of these (*fzlA*^{UN1}, *fzlA*^{NH2}, *fzlA*^{NH3}) (**Fig. 23A** and **Fig. 24**). The proteins corresponding to each of these three mutant alleles bound to FtsZ to some extent and, conversely, the alleles corresponding to binding-deficient mutant proteins (*fzlA*^{NB1} & *fzlA*^{NB2}) were unable to complement loss of *fzlA*. These observations indicate that the FzlA-FtsZ interaction is essential for viability and division. Additionally, the alleles corresponding to the proteins that bound FtsZ and formed helices *in vitro*, but themselves caused cell elongation and very severe growth defects (*fzlA*^{UE1} & *fzlA*^{UE2}) *in* *vivo,* also could not complement loss of *fzlA*. Since the residues altered in the proteins corresponding with these two mutant alleles do not appear to be necessary for interaction with FtsZ *in vitro*, we propose that they mediate an unknown, but essential activity distinct from FtsZ binding. Interestingly, although *fzlA*^{WB1} cells were not particularly sick in the FzlA depletion experiment (**Fig. 11**), *fzlA*^{WB1} could not replace WT *fzlA* on the chromosome. This was somewhat surprising, but we reason that since induction with vanillate causes overexpression of the mutant allele (**Fig. 13**), higher protein levels may compensate for FzlA^{WB1}'s weak affinity for FtsZ.

2.9 Mutant *fzlA* strains display growth and shape defects

We characterized the phenotypes of the *fzlA* allelic exchange strains in detail in order to further assess the link between *in vitro* activity of FzlA and its *in vivo* function. *fzlA*^{UN1} and *fzlA*^{NH3} grew similarly to WT by spot dilution (**Fig. 23B**), but displayed a moderate reduction in growth rate (**Fig. 23C**) and were elongated (**Fig. 23A, 23D**). The phenotype of *fzlA*^{NH2} was much more severe, as evidenced by reduced colony size and number (**Fig. 23B**), significantly lower growth rate (**Fig. 23C**), and elongated and filamentous cells (**Fig. 23A, 23D**). The steady state protein levels of FzlA^{UN1} and FzlA^{NH3} were similar to WT, while there was a moderate increase in levels of FzlA^{NH2} (**Fig. 24)**. The mild overexpression of *fzlA*^{NH2} is unlikely to underlie the morphological defects observed, however. As previously mentioned, overexpression of *fzlA* (Goley *et al.*, 2010b), *mCherry-fzlA*, or many of the *mCherry-fzlA* mutant variants we tested (**Fig. 13**), did not result in significant cell length defects.

We sought to quantify cell shape abnormalities of each mutant strain using Celltool (Pincus and Theriot, 2007). To this end, we synchronized mutant and WT cells to minimize cell cycle-dependent differences in shape and imaged them prior to the initiation of constriction. Cell contours from WT and the three mutant strains were extracted and principle component analysis (PCA) was performed to determine variation in shape across the four populations. The modes which accounted for the most variation from mean cell shape roughly reflected cell length, curvature, and width (**Fig. 23E**). Each mutant strain, but particularly *fzlA*^{NH2}, was elongated compared to WT, consistent with our cell length measurements of a mixed population of cells. In addition, *fzlA*^{NH2} cells and to a lesser extent, *fzlA*^{NH3} cells, were skinnier than WT. Cell curvature did not appear to be affected by mutations in *fzlA*. In sum, the three *fzlA* strains capable of allelic exchange were distinct from WT in growth rate, cell length, and cell width, with *fzlA*^{NH2} having the most severe phenotype.

Characterizing the phenotypes of the allelic exchange strains allowed us to more precisely correlate the biochemical activity of their corresponding mutant proteins with their division defects. While FzlA^{NH1}, FzlA^{NH2}, and FzlA^{NH3} were found to bind FtsZ, they do not form helices or higher order structures (**Fig. 18A-C**). As shown above, expression of each of these mutant genes in a FzlA depletion background (*fzlA*^{NH1}) or on its own (*fzlA*^{NH2}, *fzlA*^{NH3}) led to division defects. *fzlA*^{NH2} and *fzlA*^{NH3} had severe and mild deficiencies, respectively, in growth rate, length, and shape. *fzlA*^{NH1}, on the other hand, was not capable of allelic replacement. From this we conclude that, while FzlA-FtsZ helices are not necessarily required for division, loss of these structures *in vitro* does correlate with a decrease in division efficiency. The mechanisms behind the mild growth phenotypes observed in *fzlA*^{UN1}, which still forms helices, are not currently clear. We observed a slight, but not statistically significant, reduction in FzlA^{UN1} co-pelleting, which might reflect mildly reduced binding affinity for FtsZ (**Fig. 18Ai**).

2.10 *fzlA* mutant strains display reduced constriction rates

Mutation of FzlA has a clear effect on the efficiency of division. Additionally, we previously showed that depletion of FzlA leads cells to grow into smooth filaments without affecting divisome assembly, indicating a role in the constriction process itself (Goley *et al.*, 2010b). We therefore hypothesized that FzlA regulates the rate of constriction and that this rate may be impaired in the *fzlA* mutant strains. To address this possibility, we performed single-cell timelapse microscopy on WT, $fzlA^{UN1}$, $fzlA^{NH2}$, and $fzlA^{NH3}$ cells. Cells from each strain were synchronized, then placed onto an agarose pad for imaging by phase-contrast microscopy at five minute intervals (**Fig. 25A**). MicrobeJ (Ducret *et al.*, 2016) was used to track individual cells, quantify cell length and width at each time point, and mark time of constriction initiation. The time of completion of division was manually scored for each cell. From these data, the number of frames required to complete constriction was determined for single cells, giving the constriction time. We then calculated constriction rate by dividing the change in cell width during constriction by constriction time (**Fig. 25B**). The constriction rates for $fzlA^{UN1}$ (11.7 ± 0.1 nm/min) and $fzlA^{NH3}$ (11.7 ± 0.2 nm/min) were decreased compared to WT (13.6 ± 0.2 nm/min). Consistent with the more severe phenotype of $fzlA^{NH2}$, these cells constricted even more slowly (9.3 ± 0.2 nm/min).

The decrease in constriction rates observed for the *fzlA* mutant strains might be explained by an overall decrease in the rate of cell wall synthesis. If this was the case, we would expect to see a corresponding decrease in elongation rate, which also depends on cell wall synthesis, for each strain. Elongation rate during constriction was actually increased by a small degree for $fzlA^{UN1}$ (31.4 ±0.2 nm/min) and $fzlA^{NH3}$ (31.9 ±0.2 nm/min), compared to WT (28.2 ±0.2 nm/min), whereas it was slightly decreased for $fzlA^{NH2}$ (25.2 ±0.2 nm/min) (**Fig. 25C**). We examined the ratio of constriction rate to elongation rate for cells of each strain to account for possible global differences in cell wall synthesis (**Fig 25D**). Importantly, we found that this ratio decreased by 20-25% in each mutant strain compared to WT. We observed similar trends when we compared constriction rate to the elongation rate prior to constriction or to the elongation rate during constriction. We therefore conclude that the decrease in constriction rate of each mutant is not merely due to a decrease in global cell wall production, but rather includes a constriction-specific defect.

We additionally observed an increase in the time of constriction initiation (pre-constriction time) in *fzlA*^{NH2} cells (**Fig. 26A**), indicating that this mutation of FzlA results in delayed constriction onset. The change in constriction timing is correlated with a slight increase in the change in cell length before constriction (**Fig. 26B**). Finally, we found in all of the *fzlA* allelic exchange mutants that the decreased constriction rates (**Fig. 25D**) and increased constriction times are correlated with greater changes in length during constriction (**Fig. 26C, D**), as expected.

To further validate the observed differences in constriction versus elongation rates for the *fzlA* mutants, we assessed cell pole shape. Pole shape is indicative of the relative rates of constriction and elongation: a mutant strain that constricts faster (without a corresponding increase in elongation rate) forms blunter poles, while one that constricts slower (without a corresponding decrease in elongation rate) forms more tapered, pointed poles. We therefore determined the maximum instantaneous curvature at the cell poles as a readout for pole "pointiness" (**Fig. 25E**). *fzlA*^{NH2} cells, and to a lesser degree *fzlA*^{UN1} and *fzlA*^{NH3} cells, were found to have significantly "pointier" poles than WT. These data are consistent with our observation that while the constriction rate (i.e. rate of decrease of the diameter of the cell) had been lowered, the elongation rate (i.e. rate of longitudinal insertion of cell wall material) was not affected to the same degree. We conclude that FzlA, through its interaction with FtsZ, plays a specific role in regulating the rate of constriction during *C. crescentus* division.

2.11 Discussion

In this study, we undertook a structure-function approach to characterize the role of FzlA in division in *C. crescentus*. We solved the structure of FzlA and found that it forms a GST-like dimer, then created a library of point mutants with the goal of altering its interaction with FtsZ. After correlating *in vivo* localization and function with *in vitro* activity towards FtsZ for each mutant allele and corresponding protein, we demonstrated that FzlA binding to FtsZ is required for division (**Fig. 27**). Further, the ability of FzlA to curve FtsZ filaments, while not essential, contributes to the efficiency of division (**Fig. 27**). Importantly, FzlA appears to play a key role in determining cell constriction rate through its interaction with FtsZ (**Fig. 27**).

The structural, BTH analysis, and co-immunoprecipitation data provide evidence that FzlA forms a dimer. In the co-immunoprecipitation, 3xFLAG-FzlA is able to pull down a roughly equimolar amount of mCherry-FzlA and other FzlA species that are not reactive with the FLAG antibody (e.g. mCherry-FzlA and 3xFLAG-FzlA degradation products), suggesting the interaction is unlikely to be the result of binding to a bridging protein (**Fig. 8B**). That FzlA dimerizes potentially provides insight into how FzlA is able to mold FtsZ protofilaments into double stranded helices. The most straightforward model is that monomers within a FzlA dimer may bind to FtsZ subunits on opposing strands, positioning them in an offset orientation that causes twisting and helix formation upon polymerization. Alternatively, it is possible that each monomer within a FzlA dimer binds to discrete FtsZ subunits on a single strand, imposing a slight twist. Each strand may then bind to a second either through intrinsic lateral interactions or potentially via self-association of FzlA dimers. In any case, since we never observed highly curved single FtsZ filaments in the presence of WT or any mutant FzlA protein, we propose that FzlA's curvature-inducing activity requires and/or is linked to pairing of FtsZ filaments.

FtsZ has been shown to exist in a curved conformation *in vivo* (Li *et al.*, 2007), but little is known about the coordination and specific function of curved conformations of FtsZ. So far, only a few proteins have been implicated in FtsZ curvature regulation: *B. subtilis* ZapA forms mini-rings with FtsZ in the absence of nucleotide (Gueiros-Filho and Losick, 2002), *Thermotoga maritima* FtsA curves FtsZ filaments on membranes through the repeat distance mismatch (Szwedziak *et al.*, 2012; Szwedziak *et al.*, 2014; Ghosal and Löwe, 2015), and FzlA curves FtsZ through the formation of double-stranded helices (Goley *et al.*, 2010b). In the current study, we focused on the FtsZ-FzlA interaction and have specifically identified sites that contribute to binding to FtsZ. Mutation of one set of residues (D109 and E122 [FzlA^{WB1}]) weakens interaction with FtsZ, while perturbation of others (W38, R124 [FzlA^{NB1}] and E119 [FzlA^{NB2}]) completely eliminates binding. In addition, we identified residues (P131, L136, R137 [FzlA^{NH1}], R140, E141 [FzlA^{NH2}], and R144 [FzlA^{NH3}]) that when mutated, retained some ability to bind but were no longer able to curve FtsZ filaments. Satisfyingly, these residues map to the same face on FzlA's surface (**Fig. 6C**). The residues required for curvature all border one another and while the residues required for binding are nearby on the same face, they are not directly adjacent to each other. This region of FzlA is likely in physical contact with FtsZ, though not all of these residues necessarily directly interact with FtsZ.

Though our mutational analysis suggests a link between FzlA-FtsZ helices and division efficiency, we surprisingly found that the ability of FzlA to interact with FtsZ and promote formation of helices is not sufficient for division. Two mutant proteins (FzlA^{UE1} & FzlA^{UE2}) localize *in vivo*, robustly bind to FtsZ, and form helices, yet their corresponding strains are unable to function in division. The altered residues in these mutant proteins (Y223, D227, and F228) are located close to the C-terminus of FzlA, a region that is spatially distant from the FtsZ binding residues on the surface of FzlA; this separation likely explains why their mutation had little impact on interaction with FtsZ (**Fig. 6C**). The Y223A (*fzlA*^{UN2}) and F228A (*fzlA*^{W11}) single mutant strains were viable, while the D227K (*fzlA*^{UE2}) mutant strain was indistinguishable from the triple mutant strain (*fzlA*^{UE1}), suggesting that mutation of D227 (*fzlA*^{UE2}) is largely responsible for the severe division defect associated with mutation of the C-terminus (**Fig. 12** and **Fig. 11**). Interestingly, the C-terminus of FzlA is a highly acidic region of about 20 amino acids lacking secondary structure, making it a possible protein interaction site. The C-terminus may regulate FzlA's interaction with itself, though we did not observe an interaction of the isolated C-terminus with FzlA by BTH analysis (data not shown). Alternatively, the C-terminal tail may bind to an unidentified, essential division protein, possibly through residue D227.

Previous work has correlated FtsZ curvature with membrane deformation *in vitro*, suggesting a role in force generation (Osawa *et al.*, 2009). Though other studies indicate FtsZ polymers can occupy a curved conformation *in vivo* (Lu *et al.*, 2000; Li *et al.*, 2007; Li *et al.*, 2013), FtsZ curvature has not previously been linked to an effect on division in cells. Through our combination of *in vivo* phenotypic characterization and biochemical assays, we describe a mutant protein (FzlA^{NH2}) that binds FtsZ, but is incapable of forming helices, and that is associated with severe growth, division, and shape defects. Interestingly, loss of helix formation yielded a range of phenotypes in other mutant strains, from a milder effect on division and constriction rate (*fzlA*^{NH3}), to an inability to complement loss of *fzlA* (*fzlA*^{NH1}). We conclude that, though not strictly essential, FzlA-induced FtsZ curvature is correlated with efficient division. Based on previously described models (Erickson *et al.*, 2010), it is possible that FzlA-mediated FtsZ curvature directly enables constriction through contractile force generation.

It is important to note that the structure of the FzlA-FtsZ complex *in vivo* is currently unknown. That FzlA and FtsZ form helices *in vitro* does not necessarily suggest they form these exact structures *in vivo.* Indeed, highly curved or helical FtsZ polymers have not been observed by cryo-electron tomography (cryo-ET) in *C. crescentus* cells (Li *et al.*, 2007; Szwedziak *et al.*, 2014; Yao *et al.*, 2017). However, it is possible that FzlA and FtsZ do form highly curved structures *in vivo* that have not yet been resolved by cryo-ET since we lack methods for specifically labeling proteins for cryo-ET imaging. Alternatively, or in addition, the highly curved helices observed *in vitro* by TEM may be in a relaxed or unconstrained state; in cells, they may be constrained through membrane attachment to appear less curved (i.e. to follow the curvature of the cell membrane, much like is proposed for crescentin (Cabeen *et al.*, 2009)). Although demonstration of helix formation by TEM does not necessarily indicate helix formation in cells, the properties of FzlA that allow it to promote helix formation *in vitro* are clearly important for its role in promoting constriction in cells.

Our observations also indicate that the interaction of FzlA with FtsZ filaments influences constriction rate, which logically would be mediated through peptidoglycan (PG) metabolism. Recent work has shown that FtsZ dynamics regulate PG synthesis, and that slowing FtsZ turnover by reducing its GTPase rate causes cell envelope morphology defects in *E. coli* and slowed constriction rate in *B. subtilis* (Bisson-Filho *et al.*, 2017; Yang *et al.*, 2017). Our study provides evidence that FtsZ regulates constriction rate in *C. crescentus*, but also suggests that FtsZ polymer structure may be important for this regulation. Interestingly, while mutation of

FzlA lowered the constriction rate (68.4% of WT constriction rate), the cell elongation rate was not altered to the same degree (89.3% of WT elongation rate) (**Fig. 25C**). Partial inactivation of the septal PG transpeptidase FtsI in *E. coli* also leads to a decrease in constriction rate compared to elongation rate (Coltharp *et al.*, 2016) and to formation of pointed cell poles (Taschner *et al.*, 1988; Costa *et al.*, 2008). These data not only confirm that mutation of FzlA has a greater impact on constriction rate over elongation rate, but also suggest a potential genetic link between FzlA and the PG synthase FtsI.

The observation that the cell poles become more "pointy" in the *fzlA*^{NH2} mutant strain indicates that new cell wall material is still being added at the division site, but with a slower decrease in cell diameter than for WT. We can envision at least two possible mechanisms underlying this apparent uncoupling of PG synthesis rate (i.e. elongation rate) and constriction rate. In the first, FzlA influences the enzymatic activity of cell wall enzymes specific to division (e.g. FtsW and FtsI), and when FzlA is mutated to slow the constriction rate, the total activity of these enzymes is reduced. In this case, much of the new material being inserted at midcell must be mediated by the elongasome (e.g. RodA and PBP2) or general PG synthetic enzymes (e.g. the bifunctional PBP family) to maintain the elongation rate. Alternatively, all of the new material being inserted at midcell is synthesized by the divisome in the *fzlA*^{NH2} mutant strain. In this case, the directionality of insertion in a radial direction – but not overall enzymatic activity of PG enzymes in the divisome – requires input from FzlA and FtsZ.

The role of FtsZ in defining the rate of division, as well as the contribution of FtsZ curvature to division, have been longstanding questions in the field. Through mutational analysis, we provide evidence in this study that a regulator of FtsZ curvature, FzlA, affects the rate of constriction for *C. crescentus* cytokinesis. Future work will be aimed at determining if the

FzlA-FtsZ interaction facilitates division through force generation, by communication with PG remodeling enzymes, or a combination of the two.

2.12 Tables

Table 1. Crystallographic data.

	FzlA native	*FzlA mercury derivative*
Components	*Caulobacter crescentus* FzlA	*Caulobacter crescentus* FzlA
GenBank IDs	ACL97219.2	ACL97219.2
UNIPROT	A0A0H3CDY2	A0A0H3CDY2
Data collection		
Beamline	Cu anode	Cu anode
Wavelength [Å]	1.54	1.54
Crystal		
Space group	$I2_13$	$I2_13$
Cell [Å]	124.33	121.77
Scaling		
Resolution [Å]	2.0	3.0
Completeness [%][i]	97.3 (92.6)	99.7 (100.0)
Multiplicity[i]	4.9 (4.7)	11.9 (12.0)
Ano completeness [%][i]		99.6 (100.0)
Ano multiplicity[i]		6.3 (6.2)
Ano correlation[i,ii]		0.285
$I / \sigma I$[i]	7.3 (1.7)	4.1 (0.5)
R_{pim}[i]	0.043 (0.226)	0.081 (0.687)
CC1/2[i, ii]	0.997 (0.857)	0.996 (0.648)
Phasing		
Scatterer / mode		Hg
Number of sites		2
Refinement		
Residues	3-228	
Resolution	2 Å	
R-factor, R-free	0.161, 0.200	
B average[iii]	28.4 Å^2	
Geometry bonds/angles[iv]	0.012 Å, 1.298°	
Ramachandran[v]	97.3%/0.0%	
PDB ID	**5NR1**	

[i] Values in parentheses refer to the highest recorded resolution shell.

[ii] Correlation coefficient between half sets (CCP4 SCALA).

[iii] Temperature factors averaged for all atoms.

[iv] RMS deviations from ideal geometry for bond lengths and restraint angles.

[v] Percentage of residues in the most and additionally favoured regions of the Ramachandran plot and percentage of outliers (CCP4 PROCHECK).

Table 2. FzlA mutant phenotypes and activity.

			P$_{van}$* mChy-mutant *fzlA*, *P$_{xyl}$* *fzlA			**mutant *fzlA* (allelic exchange)**			**High Speed Pellet**	**Low Speed Pellet**		
Mutant Class	**Name**	**Residue Mutations**	**Doubling Time (min)**	**Max OD$_{600}$**	**FzlA Localization**	**Doubling Time (min)**	**Max OD$_{600}$**	**Cell Length (µm)**	**Fold change of FzlA in pellet**	**Fold change of FzlA in pellet**	**% of FtsZ GTPase rate**	**Forms Helices**
WT	FzlA	n/a	131.8 ± 1.3	2.27 ± 0.0024	Midcell	108.4 ± 0.7	1.45 ± 0.03	2.71 ± 0.04	20.43 ± 1.09	11.07 ± 1.22	Trial 1: 60.63 ± 2.65 Trial 2: 48.89 ± 5.51	Y
Weakened **B**inding to FtsZ	FzlA^{WB1}	D109R E122K	135.1 ± 2.1	2.01 ± 0.0409	Diffuse	-	-	-	1.14 ± 0.13*	1.25 ± 0.08*	85.52 ± 5.32	Y
Unknown **N**on-essential activity	FzlA^{UN1}	P131A	143.4 ± 1.6	2.17 ± 0.0053	Midcell	127.3 ± 1.3	1.19 ± 0.0172	3.70 ± 0.1	9.85 ± 0.84	9.86 ± 1.56	55.69 ± 4.28	Y
Unknown **E**ssential activity	FzlA^{UE1}	Y223A D227K F228A	372.4 ± 19.6	0.07 ± 0.0004	Midcell	-	-	-	5.85 ± 0.33	6.10 ± 0.55	77.33 ± 8.05	Y
	FzlA^{UE2}	D227K	284.0 ± 10.0	0.19 ± 0.0206	Midcell	-	-	-	59.02 ± 2.45	12.26 ± 0.33	42.63 ± 4.28	Y
No **B**inding to FtsZ	FzlA^{NB1}	W38A R124D	142.0 ± 1.0	0.79 ± 0.0102	Diffuse	-	-	-	0.91 ± 0.14	1.25 ± 0.15	96.29 ± 6.32	N
	FzlA^{NB2}	E119K	158.9 ± 0.2	0.32 ± 0.0278	Diffuse	-	-	-	1.24 ± 0.05	1.18 ± 0.16	98.90 ± 5.77	N
No **H**elices	FzlA^{NH1}	P131A L136A R137E	146.4 ± 3.0	1.00 ± 0.06	Midcell	-	-	-	2.34 ± 0.22	1.03 ± 0.02	86.25 ± 6.62	N
	FzlA^{NH2}	R140D E141K	142.8 ± 2.0	2.02 ± 0.0208	Midcell	201.6 ± 2.8	0.55 ± 0.0094	4.70 ± 0.15	7.21 ± 0.18	1.30 ± 0.29	84.95 ± 5.65	N
	FzlA^{NH3}	R144D	145.4 ± 2.2	2.14 ± 0.03	Midcell	132.9 ± 4.1	1.28 ± 0.0182	3.43 ± 0.07	3.51 ± 0.05	1.00 ± 0.18	89.05 ± 4.52	N

Values shown as mean ± SEM. For co-pelleting data, values are reported as fold change of % FzlA in pellet alone vs. with FtsZ.
*: FzlA^{WB1} had significant pelleting on its own, making the fold change of FzlA in pellet appear low. However, this mutant still forms helices, indicating it binds FtsZ at least weakly.

Table 3. Additional FzlA mutant phenotype and activity.

			P_{van} mChy-mutant fzlA, P_{xyl} fzlA		
Mutant Class	**Name**	**Residue Mutations**	**Doubling Time (min)**	**Max OD$_{600}$**	**FzlA Localization**
Poor **St**ability	FzlA^{ST1}	E25K	-	-	No signal
	FzlA^{ST2}	R94D E96K R98D	-	-	Diffuse
	FzlA^{ST3}	E151K K188D D189R	-	-	No signal
	FzlA^{ST4}	W159A W196A K199D	-	-	Diffuse
	FzlA^{ST5}	G183W V185A	122.9 ± 2.9	1.85 ± 0.0327	Diffuse
	FzlA^{ST6}	W187A K194E	-	-	Diffuse
	FzlA^{ST7}	K201D S202A R203D P204A	-	-	Diffuse
Poor **Sol**ubility	FzlA^{SOL1}	R20D	-	-	Diffuse
	FzlA^{SOL2}	R99D W103A D105K	-	-	Diffuse
	FzlA^{SOL3}	D109R R127D	133.0 ± 0.7	2.24 ± 0.0355	Diffuse
	FzlA^{SOL4}	E111K H146D	150.9 ± 4.2	0.85 ± 0.0425	Diffuse
	FzlA^{SOL5}	W187A	-	-	Diffuse
	FzlA^{SOL6}	R207D L210A	144.6 ± 0.6	1.63 ± 0.0225	Midcell
WT-like	FzlA^{W1}	P14A	-	-	Midcell
	FzlA^{W2}	R27D E81K E83K	-	-	Midcell
	FzlA^{W3}	K60D H61D R63D	-	-	Midcell
	FzlA^{W4}	R89D D90R	-	-	Midcell
	FzlA^{W5}	K120D D184R	-	-	Midcell
	FzlA^{W6}	D132R	-	-	Midcell
	FzlA^{W7}	L153A R157D	-	-	Midcell

	FzlA^{W8}	D158R R163D R164D	-	-	Midcell
	FzlA^{W9}	D212R R213D	-	-	Midcell
	FzlA^{W10}	P219A H222D	-	-	Midcell
	FzlA^{W11}	F228A	-	-	Midcell
Unknown **N**on-essential activity	FzlA^{UN2}	Y223A	-	-	Midcell

Values shown as mean ± SEM. For co-pelleting data, values are reported as fold change of % FzlA in pellet alone vs. with FtsZ.

2.13 Figures and Legends

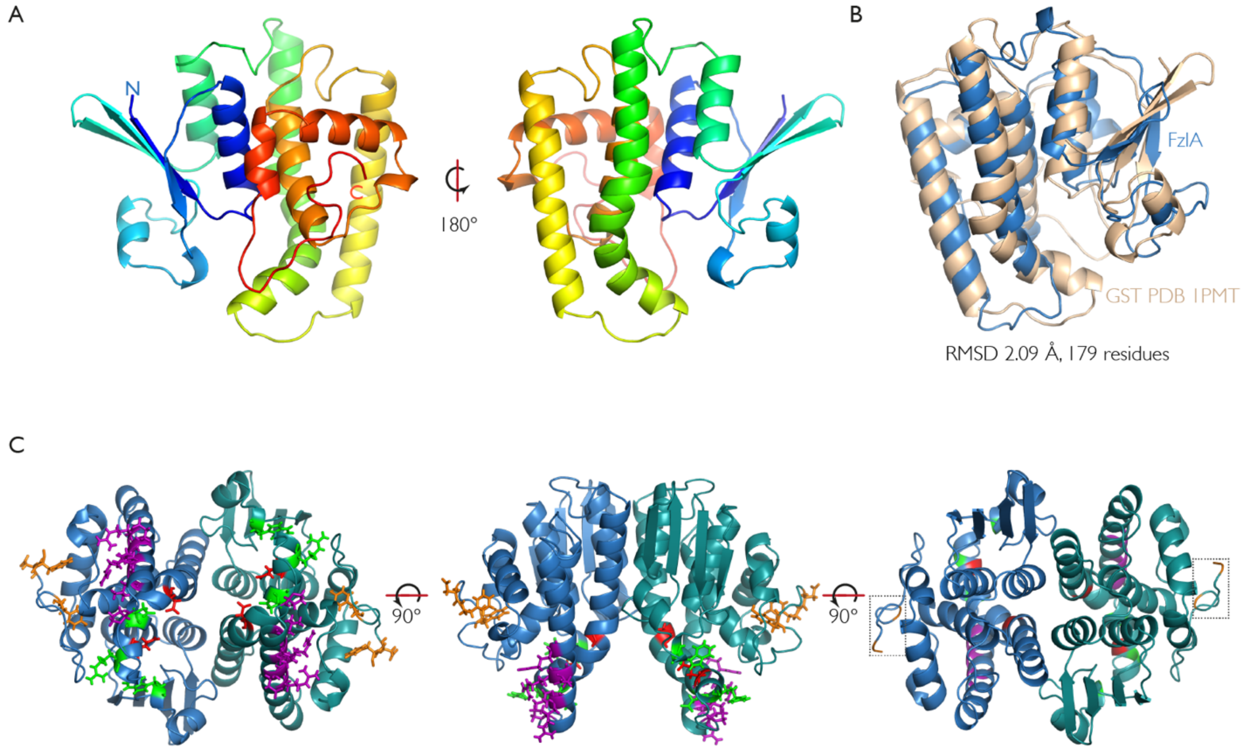

Figure 6. FzlA forms a homodimer in the GST structural family.

(A) Ribbon plot outlining the crystal structure of a FzlA monomer at 2 Å resolution. The structure is shown in rainbow colors from the N-terminus in blue to the C-terminus in red.

(B) A superposition between PDB 1PMT (RMSD of 2.09 Å over 179 Cα atoms) (cream) and FzlA (blue) is shown.

(C) A FzlA dimer with the relevant mutations shown: WB and UN mutations (D109R E122K and P131A) – red; UE mutations (Y223A D227K F228A) – orange; NB mutations (W38A R124D and E119K) – green; NH mutations (P131A L136A R137E, R140D E141K, and R144D) – purple. The C-termini are boxed.

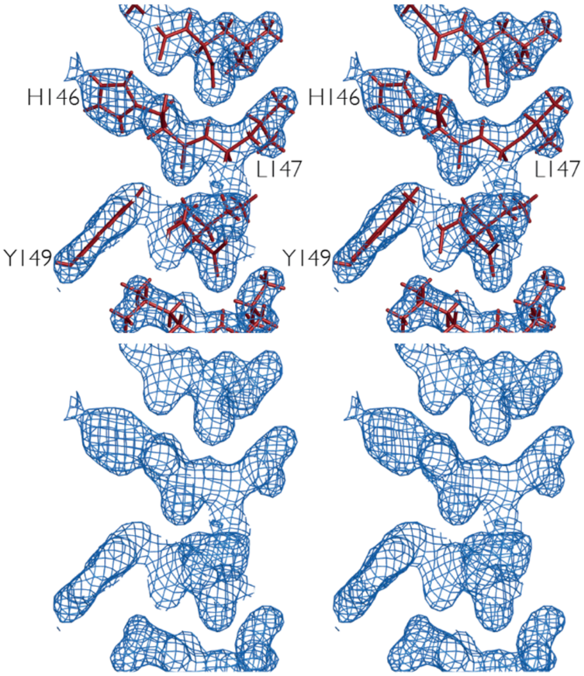

Figure 7. Close-up of a stereo image of the electron density map of FzlA.

Shown are wall-eyed stereo images of the 2Fo-Fc map contoured at the sigma level 1.0. Views of the map with and without fitted atomic model are presented next to each other displaying H146, L147 and Y149.

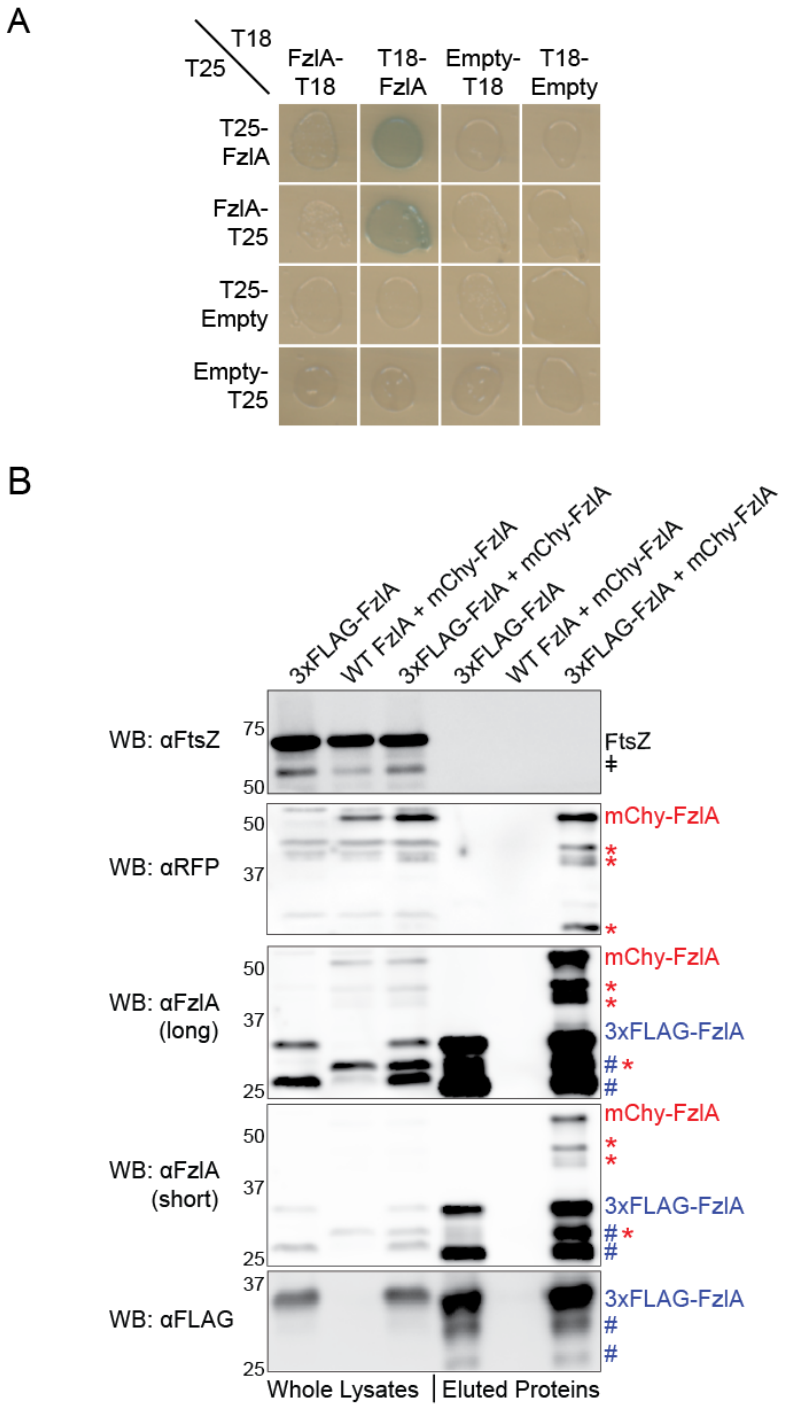
A
T18
T25
FzlA-T18
T18-FzlA
Empty-T18
T18-Empty
T25-FzlA
FzlA-T25
T25-Empty
Empty-T25
B
3xFLAG-FzlA
WT FzlA + mChy-FzlA
3xFLAG-FzlA + mChy-FzlA
3xFLAG-FzlA
WT FzlA + mChy-FzlA
3xFLAG-FzlA + mChy-FzlA
WB: αFtsZ
75
50
FtsZ
ǂ
WB: αRFP
50
37
mChy-FzlA
*
*
*
WB: αFzlA (long)
50
37
25
mChy-FzlA
*
*
3xFLAG-FzlA
# *
#
WB: αFzlA (short)
50
37
25
mChy-FzlA
*
*
3xFLAG-FzlA
# *
#
WB: αFLAG
37
25
3xFLAG-FzlA
#
#
Whole Lysates
Eluted Proteins

Figure 8. FzlA self-interacts *in vivo*.

(A) Cultures of *E. coli* BTH101 strains producing the indicated FzlA fusions or carrying empty vector controls spotted on plates containing IPTG and X-Gal. T18-FzlA interacts with both N- and C-terminal T25 FzlA fusions.

(B) mCherry-FzlA co-immunoprecipitates with 3xFLAG-FzlA from *C. crescentus* cell lysates. Western blot analysis of whole cell lysates of strains producing the indicated FzlA variants (left) and eluates from samples of the same strains obtained by immunoprecipitation with α-FLAG resin and elution with FLAG peptide (right). Cultures were grown to log phase and induced for 1hr with vanillate before preparation of lysates and immunoprecipitation. Antibodies used for western blotting (WB) are indicated to the left of the blots. Long=longer exposure. Short = shorter exposure. ‡ = FtsZ degradation product. Red = mCherry-FzlA derived species. * = mCherry-FzlA degradation products. Blue = 3xFLAG-FzlA derived species. # = 3xFLAG-FzlA degradation products. mChy = mCherry. Strain key: 3xFLAG-FzlA (EG2217), WT FzlA + mChy-FzlA (EG2451), 3xFLAG-FzlA+ mChy-FzlA (EG2452).

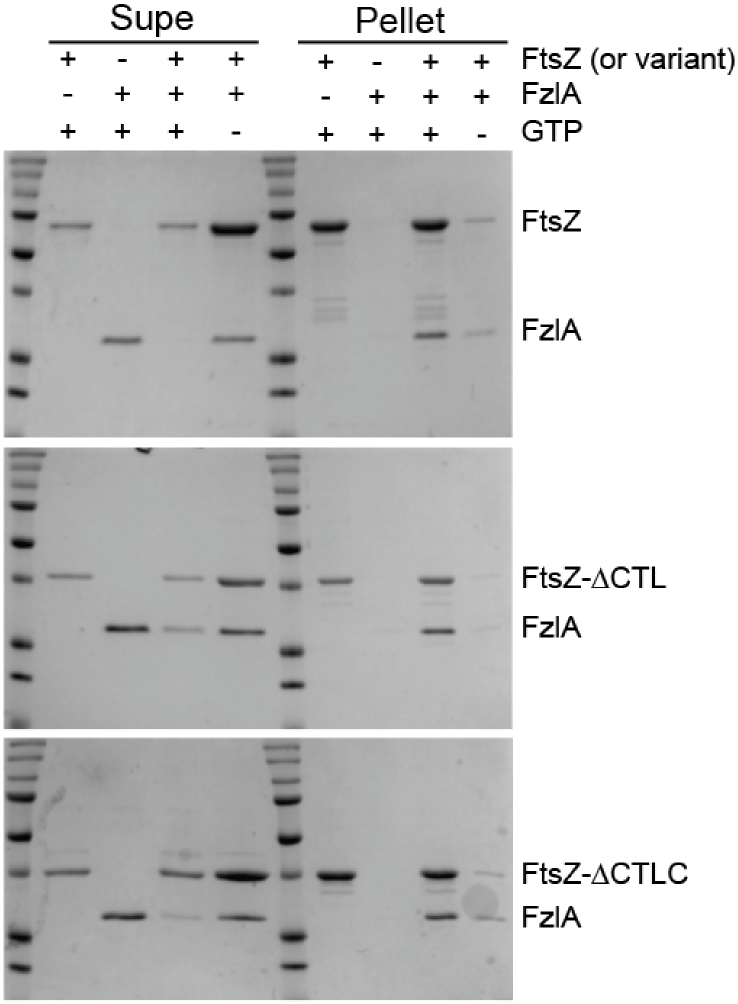

Supe
Pellet
+ - + + + - + + FtsZ (or variant)
- + + + - + + + FzlA
+ + + - + + + - GTP
FtsZ
FzlA
FtsZ-ΔCTL
FzlA
FtsZ-ΔCTLC
FzlA

Figure 9. FzlA Interacts with the GTPase domain of FtsZ.

Coomassie-stained SDS-PAGE gels of supernatant and pellet fractions from high-speed co-sedimentation assays of 3 μM His$_6$-FzlA + 3 μM FtsZ (top), 3 μM FtsZΔCTL (middle), and 3 μM FtsZΔCTLC (bottom). Both His$_6$-FzlA and each FtsZ variant are preferentially recruited to the pellet in the presence of GTP. Reactions were performed in HEK50 polymerization buffer (50 mM HEPES-KOH [pH 7.2], 50 mM KCl, 0.1 mM EDTA) with 2 mM GTP, 2.5 mM $MgCl_2$, and 0.05% Triton X-100.

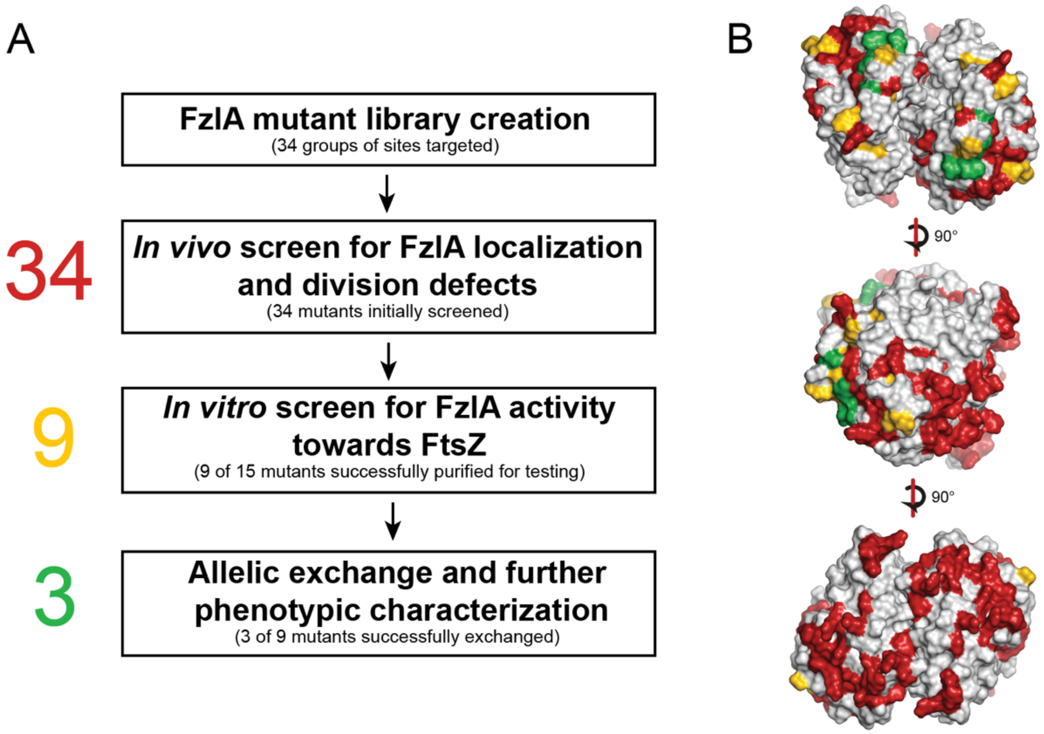
A
B
FzlA mutant library creation
(34 groups of sites targeted)
34
In vivo screen for FzlA localization and division defects
(34 mutants initially screened)
9
In vitro screen for FzlA activity towards FtsZ
(9 of 15 mutants successfully purified for testing)
3
Allelic exchange and further phenotypic characterization
(3 of 9 mutants successfully exchanged)
90°
90°

Figure 10. Structure-function analysis workflow.

(A) A list of conserved, charged, and surface exposed residues were identified from the FzlA structure as potential sites of interaction with FtsZ. A library of non-conservative point mutants of 34 groups of residues was made in which the mutant proteins were fused to mCherry, with expression driven by a vanillate inducible promoter. These constructs were placed in a background where WT FzlA expression was controlled by xylose. We depleted these cells of WT FzlA and induced with vanillate, then screened for mCherry-FzlA localization and division defects using fluorescence microscopy, growth rate analysis, and spot dilution. Twenty-five mutant genes were either associated with wild-type looking strains or yielded protein that was unstable *in vivo* or insoluble *in vitro*, so were not further characterized. Nine mutant proteins associated with strains displaying a range of FzlA localization and division phenotypes were soluble when purified. We screened these mutant proteins for activity towards FtsZ *in vitro*, using co-pelleting, right-angle light scattering (RALS), and transmission electron microscopy (TEM). We successfully performed allelic exchange on three of these nine mutant alleles, and further characterized their phenotypes by assessing cell length, shape, constriction rate, and elongation rate.

(B) Dimer of FzlA showing sites originally targeted for *in vivo* screening (red), sites tested biochemically (yellow), and sites that allowed for allelic exchange (green).

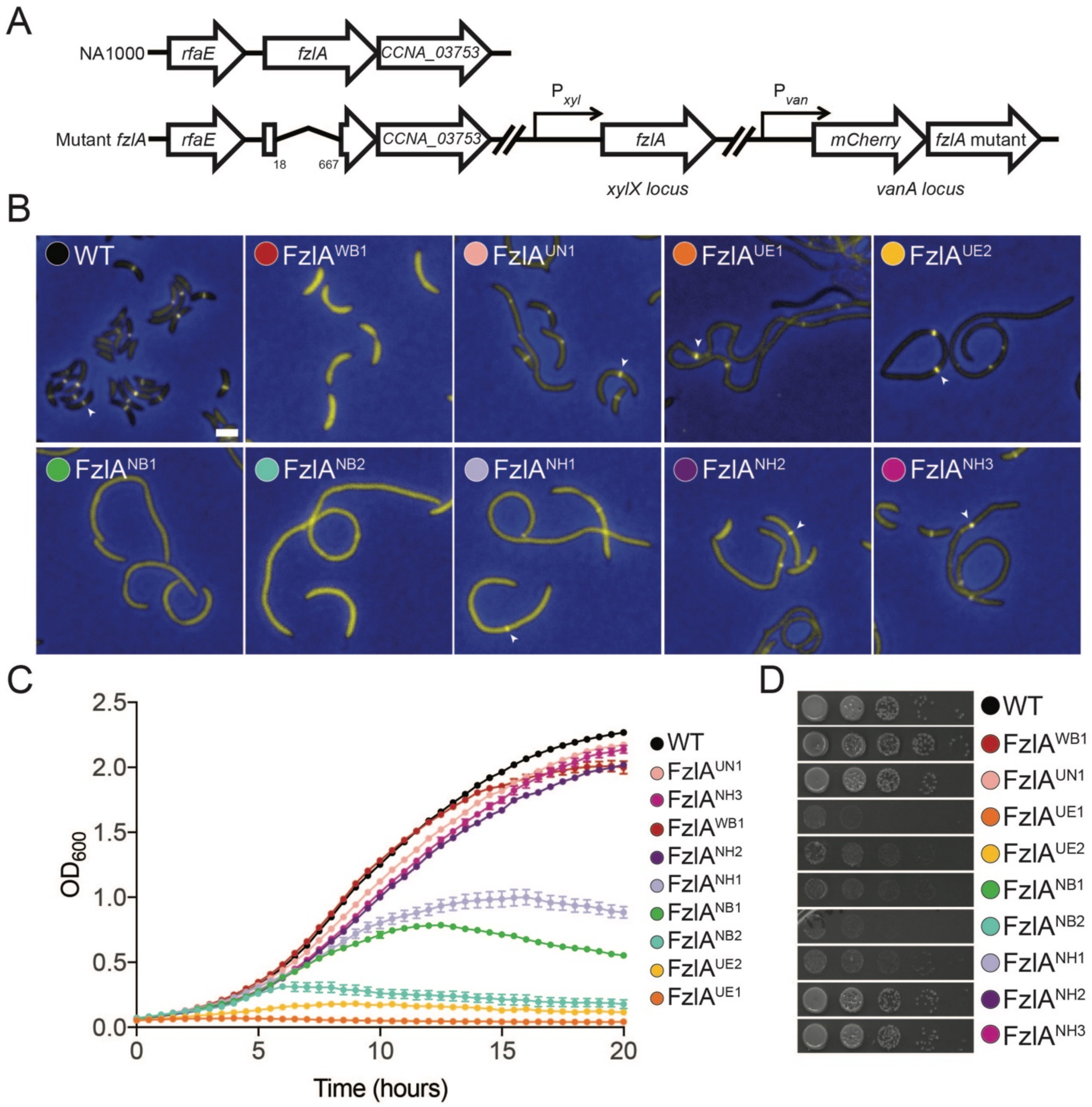

Figure 11. *fzlA* mutant strains display a range of division and localization deficiencies.

(A) Cartoon depicting genetic backgrounds for *in vivo* testing. In these strains, *fzlA* has been deleted at the native locus and a xylose-inducible copy of *fzlA* is at the *xylX* locus. A vanillate-inducible copy of the *mCherry-fzlA* variant is integrated at the *vanA* locus.

(B) Merged fluorescence and phase contrast microscopy images depicting mCherry-FzlA mutant protein (yellow) localization in cells depleted of WT FzlA and grown with vanillate to induce the indicated mCherry-FzlA variant for 24 hours prior to imaging. White arrowheads mark localized FzlA bands. Scale bar = 2 µm.

(C) Growth curves of the same strains as in (B) grown with vanillate and depleted of WT FzlA for 24 hours prior to the start of the experiment. Mean of three technical replicates ± SEM is shown.

(D) Spot dilutions of strains as in (B), plated on PYE agar with vanillate, without pre-depletion of WT FzlA. Strain key: WT (EG1310), FzlA$^{\mathrm{WB1}}$ (EG1435), FzlA$^{\mathrm{UN1}}$ (EG1312), FzlA$^{\mathrm{UE1}}$ (EG1313), FzlA$^{\mathrm{UE2}}$ (EG1621), FzlA$^{\mathrm{NB1}}$ (EG1430), FzlA$^{\mathrm{NB2}}$ (EG1438), FzlA$^{\mathrm{NH1}}$ (EG1311), FzlA$^{\mathrm{NH2}}$ (EG1441), FzlA$^{\mathrm{NH3}}$ (EG1442).

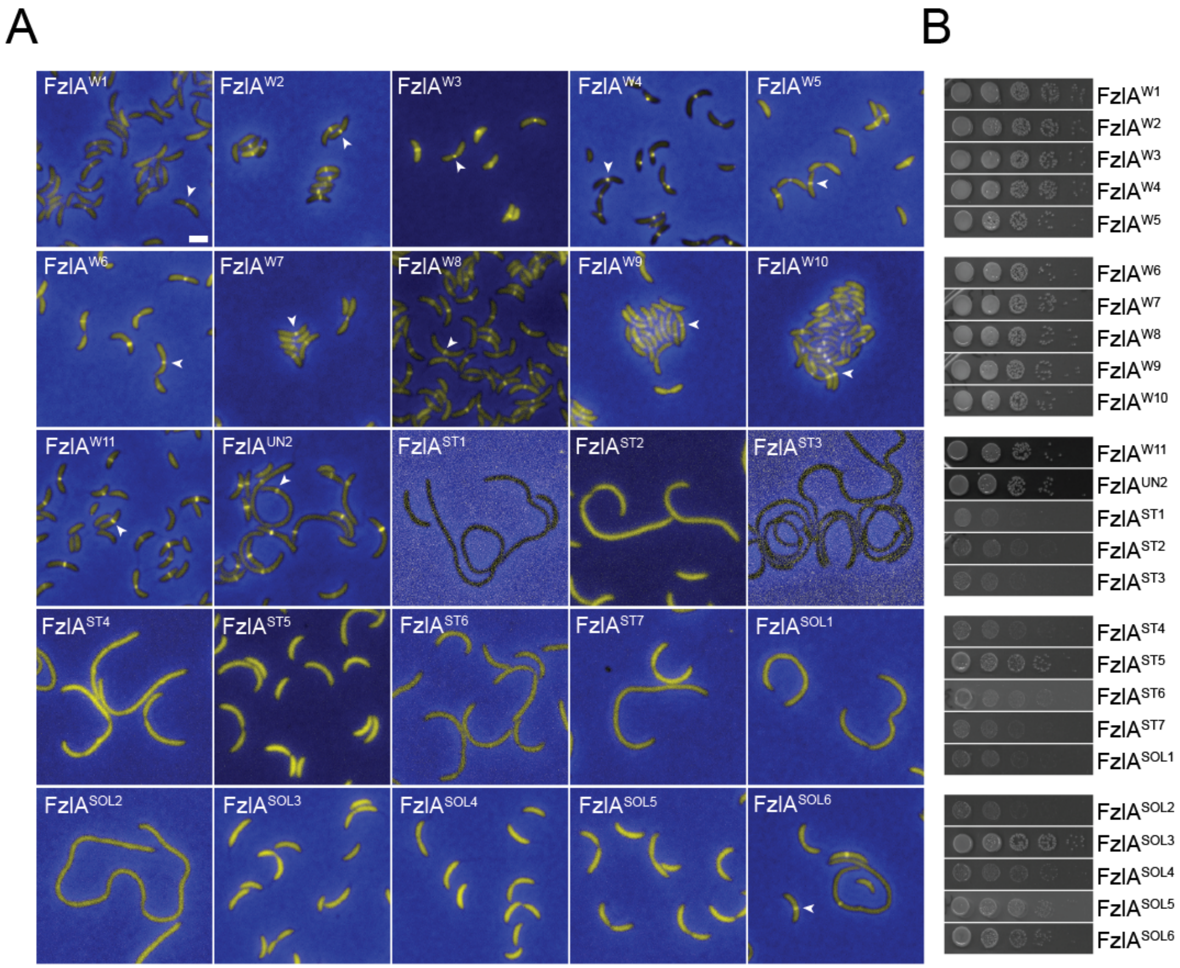
A
B
FzlA^W1
FzlA^W2
FzlA^W3
FzlA^W4
FzlA^W5
FzlA^W6
FzlA^W7
FzlA^W8
FzlA^W9
FzlA^W10
FzlA^W11
FzlA^UN2
FzlA^ST1
FzlA^ST2
FzlA^ST3
FzlA^ST4
FzlA^ST5
FzlA^ST6
FzlA^ST7
FzlA^SOL1
FzlA^SOL2
FzlA^SOL3
FzlA^SOL4
FzlA^SOL5
FzlA^SOL6

Figure 12. Many *fzlA* mutant strains displayed wild-type phenotypes or were unstable or insoluble.

(A) Merged fluorescence microscopy images depicting mCherry-FzlA mutant protein (yellow) localization in cells in Δ*fzlA* P_{xyl}-*fzlA* P_{van}-*mCherry-fzlA* mutant backgrounds (labels indicate mutant alleles fused to mCherry, with expression driven by P_{van}). Cells were depleted of WT FzlA and grown with vanillate for 24 hours prior to imaging. White arrowheads mark localized FzlA bands. Scale bar = 2 µm.

(B) Spot dilutions of Δ*fzlA* P_{xyl}-*fzlA*, P_{van}-*mCherry-fzlA* mutant strains, plated on PYE-agar with vanillate. Strain key: FzlA^{W1} (EG1426), FzlA^{W2} (EG1428), FzlA^{W3} (EG1431), FzlA^{W4}

(EG1432), FzlA^{W5} (EG1439), FzlA^{W6} (EG1440), FzlA^{W7} (EG1443), FzlA^{W8} (EG1444), FzlA^{W9} (EG1455), FzlA^{W10} (EG1456), FzlA^{W11} (EG2304), FzlA^{UN2} (EG2302), FzlA^{ST1} (EG1429), FzlA^{ST2} (EG1433), FzlA^{ST3} (EG1454), FzlA^{ST4} (EG1450), FzlA^{ST5} (EG1451), FzlA^{ST6} (EG1314), FzlA^{ST7} (EG1452), FzlA^{SOL1} (EG1427), FzlA^{SOL2} (EG1434), FzlA^{SOL3} (EG1436), FzlA^{SOL4} (EG1437), FzlA^{SOL5} (EG1315), FzlA^{SOL6} (EG1453).

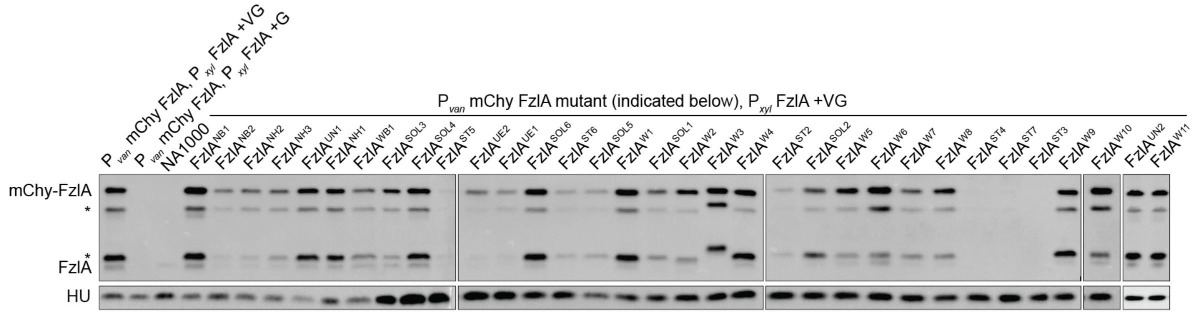
P$_{van}$ mChy FzlA, P$_{xyl}$ FzlA +VG
P$_{van}$ mChy FzlA, P$_{xyl}$ FzlA +G
NA1000
P$_{van}$ mChy FzlA mutant (indicated below), P$_{xyl}$ FzlA +VG
FzlA^{NB1}
FzlA^{NB2}
FzlA^{NH2}
FzlA^{NH3}
FzlA^{UN1}
FzlA^{NH1}
FzlA^{WB1}
FzlA^{SOL3}
FzlA^{SOL4}
FzlA^{ST5}
FzlA^{UE2}
FzlA^{UE1}
FzlA^{SOL6}
FzlA^{ST6}
FzlA^{SOL5}
FzlA^{W1}
FzlA^{SOL1}
FzlA^{W2}
FzlA^{W3}
FzlA^{W4}
FzlA^{ST2}
FzlA^{SOL2}
FzlA^{W5}
FzlA^{W6}
FzlA^{W7}
FzlA^{W8}
FzlA^{ST4}
FzlA^{ST7}
FzlA^{ST3}
FzlA^{W9}
FzlA^{W10}
FzlA^{UN2}
FzlA^{W11}
mChy-FzlA
*
*
FzlA
HU

Figure 13. Protein levels of mCherry-FzlA under induction conditions.

α-FzlA (top) and α-HU (bottom, loading control) immunoblot of Δ*fzlA* P$_{xyl}$-*fzlA* P$_{van}$-*mCherry-fzlA* mutant strain lysates depleted of WT FzlA and grown for 24 hours with vanillate and glucose. *=degradation product. V = vanillate, G = glucose. The strain containing *mCherry-fzlA*^{ST1} was severely sick and did not reach log phase in 24 hours. It was therefore not included in immunoblot analysis. Strain key: P$_{van}$ mChy FzlA, P$_{xyl}$ FzlA (EG1310), FzlA^{NB1} (EG1430), FzlA^{NB2} (EG1438), FzlA^{NH2} (EG1441), FzlA^{NH3} (EG1442), FzlA^{UN1} (EG1312), FzlA^{NH1} (EG1311), FzlA^{WB1} (EG1435), FzlA^{SOL3} (EG1436), FzlA^{SOL4} (EG1437), FzlA^{ST5} (EG1451), FzlA^{UE2} (EG1621), FzlA^{UE1} (EG1313), FzlA^{SOL6} (EG1453), FzlA^{ST6} (EG1314), FzlA^{SOL5} (EG1315), FzlA^{W1} (EG1426), FzlA^{SOL1} (EG1427), FzlA^{W2} (EG1428), FzlA^{W3} (EG1431), FzlA^{W4} (EG1432), FzlA^{ST2} (EG1433), FzlA^{SOL2} (EG1434), FzlA^{W5} (EG1439), FzlA^{W6} (EG1440), FzlA^{W7} (EG1443), FzlA^{W8} (EG1444), FzlA^{ST4} (EG1450), FzlA^{ST7} (EG1452), FzlA^{ST3} (EG1454), FzlA^{W9} (EG1455), FzlA^{W10} (EG1456), FzlA^{UN2} (EG2302), FzlA^{W11} (EG2304).

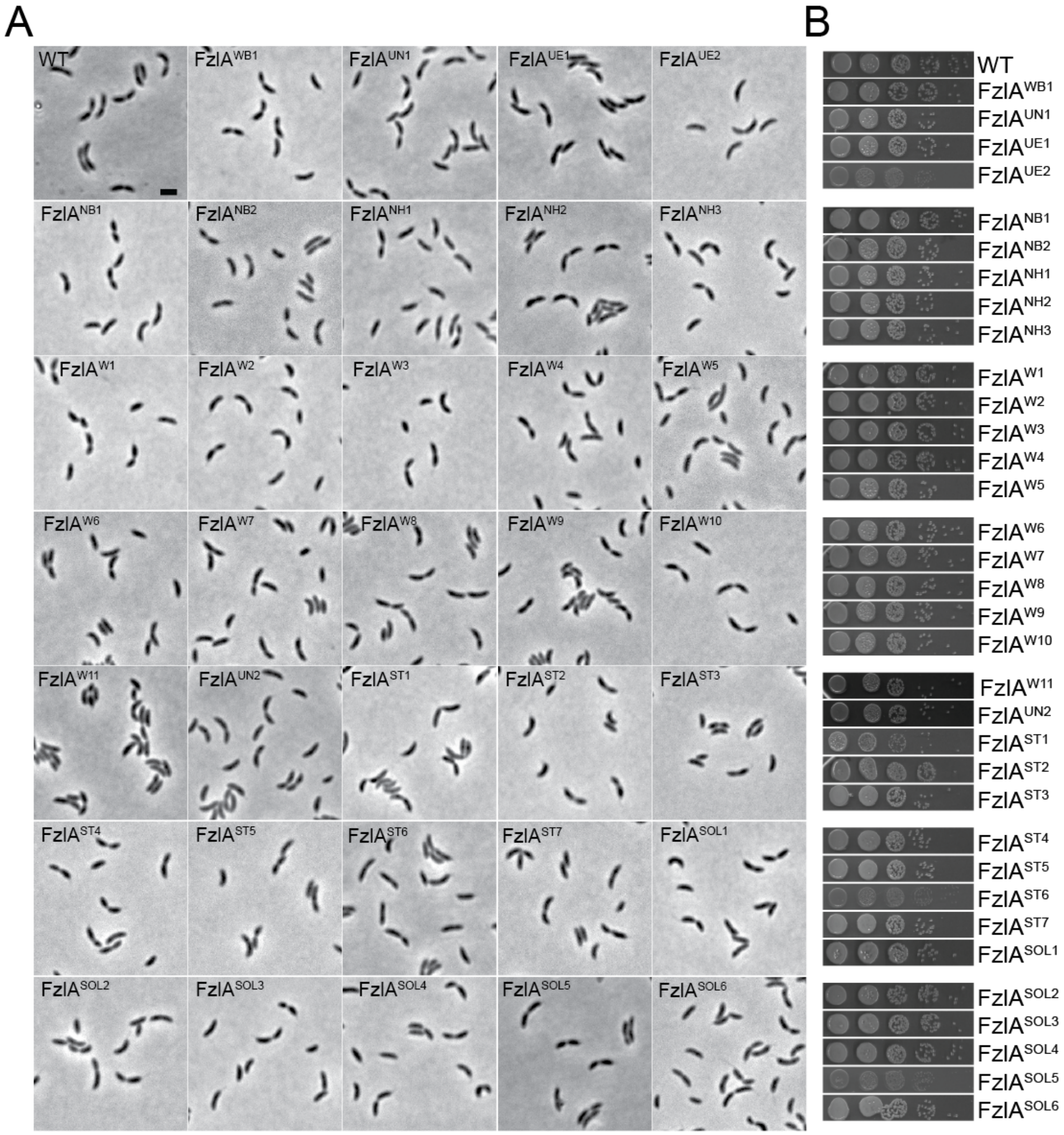
A
B
WT
FzlA^{WB1}
FzlA^{UN1}
FzlA^{UE1}
FzlA^{UE2}
FzlA^{NB1}
FzlA^{NB2}
FzlA^{NH1}
FzlA^{NH2}
FzlA^{NH3}
FzlA^{W1}
FzlA^{W2}
FzlA^{W3}
FzlA^{W4}
FzlA^{W5}
FzlA^{W6}
FzlA^{W7}
FzlA^{W8}
FzlA^{W9}
FzlA^{W10}
FzlA^{W11}
FzlA^{UN2}
FzlA^{ST1}
FzlA^{ST2}
FzlA^{ST3}
FzlA^{ST4}
FzlA^{ST5}
FzlA^{ST6}
FzlA^{ST7}
FzlA^{SOL1}
FzlA^{SOL2}
FzlA^{SOL3}
FzlA^{SOL4}
FzlA^{SOL5}
FzlA^{SOL6}

Figure 14. ***fzlA*** **mutant strains grown with xylose to induce WT FzlA grow normally.**

(A) Phase contrast images depicting mutant cells with Δ*fzlA* P_{xyl}-*fzlA* P_{van}-*mCherry-fzlA* mutant backgrounds. Cells were grown with xylose. Scale bar = 2 μm.

(B) Spot dilutions of Δ*fzlA* P_{xyl}-*fzlA* P_{van}-*mCherry-fzlA* mutant strains, plated on PYE-agar with xylose. Strain key: WT (NA1000), FzlA^{WB1} (EG1435), FzlA^{UN1} (EG1312), FzlA^{UE1} (EG1313), FzlA^{UE2} (EG1621), FzlA^{NB1} (EG1430), FzlA^{NB2} (EG1438), FzlA^{NH1} (EG1311), FzlA^{NH2} (EG1441), FzlA^{NH3} (EG1442), FzlA^{W1} (EG1426), FzlA^{W2} (EG1428), FzlA^{W3} (EG1431), FzlA^{W4} (EG1432), FzlA^{W5} (EG1439), FzlA^{W6} (EG1440), FzlA^{W7} (EG1443), FzlA^{W8} (EG1444), FzlA^{W9} (EG1455), FzlA^{W10} (EG1456), FzlA^{W11} (EG2304), FzlA^{UN2} (EG2302), FzlA^{ST1} (EG1429), FzlA^{ST2} (EG1433), FzlA^{ST3} (EG1454), FzlA^{ST4} (EG1450), FzlA^{ST5} (EG1451), FzlA^{ST6} (EG1314), FzlA^{ST7} (EG1452), FzlA^{SOL1} (EG1427), FzlA^{SOL2} (EG1434), FzlA^{SOL3} (EG1436), FzlA^{SOL4} (EG1437), FzlA^{SOL5} (EG1315), FzlA^{SOL6} (EG1453).

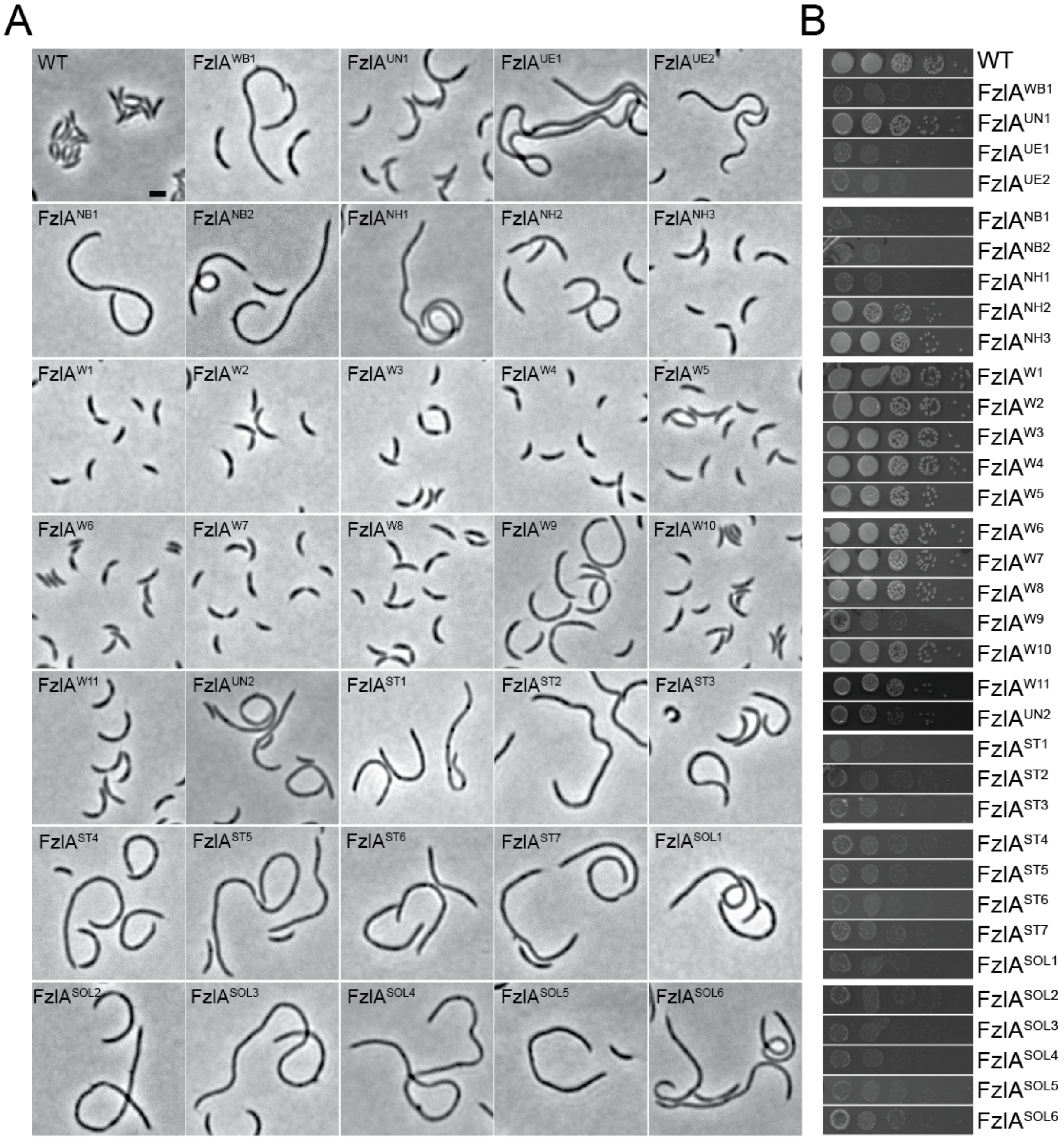
A
B
WT
FzlA^{WB1}
FzlA^{UN1}
FzlA^{UE1}
FzlA^{UE2}
FzlA^{NB1}
FzlA^{NB2}
FzlA^{NH1}
FzlA^{NH2}
FzlA^{NH3}
FzlA^{W1}
FzlA^{W2}
FzlA^{W3}
FzlA^{W4}
FzlA^{W5}
FzlA^{W6}
FzlA^{W7}
FzlA^{W8}
FzlA^{W9}
FzlA^{W10}
FzlA^{W11}
FzlA^{UN2}
FzlA^{ST1}
FzlA^{ST2}
FzlA^{ST3}
FzlA^{ST4}
FzlA^{ST5}
FzlA^{ST6}
FzlA^{ST7}
FzlA^{SOL1}
FzlA^{SOL2}
FzlA^{SOL3}
FzlA^{SOL4}
FzlA^{SOL5}
FzlA^{SOL6}

Figure 15. *fzlA* mutant strains grown without inducers display a range of growth phenotypes that correlate with their activities in the presence of vanillate.

(A) Phase contrast images depicting mutant cells with Δ*fzlA* P$_{xyl}$-*fzlA* P$_{van}$-*mCherry-fzlA* mutant backgrounds. Cells were grown without inducers and with glucose to repress the P$_{xyl}$ promoter for 24 hours prior to imaging. (FzlA^{ST1} cells displayed severe growth defects and did not reach log phase in 24 hours. These cells were imaged after 48 hours.) Scale bar = 2 µm. Note that for WT cells and strains with mutant *fzlA* genes that support division, leaky expression from the P_{van} promoter is sufficient to support growth.

(B) Spot dilutions of Δ*fzlA* P_{xyl}-*fzlA* P_{van}-*mCherry-fzlA* mutant strains, plated on PYE-ager with glucose and without inducers. Strain key: WT (NA1000), $FzlA^{WB1}$ (EG1435), $FzlA^{UN1}$ (EG1312), $FzlA^{UE1}$ (EG1313), $FzlA^{UE2}$ (EG1621), $FzlA^{NB1}$ (EG1430), $FzlA^{NB2}$ (EG1438), $FzlA^{NH1}$ (EG1311), $FzlA^{NH2}$ (EG1441), $FzlA^{NH3}$ (EG1442), $FzlA^{W1}$ (EG1426), $FzlA^{W2}$ (EG1428), $FzlA^{W3}$ (EG1431), $FzlA^{W4}$ (EG1432), $FzlA^{W5}$ (EG1439), $FzlA^{W6}$ (EG1440), $FzlA^{W7}$ (EG1443), $FzlA^{W8}$ (EG1444), $FzlA^{W9}$ (EG1455), $FzlA^{W10}$ (EG1456), $FzlA^{W11}$ (EG2304), $FzlA^{UN2}$ (EG2302), $FzlA^{ST1}$ (EG1429), $FzlA^{ST2}$ (EG1433), $FzlA^{ST3}$ (EG1454), $FzlA^{ST4}$ (EG1450), $FzlA^{ST5}$ (EG1451), $FzlA^{ST6}$ (EG1314), $FzlA^{ST7}$ (EG1452), $FzlA^{SOL1}$ (EG1427), $FzlA^{SOL2}$ (EG1434), $FzlA^{SOL3}$ (EG1436), $FzlA^{SOL4}$ (EG1437), $FzlA^{SOL5}$ (EG1315), $FzlA^{SOL6}$ (EG1453).

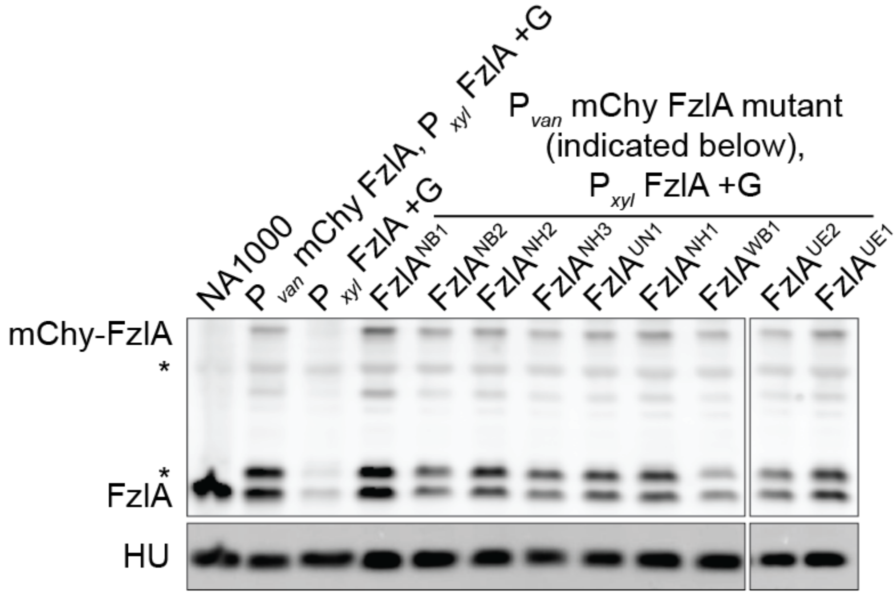
NA1000
P van mChy FzlA, P xyl FzlA +G
P xyl FzlA +G
P van mChy FzlA mutant (indicated below), P xyl FzlA +G
FzlA^NB1
FzlA^NB2
FzlA^NH2
FzlA^NH3
FzlA^UN1
FzlA^NH1
FzlA^WB1
FzlA^UE2
FzlA^UE1
mChy-FzlA
*
*
FzlA
HU

Figure 16. Protein levels of mCherry-FzlA under depletion conditions.

α-FzlA (top) and α-HU (bottom, loading control) immunoblot of Δ*fzlA* P_{xyl}-*fzlA* P_{van}-*mCherry-fzlA* mutant strain lysates depleted of WT FzlA and grown for 24 hours with glucose. *=degradation product. G = glucose. Only strains that were biochemically characterized are shown. Strain key: NA1000 (WT), P_{van} mChy FzlA, P_{xyl} FzlA (EG1310), P_{xyl} FzlA (EG312), FzlA^{NB1} (EG1430), FzlA^{NB2} (EG1438), FzlA^{NH2} (EG1441), FzlA^{NH3} (EG1442), FzlA^{UN1} (EG1312), FzlA^{NH1} (EG1311), FzlA^{WB1} (EG1435),), FzlA^{UE2} (EG1621), FzlA^{UE1} (EG1313).

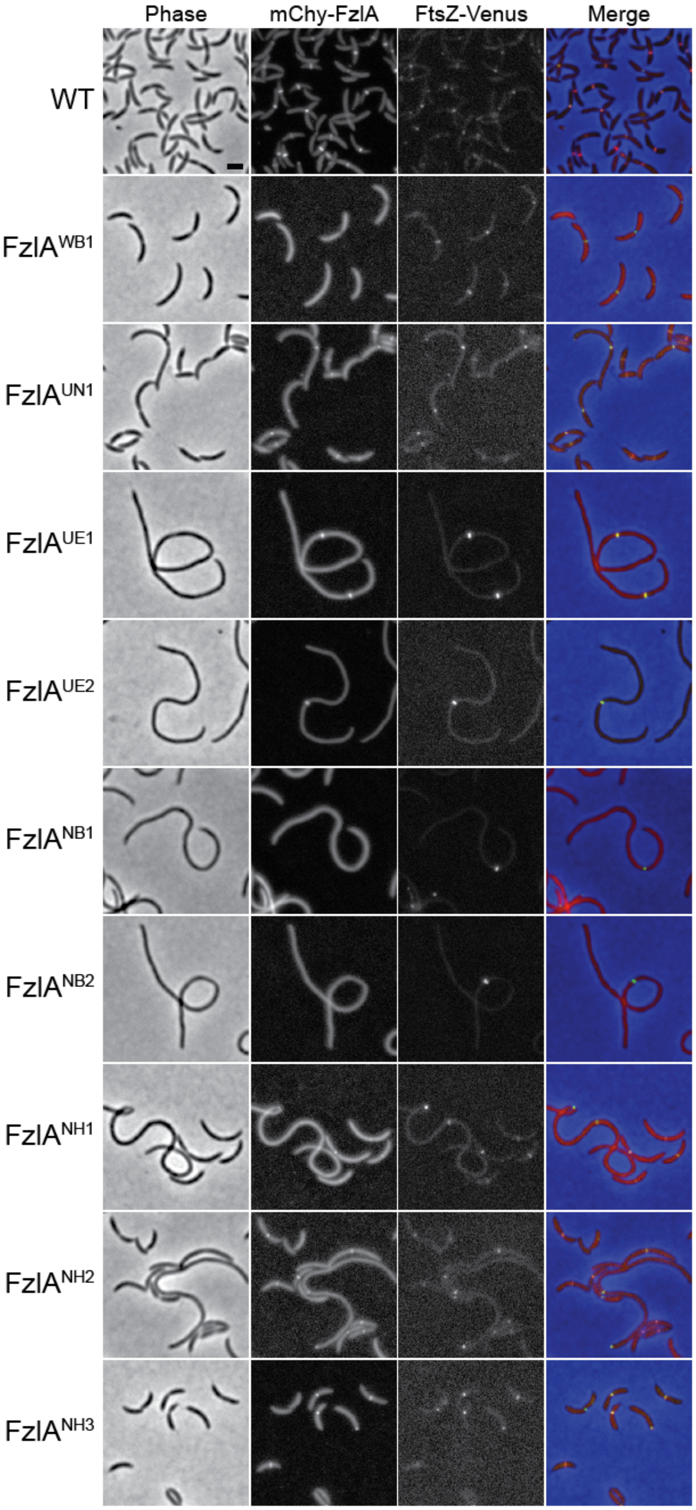
Phase
mChy-FzlA
FtsZ-Venus
Merge
WT
FzlA^{WB1}
FzlA^{UN1}
FzlA^{UE1}
FzlA^{UE2}
FzlA^{NB1}
FzlA^{NB2}
FzlA^{NH1}
FzlA^{NH2}
FzlA^{NH3}

Figure 17. FtsZ forms rings in cells expressing *fzlA* mutant alleles.

Merged fluorescence microscopy images depicting mCherry-FzlA mutant protein (red) and FtsZ-Venus (green) localization in cells with Δ*fzlA* P_{xyl}-*fzlA* P_{van}-*mCherry-fzlA* mutant backgrounds that carry a low copy plasmid containing P_{lac}-FtsZ-Venus. Cells were depleted of WT FzlA and grown with vanillate for 24 hours prior to imaging. IPTG was not added as we found that leaky expression was sufficient for low levels of FtsZ-Venus expression. Yellow indicates co-localization of mCherry-FzlA and FtsZ-Venus. Scale bar = 2 μm. Strain key: WT (EG1760), FzlA^{WB1} (EG1762), FzlA^{UN1} (EG1628), FzlA^{UE1} (EG1767), FzlA^{UE2} (EG1766), FzlA^{NB1} (EG1761), FzlA^{NB2} (EG1765), FzlA^{NH1} (EG1770), FzlA^{NH2} (EG1629), FzlA^{NH3} (EG1768).

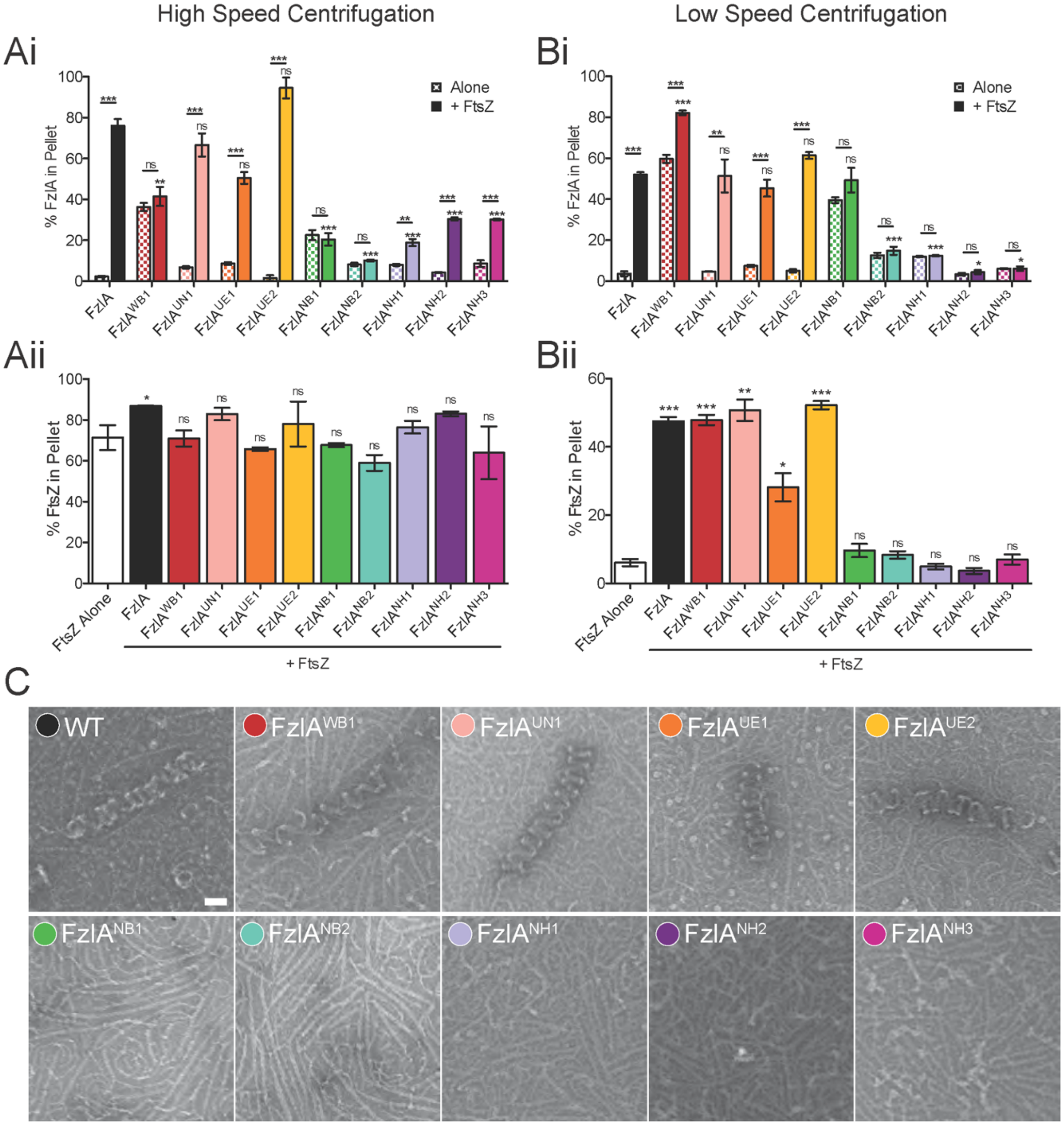

Figure 18. FtsZ binding and/or helix formation is perturbed for a number of FzlA mutant proteins.

(A-B) Quantification of the percent of WT or mutant FzlA protein (i) or FtsZ (ii) found in the pellet after high speed (A) and low speed (B) centrifugation of 4 μM FzlA variant ± 2 μM FtsZ under polymerizing conditions. Mean ± SEM is shown. For WT controls (FzlA alone, FtsZ alone, and FtsZ + FzlA), representative experiments in triplicate are shown, as these controls were run numerous times. For (i), unpaired t-tests were performed to analyze the difference between a given FzlA mutant protein alone vs. with FtsZ. Either unpaired t-tests or a one way ANOVA with Dunnett's multiple comparison test was performed to assess differences between each FzlA mutant protein + FtsZ and WT FzlA + FtsZ (lower asterisks), depending on the number of mutants in a particular run. For (ii), a one way ANOVA with Dunnett's multiple comparison test was performed to assess differences between WT FzlA or mutant FzlA + FtsZ vs. FtsZ alone. For all statistical tests, $^{ns}P>0.05$, $^{*}P\leq0.05$, $^{**}P\leq0.01$, $^{***}P\leq0.001$ and n=3 for each sample. For the Commassie-blue SDS-PAGE gels from which pelleting data is drawn, see the supporting information.

(C) Negative stain TEM images of 4 µM FzlA variant + 2 µM FtsZ under polymerizing conditions. Scale bar = 50 nm.

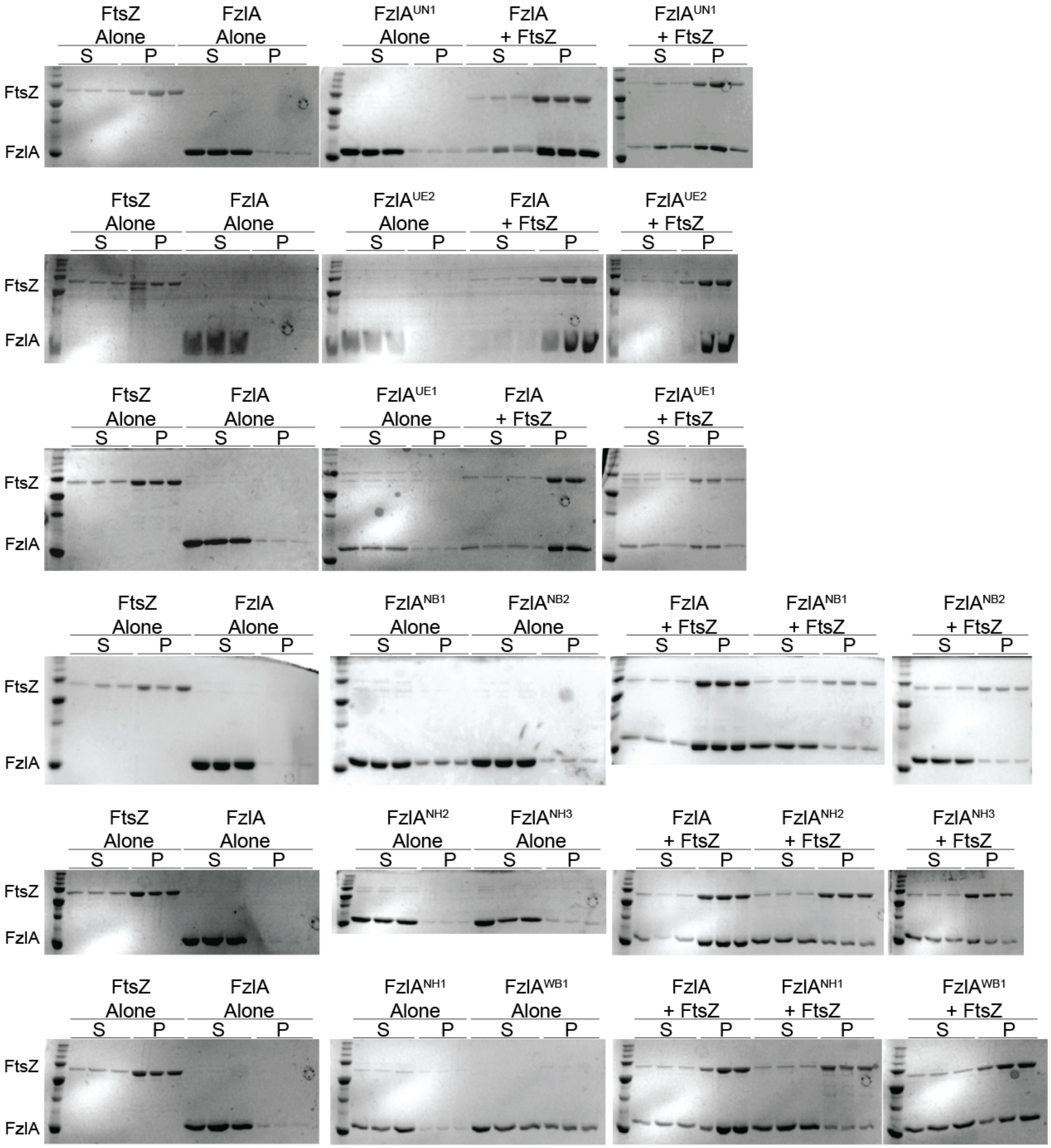
FtsZ Alone
FzlA Alone
FzlA^UN1 Alone
FzlA + FtsZ
FzlA^UN1 + FtsZ
FzlA^UE2 Alone
FzlA^UE2 + FtsZ
FzlA^UE1 Alone
FzlA^UE1 + FtsZ
FzlA^NB1 Alone
FzlA^NB2 Alone
FzlA^NB1 + FtsZ
FzlA^NB2 + FtsZ
FzlA^NH2 Alone
FzlA^NH3 Alone
FzlA^NH2 + FtsZ
FzlA^NH3 + FtsZ
FzlA^NH1 Alone
FzlA^WB1 Alone
FzlA^NH1 + FtsZ
FzlA^WB1 + FtsZ
S
P
FtsZ
FzlA

Figure 19. High speed co-pelleting of FzlA mutant proteins and FtsZ.

Coomassie-blue stained SDS-PAGE gels of FtsZ (2 µM) and FzlA mutant proteins (4 µM) that have been co-sedimented at high speed under polymerizing conditions, used for quantification (main text). S=supernatant, P=pellet. Experiments performed in triplicate, as shown. Each row shows samples run on the same day. Control experiments with FtsZ and WT FzlA were run each time for comparison to different FzlA mutants and to control for day-to-day variations.

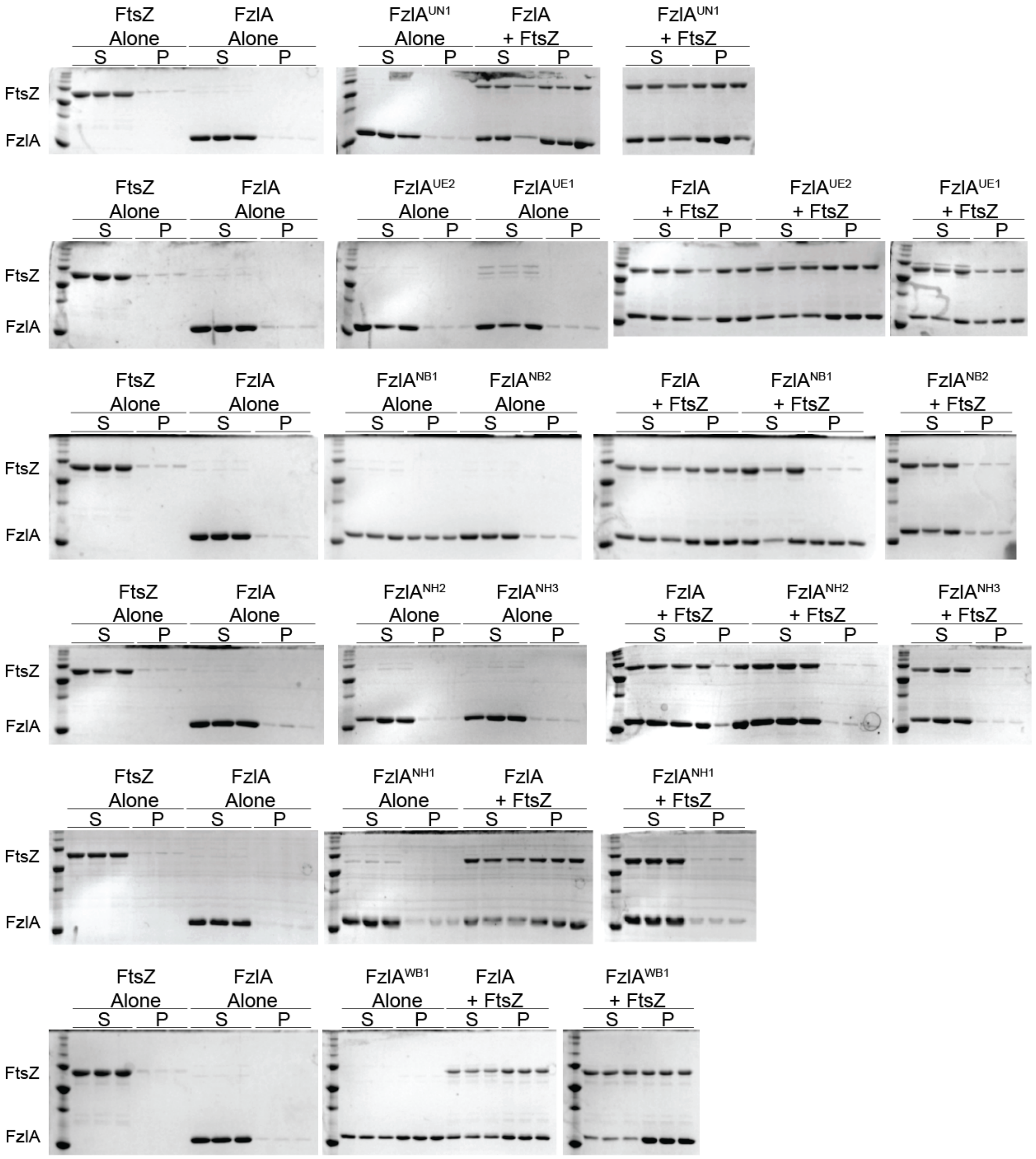
FtsZ Alone
FzlA Alone
FzlA^{UN1} Alone
FzlA + FtsZ
FzlA^{UN1} + FtsZ
S
P
FtsZ
FzlA
FtsZ Alone
FzlA Alone
FzlA^{UE2} Alone
FzlA^{UE1} Alone
FzlA + FtsZ
FzlA^{UE2} + FtsZ
FzlA^{UE1} + FtsZ
S
P
FtsZ
FzlA
FtsZ Alone
FzlA Alone
FzlA^{NB1} Alone
FzlA^{NB2} Alone
FzlA + FtsZ
FzlA^{NB1} + FtsZ
FzlA^{NB2} + FtsZ
S
P
FtsZ
FzlA
FtsZ Alone
FzlA Alone
FzlA^{NH2} Alone
FzlA^{NH3} Alone
FzlA + FtsZ
FzlA^{NH2} + FtsZ
FzlA^{NH3} + FtsZ
S
P
FtsZ
FzlA
FtsZ Alone
FzlA Alone
FzlA^{NH1} Alone
FzlA + FtsZ
FzlA^{NH1} + FtsZ
S
P
FtsZ
FzlA
FtsZ Alone
FzlA Alone
FzlA^{WB1} Alone
FzlA + FtsZ
FzlA^{WB1} + FtsZ
S
P
FtsZ
FzlA

Figure 20. Low speed co-pelleting of FzlA mutant proteins and FtsZ.

Coomassie-blue stained SDS-PAGE gels of FtsZ (2 µM) and FzlA mutant proteins (4 µM) that have been co-sedimented at low speed under polymerizing conditions, used for quantification (main text). S=supernatant, P=pellet. Experiments performed in triplicate, as shown. Each row shows samples run on the same day. Control experiments with FtsZ and WT FzlA were run each time for comparison to different FzlA mutants and to control for day-to-day variations.

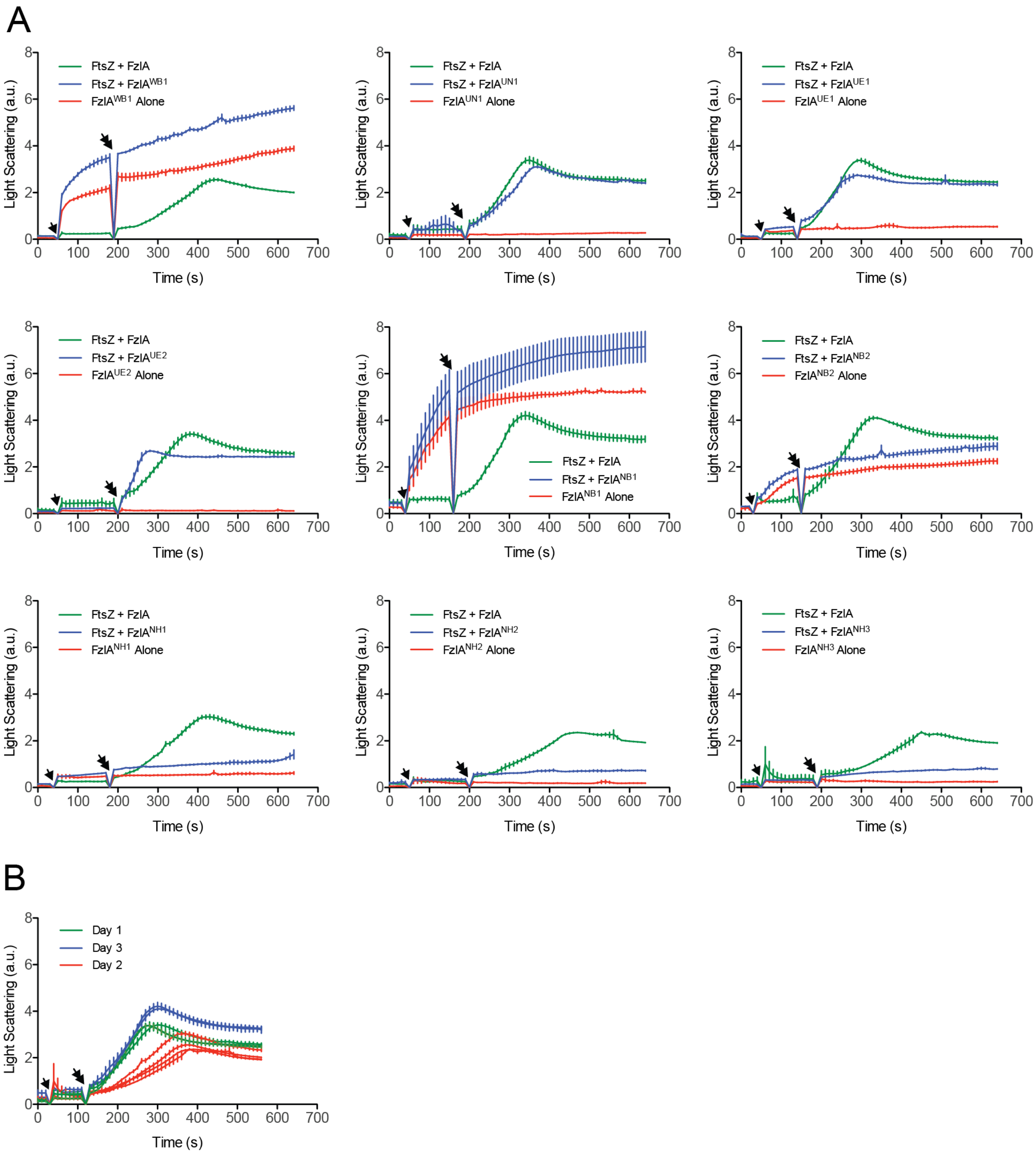

Figure 21. Some FzlA mutant proteins are able to form higher order structures in the presence of FtsZ.

(A) Plots of RALS over time for 4 μM FzlA WT or mutant protein ± 2 μM FtsZ. Mean ± SEM is shown. Cuvettes containing FtsZ received injections of FzlA mutant protein (single arrow), then

2 mM GTP (double arrow) to induce polymerization. Experiments were performed in triplicate (except for FzlA$^{\mathrm{UE1}}$ alone, which was done in duplicate). Some mutant proteins (WB1, NB1, NB2) displayed self-association on their own, as evidenced by an increase in signal without FtsZ (red lines).

(B) Plot of RALS over time for the FtsZ + FzlA control reaction for each experiment shown in panel A. Experiments were performed on three separate days, with the relevant mutant proteins noted: Day 1 (FzlA$^{\mathrm{UE1}}$, FzlA$^{\mathrm{UE2}}$, FzlA$^{\mathrm{UN1}}$), Day 2 (FzlA$^{\mathrm{WB1}}$, FzlA$^{\mathrm{Nh1}}$, FzlA$^{\mathrm{NH2}}$, FzlA$^{\mathrm{NH3}}$), and Day 3 (FzlA$^{\mathrm{NB1}}$, FzlA$^{\mathrm{NB2}}$). FtsZ + FzlA displayed mild variability in terms of rate of light scattering and maximum intensity, but the characteristic shape of the curve remained relatively constant.

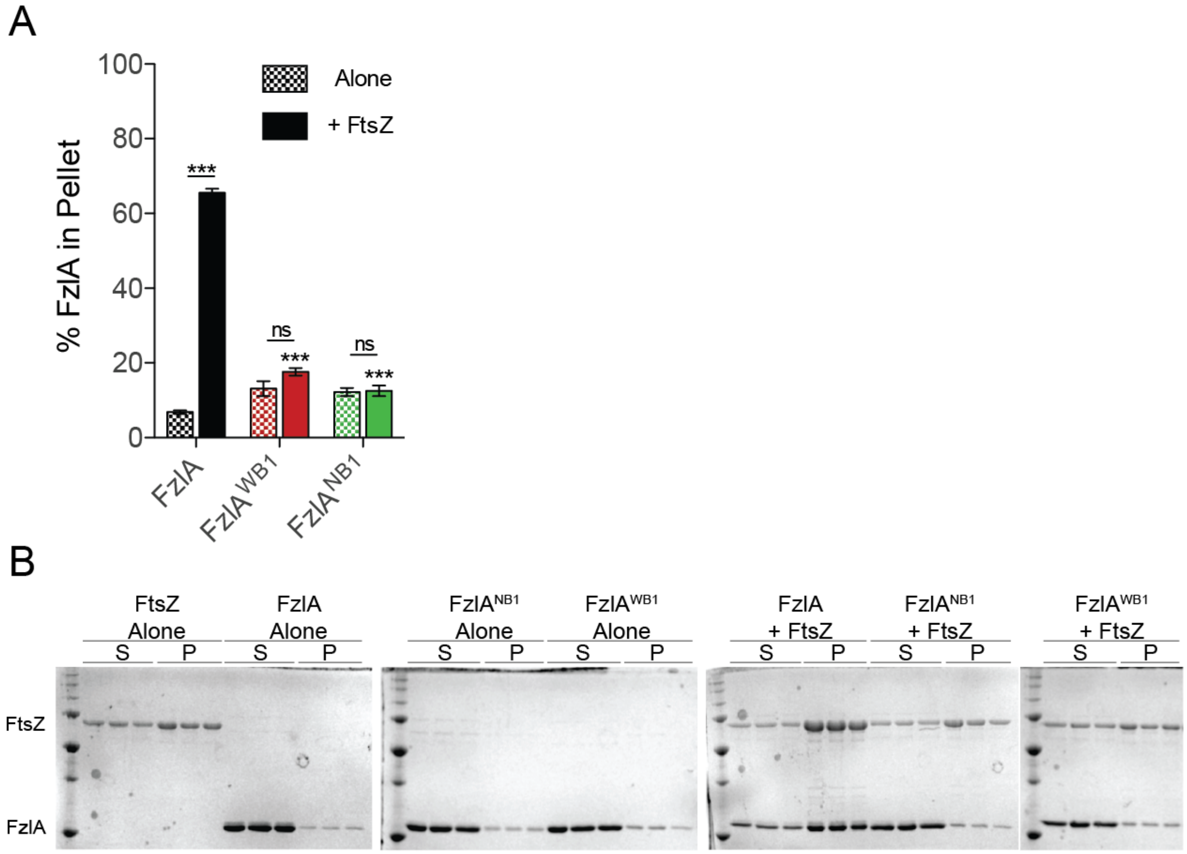

Figure 22. High speed co-pelleting of FzlA^{WB1} or FzlA^{NB1} and FtsZ.

(A-B) Quantification of percent FzlA found in pellet (A) and Coomassie-blue stained SDS-PAGE gels (B) of FtsZ (4 µM) and FzlA mutant protein (4 µM) that have been co-sedimented at high speed in HEK50 polymerization buffer (50 mM HEPES, 50 mM KCl, pH 7.2; 2 mM GTP; 10 mM $MgCl_2$). For (A), a one way ANOVA with Dunnett's multiple comparison test was performed to assess differences between each FzlA mutant protein + FtsZ and WT FzlA + FtsZ (lower asterisks). Unpaired t-tests were performed to analyze the difference between a given FzlA mutant protein alone vs. with FtsZ. For all statistical tests, $^{ns}P>0.05$, $^{***}P\leq0.001$ and n=3 for each sample. For (B), S=supernatant, P=pellet.

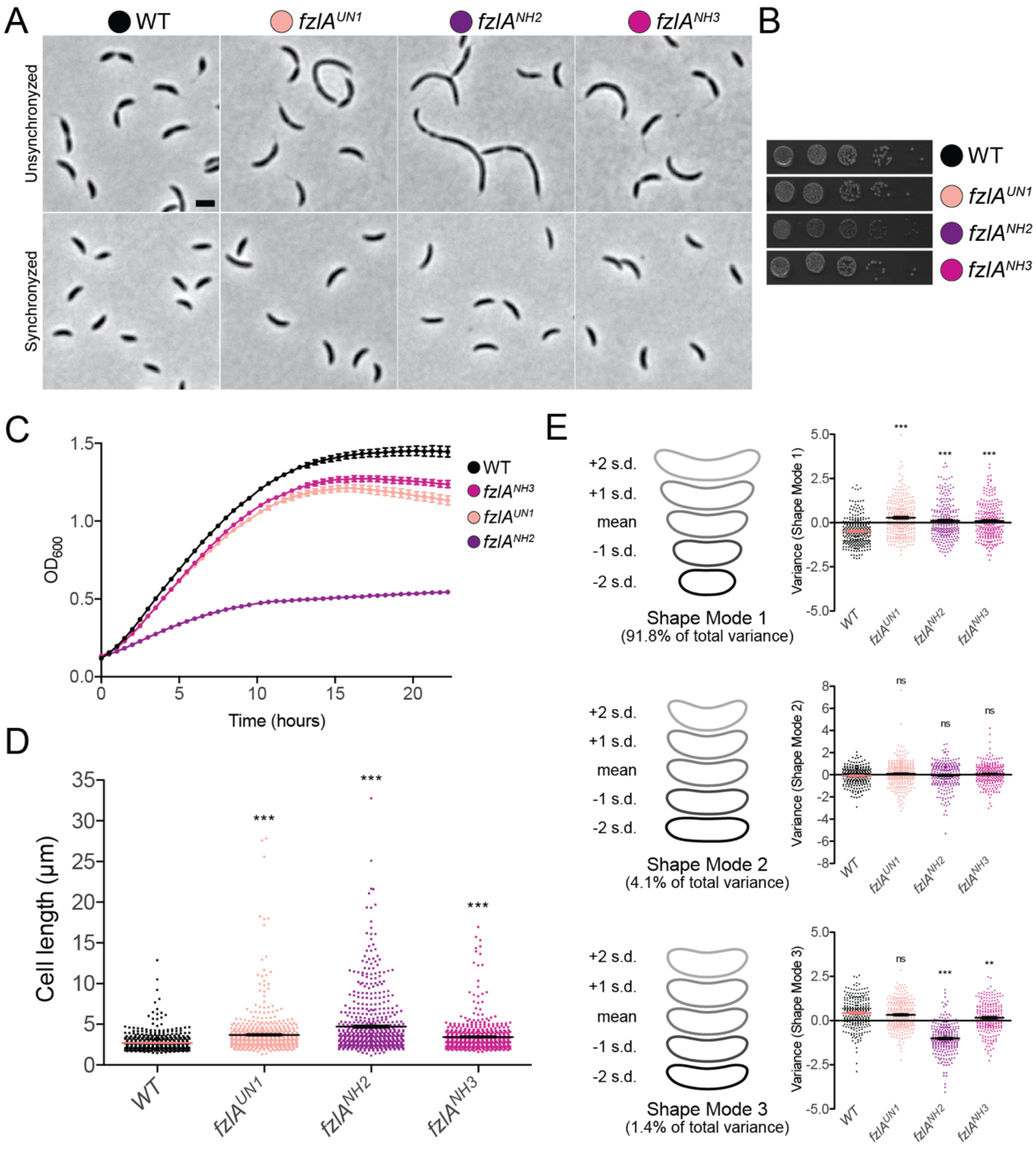

Figure 23. Three *fzlA* mutant genes are capable of allelic replacement, causing a range of division and morphological defects.

(A) Phase contrast images of unsynchronized (top) and synchronized (bottom) cells from strains carrying mutant *fzlA* alleles as the only copy. Scale bar = 2 µm.

(B) Spot dilutions of mutant *fzlA* allelic exchange strains.

(C) Growth curves of mutant *fzlA* allelic exchange strains. Mean of three technical replicates ± SEM is shown.

(D) Lengths of unsynchronized cells from *fzlA* allelic exchange strains. Mean ± SEM is shown. A one way ANOVA with a Kruskal-Wallis test was performed to analyze differences compared to WT: $^{***}P \leq 0.001$. From left to right, n= 610, 618, 607, 610. E. PCA of cell shape in synchronized *fzlA* allelic exchange strains. For each of the three shape modes that account for most of the variance in the population, mean cell contour ± 1 or 2 standard deviations (s.d.) is shown (left). Shape mode values for cells in each strain are plotted and mean ± SEM is indicated (right). A one way ANOVA with with a Kruskal-Wallis test was performed to assess differences compared to WT: $^{ns}P > 0.05$, $^{**}P \leq 0.01$, $^{***}P \leq 0.001$. From left to right, n=261, 288, 249, 245. Strain key: WT (NA1000), $fzlA^{UN1}$ (EG1908), $fzlA^{NH2}$ (EG1600), $fzlA^{NH3}$ (EG1909).

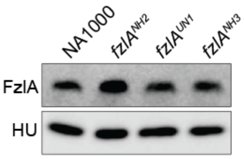
NA1000
fzlA^NH2
fzlA^UN1
fzlA^NH3
FzlA
HU

Figure 24. Protein levels of FzlA in *fzlA* allelic exchange strains.

α-FzlA (top) and α-HU (bottom) immunoblots of *fzlA* allelic exchange strain lysates. Strain key: NA1000 (WT), *fzlA*^{NH2} (EG1600), *fzlA*^{UN1} (EG1671), *fzlA*^{NH3} (EG1909).

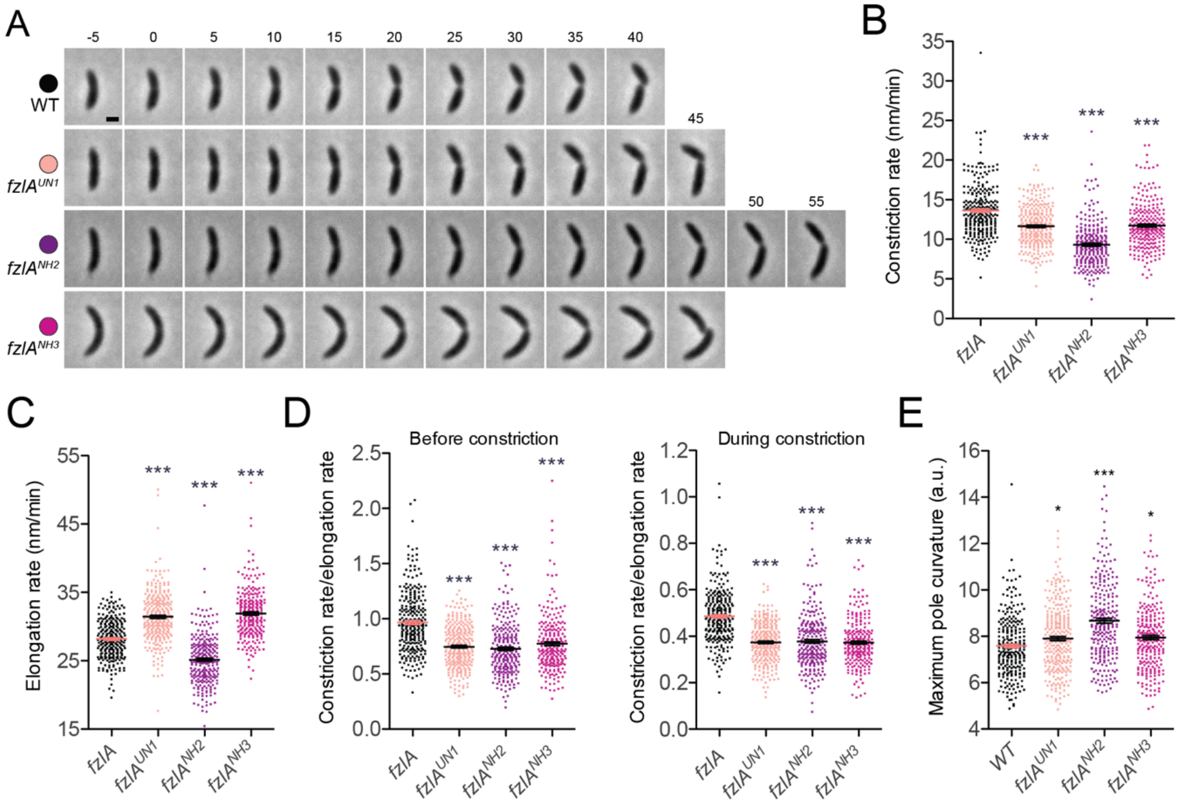

Figure 25. *fzlA* mutant strains show protracted constriction.

(A) Phase contrast images of representative constricting cells from *fzlA* allelic exchange strains, acquired at 5 minute intervals. For each strain, constriction begins in the second frame (t=0) and ends upon cell separation in the last frame. Scale bar = 1 µm.

(B-C) Plots of constriction rate (B) and elongation rate during constriction (C) for a population of synchronized cells from each *fzlA* strain, calculated from single cell microscopy data. Mean ± SEM is shown. One way ANOVA tests with Tukey's multiple comparison test were performed to analyze differences compared to WT: ***P≤0.001. From left to right, n= 271, 295, 260, 249 (B) and 266, 293, 258, 246 (C).

(D) Plots of the ratio of constriction rate to elongation rate before constriction (left) and during constriction (right) for a population of synchronized cells from each *fzlA* strain, calculated from single cell microscopy data. Mean ± SEM is shown. One way ANOVA tests with Tukey's multiple comparison test were performed to analyze differences compared to WT: $^{***}P \leq 0.001$. From left to right, n=271, 295, 260, 249 (left) and 266, 293, 258, 246 (right).

(E) Plot of the maximum curvature of the poles for a synchronized population of single cells for each *fzlA* allelic exchange strain. Mean ± SEM is shown. A one way ANOVA with a Kruskal-Wallis test was performed to analyze differences compared to WT: $^{*}P \leq 0.05$, $^{***}P \leq 0.001$. From left to right, n= 261, 288, 249, 245. Strain key: WT (NA1000), $fzlA^{UN1}$ (EG1908), $fzlA^{NH2}$ (EG1600), $fzlA^{NH3}$ (EG1909).

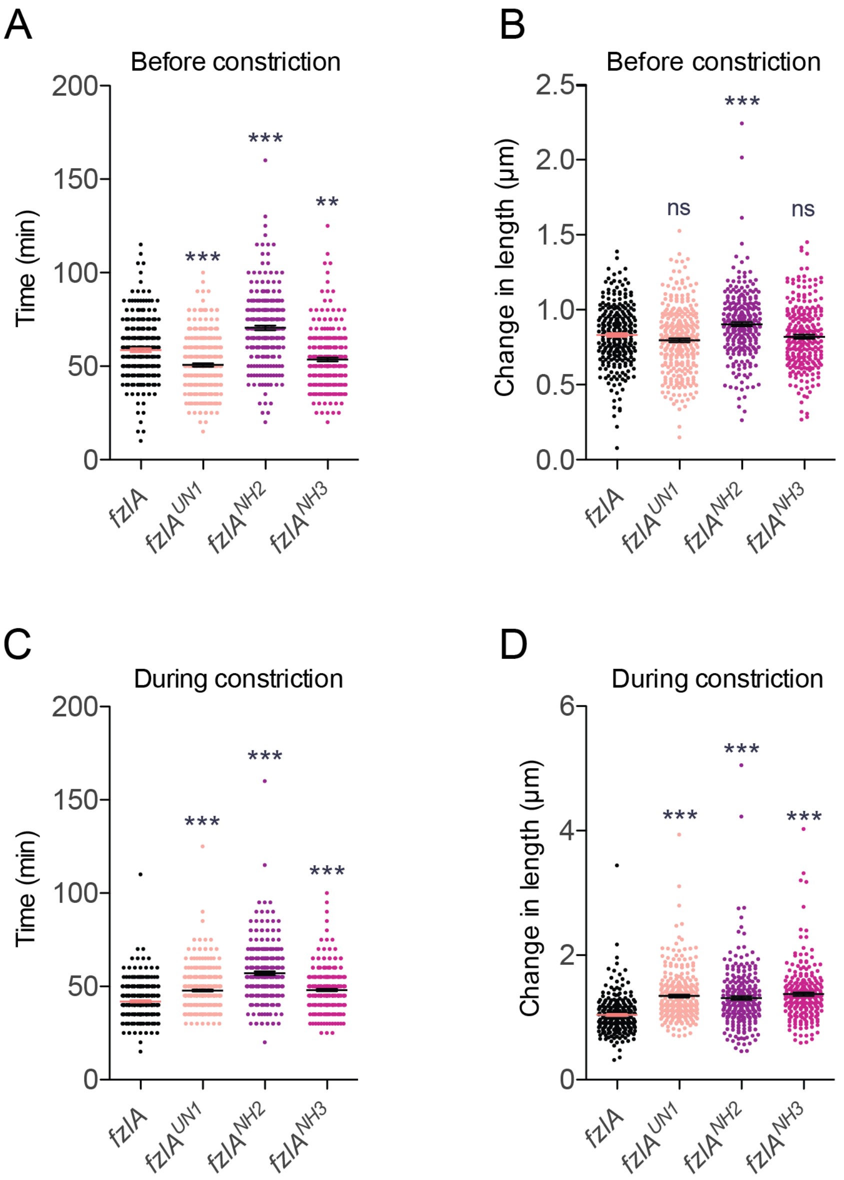

Figure 26. Pre-constriction time and change in cell length for *fzlA* allelic exchange strains. (A-D) Plots of pre-constriction time (A), change in cell length before constriction (B), constriction time (C) and change in cell length during constriction (D) for a population of synchronized cells from each *fzlA* strain, calculated from single cell microscopy data. Pre-constriction time was calculated by determining the number of frames from initial image acquisition until cells began to divide, then converting to minutes. Constriction time was

calculated by counting the number of frames from constriction initiation until cell separation, then converting into minutes. Mean ± SEM is shown. A one way ANOVA with Tukey's multiple comparison test was performed to analyze differences compared to WT: $^{ns}P>0.05$, $^{**}P\leq0.01$, $^{***}P\leq0.001$. From left to right, n= 271, 295, 260, 249 (A, B, C) and 266, 293, 258, 246 (D). Strain key: *fzlA* (NA1000), *fzlA*^{UN1} (EG1908), *fzlA*^{NH2} (EG1600), *fzlA*^{NH3} (EG1909).

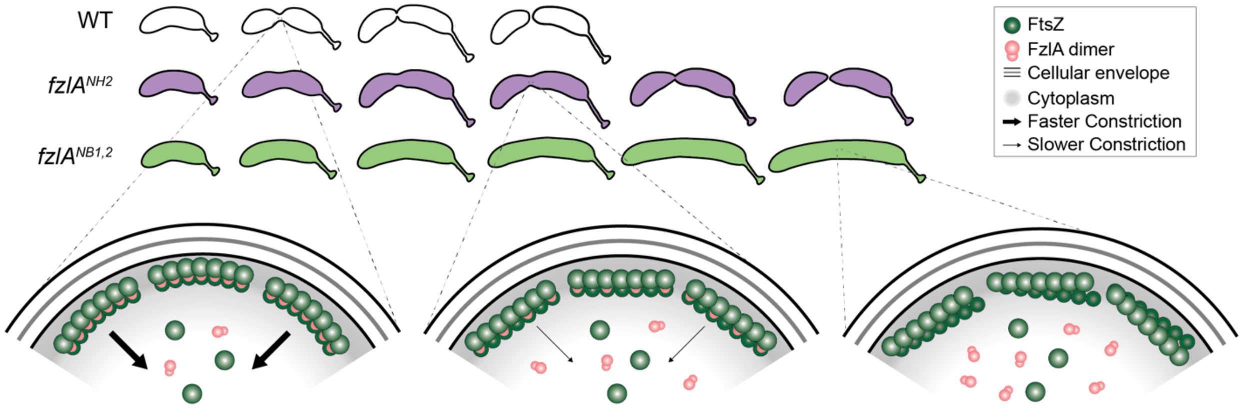
WT
fzlA^{NH2}
fzlA^{NB1,2}
FtsZ
FzlA dimer
Cellular envelope
Cytoplasm
Faster Constriction
Slower Constriction

Figure 27. Model of FzlA function in regulating constriction

Full interaction with FtsZ, including helix formation, is required for wild-type constriction rate. Top: Constriction is shown for normally dividing WT cells (white) and slower dividing *fzlA*^{NH2} cells (purple). *fzlA*^{NB1,2} cells (bright green) grow, but do not constrict or divide. Bottom: Close-up of the division septa, depicting FtsZ (dark green) bound to WT or mutant FzlA protein (pink). WT FzlA binds and curves FtsZ, and corresponds with normal, fast constriction (bottom left). FzlA^{NH2} binds, but does not curve FtsZ filaments, and correlates with slower constriction (bottom middle). (Note, FzlA^{NH2} is shown to bundle FtsZ filaments, however it is unclear by TEM if this is indeed the case.) FzlA^{NB1-2} mutant proteins do not bind or curve FtsZ, which prohibits constriction and division (bottom right).

Chapter 3. An essential regulator of bacterial division links FtsZ to cell wall synthase activation

3.1 Introduction

Bacterial division is driven by the insertion of new cell wall material at midcell in a tightly regulated manner, allowing for determination of cell shape and maintenance of envelope integrity (Cabeen and Jacobs-Wagner, 2005; Woldemeskel and Goley, 2017). The cell wall is made of peptidoglycan (PG), a meshwork consisting of glycan strands crosslinked by peptide stems (Gan *et al.*, 2008; Huang *et al.*, 2008). PG synthesis requires the coordination of glycan polymerization and peptide crosslinking by either coupled monofunctional glycosyltransferases (GTases) and transpeptidases (TPases), or bifunctional enzymes that contain both activities, with these proteins being more generally referred to as PG synthases (Cabeen and Jacobs-Wagner, 2005).

Monofunctional PG synthase pairs have been implicated as the primary synthetic enzymes of the elongation (elongasome) and division (divisome) machineries. A paradigm has been proposed whereby a shape, elongation, division, and sporulation (SEDS) family GTase is functionally coupled to a penicillin binding protein (PBP) TPase, which together facilitate cell wall synthesis (Meeske *et al.*, 2016; Rohs *et al.*, 2018; Taguchi *et al.*, 2019). Through characterization of the elongation-specific PG synthases RodA and PBP2 in *Escherichia coli*, it has been postulated that SEDS-PBP enzymes require activation to function (Rohs *et al.*, 2018). Specifically, mutations in RodA or PBP2 that increase GTase activity *in vitro* and PG synthesis in cells render other components of the elongasome non-essential, arguing that their normal function is to activate the RodA-PBP2 complex (Rohs *et al.*, 2018). Intriguingly, analogous mutations in the division-specific SEDS-PBP enzymes, FtsW and FtsI, allow cells to constrict faster than normal (Lambert *et al.*, 2018), indicating that these mutations promote formation of an activated PG synthase complex (Modell *et al.*, 2014; Rohs *et al.*, 2018). However, it is unclear precisely how SEDS-PBP activation normally occurs during division.

Recent studies have established that the conserved cytoskeletal protein FtsZ (Vaughan *et al.*, 2004; Sundararajan and Goley, 2017), which recruits the division machinery to a ring-like structure at midcell (Fu *et al.*, 2010; Goley *et al.*, 2011; Holden *et al.*, 2014), is coupled to PG synthesis activation during division. In multiple organisms, the C-terminal linker domain of FtsZ was found to be required for regulating cell wall integrity (Buske and Levin, 2013; Gardner *et al.*, 2013; Sundararajan *et al.*, 2015) and shape, as well as PG chemistry (Sundararajan *et al.*, 2015; Howell *et al.*, 2019). Moreover, in *E. coli* and *Bacillus subtilis*, FtsZ dynamics were demonstrated to drive PG synthase dynamics in both organisms, as well as division site shape in *E. coli* and constriction rate in *B. subtilis* (Bisson-Filho *et al.*, 2017; Yang *et al.*, 2017). Collectively these data indicate that, at least in some organisms, FtsZ acts as a "dynamic scaffold" or "dynamic activator" of PG synthesis likely impinging on FtsWI. However, the signaling pathway connecting these two endpoints remains unresolved.

We previously demonstrated that an essential FtsZ-binding protein, FzlA (Goley *et al.*, 2010b), is required for division and regulates the rate of constriction in the α-proteobacterium *Caulobacter crescentus* (Lariviere *et al.*, 2018). Mutations in FzlA with diminished affinity for FtsZ were found to have slower constriction rates and altered cell pole shape, indicative of reduced PG synthetic activity during division (Lariviere *et al.*, 2018). We therefore postulated that FzlA facilitates a link between FtsZ and PG synthesis by serving as an upstream activator of PG synthases and, here, set out to test this hypothesis.

3.2 *fzlA* lies upstream of *ftsWI* in a PG synthesis pathway

We reasoned that if FzlA impacts constriction through PG synthases, it likely acts on the division-specific SEDS family GTase FtsW and/or the monofunctional PBP TPase FtsI. To assess if FzlA is required for activation of FtsWI, we exploited fast-constricting strains containing hyperactive mutant variants of FtsI and/or FtsW termed *ftsW**I** (Modell *et al.*, 2014; Lambert *et al.*, 2018) and *ftsW** (Modell *et al.*, 2014). *ftsW**I** bears the mutations F145L and A246T in FtsW and I45V in FtsI, whereas *ftsW** contains only the FtsW A246T mutation (Modell *et al.*, 2014). These mutations are thought to stabilize an activated form of the FtsWI complex (Modell *et al.*, 2014; Rohs *et al.*, 2018), leading to increased rates of constriction (Lambert *et al.*, 2018) via unrestrained PG synthesis.

If *fzlA* lies upstream of *ftsWI* in a PG synthesis pathway, then the hyperactive variants *ftsW**I** and/or *ftsW** may bypass the essentiality of *fzlA*. Accordingly, we found that *fzlA* could be readily deleted in either the *ftsW**I** or *ftsW** strain backgrounds (**Fig. 28A-B**). This is a particularly striking finding given that depletion of FzlA in a WT background completely inhibits division and induces cell filamentation and death (Goley *et al.*, 2010b). Interestingly, a number of *ftsW**I*/ftsW** Δ*fzlA* cells appeared to be "S"-shaped with the direction of curvature in future daughter cells facing opposite directions, as opposed to the characteristic "C"-shape of pre-divisional WT and *ftsW**I* Caulobacter* cells (**Fig. 28A**, asterisk, discussed further below). Strains lacking *fzlA* displayed a slight reduction in colony forming units, compared to the corresponding hyperactive PG synthase mutant strains (**Fig. 28C**), whereas growth rate was unaffected (**Fig. 28D**). Additionally, _ftsW**I*/ftsW*_ Δ_fzlA_ cells displayed an increase in length (**Fig. 28E**), suggesting a division defect. Because _ftsW*_ Δ_fzlA_ cells are longer than _ftsW**I*_ Δ_fzlA_ cells, we conclude that _ftsW**I*_ suppresses loss of _fzlA_ better than the single mutant.

We also observed that _ftsW**I*_ suppresses length, width, shape, and fitness defects associated with slowly constricting _fzlA_ point mutants _fzlA_^{NH2} and _fzlA_^{NH3} (**Fig. 29**), further indicating that hyperactivated _ftsWI_ are dominant to, and likely downstream of _fzlA_. To determine the contribution of the FtsZ-FzlA interaction to activation of FtsWI, we assessed cell morphology, fitness, and cell length of _ftsW**I*_ strains containing FzlA mutants with decreasing affinity for FtsZ (Lariviere _et al._, 2018) (**Fig. 30**; FzlA > FzlA$^{\mathrm{NH2}}$ = FzlA$^{\mathrm{NH3}}$ > FzlA$^{\mathrm{NH1}}$; FzlA$^{\mathrm{NB2}}$, FzlA$^{\mathrm{NB1}}$ = no binding). We found that decreased affinity of FzlA towards FtsZ correlated with an increase in cell length (**Fig. 30E**), indicating that high-affinity binding to FtsZ is required for FzlA to contribute to the FtsWI activation pathway. We term this activation pathway the [FtsZ-FzlA]-FtsWI signaling pathway.

We previously showed that mutation of FzlA's conserved C-terminus inhibits division, but does not affect binding to FtsZ, suggesting the C-terminus might facilitate an essential interaction with another protein (Lariviere _et al._, 2018). We reasoned that if this other essential interaction is involved in the PG synthesis activation pathway, then FzlA's C-terminus should be mutable in an _ftsW**I*_ background. Indeed, _fzlA_^{UE2}, which encodes a charge reversal mutation in the C-terminus of FzlA normally preventing division but not FtsZ-binding, phenocopies loss of _fzlA_ in an _ftsW**I*_ background. _ftsW**I* fzlA_^{UE2} cells are slightly elongated and "S"-shaped (**Fig. 31A**), but have normal cell growth, viability, and FzlA levels (**Fig. 31B-D**). Because the 5' end of _fzlA_'s coding sequence overlaps with the non-essential downstream gene, _CCNA_03753_, we exogenously expressed _fzlA_^{UE2} in an _ftsW**I*_ Δ_fzlA_ background to leave _CCNA_03753_ intact. Again, cells became slightly elongated and “S”-shaped in the presence of *fzlA*^{UE2} (**Fig. 31E**), with no major impact on growth or viability compared to exogenous expression of *fzlA* (**Fig. 31F-H**), confirming that change in cell shape is due to mutation of FzlA’s C-terminus. Because FzlA’s C-terminus becomes dispensable upon hyperactivation of *ftsW**I**, we propose that the C-terminus facilitates interaction with another essential factor in the PG synthesis activation pathway.

3.3 *ftsW**I** specifically permits loss of *fzlA*

To assess the specificity of the *fzlA*-*ftsWI* genetic interaction and potentially identify additional components of this pathway, we performed comparative transposon sequencing (Tn-Seq) on WT and *ftsW**I** strains. Surprisingly, *fzlA* was the only essential gene to become non-essential in the *ftsW**I** background, with few insertions in WT but plentiful insertions in *ftsW**I** cells (**Fig. 28F-G**). All other known essential division genes, e.g. *ftsZ* (**Fig. 28G**), had few transposon insertions in either background; examination of known division genes’ insertion profiles showed all domains remain essential in *ftsW**I**. These data indicate that *ftsW**I** specifically rescues loss of *fzlA*, confirming that FzlA is normally required for activation of FtsWI. We expect that other essential division proteins participate in this pathway too, but that they have additional essential functions.

3.4 FzlA contributes to efficient division in a hyperactive PG synthase background

Given that cells lacking *fzlA* in the hyperactive PG synthase backgrounds were elongated, we assessed constriction rate and division efficiency of *ftsW**I** and *ftsW** cells ± *fzlA* using time-lapse microscopy and MicrobeJ to track division (Ducret *et al.*, 2016; Lariviere *et al.*, 2018) (**Fig. 32A**). Consistent with previous findings (Lambert *et al.*, 2018), *ftsW**I** and *ftsW** cells constrict more quickly than WT (**Fig. 32B**). Intriguingly, the hyperactive PG synthase strains lacking *fzlA* constricted significantly more slowly than the corresponding strain with *fzlA* present, with constriction rates cut nearly in half (**Fig. 32B**). This suggests that hyperactivated FtsWI are not sufficient for efficient division and underscores the importance of FzlA in dictating constriction rate. As with cell length and fitness, *ftsW**I** acted as a better suppressor to *fzlA* deletion, allowing for a faster constriction rate than did *ftsW** (**Fig. 32B**).

To ensure that changes in constriction rate were not due to global differences in PG synthesis, we determined elongation rates across strains (**Fig. 32C**), which enabled calculation of the ratio of constriction to elongation rate (**Fig. 32D**). We saw the same trend as for constriction rate itself, with *ftsW**I** and *ftsW** mutant strains having higher ratios of constriction to elongation and loss of *fzlA* giving lower ratios (**Fig. 32D**). Interestingly, elongation rate was inversely correlated with constriction rate in all mutant strains (**Fig. 32C-D**), perhaps reflecting competition between the elongasome and divisome for PG precursor substrate (Coltharp *et al.*, 2016). Altogether, these data support the conclusion that alterations to the [FtsZ-FzlA]-FtsWI pathway affect constriction to a greater extent than they affect elongation, with FzlA increasing the constriction rate in both WT and hyperactive PG synthase mutant backgrounds.

While tracking division in *ftsW**I*/ftsW** Δ*fzlA* cells, we noticed that some cells initiated, then aborted division at one location, before successfully dividing at a second (or third or fourth) site (**Fig. 32E**). We found that 16.6-19.5% of *ftsW*/ftsW**I* ΔfzlA* cells aborted division at one site before successfully dividing at another, compared to a 0-0.3% failure rate for WT or hyperactive PG synthase cells with *fzlA* present (**Fig. 32F**). These data further demonstrate that *ftsW**I** are not sufficient for efficient division, and that *fzlA* is required to ensure division processivity and efficiency.

3.5 *fzlA* is required for maintenance of proper cell shape

As mentioned earlier, deletion of *fzlA* in the hyperactive PG synthase backgrounds impacted global cell morphology, with many pre-divisional cells appearing "S-shaped". By scanning electron microscopy (SEM), we saw a relatively high frequency of S-shaped *ftsW**I* ΔfzlA* cells, whereas most WT or *ftsW**I** cells displayed the typical "C-shaped" morphology characteristic of *Caulobacter* (**Fig. 33A**). To quantify S-shape frequency, we utilized Celltool to isolate variance in cell shape to shape modes (Pincus and Theriot, 2007; Lariviere *et al.*, 2018). Shape mode 3 captured the variation due to degree of S- versus C-shape and we set a cutoff such that cells with a standard deviation |sd| > 1 from the mean for this shape mode are considered S-shaped (**Fig. 33B-C**). We found a significant difference in variance in degree of S-shape across populations (**Fig. 33B**), corresponding with a large difference in S-shaped cells across strains: 26.9% of dividing *ftsW**I* ΔfzlA* cells are S-shaped, compared to 2.4% of WT and 1.1% of *ftsW**I** cells (**Fig. 33D**).

To shed light on the origin of S-shape, we next asked at what point during growth do *ftsW**I* ΔfzlA* cells begin to adopt this morphology. Using time-lapse microscopy, we observed that *ftsW**I* ΔfzlA* cells were C-shaped at the beginning of the cell cycle and began to twist or rotate about the division plane after constriction initiated. S-shape only became apparent in the latter part of constriction, when daughters had rotated ~180° relative to each other (**Fig. 33E**). This finding suggests that the [FtsZ-FzlA]-FtsWI pathway determines geometry of PG insertion at the site of division in a manner that influences global cell morphology, normally constraining cells in their characteristic C-shape as constriction progresses.

Changes in division site shape and formation of S-shaped cells have been previously linked to aberrant localization of FtsZ and the elongation factor, MreB, respectively (Bi and Lutkenhaus, 1992; Addinall and Lutkenhaus, 1996; Charbon *et al.*, 2009; Yang *et al.*, 2017). However, mNG-FtsZ and Venus-MreB localization in *ftsW**I* ΔfzlA* cells was comparable to *ftsW**I** cells (**Fig. 34A-B**). Additionally, imaging with HADA did not reveal any gross changes in PG synthesis localization (**Fig. 34C**). Together, these findings suggest that cell twisting is likely induced by a finer scale alteration of PG synthesis at the division site due to disruption of the [FtsZ-FzlA]-FtsWI pathway. Finally, we observed that affinity of mutant FzlA for FtsZ was inversely correlated with the frequency of S-shaped cells (**Fig. 35**), demonstrating that the FtsZ-FzlA interaction is important for maintaining proper morphology.

3.6 The [FtsZ-FzlA]-FtsWI pathway contributes to resistance to PBP-targeting antibiotics

Because FzlA is important for regulation of PG synthesis in the context of determining constriction rate and cell shape, we hypothesized that it might also contribute to resistance to cell wall-targeting antibiotics. *ftsW**I*,* as has been previously shown (Modell *et al.*, 2014), displayed sensitivity to cephalexin (**Fig. 36A**), which inhibits FtsI and other penicillin-binding proteins in *Caulobacter* (Pogliano *et al.*, 1997; Costa *et al.*, 2008). Interestingly, deletion of *fzlA* in the *ftsW**I** background exacerbated sensitivity to cephalexin (**Fig. 36A**). We found a similar trend upon treatment with mecillinam, which targets the elongation-specific PG synthase PBP2 (Spratt and Pardee, 1975; Spratt, 1977a), whereby the minimum inhibitory concentration (MIC) for *ftsW**I** cells was decreased compared to WT, with deletion of *fzlA* further lowering the MIC (**Fig. 36B**). However, neither *ftsW**I** nor *ftsW**I* ΔfzlA* cells displayed sensitivity to the β-lactam ampicillin or antibiotics that block other aspects of cell wall synthesis (**Fig. 37A**). *fzlA* therefore supports robust cell wall synthesis in the presence of PBP-inactivating drugs, perhaps by compensating for partial PBP-inactivation by boosting the intensity of cell wall synthesis activation signaling. To determine if the interaction between FtsZ and FzlA is important for maintaining cell wall integrity, we assessed sensitivity to cephalexin using the panel of *fzlA* mutants which display varying affinities towards FtsZ (**Fig. 37B**). We found that mutants with decreased FzlA affinity towards FtsZ in fact became more sensitive to cephalexin (**Fig. 37B**), demonstrating that the entire [FtsZ-FzlA]-FtsWI pathway is required for promoting cell wall integrity during antibiotic treatment.

Since *ftsW**I** cells are more sensitive to perturbation of other PG synthetic activities even when *fzlA* is present, we asked if any normally non-essential division genes become more important for fitness in an *ftsW**I** background, as they might help bolster resistance to assaults on PG synthesis. Examination of the *ftsW**I** Tn-Seq data indicated that *pbpX* (encoding a bifunctional PG synthase) (Yakhnina and Gitai, 2013; Strobel *et al.*, 2014), and to a lesser extent *ftsX* (encoding a cell separation factor) (Meier *et al.*, 2017) and *dipM* (encoding an envelope maintenance/cell separation factor) (Goley *et al.*, 2010a; Möll *et al.*, 2010; Meier *et al.*, 2017; Zielińska *et al.*, 2017), had fewer transposon insertions in an *ftsW**I** background than in WT (**Fig. 28F** and **Fig. 38A-B**). Depletion of the otherwise nonessential DipM or PbpX completely inhibited growth of *ftsW**I** cells (**Fig. 38C**), validating our Tn-Seq results. Because *ftsW**I** cells have misregulated division site PG synthase activity, we suspect that DipM and PbpX become important for ensuring robust PG synthesis during constriction. Surprisingly, the normally non-essential *nhaA* locus, coding for a putative sodium-proton antiporter (Zuleta *et al.*, 2003), was also predicted by Tn-Seq to become essential in *ftsW**I** cells (**Fig. 28F** and **Fig. 38A-B**). Disruption of *nhaA* in the presence of sucrose has been shown to arrest division (Zuleta *et al.*, 2003), suggesting *nhaA* may be important for osmoregulation during division under certain conditions, possibly explaining its apparent synthetic lethality with *ftsW**I**.

3.7 The *fzlA-ftsW* genetic interaction is conserved in diverse α-proteobacteria

To assess the conservation of FzlA's role in regulating PG synthesis, we sought to characterize the genetic interaction between *fzlA* and PG synthases in another α-proteobacterium, *Agrobacterium tumefaciens*. While *A. tumefaciens* and *Caulobacter* display disparate growth patterns (Aaron *et al.*, 2007; Brown *et al.*, 2012; Kuru *et al.*, 2012; Figueroa-Cuilan and Brown, 2018), the components of the division machinery are largely conserved. To test if the genetic interaction between *fzlA* and *ftsW* is conserved, we made an IPTG-dependent FzlA depletion construct in a WT background or in a background with a single hyperactivating mutation in *A. tumefaciens ftsW* (F137L, equivalent to *Caulobacter* FtsW F145L) at the *ftsW* locus. Depletion of FzlA in a WT background resulted in reduced viability, division arrest, and ectopic pole formation at midcell (**Fig. 39**), reminiscent of FtsW depletion in *A. tumefaciens* (Howell *et al.*, 2019). Importantly, we found that the decrease in viability and morphology defects associated with depletion of FzlA were rescued by *ftsW F137L* (**Fig. 39**). These data indicate that FzlA's essential role in regulating division-specific PG synthesis is conserved in another α-proteobacterium and further highlight the importance of FzlA as a key regulator of constriction and cell morphology.

3.8 Discussion

Here we have described a conserved PG synthesis activation pathway in which FtsZ and FzlA, likely via its C-terminus, regulates PG synthesis during division in α-proteobacteria by signaling to FtsWI (solid arrow) and/or possibly by influencing FtsZ dynamics (dashed arrow) (**Fig. 40**, left). Specifically, the [FtsZ-FzlA]-FtsWI pathway determines geometry of cell wall insertion at the site of division, sets the constriction rate, and promotes cell wall integrity (**Fig. 40**, left). FtsW**I* can still receive input from FzlA which, in combination with their intrinsic hyperactivity, leads to shorter, faster-constricting cells with sensitivity to cell wall antibiotics (**Fig. 40**, middle). In the absence of *fzlA*, *ftsW**I** cells lose critical regulation of PG synthesis, leading to rotation during division, slower constriction, and increased sensitivity to cell wall antibiotics (**Fig. 40**, right). We establish FzlA as a critical participant in signaling from FtsZ to FtsWI and demonstrate that this division-specific SEDS-PBP pair require FzlA-dependent activation for normal division.

On a molecular level, how does FzlA provide input into the PG synthesis process? We can envision at least two potential mechanisms. In the first, FzlA influences PG synthesis by regulating FtsZ superstructure or dynamics. According to this model, FzlA would function analogously to ZipA or FtsA, which have been proposed to contribute to constriction, at least in part, by influencing FtsZ assembly properties (Hale and de Boer, 1997; Hale *et al.*, 2000; Tsang and Bernhardt, 2015; Haeusser *et al.*, 2015; Du *et al.*, 2016; Schoenemann *et al.*, 2018). FtsW**I* hyperactivation could suppress loss of *fzlA* by overcoming the requirement for regulation by FtsZ dynamics or, perhaps less likely, by restoring the requisite dynamic properties of FtsZ. We previously demonstrated that FzlA can alter FtsZ superstructure and reduce its turnover *in vitro* under certain biochemical conditions (Lariviere *et al.*, 2018), which would be consistent with this model. However, our prior identification of FzlA mutants (e.g. FzlA^{NH3}) that fail to alter FtsZ superstructure or dynamic properties *in vitro* but that, nevertheless, function in division suggests that these effects on FtsZ assembly properties are not required for activation of constriction (Lariviere *et al.*, 2018). We cannot, however, rule out the possibility that FzlA contributes to PG synthesis activation by influencing FtsZ dynamics.

We favor a model in which FzlA serves as a bridge between FtsZ and the conserved core PG synthesis activation pathway, transducing a cell wall synthesis activation signal. We have no evidence that FzlA and FtsWI directly interact, and hypothesize that other intermediary factor(s) transduce the activation signal from FzlA to FtsWI. Our finding that FzlA's normally essential C-terminus, which is not involved in FtsZ binding (Lariviere *et al.*, 2018), becomes non-essential in an *ftsW**I** background implicates this region of the protein as the likely interface with the downstream division activation pathway. Genetic studies in *E. coli* have implicated a number of divisome proteins as part of the core divisome activation machinery, including FtsA, FtsN, FtsK, and FtsQLB (Geissler and Margolin, 2005; Grainge, 2010; Liu *et al.*, 2015; Tsang and Bernhardt, 2015), each of which is essential and conserved in *Caulobacter*. FtsN is proposed to signal to FtsQLB, either directly or through FtsA, to lead to FtsWI activation (Liu *et al.*, 2015; Tsang and Bernhardt, 2015; Du *et al.*, 2016), with FtsK also playing a role in constriction licensing (Geissler and Margolin, 2005; Grainge, 2010). According to our signal transduction model, FzlA contributes to this activation signal by providing regulatory input via its C-terminus into the core conserved signaling pathway. The two models described above are not mutually exclusive; indeed, the two may work in concert (**Fig. 40**). Future work will clarify how FzlA contributes to PG synthesis activation.

That cells become "S"-shaped upon deletion of *fzlA* and hyperactivation of *ftsW**I** suggests that regulation of cell wall synthesis during division is required to globally maintain cell shape. Although further studies will be required to inform the precise mechanism of cell twisting, we propose a few potential models. If FzlA influences FtsZ dynamics, then loss of *fzlA* could result in aberrant FtsZ movement and misdirection of PG synthesis dynamics that ultimately induces rotation, somewhat reminiscent of the D158A and D212G *ftsZ* mutants in *E. coli* (Yang *et al.*, 2017). In those mutants, FtsZ forms helical structures that induce helical septa. For a similar model to hold in *Caulobacter*, the scale on which dynamics are altered would need to be significantly more finely focused, since FtsZ localization and septum morphology is obviously aberrant in the *E. coli ftsZ* mutants, but not in *ftsW**I* ΔfzlA* cells. Alternatively, loss of *fzlA* may impact PG synthase dynamics independent of FtsZ dynamics, effectively uncoupling the two, but still leading to aberrant movement of PG synthases and altered patterning of PG insertion. Finally, FzlA may be required for balanced transpeptidation and transglycosylation activities, thereby impacting PG chemistry and cell shape, as is the case for maintenance of helical shape in *Helicobacter pylori* (Sycuro *et al.*, 2010).

More broadly, our model advances the idea that regulation of SEDS-PBP pairs for growth and division is conserved at numerous levels. The finding that FzlA governs division-specific PG synthesis in both *Caulobacter* and *A. tumefaciens* argues that α-proteobacteria require FzlA as a part of a conserved and dedicated pathway to activate FtsWI. FzlA is absent outside of this clade, however, so we propose that other divisome components play equivalent roles in contributing to FtsWI activation in other organisms. On a greater scale, our findings expand the paradigm for PG synthesis by SEDS-PBP PG synthase pairs in bacteria and provide evidence that the requirement for PG synthase activation is conserved. Elongation is facilitated by the coordination of the SEDS family GTase RodA and the monofunctional TPase PBP2, orthologs to FtsW and FtsI, respectively (Rohs *et al.*, 2018). During elongation activation (in *E. coli*) these PG synthases are activated by another protein, MreC, forming an activated complex that in turn regulates assembly and directional motion of the polymerizing scaffold MreB (Rohs *et al.*, 2018). In this system, hyperactivating mutations in RodA or PBP2 allow for bypass of the activator, MreC, similar to our finding that FtsW**I* can bypass the activator FzlA. Our data provide experimental support for the proposal that the requirement for activation of the SEDS-PBP pair of PG synthases is generally conserved for elongation and division.

There are prominent differences between the models for elongasome and divisome activation, however. Containing fewer proteins than the divisome, the elongasome is akin to a stripped down version of the divisome (Szwedziak and Löwe, 2013), with hyperactive RodA or PBP2 rendering dispensable all elongasome components save MreB and the PG synthases (Rohs *et al.*, 2018). Thus for elongation, the cell needs an activated SEDS-PBP pair and a spatial regulator to orient their motion (Rohs *et al.*, 2018). Conversely, hyperactive FtsWI in *Caulobacter* only allows for disruption of FzlA, with the rest of the divisome remaining essential. Since division requires invagination and fission of all layers of the envelope in coordination with DNA segregation and cell cycle progression, this added complexity necessitates functions beyond PG synthesis and remodeling. Further, whereas PG synthesis during elongation comprises insertion of new PG in the same plane as old cell wall material, PG synthesis during constriction requires a lasting, directional change to shape the new cell poles. So while there are key similarities in the paradigm of PG synthase activation, regulation of division likely requires a more complicated network of inputs to manage the additional outputs and constraints discussed above. In summation, this work provides evidence that the requirement for

SEDS-PBP activation is conserved across multiple modes of PG synthesis, which has broad implications for determining the speed of division, cell shape, and cell wall robustness.

3.9 Figures and Legends

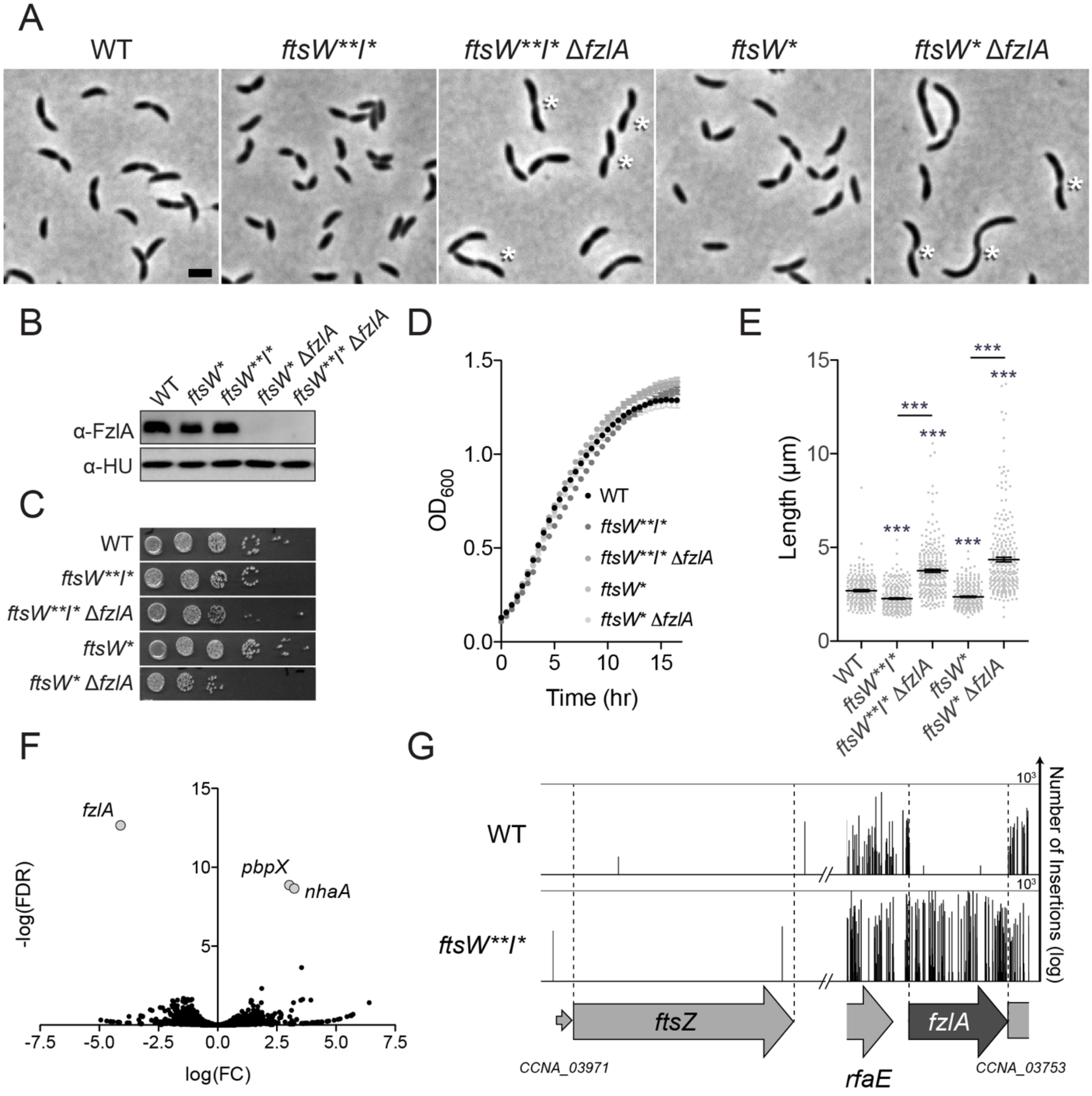

Figure 28. Hyperactive *ftsWI* mutants suppress loss of *fzlA*.

(A) Micrographs of WT *Caulobacter* and PG synthase hyperactive mutant cells +/- *fzlA*. White asterisks mark S-shaped cells. Scale bar: 2 μm.

(B) α-FzlA immunoblot (top) and α-HU immunoblot (bottom, loading control) of the indicated strains.

(C, D) Spot dilutions (diluted ten-fold) (C) and growth curves (D) of the indicated strains.

(E) Lengths of unsynchronized cells from the indicated strains. Mean ± SEM shown. Kruskal-Wallis tests with Dunn's post-test were performed to compare WT and the indicated strains: $^{***}P \leq 0.001$. From left to right, $n = 254, 262, 261, 260, 258$.

(F) Volcano plot of the negative $\log_{10}$ of the false discovery rate (-log(FDR)) vs. $\log_2$ of the fold change of each gene in WT vs. *ftsW**I** strains determined by Tn-Seq analysis.

(G) Plot of transposon insertion frequency in essential division genes in WT (top) vs. *ftsW**I** (bottom) cells determined by Tn-Seq analysis.

Strain key (*Caulobacter*): WT (EG865 A-E; EG2366 F-G), *ftsW**I** (EG1557), *ftsW**I** Δ*fzlA* (EG2170), *ftsW** (EG1556), *ftsW** Δ*fzlA* (EG2166).

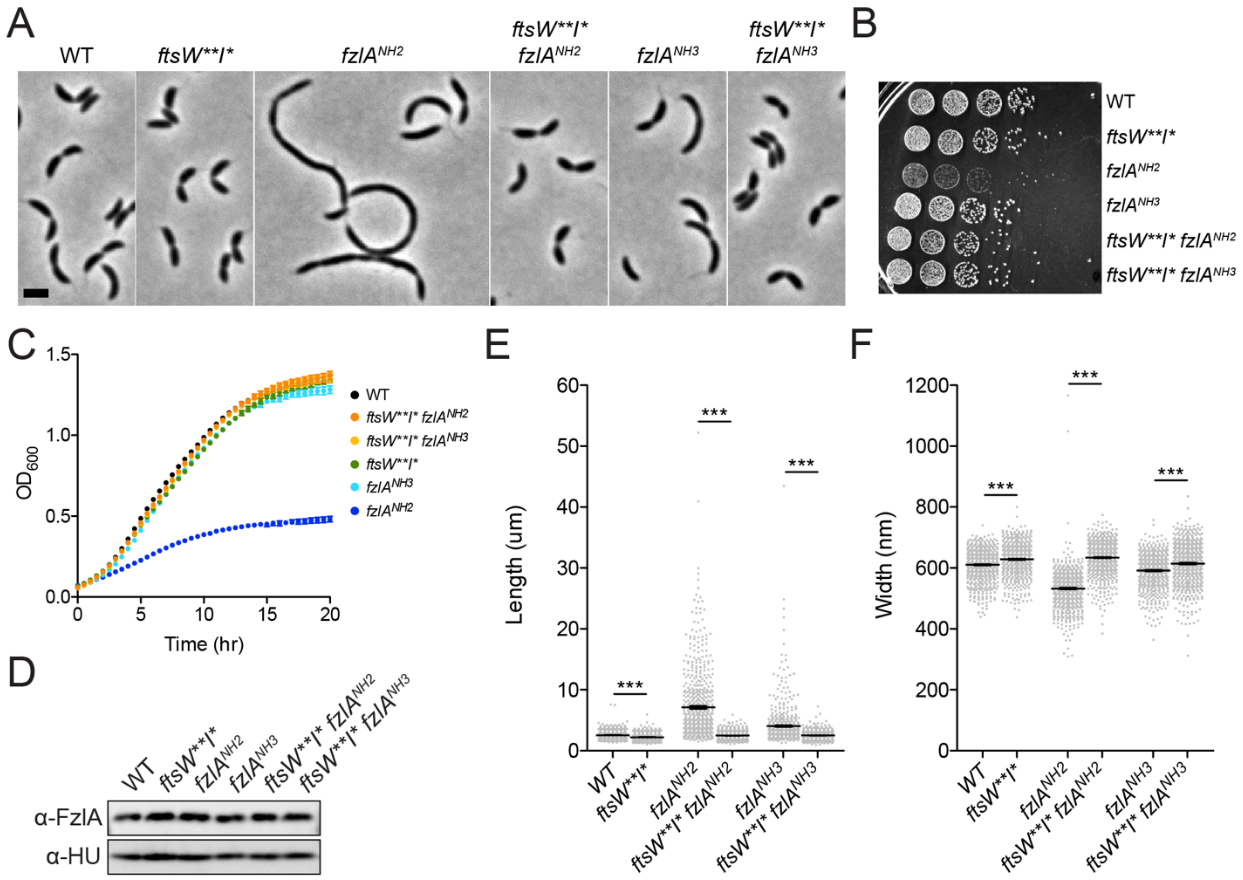

Figure 29. _ftsWI*_ rescue the fitness/morphological defects of two _fzlA_ mutants.**

(A) Phase contrast microscopy images depicting cells of the indicated strains. Scale bar = 2 µm.

(B, C) Spot dilutions (diluted ten-fold) (B) and growth curves (C) of the indicated strains.

(D) α-FzlA immunoblot (top) and α-HU immunoblot (bottom, loading control) of the indicated strains.

(E, F) Lengths (E) and widths (F) of unsynchronized cells from the indicated strains. Mean ± SEM shown. Kruskal-Wallis tests with Dunn's post-test were performed to analyze differences compared to the indicated strains: $^{***}P \leq 0.001$. From left to right, n = 674, 609, 606, 653, 618, 645. Strain key (_Caulobacter crescentus_): WT (EG865), _ftsW**I* fzlA_ (EG1557), _fzlA_^{NH2} (EG1600), _ftsW**I* fzlA_^{NH2} (EG2111), _fzlA_^{NH3} (EG1909), _ftsW**I* fzlA_^{NH3} (EG2489).

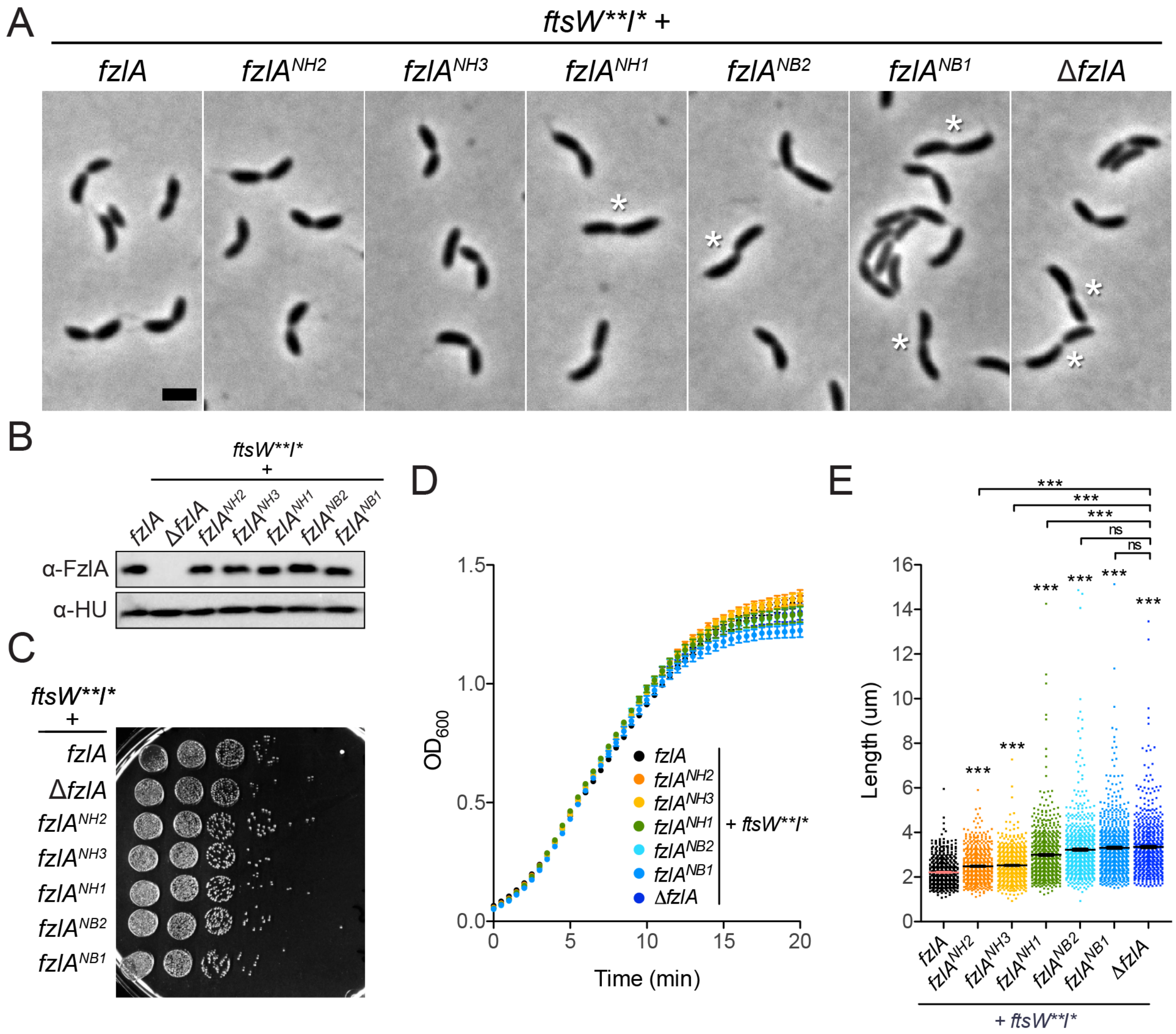

Figure 30. In the presence of hyperactive PG synthases, the interaction between FtsZ and FzlA determines division efficiency, but not growth rate or viability.

(A) Phase contrast microscopy images depicting cells of the indicated strains. White asterisks mark S-shaped cells. Scale bar = 2 µm.

(B) α-FzlA immunoblot (top) and α-HU immunoblot (bottom, loading control) of the indicated strains.

(C, D) Spot dilutions (diluted ten-fold) (C) and growth curves (D) of the indicated strains. (E) Lengths of unsynchronized cells from the indicated strains. Mean ± SEM shown. Kruskal-Wallis tests with Dunn's post-test were performed to analyze differences compared to WT and the indicated strains: $^{ns}P>0.05$, $^{***}P\leq 0.001$. From left to right, *n* = 609, 653, 645, 688, 674, 729, 612. Strain key (*Caulobacter crescentus*): _ftsW**I* fzlA_ (EG1557), _ftsW**I* fzlA_^{NH2} (EG2111), _ftsW**I* fzlA_^{NH3} (EG2489), _ftsW**I* fzlA_^{NH1} (EG2492), _ftsW**I* fzlA_^{NB2} (EG2485), _ftsW**I* fzlA_^{NB1} (EG2495), _ftsW**I*_ Δ_fzlA_ (EG2170).

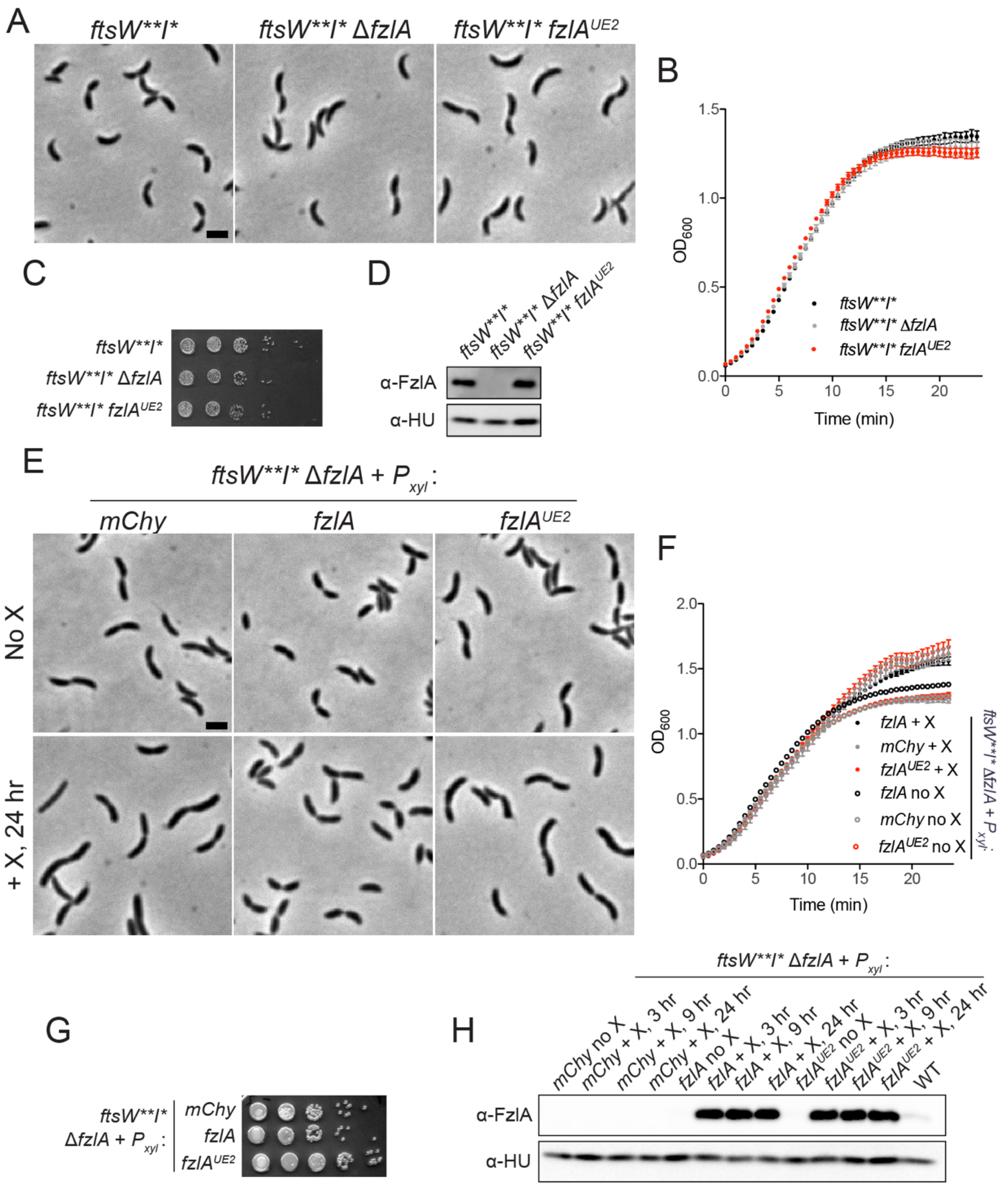

Figure 31. Mutation of FzlA's essential C-terminus phenocopies loss of *fzlA* in an *ftsWI** background.**

(A) Phase contrast microscopy images depicting cells of the indicated strains. Scale bar = 2 μm.

(B,C) Growth curves (B) and spot dilutions (diluted ten-fold) (C) of the indicated strains.

(D) α-FzlA immunoblot (top) and α-HU immunoblot (bottom, loading control) of the indicated strains.

(E) Phase contrast microscopy images depicting cells of the indicated strains with no xylose (top) or incubated in the presence of 0.24% xylose (bottom) for 24 hours to control expression of the indicated gene. Scale bar = 2 µm.

(F) Growth curves of the indicated strains with no xylose (no X) or incubated in the presence of 0.24% xylose (+X) to control expression of the indicated gene.

(G) Spot dilutions (diluted ten-fold) of the indicated strains.

(H) α-FzlA immunoblot (top) and α-HU immunoblot (bottom, loading control) of the indicated strains with no xylose (no X) or incubated in the presence of 0.24% xylose (+X) for 3, 9, or 24 hours to control expression of the indicated gene. Strain key (_Caulobacter crescentus_): _ftsW**I*_ (EG1557), _ftsW**I* ΔfzlA_ (EG2170), _ftsW**I*_ $fzlA^{UE2}$ (EG2895), _ftsW**I* ΔfzlA_ + P_{xyl} _mChy_ (EG2879), _ftsW**I* ΔfzlA_ + P_{xyl} _fzlA_ (EG2866), _ftsW**I* ΔfzlA_ + P_{xyl} $fzlA^{UE2}$ (EG2874).

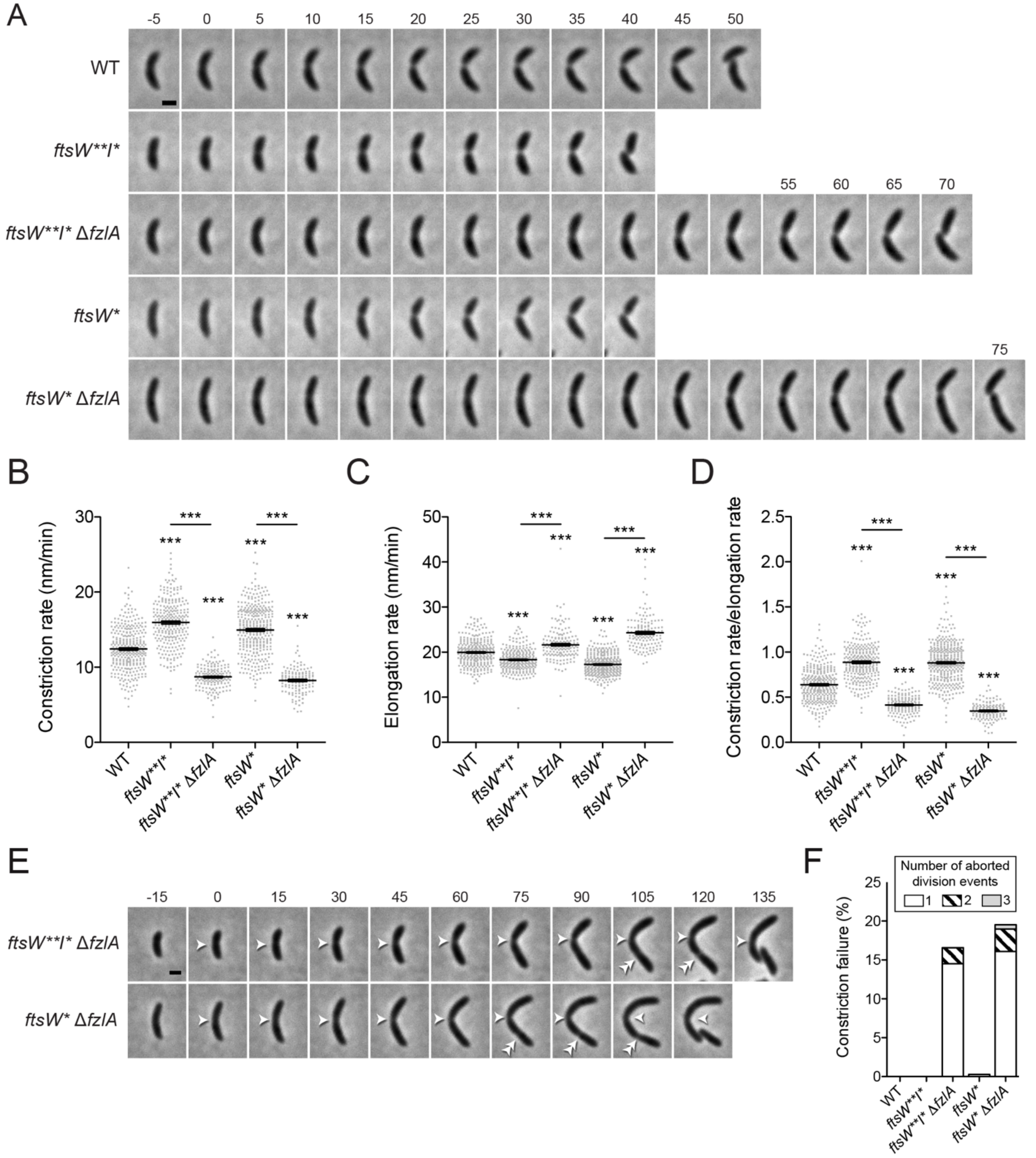

Figure 32. FzlA contributes to efficient division in a hyperactive PG synthase background.

(A) Time-lapse micrographs of constriction in WT or PG synthase hyperactive mutant cells +/- *fzlA*. Constriction starts at t=0 and concludes in the last frame upon cell separation. Time relative to constriction initiation (minutes) is indicated. Scale bar: 1 µm.

(B, C, D) Plots of constriction rate (B), total elongation rate (C), and ratio of constriction rate to total elongation rate (D) for a population of synchronized cells from each indicated strain, calculated from single cell microscopy data. Mean ± SEM shown. Kruskal-Wallis tests with Dunn's post-test were performed to compare WT and the indicated strains: $^{***}P \leq 0.001$. From left to right, *n* = 324, 280, 161, 366, 139 (B) and 321, 280, 161, 363, 139 (C, D).

(E) Micrographs of constriction failure at the initial division site (single white arrowhead), then initiation and completion at a second site (double white arrowhead) in Δ*fzlA* cells. As in (A), constriction initiates at t=0 and concludes in the last frame. Scale bar: 1 μm.

(F) Plot of the constriction failure rate in cells in which constriction initiated, then failed at one division site and subsequently initiated and finished at another division site. "Number of aborted division events" refers to the number of times a cell abandoned division at distinct sites within the cell. The y-axis indicates the percentage of cells out of the whole population that aborted division at least once. From left to right, *n* = 324, 280, 193, 368, 174.

Strain key (*Caulobacter*): WT (EG865), *ftsW**I** (EG1557), *ftsW**I** Δ*fzlA* (EG2170), *ftsW** (EG1556), *ftsW** Δ*fzlA* (EG2166).

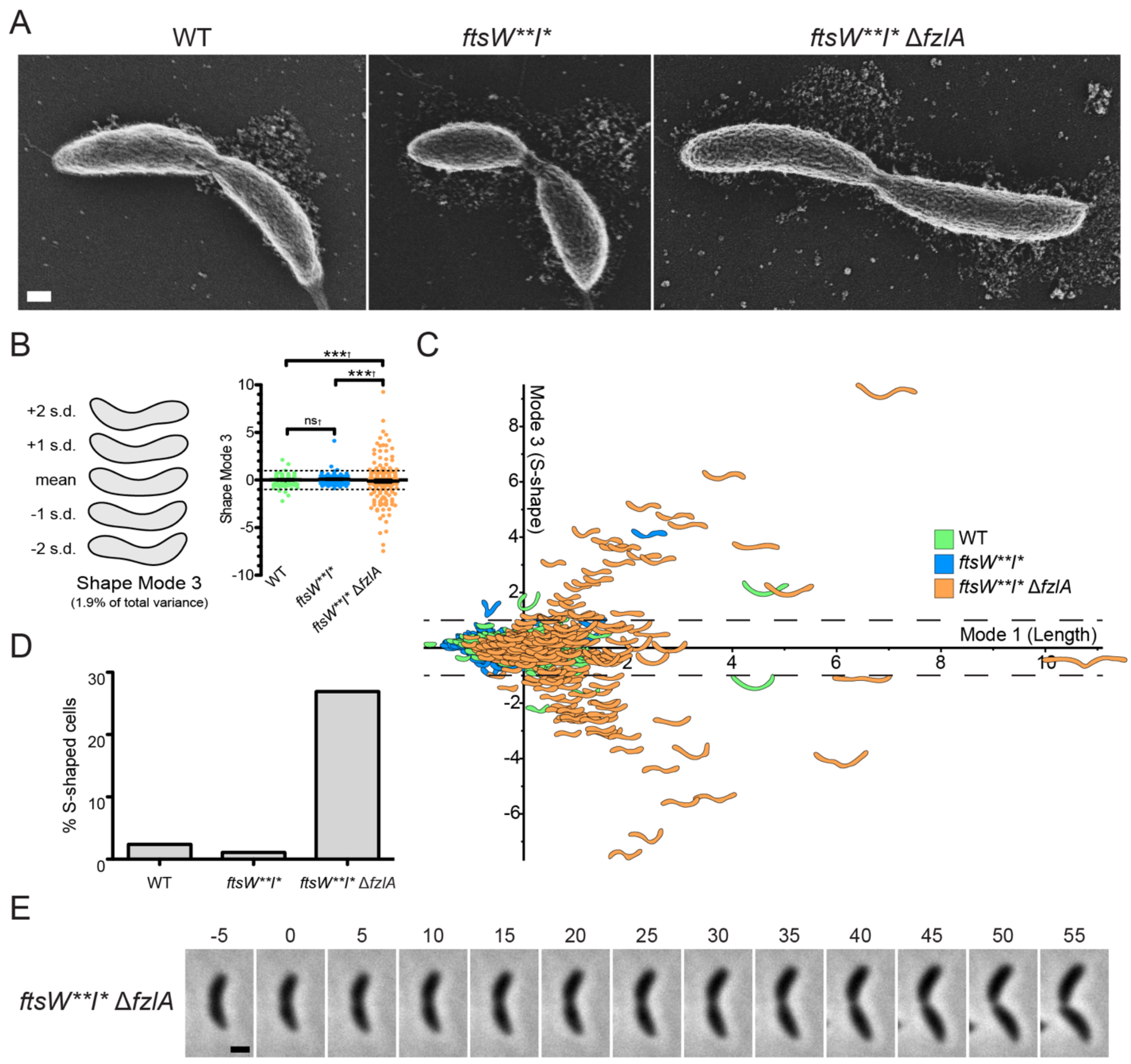

Figure 33. *fzlA* is required for global shape maintenance.

(A) SEM images of cells from the indicated strains. Scale bar: 200 nm.

(B) PCA of cell shape in a population of cells that have initiated constriction from the indicated strains. Shape mode 3 approximately captures degree of S-shape in cells. Mean cell contour ± 1 or 2 standard deviations (s.d.) is shown (left). Shape mode values for cells in each strain are plotted and mean ± SEM is shown (right). The dashed line drawn at s.d.=1 indicates the cutoff for S-shaped cells (cells with an |s.d.| ≥ 1 are considered to be S-shaped). A Brown-Forsythe

Levene-type test (used in populations not assumed to be normally distributed) was performed using R to compare population variances (†): $^{ns}P>0.05$, $^{***}P\leq0.001$. From left to right, n = 292, 279, 290.

(C) Plot of shape mode 3 (S-shape) vs. shape mode 1 (length) values for a population of cells that have initiated constriction from the indicated strains. The dashed lines drawn at |s.d.|=1 indicates the cutoff for S-shaped cells.

(D) Plot of percentage of S-shaped cells present in a population of cells that have initiated constriction from the indicated strains. Cells from (B) with an |s.d.| ≥ 1 are considered S-shaped.

(E) Micrographs of cell twisting during division in an *ftsW**I** Δ*fzlA* cell. Constriction starts at t=0 minutes and concludes in the last frame upon cell separation. Scale bar: 1 μm.

Strain key (*Caulobacter*): WT (EG865), *ftsW**I** (EG1557), *ftsW**I** Δ*fzlA* (EG2170).

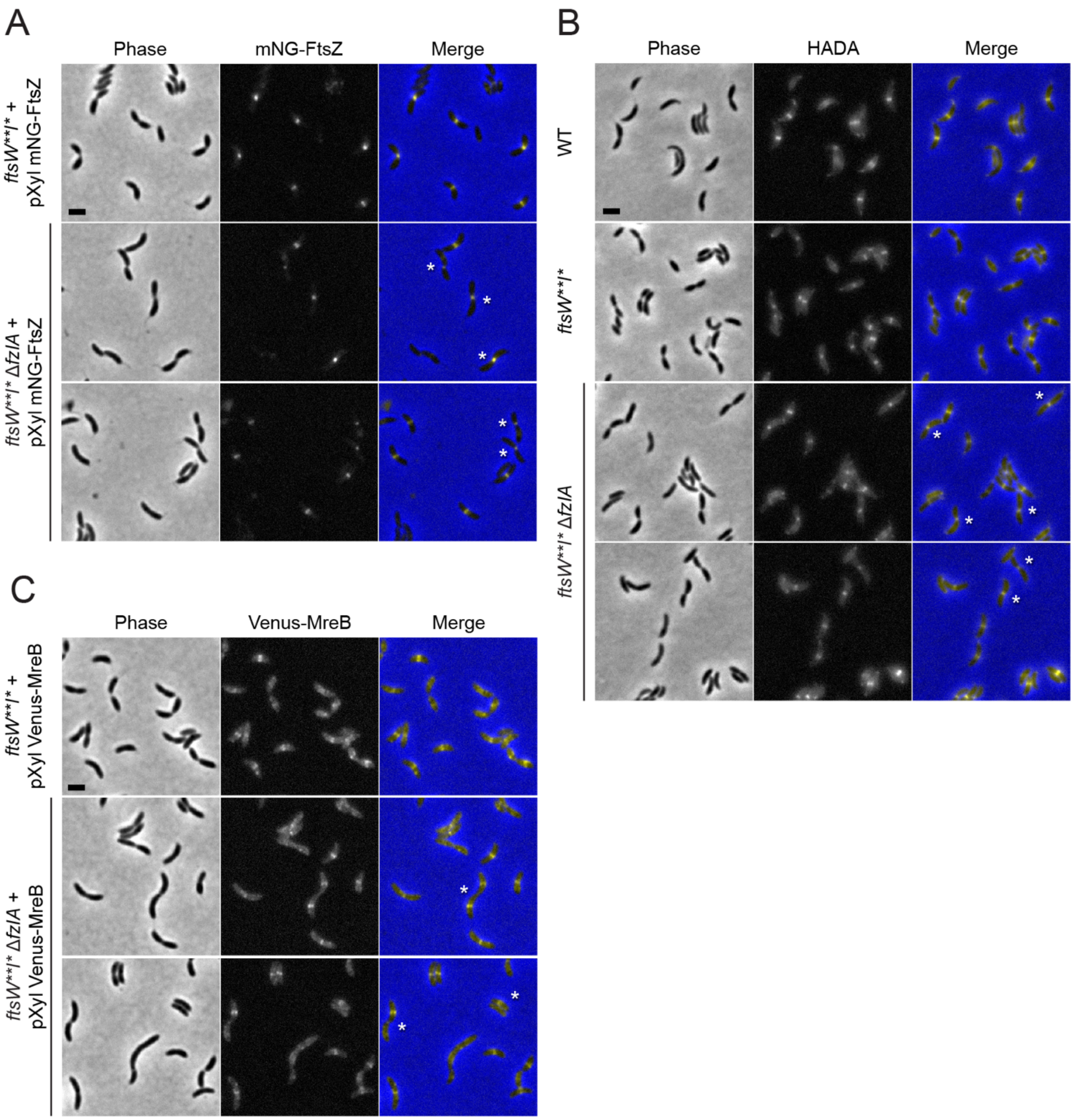
A
Phase
mNG-FtsZ
Merge
ftsW**I* + pXyl mNG-FtsZ
ftsW**I* ΔfzlA + pXyl mNG-FtsZ
B
Phase
HADA
Merge
WT
ftsW**I*
ftsW**I* ΔfzlA
C
Phase
Venus-MreB
Merge
ftsW**I* + pXyl Venus-MreB
ftsW**I* ΔfzlA + pXyl Venus-MreB

Figure 34. FtsZ, MreB, and PG synthesis localization is unaffected in *ftsWI* ΔfzlA* cells.** (A) Phase contrast, fluorescence, and merged microscopy images depicting mNG-FtsZ localization in cells of the indicated strains in the presence of inducer (xylose). White asterisks mark S-shaped cells. Scale bar = 2 μm.

(B) Phase contrast, fluorescence, and merged microscopy images depicting Venus-MreB localization in cells of the indicated strains in the presence of inducer (xylose). White asterisks mark S-shaped cells. Scale bar = 2 µm.

(C) Phase contrast, fluorescence, and merged microscopy images depicting HADA localization in cells of the indicated strains after a 5 minute HADA pulse. White asterisks mark S-shaped cells. Scale bar = 2 µm. Strain key (*Caulobacter crescentus*): *ftsW**I* + pXyl mNG-ftsZ* (EG2157), *ftsW**I* ΔfzlA + pXyl mNG-ftsZ* (EG2326), *ftsW**I* + pXyl Venus-mreB* (EG2377), *ftsW**I* ΔfzlA + pXyl Venus-mreB* (EG2378), WT (EG865), *ftsW**I** (EG1557), *ftsW**I* ΔfzlA* (EG2170).

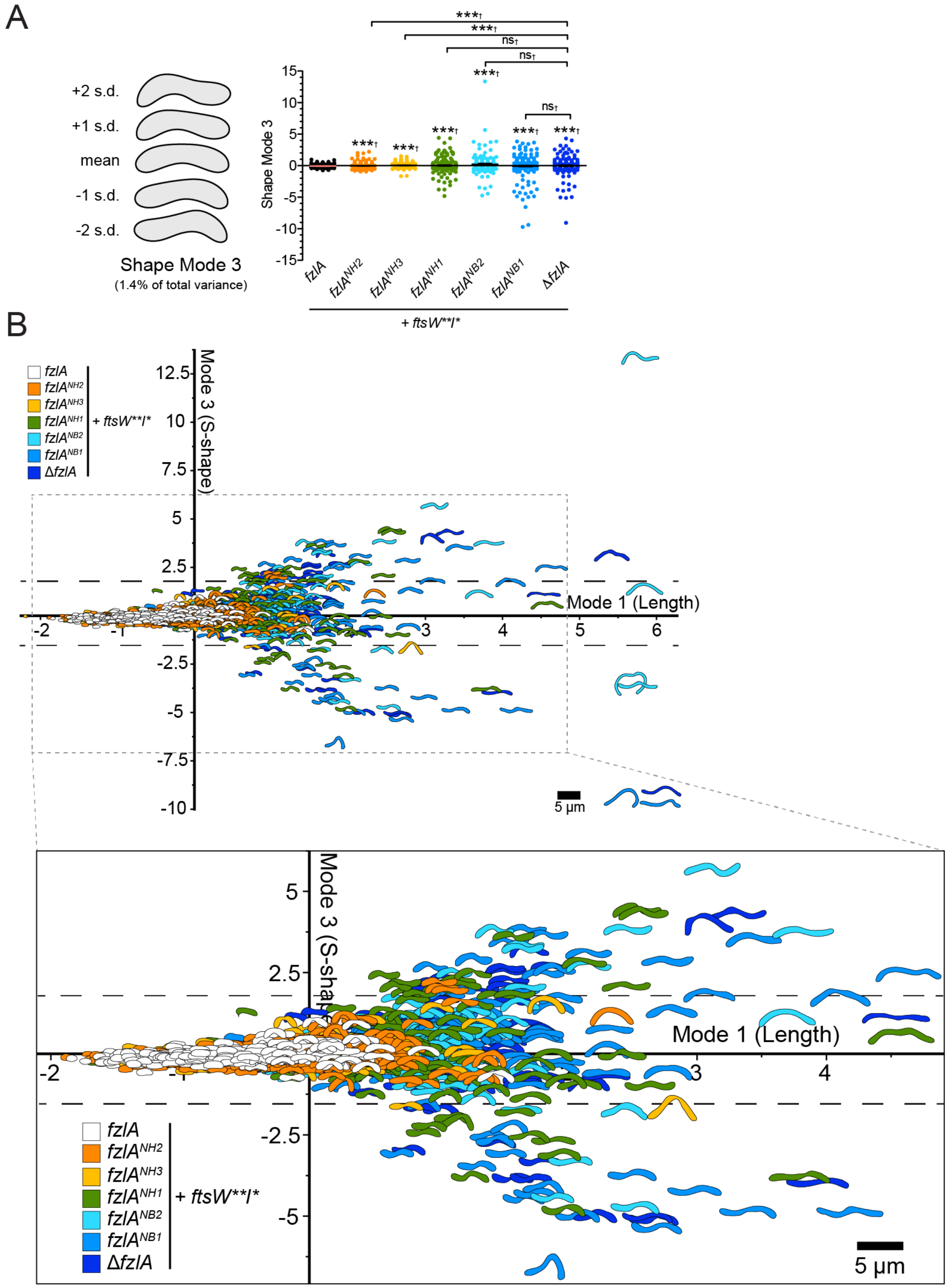

Figure 35. Interaction of FtsZ with FzlA is necessary for proper division site shape maintenance.

(A) PCA of cell shape in a population of unsynchronized cells (not all cells are necessarily actively constricting) from the indicated strains. Shape mode 3 approximately captures degree of S-shape in cells. Mean cell contour ± 1 or 2 standard deviations (s.d.) is shown (left). Shape mode values for cells in each strain are plotted and mean ± SEM is shown (right). A Brown-Forsythe Levene-type test (which is used in populations not assumed to be normally distributed) was performed to determine differences between population variances (†): $^{ns}P>0.05$, $^{***}P\leq0.001$. From left to right, n = 269, 375, 218, 250, 177, 289, 211.

(B) Plot of shape mode 3 (degree of S-shape) vs. shape mode 1 (length) values in a population of unsynchronized cells (not all cells are necessarily actively constricting) from the indicated strains. The dashed lines qualitatively demark the boundary between cells that appear to be S-shaped and those that display normal curvature. Inset presents a zoomed in view of the highlighted region of interest. Strain key (*Caulobacter crescentus*): *ftsW**I* fzlA* (EG1557), *ftsW**I* fzlA*^{NH2} (EG2111), *ftsW**I* fzlA*^{NH3} (EG2489), *ftsW**I* fzlA*^{NH1} (EG2492), *ftsW**I* fzlA*^{NB2} (EG2485), *ftsW**I* fzlA*^{NB1} (EG2495), *ftsW**I** Δ*fzlA* (EG2170).

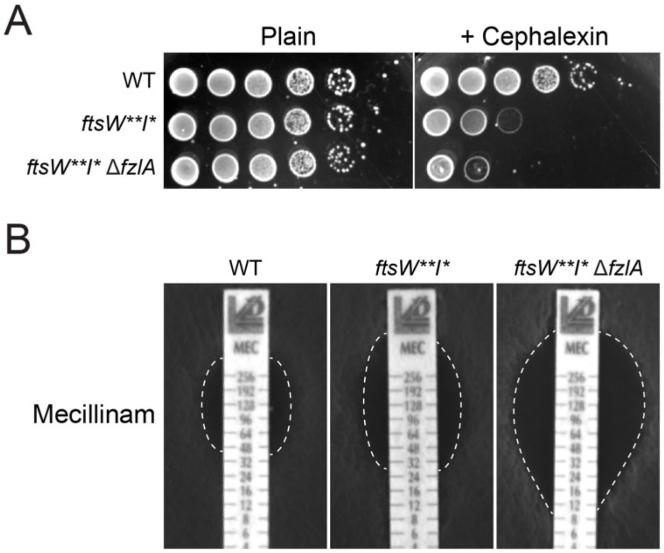
A
Plain
+ Cephalexin
WT
ftsW**I*
ftsW**I* ΔfzlA
B
WT
ftsW**I*
ftsW**I* ΔfzlA
Mecillinam
MEC
256
192
128
96
64
48
32
24
16
12
8
6

Figure 36. Loss of *fzlA* leads to increased cell wall antibiotic sensitivity.

(A) Spot dilutions (diluted ten-fold) of the indicated strains plated on PYE ± cephalexin (6 μg/ml).

(B) Plates of the indicated strains grown in the presence of mecillinam minimum inhibitory concentration (MIC) test strips, with antibiotic concentration decreasing from top to bottom. The zone of clearance is highlighted in white (dashed line).

Strain key (*Caulobacter*): WT (EG865), *ftsW**I** (EG1557), *ftsW**I** Δ*fzlA* (EG2170).

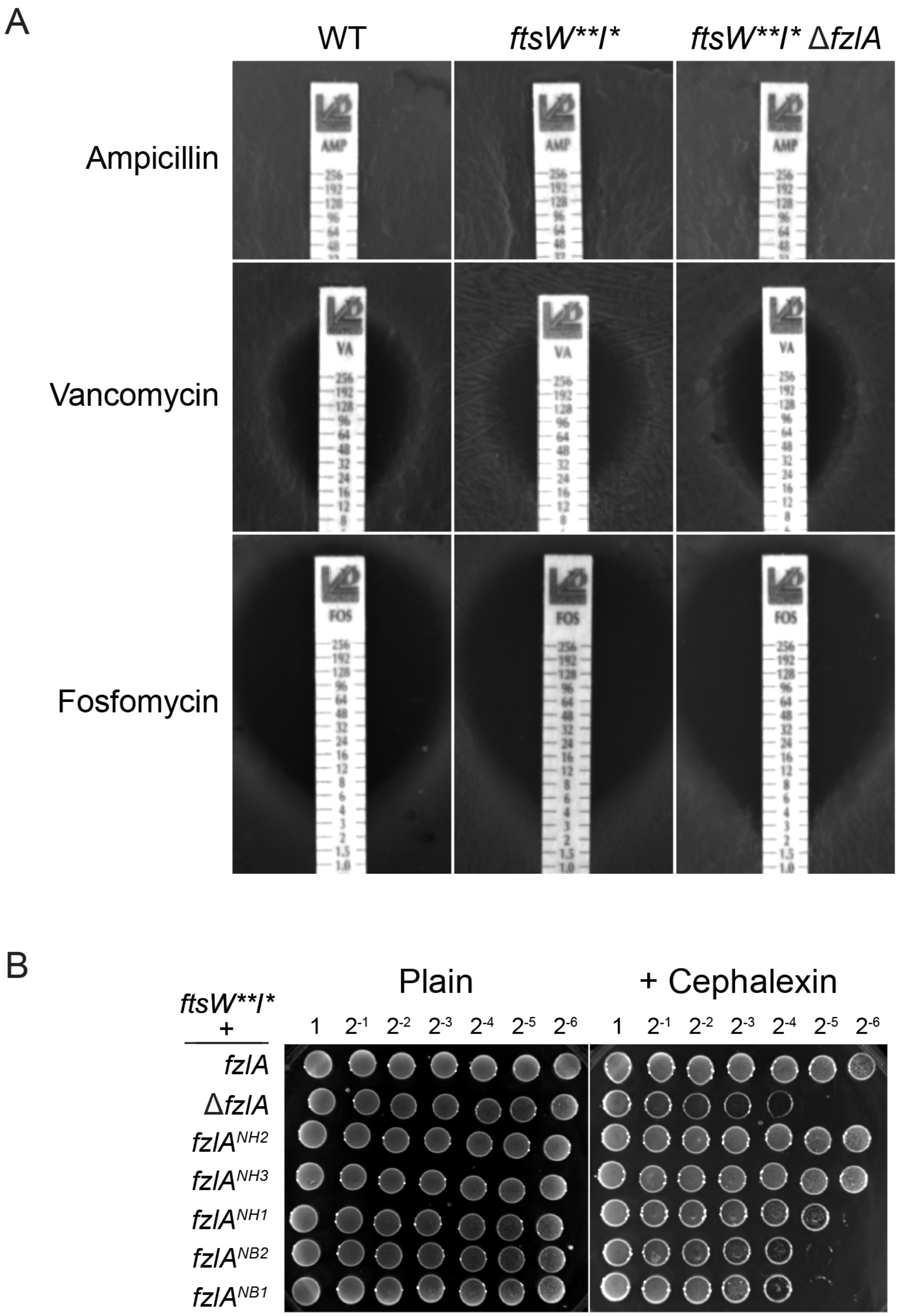
A
WT
ftsW**I*
ftsW**I* ΔfzlA
Ampicillin
Vancomycin
Fosfomycin
AMP
VA
FOS
256
192
128
96
64
48
32
24
16
12
8
6
4
3
2
1.5
1.0
B
Plain
+ Cephalexin
ftsW**I* +
1
2^{-1}
2^{-2}
2^{-3}
2^{-4}
2^{-5}
2^{-6}
fzlA
ΔfzlA
$fzlA^{NH2}$
$fzlA^{NH3}$
$fzlA^{NH1}$
$fzlA^{NB2}$
$fzlA^{NB1}$

Figure 37. Effect of loss of FzlA and FzlA-FtsZ interaction on resistance to cell wall antibiotics.

(A) Plates of the indicated strains grown in the presence of antibiotic minimum inhibitory concentration (MIC) test strips, with antibiotic concentration decreasing from top to bottom. (B) Spot dilutions (diluted two-fold) of the indicated strains plated on PYE ± cephalexin (6 µg/ml). Strain key (*Caulobacter crescentus*): WT (EG865), *ftsW**I* fzlA* (EG1557), *ftsW**I* fzlA*^{NH2} (EG2111), *ftsW**I* fzlA*^{NH3} (EG2489), *ftsW**I* fzlA*^{NH1} (EG2492), *ftsW**I* fzlA*^{NB2} (EG2485), *ftsW**I* fzlA*^{NB1} (EG2495), *ftsW**I** Δ*fzlA* (EG2170), *fzlA*^{NH2} (EG1600), *fzlA*^{NH3} (EG1909).

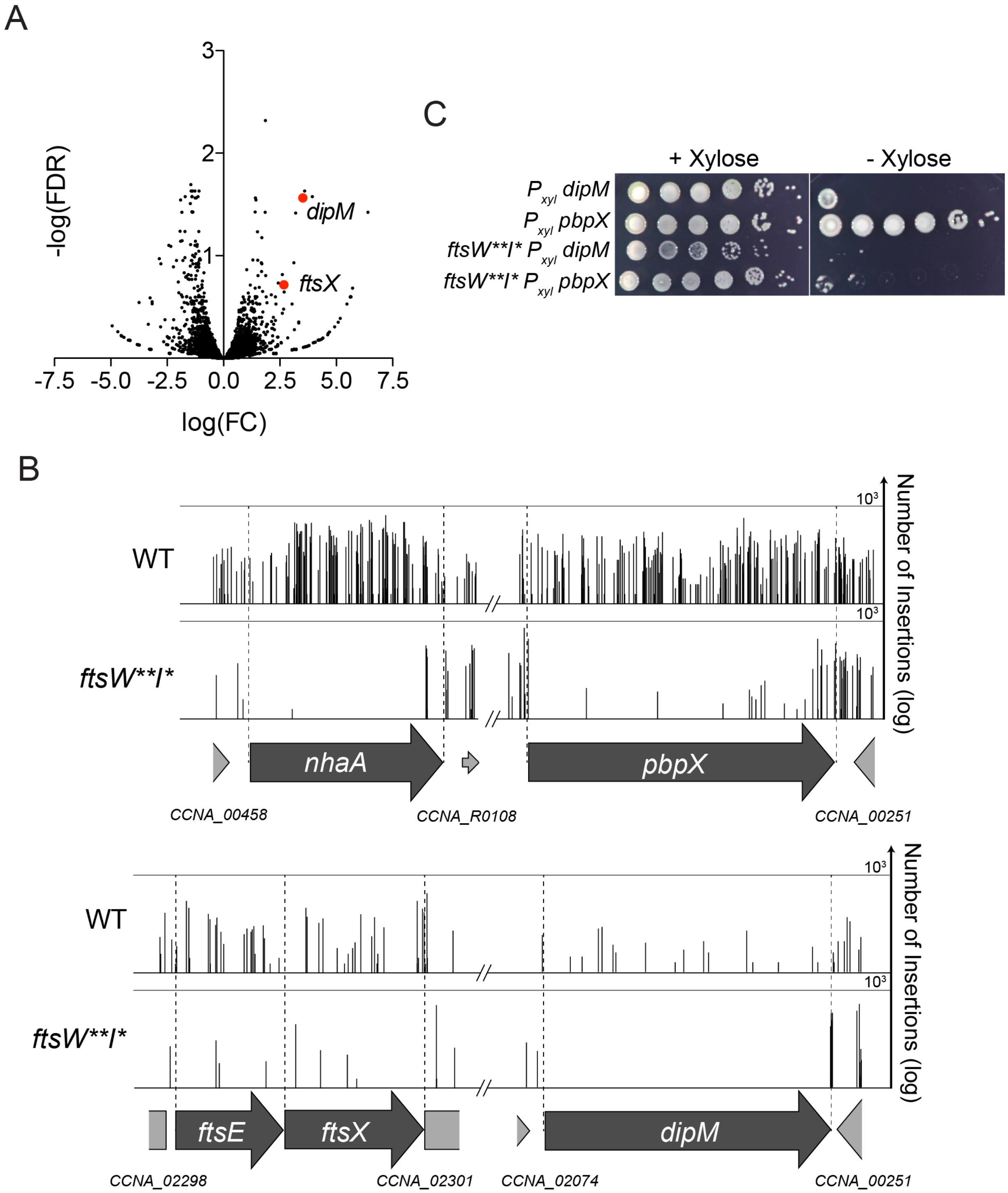

Figure 38. Multiple non-essential division genes become essential in a hyperactive PG synthase background.

(A) Volcano plot of the negative $\log_{10}$ of the false discovery rate (-log(FDR)) vs. $\log_2$ of the fold change of each gene in WT vs. *ftsW**I** strains determined by Tn-Seq analysis. This is a zoomed in and cropped view of the volcano plot from Figure 1F.

(B) Plot of transposon insertion frequency in essential division genes in WT (top) vs. *ftsW**I** (bottom) cells. Genetic loci are annotated below the plot. Number of reads is displayed on a logarithmic scale.

(C) Spot dilutions (diluted ten-fold) of the indicated strains grown +/- xylose (to induce gene expression) or +/- glucose (non-inducer control).

Strain key (*Caulobacter*): WT (EG2366), *ftsW**I** (EG1557), *P_{xyl} dipM* (EG2771), *P_{xyl} pbpX* (EG2772), *ftsW**I* dipMΔC P_{xyl} dipM* (EG2779), *ftsW**I* pbpXΔC P_{xyl} pbpX* (EG2781).

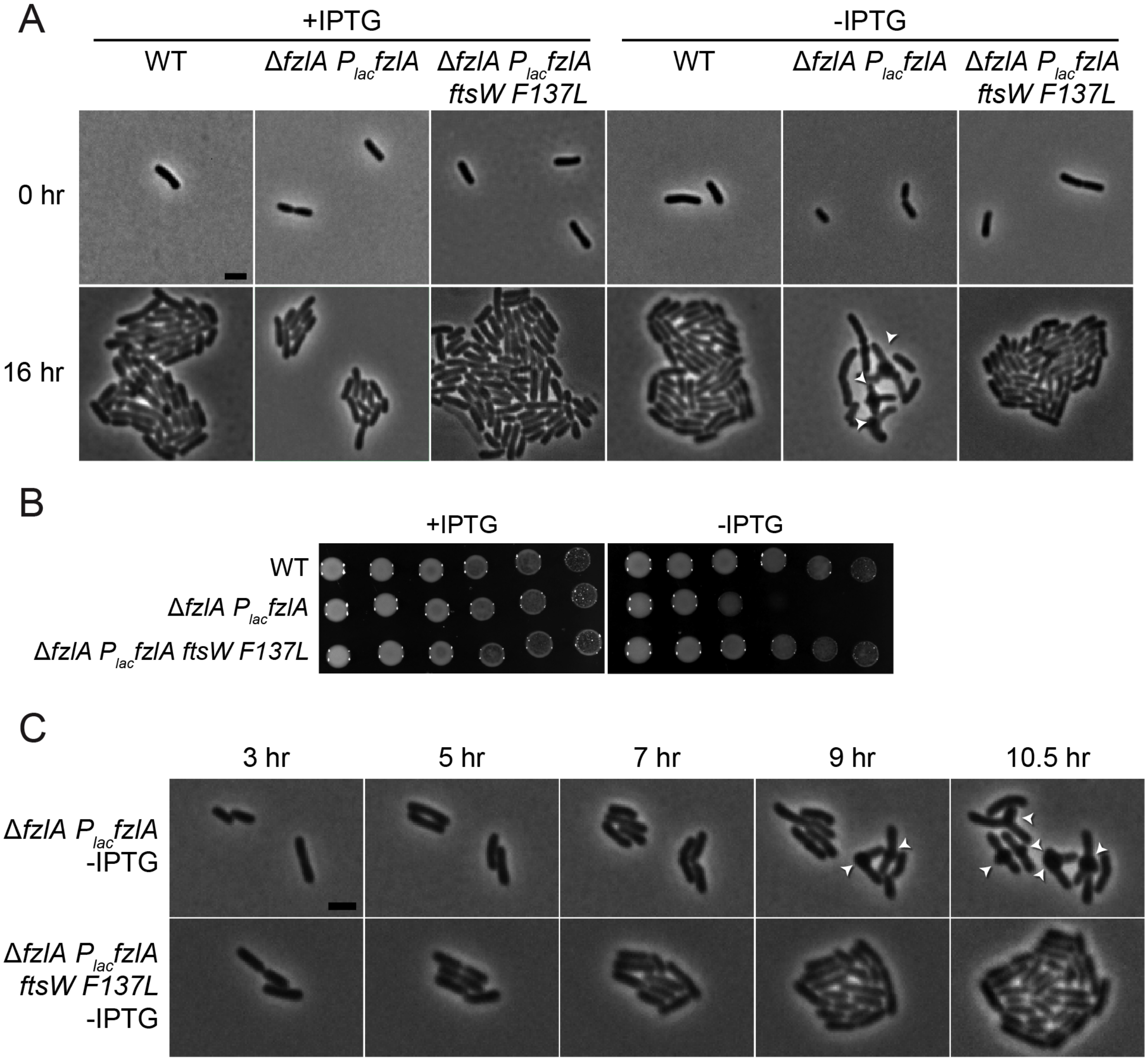
A
+IPTG
-IPTG
WT
ΔfzlA P lac fzlA
ΔfzlA P lac fzlA ftsW F137L
WT
ΔfzlA P lac fzlA
ΔfzlA P lac fzlA ftsW F137L
0 hr
16 hr
B
+IPTG
-IPTG
WT
ΔfzlA P lac fzlA
ΔfzlA P lac fzlA ftsW F137L
C
3 hr
5 hr
7 hr
9 hr
10.5 hr
ΔfzlA P lac fzlA -IPTG
ΔfzlA P lac fzlA ftsW F137L -IPTG

Figure 39. The ability of hyperactive *ftsW* to suppress loss of *fzlA* is conserved.

(A) Micrographs of PG synthase hyperactive mutant cells ± FzlA in *Agrobacterium tumefaciens*. *fzlA* was induced where indicated with IPTG and depleted where indicated upon removal of IPTG, then grown for 16 hours on agarose pads. White arrowheads mark ectopic poles at midcell. Scale bar: 2 µm.

(B) Spot dilutions (diluted ten-fold) of the indicated strains grown in the presence or absence of IPTG to control *fzlA* expression, in *A. tumefaciens*.

(C) Phase contrast time-lapse microscopy images depicting WT and PG synthase hyperactive mutant cells depleted of FzlA over time. White arrowheads mark ectopic poles at midcell. Scale bar: 2 μm.

Strain key (*A. tumefaciens*): WT (PBA44)(Figueroa-Cuilan *et al.*, 2016); Δ*fzlA* P_{lac}*fzlA* (PBA199); Δ*fzlA* P_{lac}*fzlA ftsWF137L* (PBA232).

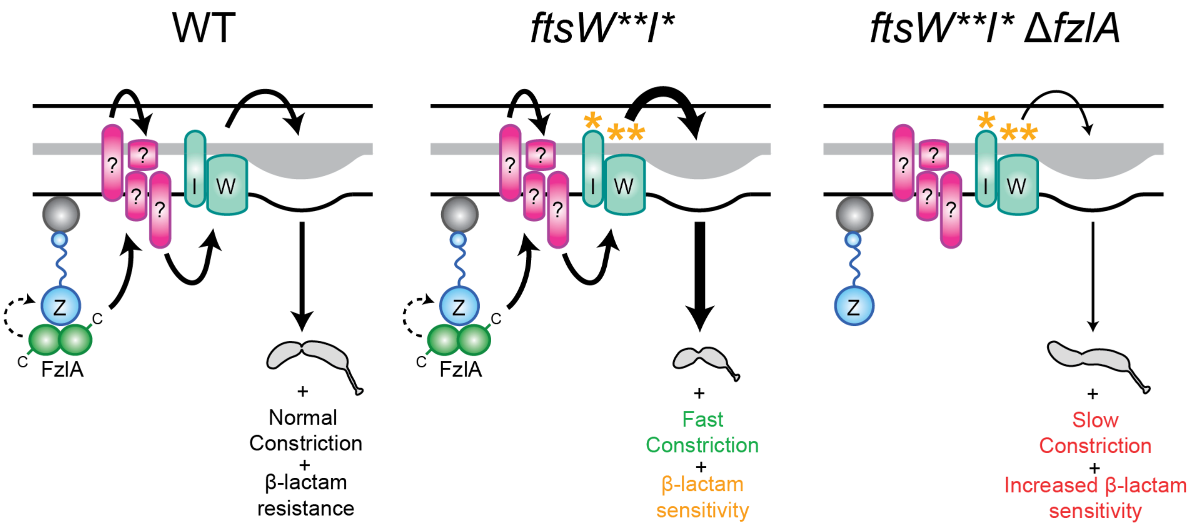
WT
ftsW**I*
ftsW**I* ΔfzlA
?
I
W
Z
C
FzlA
+
Normal
Constriction
+
β-lactam
resistance
Fast
Constriction
β-lactam
sensitivity
Slow
Constriction
Increased β-lactam
sensitivity

Figure 40. FzlA is required for activation of FtsWI and regulates the geometry of PG insertion.

FzlA is required for activation of FtsWI and likely signals (solid arrow) through unidentified intermediate factor(s), possibly via its C-terminus, in a manner dependent on interaction with FtsZ to effect normal cell shape, normal constriction rate, and antibiotic resistance (left). FzlA may also or alternatively contribute to cell wall synthesis activation by influencing FtsZ dynamics (dashed arrow, left). FtsW**I* can still receive input from FzlA (either through signaling, influence of FtsZ dynamics or some combination of both), which in addition to its own hyperactivity, leads to faster constriction and antibiotic sensitivity likely associated with positive misregulation of PG insertion (middle). FtsW**I* can function in the absence of FzlA, but with misregulated activity, leading to twisting during constriction, slower constriction speed, and increased antibiotic sensitivity (right).

Materials and Methods

4.1 Plasmid construction

Plasmids were created using standard molecular cloning procedures including PCR, restriction digestion, and ligation, unless otherwise indicated. Creation of the *fzlA* mutant gene library was performed using Multi Site-Directed Mutagenesis Kit (Agilent Genomics), described briefly here. First, a list of potential FtsZ-interacting residues was first complied based on a number of criteria. Residues chosen were generally surface-exposed, charged, conserved across α-proteobacteria or a combination of these factors. Mutagenesis was then performed using a QuikChange Lightning Multi Site-Directed Mutagenesis Kit (Agilent Genomics). Primers were designed using Agilent's QuikChange Primer Design Program and contained 1-4 mutated residues each. The resulting mutations were non-conservative, containing either charge reversals (for charged residues) or dissimilar amino acids (eg, Ala for Trp). Mutations were made in pEG910 (pVCHYN-2 *fzlA*), a plasmid encoding a vanillate-inducible *mCherry-fzlA* fusion, for use in *in vivo* screening. Mutagenesis of *ftsW* for *A. tumefaciens* was similarly performed using a QuikChange Lightning Multi Site-Directed Mutagenesis Kit (Agilent Genomics), with primers designed using Agilent's QuikChange Primer Design Program, as described above and previously (Lariviere *et al.*, 2018). Finally, pEG1345 was constructed using an NEBuilder HiFi DNA Assembly Cloning Kit (NEB).

4.2 Strains

Caulobacter crescentus strains were derived from the NA1000 WT strain. Unless otherwise indicated, *Caulobacter* colonies were isolated from solid 1.5% agar peptone yeast extract (PYE) plates grown at 30 °C and cells were grown in liquid culture in PYE shaking at 30 °C (Meier *et al.*, 2016). Antibiotic MIC analysis was performed using antibiotic test strips (Liofilchem), which include a concentration gradient of 0.016-256 mg/L for all antibiotics tested. Inducers and antibiotics were added to liquid (and solid) PYE media at the following concentrations: 0.3 (0.3)% xylose, 0.3 (0.3)% glucose, 0.5 (0.5) mM vanillate, 5 (25) μg ml^{-1} kanamycin, 25 (100) μg ml^{-1} spectinomycin, (5 μg ml^{-1}) streptomycin, and 1 (1) μg ml^{-1} chloramphenicol. Where indicated, *Caulobacter* cells were treated with 6 μg ml^{-1} of cephalexin. Prior to induction or depletion, cells were washed three times in plain PYE.

A. tumefaciens were grown in *A. tumefaciens* glucose and $(NH_4)_2SO_4$ (ATGN) minimal medium (Morton and Fuqua, 2012), with 0.5% glucose at 28°C. *E. coli* strains were grown in LB medium at 37°C. IPTG was added at a concentration of 1 mM when necessary. To make the Δ*fzlA* P_{lac}*fzlA* strain (PBA199), first, a mini-Tn7 vector containing IPTG inducible *fzlA*, along with the pTNS3 helper plasmid, were introduced into Δ*tetRA* a-*att*Tn7 cells (PBA44) via electroporation as previously described (Figueroa-Cuilan *et al.*, 2016). Deletion of *fzlA* (for PBA199) and allelic exchange of *ftsW* (for PBA232) were subsequently performed by transferring the corresponding suicide vector to *A. tumefaciens* via conjugation with *E. coli* S17.

4.3 Spot dilutions, growth analysis, and synchrony

Spot dilutions for *Caulobacter* were performed by serially diluting cells at the indicated fraction (1/10 or 1/2), before plating. Growth rates were obtained by measuring optical density at 600 nm

(OD_{600}) values every 30 minutes of cells grown in a 96-well plate shaking at 30°C, using a Tecan Infinite 200 Pro plate reader. *Caulobacter* cell synchrony was performed as previously described (Goley *et al.*, 2011). Briefly, log phase cells were washed with M2 salts (6.1 mM Na_2HPO_4, 3.9 mM KH_2PO_4, 9.3 mM NH_4Cl) (Hottes *et al.*, 2004), resuspended in 1:1 M2:Percoll, then centrifuged at 11,200 x *g*. The swarmer band was isolated, and cells were subsequently washed twice in M2, then resuspended in PYE.

For *A. tumefaciens* spot dilutions, cells were grown overnight in ATGN minimal medium in the presence of IPTG at 1 mM concentration, washed, then pre-depleted of IPTG for 16 hours where indicated. Cells were then serially diluted (ten-fold) and spotted on ATGN minimal medium with the presence or absence of IPTG.

4.4 Protein Purification

FtsZ, FtsZΔCTL, and FtsZΔCTLC were expressed in *E. coli* Rosetta (DE3) pLysS and purified as previously described (Sundararajan *et al.*, 2015). To purify His_6-FzlA for crystallization and co-sedimentation, FzlA (GenBank ID ACL97219.2, UNIPROT number A0A0H3CDY2) was cloned with an N-terminal His_6-tag. The protein was expressed at 37°C in *E. coli* C41 (DE3) cells for 4 hours. Cells were lysed in buffer A (50 mM Tris, 300 mM NaCl, 40 mM imidazole, pH 8.0) by passing through a Constant Systems cell disruptor at 25 kpsi. The soluble fraction was loaded on a nickel column (2x5 ml HisTrap, GE Healthcare), washed thoroughly with 250 ml buffer A and the protein was eluted by 0-1 M imidazole gradient. Peak fractions were pooled, concentrated and subjected to size-exclusion chromatography on Sephacryl S200 (GE Healthcare) in buffer B (50 mM Tris, 300 mM NaCl, pH 8.0). Peak fractions were concentrated to 10 mg/ml and stored at -80°C.

To purify untagged FzlA for biochemical characterization, His_6-SUMO-FzlA or FzlA mutant was first expressed at 30°C in Rosetta (DE3) pLysS *E. coli* cells for 4 hours following induction with 0.25 to 1mM isopropylthioglactoside (IPTG). Cells were pelleted by centrifugation at 6,000 x g for 10 minutes at 4°C, then resuspended in 40 ml buffer A (50 mM HEPES-KOH, 300 mM KCl, 20 mM imidazole, 10% glycerol, pH 7.2) per 1 L of culture, and snap frozen in liquid nitrogen. The cell suspension was thawed and incubated at room temperature for 1 hour, after receiving the following additives: 1 mg ml^{-1} lysozyme, 2 mM phenylmethyl sulphonyl fluoride (PMSF), 2 units ml^{-1} DNAse I (New England Biolabs), and 2.5 mM $MgCl_2$. Cells were sonicated, then centrifuged at 15,000 x g for 30 minutes at 4°C. The supernatant was filtered and loaded onto a HisTrap FF 1 ml nickel column (GE Life Sciences). The column was washed first with 100% buffer A, then 3% buffer B (50 mM HEPES-KOH, 300 mM KCl, 1 M imidazole, 10% glycerol, pH 7.2) to remove non-specifically bound proteins. The His_6-tagged protein eluted upon addition of 30% buffer B. Peak fractions were concentrated, then simultaneously incubated with His_6-ULP protease to cleave the His_6-SUMO tag and dialyzed overnight into buffer A. The solution was again loaded onto a HisTrap FF 1 ml nickel column and the flow through was collected, concentrated, and dialyzed overnight into storage buffer (50 mM HEPES-KOH, 300 mM KCl, 10% glycerol, pH 7.2), before being snap-frozen in liquid nitrogen and stored at -80°C.

4.5 Crystallization and structure determination

Initial conditions were identified at the MRC-LMB crystallization facility (Stock *et al.*, 2005). His_6-FzlA yielded cubic crystals in the following conditions: 50% PEG 200, 0.2 M NaCl, 0.1 M sodium potassium phosphate pH 6.2. Crystals diffracted to 2 Å and a native dataset was collected in house using a Rigaku X-ray generator. Heavy metal derivatives were obtained by soaking the native crystals with ethyl mercury thiosalicylate (EMTS). The soaked crystals diffracted to 3 Å in house. FzlA crystals belonged to spacegroup $I2_13$ with one molecule in the asymmetric unit. Cell constants were a = b = c = 124.33 Å. Initial phases were determined with autoSHARP (Vonrhein *et al.*, 2007). The model was built with MAIN (Turk, 2013) and refined with PHENIX . For more details please refer to Table 1. The structure was deposited in the Protein Data Bank (PDB) with code 5NR1.

4.6 Bacterial Two-Hybrid (BTH) Analysis

Bacterial two-hybrid testing was performed as described by Karimova et al (Karimova *et al.*, 1998). Briefly, we constructed plasmids containing genes of interest fused to the T18 and T25 domains of the adenylate cyclase gene, which were then transformed into BTH101 *E. coli* cells. Transformants were grown overnight in liquid culture with 0.5 mM IPTG, then plated on agar containing 0.5 mM IPTG and 40 μg/ml X-gal. In strains where the T18 and T25 fusions interacted, expression of β-galactosidase resulted in blue colonies.

4.7 Co-immunoprecipitation

The co-immunoprecipitation was performed as previously described (Bowman *et al.*, 2008) without crosslinking and with a few other notable differences. Cell cultures were grown to exponential phase in 1L of PYE medium, then pelleted. Pellets were washed and re-suspended in co-immunoprecipitation buffer [20mM HEPES pH 7.5, 100mM NaCl, 20% glycerol, Pierce Protease Inhibitor Tablet (1 tablet/liter)]. The cell suspension was passed through a French press at 16,000 psi three times to achieve lysis. Membranes were solubilized by the addition of

IGEPAL CA-630 (1%), sodium deoxycholate (0.5%), and 2mM EDTA. 3xFLAG-FzlA was then immunoprecipitated using anti-FLAG affinity agarose gel (Sigma), and bound proteins were eluted using excess FLAG peptide (Sigma). Samples were subjected to immunoblot analysis (see antibodies and immunoblotting section below).

4.8 FtsZ activity assays

All biochemical assays were performed with 2 μM FtsZ and 4 μM FzlA in MESK polymerization buffer (50 mM MES [pH 6.5], 50 mM KCl) unless indicated otherwise. For high speed co-sedimentation assays, unless otherwise indicated, FzlA ± FtsZ in MESK polymerization buffer containing 10 mM $MgCl_2$, 2 mM GTP, and 0.05% Triton X-100 were incubated in triplicate for 15 minutes at room temperature, then were centrifuged at 280,000 x g for 15 min at 25°C. Low speed co-sedimentation assays were similarly performed, but solutions instead contained 2.5 mM $MgCl_2$ and were centrifuged at 16,000 x g for 15 min at room temperature. Pellet and supernatant from each sample were resolved by SDS-PAGE and stained with Coomassie Brilliant Blue. Gels were imaged with a Gel Doc EZ Gel Imaging System (BioRad) and band intensity was quantified using Image Lab (BioRad). Band intensities were used to calculate the percentage of FzlA present in the pellet.

Right angle light scattering (RALS) of FzlA ± FtsZ in MESK polymerization buffer with 2.5 mM $MgCl_2$ and 2 mM GTP was measured using a Fluoromax-3 spectrofluorometer (Jobin Yvon Inc.) with 350 nm excitation and emission wavelengths and 2 nm slits. Transmission electron microscopy (TEM) was performed on FzlA ± FtsZ in MESK polymerization buffer with 2.5 mM $MgCl_2$ and 2 mM GTP using 0.75% uranyl formate staining as previously described (Sundararajan *et al.*, 2015). TEM Samples were imaged using a Philips/FEI BioTwin CM120

TEM equipped with an AMT XR80 8 megapixel CCD camera (AMT Imaging, USA). GTPase activity of FtsZ (1.75 μm) ± WT or mutant FzlA protein (3.5 μm) was measured in triplicate using a colorimetric SensoLyte MG Phosphate Assay Kit (AnaSpec), following the company's protocol.

4.9 Antibodies and Immunoblot analysis

For immunoblotting of whole cell lysates, log phase cells were pelleted, then resuspended and boiled in SDS-PAGE loading buffer. For co-immunoprecipitation, eluted samples were boiled in SDS-PAGE loading buffer. Samples were resolved by SDS-PAGE, and protein was subsequently transferred to nitrocellulose membranes. Membranes were first probed with α-FzlA (Goley *et al.*, 2010b) (1:5,000 - 1:8,000), α-HU (Bowman *et al.*, 2010) (1:50,000; loading control), α-FtsZ (1:20,000) or α-RFP (1:2,000) primary antibodies, then incubated with HRP-conjugated α-rabbit (1:10,000 - 1:20,000) secondary antibody, or probed with α-FLAG (Sigma) (1:1,000) primary antibody, then incubated with HRP-conjugated α-mouse (1:10,000) secondary antibody. Membranes were subsequently imaged with an Amersham Imager 600 RGB gel and membrane imager (GE).

4.10 Light microscopy imaging and analysis

Images of log phase *Caulobacter* cells were obtained using either phase contrast microscopy, with cells grown on either 1% agarose PYE pads or 1% agarose dH_2O pads, or, when indicated, fluorescence microscopy, with cells grown on 1% agarose dH_2O pads. For fluorescence microscopy, mNG-FtsZ expression was induced for 1 hour with xylose then imaged through the GFP filter and venus-MreB expression was induced for 2 hours with xylose then imaged through the YFP filter. For determination of PG incorporation localization, cells were pulsed with 0.82 mM HADA for 5 minutes, washed twice with PBS, then visualized through the DAPI filter. For other fluorescence imaging experiments, an ET-dsRED filter cube was used for mCherry and ET-EGFP for Venus. For time-lapse imaging, as previously described (Lariviere *et al.*, 2018), synchronized cells were placed on 1% agarose PYE pads and imaged using phase contrast microscopy at room temperature (RT), with images being acquired at 5 minute intervals at 100x. Imaging of *Caulobacter* cells was performed using a Nikon Eclipse Ti inverted microscope with a Nikon Plan Fluor × 100 (numeric aperture 1.30) oil Ph3 objective and Photometrics CoolSNAP HQ^2 cooled CCD (charge-coupled device) camera (Lariviere *et al.*, 2018). For *A. tumefaciens* phase contrast microscopy, exponentially growing cells were spotted on 1% agarose ATGN pads as previously described (Howell *et al.*, 2017), then imaged. For *A. tumefaciens* time-lapse microscopy, images were collected every ten minutes. Microscopy of *A. tumefaciens* cells was performed with an inverted Nikon Eclipse TiE with a QImaging Rolera em-c^2 1K EMCCD camera and Nikon Elements Imaging Software.

Images were processed in Adobe Photoshop. For automated determination of dimensions of log phase cells, cell length and width were measured using FIJI (Fiji: an open-source platform for biological-image analysis | Nature Methods, n.d.) and MicrobeJ software, similar to as previously described (Ducret *et al.*, 2016; Lariviere *et al.*, 2018). Constriction rate and elongation rate were also determined using MicrobeJ (Ducret *et al.*, 2016). Briefly, MicrobeJ software allowed for tracking of cells imaged by time-lapse microscopy throughout the division process, with automatic detection of constriction initiation (based on changes in positive envelope curvature near midcell) and manual determination of cell separation. Cell length was found for cells at each time point, cell width was found at the site of constriction (in chapter 2, cell width was measured approximately at midcell; in chapter 3, this method was refined to specifically determine cell width at the site of constriction), and constriction time was calculated by multiplying the number of frames in which constriction was detected by 5 (since images were acquired every 5 minutes), allowing for calculation of constriction and elongation rates. Constriction failure rate was determined by counting the number of cells which initiated constriction at one division site, failed, then ultimately divided at a separate site. Prism was used for graphing and statistical analysis of calculated terms.

4.11 Cell shape analysis

For cell shape analysis, binary masks of phase contrast images (created using ImageJ and/or FIJI) of log phase cells (synchronized cells in chapter 2; unsynchronized cells in chapter 3) were inputted into Celltool (Pincus and Theriot, 2007), allowing for creation of cell contours, similar to as previously described (Lariviere *et al.*, 2018). Following alignment of cell contours (allowing for reflection in shape analysis performed in chapter 2; not allowing for reflection for shape analysis in chapter 3), a model of cell shape was created and principal component analysis of cell shape variation is performed using Celltool (Pincus and Theriot, 2007). The model created in chapter 2 accounts for 97.3% of the variation in shape among cells in these populations and the model created in chapter 3 accounts for 99.1% of the variation in shape among cells in these populations. The shape modes of interest were either plotted as histograms displaying the cell shape across two dimensions, or as single data points. In chapter 3, R software was used to perform statistical analyses to compare population variances in shape modes across strains. Prism was used for graphing calculated terms.

Maximum pole curvature of synchronized cells was quantified via Celltool, using a plugin created by the Pincus lab (Washington Univeristy-St. Louis). Specifically, the maximum instantaneous curvature (the inverse of the radius of the oscillating disc) at the poles was determined and averaged across the two poles for each individual cell.

4.12 Scanning electron microscopy sample preparation and imaging

For SEM, log phase cells were incubated on poly-lysine (1:10) coated glass cover slip for 15 minutes, then fixed for 1 hour using fixation buffer (1% glutaraldehyde, 0.02 M cacodylate, and 3 mM $MgCl_2$). Cells were gradually dried by washing 3 times with wash buffer (3% sucrose, 0.02 M cacodylate, and 3 mM $MgCl_2$), twice with dH_2O, once each with 30%, 50%, 70%, 90%, 100% ethanol, once with 1:1 ethanol:hexamethyldisiloxane (HMDS), and once with HMDS at 5 minute intervals each, before desiccation overnight. Cover slips were mounted, then coated with a 15 nm gold palladium sputter coat. Samples were then imaged with a LEO/Zeiss Field-emission SEM.

4.13 Transposon library preparation, sequencing, and analysis

Wild type *Caulobacter crescentus* NA1000 (EG2366) or *ftsW**I** triple mutant (EG1557) cells were grown in a large culture (1 liter) to mid-log (0.4-0.6), washed of excess Mg^{2+} with 10% glycerol, and mutagenized with the Ez-Tn5 <Kan-2> transposome (Epicentre). Cells recovered by shaking at 30 °C for 90 minutes, then plated on kanamycin containing plates for 3 days at 30 °C in order to yield roughly 100-500 colonies per plate. Libraries were grown at 30 °C and comprised ~100,000-200,000 colonies each. Mutants were pooled into one library by scraping colonies from the surface of the agar and added into ~25-40 mL PYE. Pooled libraries were shaken to yield a homogenous slurry and sterile glycerol was added to 20%. Libraries were then frozen in liquid nitrogen and stored at -80 °C. Two libraries of each genetic background were prepared individually and compared as biological replicates.

Genomic DNA was extracted from one aliquot of each library using DNeasy Blood and Tissue Kit (Qiagen). Tn-Seq libraries were prepared for Illumina Next-Generation sequencing through sequential PCR amplifications using arbitrary hexamer primers and Tn5-specific primer facing outward for the first round, and indexing primer sets that include unique molecular identifier to filter artifacts arising from PCR duplicates for the second round. Libraries were then pooled and sequenced at the University of Massachusetts Amherst Genomics Core Facility on the NextSeq 550 (Illumina).

For analyses, reads were demultiplexed by index, then each sample Tn-Seq library was concatenated and clipped of the unique molecular identifier linker from the second PCR using Je (Girardot *et al.*, 2016) and the following command:

```
java -jar /je_1.2/je_1.2_bundle.jar clip F1=compiled.gz LEN=6
```

Clipped reads were then mapped back to the *Caulobacter* NA1000 genome (NCBI Reference Sequence: NC_011916.1) using BWA (Li and Durbin, 2010) and sorted using Samtools (Li *et al.*, 2009):

```
bwa mem -t2 clipped.gz | samtools sort -@2 - > sorted.bam
```

Duplicate reads were removed using Je (Girardot *et al.*, 2016) and indexed with Samtools (Li *et al.*, 2009) using the following command:

```
java -jar /je_1.2/je_1.2_bundle.jar markdupes I=sorted.bam O=marked.bam
M=METRICS.txt MM=0 REMOVE_DUPLICATES=TRUE
samtools index marked.bam
```

5' sites of inserted transposons from each library were converted into .wig files containing counts per position and viewed using Integrative Genomics Viewer (Robinson *et al.*, 2011; Thorvaldsdóttir *et al.*, 2013). Coverage and insertion frequency using a bedfile containing all open reading frames from NC_011916.1 with the outer 20% of each gene removed were determined using BEDTools (Quinlan and Hall, 2010) and the following commands:

```
bedtools genomecov -5 -bg marked.bam > marked.bed
bedtools map -a NA1000.txt -b marked.bed -c 4 > output.txt
```

Comparison of transposon insertions was performed using the edgeR package in the Bioconductor suite (Robinson *et al.*, 2010; McCarthy *et al.*, 2012) using a quasi-likelihood F-test (glmQLFit) to determine the false discovery rate adjusted p-values reported here.

4.14 Quantification and Statistical Analysis

Constriction analysis was performed using FIJI and MicrobeJ, as indicated in the Method Details section. Cell shape analysis was performed using Cellool, as indicated in the Method Details section. Tn-Seq analysis using Je, BWA, Samtools, BEDTools, Integrative Genomics Viewer, and the edgeR package in the Bioconductor suite, as indicated in the Method Details section. Prism GraphPad, and where indicated, R, were used perform statistical analyses. Information regarding individual statistical test parameters can be found in the figure legends.

4.15 Data Availability

The Tn-Seq data have been deposited on BioProject (ID: PRJNA526509) and can be accessed at https://www.ncbi.nlm.nih.gov/bioproject/?term=PRJNA526509.

References

Aaron, M., Charbon, G., Lam, H., Schwarz, H., Vollmer, W., and Jacobs-Wagner, C. (2007) The tubulin homologue FtsZ contributes to cell elongation by guiding cell wall precursor synthesis in Caulobacter crescentus. *Mol Microbiol* **64**: 938–952.

Aarsman, M.E.G., Piette, A., Fraipont, C., Vinkenvleugel, T.M.F., Nguyen-Distèche, M., and Blaauwen, T. den (2005) Maturation of the Escherichia coli divisome occurs in two steps. *Mol Microbiol* **55**: 1631–1645.

Addinall, S.G., and Lutkenhaus, J. (1996) FtsZ-spirals and -arcs determine the shape of the invaginating septa in some mutants of Escherichia coli. *Mol Microbiol* **22**: 231–237.

Alexeeva, S., Gadella, T.W.J., Verheul, J., Verhoeven, G.S., and Blaauwen, T. den (2010) Direct interactions of early and late assembling division proteins in Escherichia coli cells resolved by FRET. *Mol Microbiol* **77**: 384–398.

Allard, J.F., and Cytrynbaum, E.N. (2009) Force generation by a dynamic Z-ring in Escherichia coli cell division. *Proc Natl Acad Sci* **106**: 145–150.

Alyahya, S.A., Alexander, R., Costa, T., Henriques, A.O., Emonet, T., and Jacobs-Wagner, C. (2009) RodZ, a component of the bacterial core morphogenic apparatus. *Proc Natl Acad Sci* **106**: 1239–1244.

Anderson, D.E., Gueiros-Filho, F.J., and Erickson, H.P. (2004) Assembly dynamics of FtsZ rings in Bacillus subtilis and Escherichia coli and effects of FtsZ-regulating proteins. *J Bacteriol* **186**: 5775–5781.

Arends, S.J.R., Kustusch, R.J., and Weiss, D.S. (2009) ATP-binding site lesions in FtsE impair cell division. *J Bacteriol* **191**: 3772–3784.

Banerjee, S., F. Scherer, N., and R. Dinner, A. (2016) Shape dynamics of growing cell walls. *Soft Matter* **12**: 3442–3450.

Beaufay, F., Coppine, J., Mayard, A., Laloux, G., Bolle, X.D., and Hallez, R. (2015) A NAD-dependent glutamate dehydrogenase coordinates metabolism with cell division in Caulobacter crescentus. *EMBO J* **34**: 1786–1800.

Bernhardt, T.G., and De Boer, P.A.J. (2003) The Escherichia coli amidase AmiC is a periplasmic septal ring component exported via the twin-arginine transport pathway. *Mol Microbiol* **48**: 1171–1182.

Bhat, N.H., Vass, R.H., Stoddard, P.R., Shin, D.K., and Chien, P. (2013) Identification of ClpP substrates in Caulobacter crescentus reveals a role for regulated proteolysis in bacterial development. *Mol Microbiol* **88**: 1083–1092.

Bi, E., and Lutkenhaus, J. (1990) FtsZ regulates frequency of cell division in Escherichia coli. *J Bacteriol* **172**: 2765–2768.

Bi, E., and Lutkenhaus, J. (1992) Isolation and characterization of ftsZ alleles that affect septal morphology. *J Bacteriol* **174**: 5414–5423.

Bi, E.F., and Lutkenhaus, J. (1991) FtsZ ring structure associated with division in Escherichia coli. *Nature* **354**: 161–164.

Bisson-Filho, A.W., Hsu, Y.-P., Squyres, G.R., Kuru, E., Wu, F., Jukes, C., *et al.* (2017) Treadmilling by FtsZ filaments drives peptidoglycan synthesis and bacterial cell division. *Science* **355**: 739–743.

Biteen, J.S., Goley, E.D., Shapiro, L., and Moerner, W.E. (2012) Three-Dimensional Super-Resolution Imaging of the Midplane Protein FtsZ in Live Caulobacter crescentus Cells Using Astigmatism. *ChemPhysChem* **13**: 1007–1012.

Boer, P. de, Crossley, R., and Rothfield, L. (1992) The essential bacterial cell-division protein FtsZ is a GTPase. *Nature* **359**: 254–256.

Bowman, G.R., Comolli, L.R., Gaietta, G.M., Fero, M., Hong, S.-H., Jones, Y., *et al.* (2010) Caulobacter PopZ forms a polar subdomain dictating sequential changes in pole composition and function. *Mol Microbiol* **76**: 173–189.

Bowman, G.R., Comolli, L.R., Zhu, J., Eckart, M., Koenig, M., Downing, K.H., *et al.* (2008) A polymeric protein anchors the chromosomal origin/ParB complex at a bacterial cell pole. *Cell* **134**: 945–955.

Boyle, D.S., Khattar, M.M., Addinall, S.G., Lutkenhaus, J., and Donachie, W.D. (1997) ftsW is an essential cell-division gene in Escherichia coli. *Mol Microbiol* **24**: 1263–1273.

Brown, P.J.B., Pedro, M.A. de, Kysela, D.T., Henst, C.V. der, Kim, J., Bolle, X.D., *et al.* (2012) Polar growth in the Alphaproteobacterial order Rhizobiales. *Proc Natl Acad Sci* **109**: 1697–1701.

Buske, P.J., and Levin, P.A. (2013) A flexible C-terminal linker is required for proper FtsZ assembly in vitro and cytokinetic ring formation in vivo. *Mol Microbiol* **89**: 249–263.

Buss, J., Coltharp, C., Huang, T., Pohlmeyer, C., Wang, S.-C., Hatem, C., and Xiao, J. (2013) In vivo organization of the FtsZ-ring by ZapA and ZapB revealed by quantitative super-resolution microscopy. *Mol Microbiol* **89**: 1099–1120.

Buss, J., Coltharp, C., Shtengel, G., Yang, X., Hess, H., and Xiao, J. (2015) A Multi-layered Protein Network Stabilizes the Escherichia coli FtsZ-ring and Modulates Constriction Dynamics. *PLOS Genet* **11**: e1005128.

Buss, J.A., Peters, N.T., Xiao, J., and Bernhardt, T.G. (2017) ZapA and ZapB form an FtsZ-independent structure at midcell. *Mol Microbiol* **104**: 652–663.

Cabeen, M.T., Charbon, G., Vollmer, W., Born, P., Ausmees, N., Weibel, D.B., and Jacobs-Wagner, C. (2009) Bacterial cell curvature through mechanical control of cell growth. *EMBO J* **28**: 1208–1219.

Cabeen, M.T., and Jacobs-Wagner, C. (2005) Bacterial cell shape. *Nat Rev Microbiol* **3**: 601–610.

Camberg, J.L., Hoskins, J.R., and Wickner, S. (2009) ClpXP protease degrades the cytoskeletal protein, FtsZ, and modulates FtsZ polymer dynamics. *Proc Natl Acad Sci* **106**: 10614–10619.

Charbon, G., Cabeen, M.T., and Jacobs-Wagner, C. (2009) Bacterial intermediate filaments: in vivo assembly, organization, and dynamics of crescentin. *Genes Dev* **23**: 1131–1144.

Chen, Y., Anderson, D.E., Rajagopalan, M., and Erickson, H.P. (2007) Assembly Dynamics of Mycobacterium tuberculosis FtsZ. *J Biol Chem* **282**: 27736–27743.

Chen, Y., and Erickson, H.P. (2005) Rapid in vitro assembly dynamics and subunit turnover of FtsZ demonstrated by fluorescence resonance energy transfer. *J Biol Chem* **280**: 22549–22554.

Coltharp, C., Buss, J., Plumer, T.M., and Xiao, J. (2016) Defining the rate-limiting processes of bacterial cytokinesis. *Proc Natl Acad Sci* **113**: E1044–E1053.

Coltharp, C., and Xiao, J. (2017) Beyond force generation: Why is a dynamic ring of FtsZ polymers essential for bacterial cytokinesis? *BioEssays* **39**: n/a-n/a.

Corbin, B.D., Wang, Y., Beuria, T.K., and Margolin, W. (2007) Interaction between Cell Division Proteins FtsE and FtsZ. *J Bacteriol* **189**: 3026–3035.

Costa, T., Priyadarshini, R., and Jacobs-Wagner, C. (2008) Localization of PBP3 in Caulobacter crescentus is highly dynamic and largely relies on its functional transpeptidase domain. *Mol Microbiol* **70**: 634–651.

Dajkovic, A., Pichoff, S., Lutkenhaus, J., and Wirtz, D. (2010) Cross-linking FtsZ polymers into coherent Z rings. *Mol Microbiol* **78**: 651–668.

Daniel, R.A., Harry, E.J., and Errington, J. (2000) Role of penicillin-binding protein PBP 2B in assembly and functioning of the division machinery of Bacillus subtilis. *Mol Microbiol* **35**: 299–311.

Divakaruni, A.V., Baida, C., White, C.L., and Gober, J.W. (2007) The cell shape proteins MreB and MreC control cell morphogenesis by positioning cell wall synthetic complexes. *Mol Microbiol* **66**: 174–188.

Du, S., and Lutkenhaus, J. (2017) Assembly and activation of the Escherichia coli divisome. *Mol Microbiol* **105**: 177–187.

Du, S., Pichoff, S., and Lutkenhaus, J. (2016) FtsEX acts on FtsA to regulate divisome assembly and activity. *Proc Natl Acad Sci* **113**: E5052–E5061.

Dubey, A., and Priyadarshini, R. (2017) Amidase activity is essential for medial localization of AmiC in <Emphasis Type="Italic">Caulobacter crescentus</Emphasis>. *Curr Genet* 1–15.

Ducret, A., Quardokus, E.M., and Brun, Y.V. (2016) MicrobeJ, a tool for high throughput bacterial cell detection and quantitative analysis. *Nat Microbiol* **1**: 16077.

Durand-Heredia, J., Rivkin, E., Fan, G., Morales, J., and Janakiraman, A. (2012) Identification of ZapD as a Cell Division Factor That Promotes the Assembly of FtsZ in Escherichia coli. *J Bacteriol* **194**: 3189–3198.

Erickson, H.P., Anderson, D.E., and Osawa, M. (2010) FtsZ in Bacterial Cytokinesis: Cytoskeleton and Force Generator All in One. *Microbiol Mol Biol Rev* **74**: 504–528.

Erickson, H.P., and Osawa, M. (2017) FtsZ Constriction Force – Curved Protofilaments Bending Membranes. *Subcell Biochem* **84**: 139–160.

Erickson, H.P., Taylor, D.W., Taylor, K.A., and Bramhill, D. (1996) Bacterial cell division protein FtsZ assembles into protofilament sheets and minirings, structural homologs of tubulin polymers. *Proc Natl Acad Sci U S A* **93**: 519–523.

Federici, L., Masulli, M., Di Ilio, C., and Allocati, N. (2010) Characterization of the hydrophobic substrate-binding site of the bacterial beta class glutathione transferase from Proteus mirabilis. *Protein Eng Des Sel* **23**: 743–750.

Fenton, A.K., and Gerdes, K. (2013) Direct interaction of FtsZ and MreB is required for septum synthesis and cell division in Escherichia coli. *EMBO J* **32**: 1953–1965.

Figge, R.M., Divakaruni, A.V., and Gober, J.W. (2004) MreB, the cell shape-determining bacterial actin homologue, co-ordinates cell wall morphogenesis in Caulobacter crescentus. *Mol Microbiol* **51**: 1321–1332.

Figueroa-Cuilan, W., Daniel, J.J., Howell, M., Sulaiman, A., and Brown, P.J.B. (2016) Mini-Tn7 Insertion in an Artificial attTn7 Site Enables Depletion of the Essential Master Regulator CtrA in the Phytopathogen Agrobacterium tumefaciens. *Appl Environ Microbiol* **82**: 5015–5025.

Figueroa-Cuilan, W.M., and Brown, P.J.B. (2018) Cell Wall Biogenesis During Elongation and Division in the Plant Pathogen Agrobacterium tumefaciens. *Curr Top Microbiol Immunol* .

Fiji: an open-source platform for biological-image analysis | Nature Methods https://www.nature.com/articles/nmeth.2019. Accessed March 23, 2019.

Fraipont, C., Alexeeva, S., Wolf, B., Ploeg, R. van der, Schloesser, M., Blaauwen, T. den, and Nguyen-Distèche, M. (2011) The integral membrane FtsW protein and peptidoglycan synthase PBP3 form a subcomplex in Escherichia coli. *Microbiol Read Engl* **157**: 251–259.

Fu, G., Huang, T., Buss, J., Coltharp, C., Hensel, Z., and Xiao, J. (2010) In vivo structure of the E. coli FtsZ-ring revealed by photoactivated localization microscopy (PALM). *PloS One* **5**: e12682.

Gan, L., Chen, S., and Jensen, G.J. (2008) Molecular organization of Gram-negative peptidoglycan. *Proc Natl Acad Sci* **105**: 18953–18957.

Gardner, K.A.J.A., Moore, D.A., and Erickson, H.P. (2013) The C-terminal linker of Escherichia coli FtsZ functions as an intrinsically disordered peptide. *Mol Microbiol* **89**: 264–275.

Geissler, B., and Margolin, W. (2005) Evidence for functional overlap among multiple bacterial cell division proteins: compensating for the loss of FtsK. *Mol Microbiol* **58**: 596–612.

Gerding, M.A., Ogata, Y., Pecora, N.D., Niki, H., and Boer, P.A.J. de (2007) The trans-envelope Tol-Pal complex is part of the cell division machinery and required for proper outer-membrane invagination during cell constriction in E. coli. *Mol Microbiol* **63**: 1008–1025.

Ghosal, D., and Löwe, J. (2015) Collaborative protein filaments. *EMBO J* **34**: 2312–2320.

Girardot, C., Scholtalbers, J., Sauer, S., Su, S.-Y., and Furlong, E.E.M. (2016) Je, a versatile suite to handle multiplexed NGS libraries with unique molecular identifiers. *BMC Bioinformatics* **17**: 419.

Gitai, Z., Dye, N., and Shapiro, L. (2004) An actin-like gene can determine cell polarity in bacteria. *Proc Natl Acad Sci U S A* **101**: 8643–8648.

Glas, M., Berg van Saparoea, H.B. van den, McLaughlin, S.H., Roseboom, W., Liu, F., Koningstein, G.M., *et al.* (2015) The Soluble Periplasmic Domains of Escherichia coli Cell Division Proteins FtsQ/FtsB/FtsL Form a Trimeric Complex with Submicromolar Affinity. *J Biol Chem* **290**: 21498–21509.

Goehring, N.W., and Beckwith, J. (2005) Diverse paths to midcell: assembly of the bacterial cell division machinery. *Curr Biol CB* **15**: R514-526.

Goehring, N.W., Gonzalez, M.D., and Beckwith, J. (2006) Premature targeting of cell division proteins to midcell reveals hierarchies of protein interactions involved in divisome assembly. *Mol Microbiol* **61**: 33–45.

Goley, E.D., Comolli, L.R., Fero, K.E., Downing, K.H., and Shapiro, L. (2010a) DipM links peptidoglycan remodelling to outer membrane organization in Caulobacter. *Mol Microbiol* **77**: 56–73.

Goley, E.D., Dye, N.A., Werner, J.N., Gitai, Z., and Shapiro, L. (2010b) Imaging-based identification of a critical regulator of FtsZ protofilament curvature in Caulobacter. *Mol Cell* **39**: 975–987.

Goley, E.D., Yeh, Y.-C., Hong, S.-H., Fero, M.J., Abeliuk, E., McAdams, H.H., and Shapiro, L. (2011) Assembly of the Caulobacter cell division machine. *Mol Microbiol* **80**: 1680–1698.

Gonzalez, D., and Collier, J. (2013) DNA methylation by CcrM activates the transcription of two genes required for the division of Caulobacter crescentus. *Mol Microbiol* **88**: 203–218.

Grainge, I. (2010) FtsK--a bacterial cell division checkpoint? *Mol Microbiol* **78**: 1055–1057.

Guan, F., Yu, J., Yu, J., Liu, Y., Li, Y., Feng, X.-H., *et al.* (2018) Lateral interactions between protofilaments of the bacterial tubulin homolog FtsZ are essential for cell division. *eLife* **7**.

Gueiros-Filho, F.J., and Losick, R. (2002) A widely conserved bacterial cell division protein that promotes assembly of the tubulin-like protein FtsZ. *Genes Dev* **16**: 2544–2556.

Haakonsen, D.L., Yuan, A.H., and Laub, M.T. (2015) The bacterial cell cycle regulator GcrA is a σ70 cofactor that drives gene expression from a subset of methylated promoters. *Genes Dev* **29**: 2272–2286.

Haeusser, D.P., Rowlett, V.W., and Margolin, W. (2015) A mutation in Escherichia coli ftsZ bypasses the requirement for the essential division gene zipA and confers resistance to FtsZ assembly inhibitors by stabilizing protofilament bundling. *Mol Microbiol* **97**: 988–1005.

Hale, C.A., and Boer, P.A. de (1997) Direct binding of FtsZ to ZipA, an essential component of the septal ring structure that mediates cell division in E. coli. *Cell* **88**: 175–185.

Hale, C.A., Rhee, A.C., and Boer, P.A. de (2000) ZipA-induced bundling of FtsZ polymers mediated by an interaction between C-terminal domains. *J Bacteriol* **182**: 5153–5166.

Hale, C.A., Shiomi, D., Liu, B., Bernhardt, T.G., Margolin, W., Niki, H., and Boer, P.A.J. de (2011) Identification of Escherichia coli ZapC (YcbW) as a Component of the Division Apparatus That Binds and Bundles FtsZ Polymers. *J Bacteriol* **193**: 1393–1404.

Hayhurst, E.J., Kailas, L., Hobbs, J.K., and Foster, S.J. (2008) Cell wall peptidoglycan architecture in Bacillus subtilis. *Proc Natl Acad Sci U S A* **105**: 14603–14608.

Hocking, J., Priyadarshini, R., Takacs, C.N., Costa, T., Dye, N.A., Shapiro, L., *et al.* (2012) Osmolality-Dependent Relocation of Penicillin-Binding Protein PBP2 to the Division Site in Caulobacter crescentus. *J Bacteriol* **194**: 3116–3127.

Holden, S.J., Pengo, T., Meibom, K.L., Fernandez, C.F., Collier, J., and Manley, S. (2014) High throughput 3D super-resolution microscopy reveals Caulobacter crescentus in vivo Z-ring organization. *Proc Natl Acad Sci* **111**: 4566–4571.

Hottes, A.K., Meewan, M., Yang, D., Arana, N., Romero, P., McAdams, H.H., and Stephens, C. (2004) Transcriptional Profiling of Caulobacter crescentus during Growth on Complex and Minimal Media. *J Bacteriol* **186**: 1448–1461.

Hottes, A.K., Shapiro, L., and McAdams, H.H. (2005) DnaA coordinates replication initiation and cell cycle transcription in Caulobacter crescentus. *Mol Microbiol* **58**: 1340–1353.

Howell, M., Aliashkevich, A., Sundararajan, K., Daniel, J.J., Lariviere, P.J., Goley, E.D., *et al.* (2019) Agrobacterium tumefaciens divisome proteins regulate the transition from polar growth to cell division. *Mol Microbiol* https://onlinelibrary.wiley.com/doi/abs/10.1111/mmi.14212. Accessed January 31, 2019.

Howell, M., Daniel, J.J., and Brown, P.J.B. (2017) Live Cell Fluorescence Microscopy to Observe Essential Processes During Microbial Cell Growth. *J Vis Exp JoVE* .

Huang, K.C., Mukhopadhyay, R., Wen, B., Gitai, Z., and Wingreen, N.S. (2008) Cell shape and cell-wall organization in Gram-negative bacteria. *Proc Natl Acad Sci* pnas.0805309105.

Huitema, E., Pritchard, S., Matteson, D., Radhakrishnan, S.K., and Viollier, P.H. (2006) Bacterial Birth Scar Proteins Mark Future Flagellum Assembly Site. *Cell* **124**: 1025–1037.

Karimova, G., Dautin, N., and Ladant, D. (2005) Interaction Network among Escherichia coli Membrane Proteins Involved in Cell Division as Revealed by Bacterial Two-Hybrid Analysis. *J Bacteriol* **187**: 2233–2243.

Karimova, G., Pidoux, J., Ullmann, A., and Ladant, D. (1998) A bacterial two-hybrid system based on a reconstituted signal transduction pathway. *Proc Natl Acad Sci U S A* **95**: 5752–5756.

Kelly, A.J., Sackett, M.J., Din, N., Quardokus, E., and Brun, Y.V. (1998) Cell cycle-dependent transcriptional and proteolytic regulation of FtsZ in Caulobacter. *Genes Dev* **12**: 880–893.

Kiekebusch, D., Michie, K.A., Essen, L.-O., Löwe, J., and Thanbichler, M. (2012) Localized Dimerization and Nucleoid Binding Drive Gradient Formation by the Bacterial Cell Division Inhibitor MipZ. *Mol Cell* **46**: 245–259.

Krupka, M., Cabré, E.J., Jiménez, M., Rivas, G., Rico, A.I., and Vicente, M. (2014) Role of the FtsA C Terminus as a Switch for Polymerization and Membrane Association. *mBio* **5**: e02221-14.

Kureisaite-Ciziene, D., Varadajan, A., McLaughlin, S.H., Glas, M., Montón Silva, A., Luirink, R., *et al.* (2018) Structural Analysis of the Interaction between the Bacterial Cell Division Proteins FtsQ and FtsB. *mBio* **9**.

Kuru, E., Velocity Hughes, H., Brown, P.J., Hall, E., Tekkam, S., Cava, F., *et al.* (2012) In situ Probing of Newly Synthesized Peptidoglycan in Live Bacteria with Fluorescent D-Amino Acids. *Angew Chem Int Ed Engl* **51**: 12519–12523.

Lam, H., Schofield, W.B., and Jacobs-Wagner, C. (2006) A Landmark Protein Essential for Establishing and Perpetuating the Polarity of a Bacterial Cell. *Cell* **124**: 1011–1023.

Lambert, A., Vanhecke, A., Archetti, A., Holden, S., Schaber, F., Pincus, Z., *et al.* (2018) Constriction Rate Modulation Can Drive Cell Size Control and Homeostasis in C. crescentus. *iScience* **4**: 180–189.

Lan, G., Daniels, B.R., Dobrowsky, T.M., Wirtz, D., and Sun, S.X. (2009) Condensation of FtsZ filaments can drive bacterial cell division. *Proc Natl Acad Sci* **106**: 121–126.

Lan, G., Wolgemuth, C.W., and Sun, S.X. (2007) Z-ring force and cell shape during division in rod-like bacteria. *Proc Natl Acad Sci U S A* **104**: 16110–16115.

Lariviere, P.J., Mahone, C.R., Santiago-Collazo, G., Howell, M., Daitch, A.K., Zeinert, R., *et al.* (2019) An Essential Regulator of Bacterial Division Links FtsZ to Cell Wall Synthase Activation. *Curr Biol* **0** https://www.cell.com/current-biology/abstract/S0960-9822(19)30394-X. Accessed May 2, 2019.

Lariviere, P.J., Szwedziak, P., Mahone, C.R., Löwe, J., and Goley, E.D. (2018) FzlA, an essential regulator of FtsZ filament curvature, controls constriction rate during Caulobacter division. *Mol Microbiol* **107**: 180–197.

Laub, M.T., Chen, S.L., Shapiro, L., and McAdams, H.H. (2002) Genes directly controlled by CtrA, a master regulator of the Caulobacter cell cycle. *Proc Natl Acad Sci* **99**: 4632–4637.

Laub, M.T., McAdams, H.H., Feldblyum, T., Fraser, C.M., and Shapiro, L. (2000) Global analysis of the genetic network controlling a bacterial cell cycle. *Science* **290**: 2144–2148.

Li, H., and Durbin, R. (2010) Fast and accurate long-read alignment with Burrows-Wheeler transform. *Bioinforma Oxf Engl* **26**: 589–595.

Li, H., Handsaker, B., Wysoker, A., Fennell, T., Ruan, J., Homer, N., *et al.* (2009) The Sequence Alignment/Map format and SAMtools. *Bioinforma Oxf Engl* **25**: 2078–2079.

Li, Y., Hsin, J., Zhao, L., Cheng, Y., Shang, W., Huang, K.C., *et al.* (2013) FtsZ protofilaments use a hinge-opening mechanism for constrictive force generation. *Science* **341**: 392–395.

Li, Z., Trimble, M.J., Brun, Y.V., and Jensen, G.J. (2007) The structure of FtsZ filaments in vivo suggests a force-generating role in cell division. *EMBO J* **26**: 4694–4708.

Liu, B., Persons, L., Lee, L., and Boer, P.A.J. de (2015) Roles for both FtsA and the FtsBLQ subcomplex in FtsN-stimulated cell constriction in Escherichia coli. *Mol Microbiol* **95**: 945–970.

Liu, X., Meiresonne, N.Y., Bouhss, A., and Blaauwen, T. den (2018) FtsW activity and lipid II synthesis are required for recruitment of MurJ to midcell during cell division in Escherichia coli. *Mol Microbiol* **109**: 855–884.

Loose, M., and Mitchison, T.J. (2014) The bacterial cell division proteins FtsA and FtsZ self-organize into dynamic cytoskeletal patterns. *Nat Cell Biol* **16**: 38–46.

Löwe, J. (1998) Crystal structure determination of FtsZ from Methanococcus jannaschii. *J Struct Biol* **124**: 235–243.

Löwe, J., and Amos, L.A. (1998) Crystal structure of the bacterial cell-division protein FtsZ. *Nature* **391**: 203–206.

Löwe, J., and Amos, L.A. (1999) Tubulin-like protofilaments in Ca2+-induced FtsZ sheets. *EMBO J* **18**: 2364–2371.

Lu, C., Reedy, M., and Erickson, H.P. (2000) Straight and Curved Conformations of FtsZ Are Regulated by GTP Hydrolysis. *J Bacteriol* **182**: 164–170.

Lutkenhaus, J., Sanjanwala, B., and Lowe, M. (1986) Overproduction of FtsZ suppresses sensitivity of lon mutants to division inhibition. *J Bacteriol* **166**: 756–762.

Lyu, Z., Coltharp, C., Yang, X., and Xiao, J. (2016) Influence of FtsZ GTPase activity and concentration on nanoscale Z-ring structure in vivo revealed by three-dimensional Superresolution imaging. *Biopolymers* **105**: 725–734.

Ma, X., Ehrhardt, D.W., and Margolin, W. (1996) Colocalization of cell division proteins FtsZ and FtsA to cytoskeletal structures in living Escherichia coli cells by using green fluorescent protein. *Proc Natl Acad Sci U S A* **93**: 12998–13003.

Ma, X.-X., Jiang, Y.-L., He, Y.-X., Bao, R., Chen, Y., and Zhou, C.-Z. (2009) Structures of yeast glutathione-S-transferase Gtt2 reveal a new catalytic type of GST family. *EMBO Rep* **10**: 1320–1326.

Martin, M.E., Trimble, M.J., and Brun, Y.V. (2004) Cell cycle-dependent abundance, stability and localization of FtsA and FtsQ in Caulobacter crescentus. *Mol Microbiol* **54**: 60–74.

McAdams, H.H., and Shapiro, L. (2009) System-level design of bacterial cell cycle control. *FEBS Lett* **583**: 3984–3991.

McCarthy, D.J., Chen, Y., and Smyth, G.K. (2012) Differential expression analysis of multifactor RNA-Seq experiments with respect to biological variation. *Nucleic Acids Res* **40**: 4288–4297.

Meeske, A.J., Riley, E.P., Robins, W.P., Uehara, T., Mekalanos, J.J., Kahne, D., *et al.* (2016) SEDS proteins are a widespread family of bacterial cell wall polymerases. *Nature* **537**: 634–638.

Meier, E.L., Daitch, A.K., Yao, Q., Bhargava, A., Jensen, G.J., and Goley, E.D. (2017) FtsEX-mediated regulation of the final stages of cell division reveals morphogenetic plasticity in Caulobacter crescentus. *PLOS Genet* **13**: e1006999.

Meier, E.L., Razavi, S., Inoue, T., and Goley, E.D. (2016) A novel membrane anchor for FtsZ is linked to cell wall hydrolysis in Caulobacter crescentus. *Mol Microbiol* **101**: 265–280.

Milam, S.L., and Erickson, H.P. (2013) Rapid in vitro assembly of Caulobacter crescentus FtsZ protein at pH 6.5 and 7.2. *J Biol Chem* **288**: 23675–23679.

Mingorance, J., Tadros, M., Vicente, M., González, J.M., Rivas, G., and Vélez, M. (2005) Visualization of single Escherichia coli FtsZ filament dynamics with atomic force microscopy. *J Biol Chem* **280**: 20909–20914.

Modell, J.W., Hopkins, A.C., and Laub, M.T. (2011) A DNA damage checkpoint in Caulobacter crescentus inhibits cell division through a direct interaction with FtsW. *Genes Dev* **25**: 1328–1343.

Modell, J.W., Kambara, T.K., Perchuk, B.S., and Laub, M.T. (2014) A DNA damage-induced, SOS-independent checkpoint regulates cell division in Caulobacter crescentus. *PLoS Biol* **12**: e1001977.

Mohammadi, T., Dam, V. van, Sijbrandi, R., Vernet, T., Zapun, A., Bouhss, A., *et al.* (2011) Identification of FtsW as a transporter of lipid-linked cell wall precursors across the membrane. *EMBO J* **30**: 1425–1432.

Mohammadi, T., Sijbrandi, R., Lutters, M., Verheul, J., Martin, N.I., Blaauwen, T. den, *et al.* (2014) Specificity of the transport of lipid II by FtsW in Escherichia coli. *J Biol Chem* **289**: 14707–14718.

Möll, A., Schlimpert, S., Briegel, A., Jensen, G.J., and Thanbichler, M. (2010) DipM, a new factor required for peptidoglycan remodelling during cell division in Caulobacter crescentus. *Mol Microbiol* **77**: 90–107.

Möll, A., and Thanbichler, M. (2009) FtsN-like proteins are conserved components of the cell division machinery in proteobacteria. *Mol Microbiol* **72**: 1037–1053.

Monteiro, J.M., Pereira, A.R., Reichmann, N.T., Saraiva, B.M., Fernandes, P.B., Veiga, H., *et al.* (2018) Peptidoglycan synthesis drives an FtsZ-treadmilling-independent step of cytokinesis. *Nature* https://www.nature.com/articles/nature25506. Accessed February 20, 2018.

Morgenstein, R.M., Bratton, B.P., Nguyen, J.P., Ouzounov, N., Shaevitz, J.W., and Gitai, Z. (2015) RodZ links MreB to cell wall synthesis to mediate MreB rotation and robust morphogenesis. *Proc Natl Acad Sci U S A* **112**: 12510–12515.

Morton, E.R., and Fuqua, C. (2012) UNIT 3D.1 Laboratory Maintenance of Agrobacterium. *Curr Protoc Microbiol* **CHAPTER**: Unit3D.1.

Mukherjee, A., Dai, K., and Lutkenhaus, J. (1993) Escherichia coli cell division protein FtsZ is a guanine nucleotide binding protein. *Proc Natl Acad Sci U S A* **90**: 1053–1057.

Mukherjee, A., and Lutkenhaus, J. (1994) Guanine nucleotide-dependent assembly of FtsZ into filaments. *J Bacteriol* **176**: 2754–2758.

Mukherjee, A., and Lutkenhaus, J. (1998) Dynamic assembly of FtsZ regulated by GTP hydrolysis. *EMBO J* **17**: 462–469.

Mukherjee, A., and Lutkenhaus, J. (1999) Analysis of FtsZ assembly by light scattering and determination of the role of divalent metal cations. *J Bacteriol* **181**: 823–832.

Oliva, M.A., Cordell, S.C., and Löwe, J. (2004) Structural insights into FtsZ protofilament formation. *Nat Struct Mol Biol* **11**: 1243.

Osawa, M., Anderson, D.E., and Erickson, H.P. (2008) Reconstitution of Contractile FtsZ Rings in Liposomes. *Science* **320**: 792–794.

Osawa, M., Anderson, D.E., and Erickson, H.P. (2009) Curved FtsZ protofilaments generate bending forces on liposome membranes. *EMBO J* **28**: 3476–3484.

Osawa, M., and Erickson, H.P. (2013) Liposome division by a simple bacterial division machinery. *Proc Natl Acad Sci U S A* **110**: 11000–11004.

Osawa, M., and Erickson, H.P. (2018) Turgor Pressure and Possible Constriction Mechanisms in Bacterial Division. *Front Microbiol* **9** https://www.frontiersin.org/articles/10.3389/fmicb.2018.00111/full. Accessed February 21, 2018.

Osorio, A., Camarena, L., Cevallos, M.A., and Poggio, S. (2017) A New Essential Cell Division Protein in Caulobacter crescentus. *J Bacteriol* **199**: e00811-16.

Pacheco-Gómez, R., Roper, D.I., Dafforn, T.R., and Rodger, A. (2011) The pH Dependence of Polymerization and Bundling by the Essential Bacterial Cytoskeltal Protein FtsZ. *PLoS ONE* **6** http://www.ncbi.nlm.nih.gov/pmc/articles/PMC3125165/.

Paez, A., Mateos-Gil, P., Hörger, I., Mingorance, J., Rivas, G., Vicente, M., *et al.* (2009) Simple modeling of FtsZ polymers on flat and curved surfaces: correlation with experimental in vitro observations. *PMC Biophys* **2**: 8.

Perez, A.J., Cesbron, Y., Shaw, S.L., Villicana, J.B., Tsui, H.-C.T., Boersma, M.J., *et al.* (2019) Movement dynamics of divisome proteins and PBP2x:FtsW in cells of Streptococcus pneumoniae. *Proc Natl Acad Sci* **116**: 3211–3220.

Pichoff, S., and Lutkenhaus, J. (2005) Tethering the Z ring to the membrane through a conserved membrane targeting sequence in FtsA. *Mol Microbiol* **55**: 1722–1734.

Pichoff, S., and Lutkenhaus, J. (2007) Identification of a region of FtsA required for interaction with FtsZ. *Mol Microbiol* **64**: 1129–1138.

Pincus, Z., and Theriot, J.A. (2007) Comparison of quantitative methods for cell-shape analysis. *J Microsc* **227**: 140–156.

Poggio, S., Takacs, C.N., Vollmer, W., and Jacobs-Wagner, C. (2010) A protein critical for cell constriction in the Gram-negative bacterium Caulobacter crescentus localizes at the division site through its peptidoglycan-binding LysM domains. *Mol Microbiol* **77**: 74–89.

Pogliano, J., Pogliano, K., Weiss, D.S., Losick, R., and Beckwith, J. (1997) Inactivation of FtsI inhibits constriction of the FtsZ cytokinetic ring and delays the assembly of FtsZ rings at potential division sites. *Proc Natl Acad Sci U S A* **94**: 559–564.

Ptacin, J.L., Lee, S.F., Garner, E.C., Toro, E., Eckart, M., Comolli, L.R., *et al.* (2010) A spindle-like apparatus guides bacterial chromosome segregation. *Nat Cell Biol* **12**: 791–798.

Quardokus, E.M., and Brun, Y.V. (2002) DNA replication initiation is required for mid-cell positioning of FtsZ rings in Caulobacter crescentus. *Mol Microbiol* **45**: 605–616.

Quinlan, A.R., and Hall, I.M. (2010) BEDTools: a flexible suite of utilities for comparing genomic features. *Bioinformatics* **26**: 841–842.

Radhakrishnan, S.K., Pritchard, S., and Viollier, P.H. (2010) Coupling Prokaryotic Cell Fate and Division Control with a Bifunctional and Oscillating Oxidoreductase Homolog. *Dev Cell* **18**: 90–101.

RayChaudhuri, D., and Park, J.T. (1992) Escherichia coli cell-division gene ftsZ encodes a novel GTP-binding protein. *Nature* **359**: 251–254.

Robinson, J.T., Thorvaldsdóttir, H., Winckler, W., Guttman, M., Lander, E.S., Getz, G., and Mesirov, J.P. (2011) Integrative genomics viewer. *Nat Biotechnol* **29**: 24–26.

Robinson, M.D., McCarthy, D.J., and Smyth, G.K. (2010) edgeR: a Bioconductor package for differential expression analysis of digital gene expression data. *Bioinforma Oxf Engl* **26**: 139–140.

Rohs, P.D.A., Buss, J., Sim, S.I., Squyres, G.R., Srisuknimit, V., Smith, M., *et al.* (2018) A central role for PBP2 in the activation of peptidoglycan polymerization by the bacterial cell elongation machinery. *PLOS Genet* **14**: e1007726.

Rossjohn, J., Polekhina, G., Feil, S.C., Allocati, N., Masulli, M., Ilio, C.D., and Parker, M.W. (1998) A mixed disulfide bond in bacterial glutathione transferase: functional and evolutionary implications. *Structure* **6**: 721–734.

Rothfield, L., Justice, S., and García-Lara, J. (1999) Bacterial cell division. *Annu Rev Genet* **33**: 423–448.

Rueda, S., Vicente, M., and Mingorance, J. (2003) Concentration and assembly of the division ring proteins FtsZ, FtsA, and ZipA during the Escherichia coli cell cycle. *J Bacteriol* **185**: 3344–3351.

Sackett, M.J., Kelly, A.J., and Brun, Y.V. (1998) Ordered expression of ftsQA and ftsZ during the Caulobacter crescentus cell cycle. *Mol Microbiol* **28**: 421–434.

Sauvage, E., Derouaux, A., Fraipont, C., Joris, M., Herman, R., Rocaboy, M., *et al.* (2014) Crystal structure of penicillin-binding protein 3 (PBP3) from Escherichia coli. *PloS One* **9**: e98042.

Scheffers, D.-J., and Driessen, A.J.M. (2002) Immediate GTP hydrolysis upon FtsZ polymerization. *Mol Microbiol* **43**: 1517–1521.

Schoenemann, K.M., Krupka, M., Rowlett, V.W., Distelhorst, S.L., Hu, B., and Margolin, W. (2018) Gain-of-function variants of FtsA form diverse oligomeric structures on lipids and enhance FtsZ protofilament bundling. *Mol Microbiol* **109**: 676–693.

Schofield, W.B., Lim, H.C., and Jacobs-Wagner, C. (2010) Cell cycle coordination and regulation of bacterial chromosome segregation dynamics by polarly localized proteins. *EMBO J* **29**: 3068–3081.

Sham, L.-T., Butler, E.K., Lebar, M.D., Kahne, D., Bernhardt, T.G., and Ruiz, N. (2014) Bacterial cell wall. MurJ is the flippase of lipid-linked precursors for peptidoglycan biogenesis. *Science* **345**: 220–222.

Shapland, E.B., Reisinger, S.J., Bajwa, A.K., and Ryan, K.R. (2011) An essential tyrosine phosphatase homolog regulates cell separation, outer membrane integrity, and morphology in Caulobacter crescentus. *J Bacteriol* **193**: 4361–4370.

Shtylla, B. (2017) Mathematical modeling of spatiotemporal protein localization patterns in C. crescentus bacteria: A mechanism for asymmetric FtsZ ring positioning. *J Theor Biol* **433**: 8–20.

Söderström, B., Mirzadeh, K., Toddo, S., Heijne, G. von, Skoglund, U., and Daley, D.O. (2016) Coordinated disassembly of the divisome complex in Escherichia coli. *Mol Microbiol* **101**: 425–438.

Söderström, B., Skoog, K., Blom, H., Weiss, D.S., Heijne, G. von, and Daley, D.O. (2014) Disassembly of the divisome in Escherichia coli: evidence that FtsZ dissociates before compartmentalization. *Mol Microbiol* **92**: 1–9.

Spratt, B.G. (1977a) The mechanism of action of mecillinam. *J Antimicrob Chemother* **3**: 13–19.

Spratt, B.G. (1977b) Temperature-Sensitive Cell Division Mutants of Escherichia coli with Thermolabile Penicillin-Binding Proteins. *J Bacteriol* **131**: 293–305.

Spratt, B.G., and Pardee, A.B. (1975) Penicillin-binding proteins and cell shape in E. coli. *Nature* **254**: 516–517.

Stock, D., Perisic, O., and Löwe, J. (2005) Robotic nanolitre protein crystallisation at the MRC Laboratory of Molecular Biology. *Prog Biophys Mol Biol* **88**: 311–327.

Strauss, M.P., Liew, A.T.F., Turnbull, L., Whitchurch, C.B., Monahan, L.G., and Harry, E.J. (2012) 3D-SIM super resolution microscopy reveals a bead-like arrangement for FtsZ and the division machinery: implications for triggering cytokinesis. *PLoS Biol* **10**: e1001389.

Stricker, J., Maddox, P., Salmon, E.D., and Erickson, H.P. (2002) Rapid assembly dynamics of the Escherichia coli FtsZ-ring demonstrated by fluorescence recovery after photobleaching. *Proc Natl Acad Sci U S A* **99**: 3171–3175.

Strobel, W., Möll, A., Kiekebusch, D., Klein, K.E., and Thanbichler, M. (2014) Function and Localization Dynamics of Bifunctional Penicillin-Binding Proteins in Caulobacter crescentus. *J Bacteriol* **196**: 1627–1639.

Sundararajan, K., and Goley, E.D. (2017) Cytoskeletal Proteins in Caulobacter crescentus: Spatial Orchestrators of Cell Cycle Progression, Development, and Cell Shape. In *Prokaryotic*

Cytoskeletons. Springer, Cham, pp. 103–137 https://link.springer.com/chapter/10.1007/978-3-319-53047-5_4. Accessed September 19, 2017.

Sundararajan, K., Miguel, A., Desmarais, S.M., Meier, E.L., Huang, K.C., and Goley, E.D. (2015) The bacterial tubulin FtsZ requires its intrinsically disordered linker to direct robust cell wall construction. *Nat Commun* **6**: 7281.

Sycuro, L.K., Pincus, Z., Gutierrez, K.D., Biboy, J., Stern, C.A., Vollmer, W., and Salama, N.R. (2010) Peptidoglycan crosslinking relaxation promotes Helicobacter pylori's helical shape and stomach colonization. *Cell* **141**: 822–833.

Szwedziak, P., and Löwe, J. (2013) Do the divisome and elongasome share a common evolutionary past? *Curr Opin Microbiol* **16**: 745–751.

Szwedziak, P., Wang, Q., Bharat, T.A.M., Tsim, M., and Löwe, J. (2014) Architecture of the ring formed by the tubulin homologue FtsZ in bacterial cell division. *eLife* **3**: e04601.

Szwedziak, P., Wang, Q., Freund, S.M., and Löwe, J. (2012) FtsA forms actin-like protofilaments. *EMBO J* **31**: 2249–2260.

Taguchi, A., Welsh, M.A., Marmont, L.S., Lee, W., Sjodt, M., Kruse, A.C., *et al.* (2019) FtsW is a peptidoglycan polymerase that is functional only in complex with its cognate penicillin-binding protein. *Nat Microbiol* 1.

Taschner, P.E., Ypenburg, N., Spratt, B.G., and Woldringh, C.L. (1988) An amino acid substitution in penicillin-binding protein 3 creates pointed polar caps in Escherichia coli. *J Bacteriol* **170**: 4828–4837.

Terrana, B., and Newton, A. (1975) Pattern of unequal cell division and development in Caulobacter crescentus. *Dev Biol* **44**: 380–385.

Thanbichler, M., and Shapiro, L. (2006) MipZ, a Spatial Regulator Coordinating Chromosome Segregation with Cell Division in Caulobacter. *Cell* **126**: 147–162.

Thorvaldsdóttir, H., Robinson, J.T., and Mesirov, J.P. (2013) Integrative Genomics Viewer (IGV): high-performance genomics data visualization and exploration. *Brief Bioinform* **14**: 178–192.

Tsang, M.-J., and Bernhardt, T.G. (2015) A role for the FtsQLB complex in cytokinetic ring activation revealed by an ftsL allele that accelerates division. *Mol Microbiol* **95**: 925–944.

Turk, D. (2013) MAIN software for density averaging, model building, structure refinement and validation. *Acta Crystallogr D Biol Crystallogr* **69**: 1342–1357.

Typas, A., Banzhaf, M., Gross, C.A., and Vollmer, W. (2012) From the regulation of peptidoglycan synthesis to bacterial growth and morphology. *Nat Rev Microbiol* **10**: 123–136.

Uehara, T., Parzych, K.R., Dinh, T., and Bernhardt, T.G. (2010) Daughter cell separation is controlled by cytokinetic ring-activated cell wall hydrolysis. *EMBO J* **29**: 1412–1422.

Vaughan, S., Wickstead, B., Gull, K., and Addinall, S.G. (2004) Molecular Evolution of FtsZ Protein Sequences Encoded Within the Genomes of Archaea, Bacteria, and Eukaryota. *J Mol Evol* **58**: 19–29.

Vonrhein, C., Blanc, E., Roversi, P., and Bricogne, G. (2007) Automated Structure Solution With autoSHARP. In *Macromolecular Crystallography Protocols*. Doublié, S. (ed.). Humana Press, pp. 215–230 http://dx.doi.org/10.1385/1-59745-266-1%3A215. Accessed March 7, 2017.

Wang, S.C.E., West, L., and Shapiro, L. (2006) The Bifunctional FtsK Protein Mediates Chromosome Partitioning and Cell Division in Caulobacter. *J Bacteriol* **188**: 1497–1508.

Wang, X., and Lutkenhaus, J. (1993) The FtsZ protein of Bacillus subtilis is localized at the division site and has GTPase activity that is dependent upon FtsZ concentration. *Mol Microbiol* **9**: 435–442.

Wang, X., and Lutkenhaus, J. (1996) FtsZ ring: the eubacterial division apparatus conserved in archaebacteria. *Mol Microbiol* **21**: 313–319.

Weiss, D.S., Chen, J.C., Ghigo, J.M., Boyd, D., and Beckwith, J. (1999) Localization of FtsI (PBP3) to the septal ring requires its membrane anchor, the Z ring, FtsA, FtsQ, and FtsL. *J Bacteriol* **181**: 508–520.

White, C.L., Kitich, A., and Gober, J.W. (2010) Positioning cell wall synthetic complexes by the bacterial morphogenetic proteins MreB and MreD. *Mol Microbiol* **76**: 616–633.

Williams, B., Bhat, N., Chien, P., and Shapiro, L. (2014) ClpXP and ClpAP proteolytic activity on divisome substrates is differentially regulated following the Caulobacter asymmetric cell division. *Mol Microbiol* **93**: 853–866.

Wissel, M.C., and Weiss, D.S. (2004) Genetic analysis of the cell division protein FtsI (PBP3): amino acid substitutions that impair septal localization of FtsI and recruitment of FtsN. *J Bacteriol* **186**: 490–502.

Woldemeskel, S.A., and Goley, E.D. (2017) Shapeshifting to Survive: Shape Determination and Regulation in Caulobacter crescentus. *Trends Microbiol* **25**: 673–687.

Woldemeskel, S.A., McQuillen, R., Hessel, A.M., Xiao, J., and Goley, E.D. (2017) A conserved coiled-coil protein pair focuses the cytokinetic Z-ring in Caulobacter crescentus. *Mol Microbiol* **105**: 721–740.

Wolfe, A., Phipps, K., and Weitao, T. (2014) Viral and cellular SOS-regulated motor proteins: dsDNA translocation mechanisms with divergent functions. *Cell Biosci* **4**: 31.

Xiao, J., and Goley, E.D. (2016) Redefining the roles of the FtsZ-ring in bacterial cytokinesis. *Curr Opin Microbiol* **34**: 90–96.

Yakhnina, A.A., and Gitai, Z. (2013) Diverse Functions for Six Glycosyltransferases in Caulobacter crescentus Cell Wall Assembly. *J Bacteriol* **195**: 4527–4535.

Yang, X., Lyu, Z., Miguel, A., McQuillen, R., Huang, K.C., and Xiao, J. (2017) GTPase activity–coupled treadmilling of the bacterial tubulin FtsZ organizes septal cell wall synthesis. *Science* **355**: 744–747.

Yao, Q., Jewett, A.I., Chang, Y.-W., Oikonomou, C.M., Beeby, M., Iancu, C.V., *et al.* (2017) Short FtsZ filaments can drive asymmetric cell envelope constriction at the onset of bacterial cytokinesis. *EMBO J* **36**: 1577–1589.

Yeh, Y.-C., Comolli, L.R., Downing, K.H., Shapiro, L., and McAdams, H.H. (2010) The Caulobacter Tol-Pal Complex Is Essential for Outer Membrane Integrity and the Positioning of a Polar Localization Factor. *J Bacteriol* **192**: 4847–4858.

Yu, X.C., and Margolin, W. (1997) Ca2+-mediated GTP-dependent dynamic assembly of bacterial cell division protein FtsZ into asters and polymer networks in vitro. *EMBO J* **16**: 5455–5463.

Zielińska, A., Billini, M., Möll, A., Kremer, K., Briegel, A., Izquierdo Martinez, A., *et al.* (2017) LytM factors affect the recruitment of autolysins to the cell division site in Caulobacter crescentus. *Mol Microbiol* **106**: 419–438.

Zuleta, L.F.G., Italiani, V.C.S., and Marques, M.V. (2003) Isolation and Characterization of NaCl-Sensitive Mutants of Caulobacter crescentus. *Appl Env Microbiol* **69**: 3029–3035.

Curriculum Vitae

Patrick James Lariviere

www.linkedin.com/in/patrick-lariviere-a9a89858/ | plarivi1@gmail.com | 847-668-3969

EDUCATION

Johns Hopkins University School of Medicine, Baltimore, MD 2013-2019 (anticipated)
Ph.D., Biochemistry, Cellular, and Molecular Biology

Bowdoin College, Brunswick, ME 2009-2013
B.A., Biochemistry (Honors)

RESEARCH EXPERIENCE

Industry Research:

AstraZeneca, Cell Culture and Fermentation Intern Feb 2019-Apr 2019

- Modulated mammalian cell metabolism to enhance cell growth (in flask and bioreactor formats), viability, and antibody production.
- Optimized *in vitro* fluorescence assay to detect oxidative stress in mammalian cells.

Ph.D. Thesis Research:

Johns Hopkins University School of Medicine, Ph.D. Candidate Fall 2013-Present
Department of Biological Chemistry. Mentor: Erin D. Goley, Ph.D.

- Discovered that an essential division protein, FzlA, controls the rate of constriction in the bacterium *Caulobacter crescentus*.
- Identified a novel pathway for activation of cell wall synthesis in division, whereby FzlA links the cytokinetic ring to peptidoglycan synthesis enzymes.
- Engineered over 170 bacterial strains to facilitate investigation of mechanisms of bacterial division.
- Utilized computational and statistical methods to analyze rates of cell growth & division for 2 research projects.

Undergraduate Research:

Bowdoin College, Undergraduate Honors Student Researcher Fall 2012-Fall 2013
Department of Biology. Mentor: Bruce Kohorn, Ph.D.

- Identified members of a MAP Kinase signaling pathway involved in the stress response in the plant model organism *Arabidopsis thaliana*.

Purdue University, Summer Student Researcher (NSF funded) Summer 2012
Department of Biochemistry. Mentor: Barbara Golden, Ph.D.

- Assessed RNA enzyme kinetics of a hepatitis delta virus-like ribozyme to provide mechanistic insight into RNA self-cleavage.

Northwestern University, Summer Student Researcher Summers 2010-2011
Department of Biomedical Engineering. Mentor: Arun Sharma, Ph.D.

- Characterized the ability of a bioengineered scaffold to facilitate tissue regeneration in a rat urological injury model.

PEER-REVIEWED PUBLICATIONS

Lariviere, P.J., Mahone, C.R., Santiago-Collazo, G., Howell, M., Daitch, A.K., Zeinert, R., Chien, P., Brown, P.J.B., Goley, E.D. Activation of SEDS-PBP cell wall synthases by an essential regulator of bacterial division. *Current Biology* (2019).

Howell, M., Aliashkevich, A., Sundararajan, K., Daniel, J.J., **Lariviere, P.J.**, Cava, F., Goley, E.D., Brown, P.J.B. *Agrobacterium tumefaciens* divisome proteins regulate the transition from polar growth to cell division. *Mol. Microbiol* (2019).

Lariviere, P.J., Szwedziak, P., Mahone, C.R., Löwe, J., Goley, E.D. FzlA, an essential regulator of FtsZ filament curvature, controls constriction rate during Caulobacter division. *Mol. Microbiol.* 107, 180–197 (2018).

Sharma, A.K., Bury, M.I., Fuller, N.J., Rozkiewicz, D.I., Hota, P.V., Kollhoff, D.M., Webber, M.J., Tapaskar, N., Meisner, J.W., **Lariviere, P.J.**, DeStefano, S., Wang, D., Ameer, G.A. , Cheng, E.Y. Growth factor release from a chemically modified elastomeric poly(1,8-octanediol-co-citrate) thin film promotes angiogenesis *in vivo*. *J Biomed Mater Res Part A.* 100A:561–570. (2012).

OTHER PUBLICATIONS

Lariviere, P.J., Goley, E. D. Cell division in *Caulobacter crescentus*: A molecular-scale model. *Nature Springer* (Book chapter, in press 2019).

Lariviere, P. J. and Kohorn, Bruce. Identification of MPKs involved in the wall associated kinase regulated stress response in *Arabidopsis thaliana*. (Undergraduate Honors Thesis, 2013).

PRESENTATIONS

Oral

Plant and Microbial Cytoskeleton Gordon Research Conference, Andover NH	Aug 2018
Biogen Drug Development Conference, Cambridge MA	Jun 2018
BCMB Graduate Program Retreat, Johns Hopkins University, Cambridge MD	Oct 2017
Biological Chemistry Departmental Retreat, Johns Hopkins University, Baltimore MD	Oct 2016
BCMB Rotation Symposium, Johns Hopkins University, Baltimore MD	Dec 2013

Undergraduate Honors Research Symposium, Bowdoin College, Brunswick ME Dec 2012
Summer Student Research Symposium, Purdue University, West Lafayette IN Jun 2012

Poster
Biological Chemistry Departmental Retreat, Johns Hopkins University, Baltimore MD Sep 2018
Plant and Microbial Cytoskeleton Gordon Research Conference, Andover NH Aug 2018
ASCB-EMBO General Meeting, Philadelphia PA Dec 2017
Biological Chemistry Departmental Retreat, Johns Hopkins University, Baltimore MD Sep 2017
BCMB Graduate Program Retreat, Johns Hopkins University, St. Michaels MD Sep 2016
BCMB Graduate Program Retreat, Johns Hopkins University, St. Michaels MD Oct 2015
ASM Conference on Prokaryotic Cell Biology and Development, Washington DC Jun 2015
Biological Chemistry Departmental Retreat, Johns Hopkins University, Baltimore MD May 2015
BCMB Graduate Program Retreat, Johns Hopkins University, St. Michaels MD Oct 2014
BCMB Rotation Symposium, Johns Hopkins University, Baltimore MD Mar 2014
Undergraduate Honors Research Symposium, Bowdoin College, Brunswick ME Apr 2013
Summer Student Research Symposium, Purdue University, West Lafayette IN Jul 2012

AWARDS

Biogen Drug Development Conference **Best Team Presentation Award** Jun 2018

ADDITIONAL BIOTECHNOLOGY EXPERIENCE

JHU Technology Ventures, Technology Transfer Intern Fall 2015-Fall 2016

- Assessed commercialization potential of 15 newly disclosed biotechnology and pharmaceutical inventions.
- Communicated findings to technology transfer associates possessing a variety of technical backgrounds.

LEADERSHIP AND MENTORSHIP

Johns Hopkins University School of Medicine, Lab Mentor

- Mentored 1 undergraduate and 2 graduate rotation students in the Goley lab, teaching methods in biochemistry and cell biology, including protein purification and protein binding assays.
- Mentored 1 graduate rotation student Nov 2017-Jan 2018
- Mentored 1 graduate rotation student Feb-Apr 2017
- Mentored 1 undergraduate student Jan 2015-May 2016

Johns Hopkins University School of Medicine, Teaching Assistant

- Created 2 online learning modules, 1 in-class activity, 1 problem set, and 10 exam questions to promote and assess student learning.
- Served as teaching assistant for graduate level Bacterial Genetics Oct-Dec 2017
- Served as teaching assistant for graduate level Bacterial Genetics Oct-Dec 2016

Thread Mentoring Program, Lead Mentor Fall 2013-Fall 2017

- Led team of 3 mentors at local non-profit to provide support for a young adult in Baltimore City, resulting in high school graduation and job placement.
- Interfaced with mentee's teachers, parents, family, Thread staff, volunteers, and lawyers to promote the well-being and success of mentee.

INTERESTS

I enjoy playing/listening to music, running, softball, cooking with my spouse, and playing with my dog.